Realistic Wind Loads on Reinforced Masonry Walls

A Thesis Submitted to the College of Graduate and Postdoctoral Studies
In Partial Fulfillment of the Requirements for the Degree of Master of Science
In the Department of Civil, Geological and Environmental Engineering
University of Saskatchewan
Saskatoon

By
Nipun Tissera

Permission to Use

In presenting this thesis in partial fulfillment of the requirements for a Postgraduate degree from the University of Saskatchewan, I agree that the Libraries of this University may make it freely available for inspection. I further agree that permission for copying of this thesis in any manner, in whole or in part, for scholarly purposes may be granted by the professor or professors who supervised my thesis work or, in their absence, by the Head of the Department or the Dean of the College in which my thesis work was done. It is understood that any copying or publications or use of this thesis or parts thereof for financial gain shall not be allowed without my written permission. It is also understood that due recognition shall be given to me and to the University of Saskatchewan in any scholarly use which may be made of any material in my thesis.

Requests for permission to copy or to make other uses of materials in this thesis in whole or part should be addressed to:

Head of the Department of Civil, Geological and Environmental Engineering
University of Saskatchewan
57 Campus Drive
Saskatoon SK S7N 5A9
Canada

Or

Dean
College of Graduate and Postdoctoral Studies
University of Saskatchewan
116 Thorvaldson Building, 110 Science Place
Saskatoon, SK S7N 5C9
Canada

Abstract

Wind is a primary source of out-of-plane loads for masonry wall structural members. Although wind is a dynamic loading condition, the current body of research generally considers the behaviour of masonry walls under quasi-static load conditions, whilst the dynamic aspect is not explicitly considered. Therefore, this research intends to address this gap in knowledge.

The objective of this research was to investigate the behavioural characteristics of reinforced masonry walls subjected to realistic wind load conditions. Specifically, the intention was to examine the differences in strength and deflection characteristics of reinforced masonry walls under quasi-static and dynamic load conditions. In addition, differences in the behaviour of walls with different levels of reinforcement were examined under quasi-static and dynamic load conditions.

The experimental program consisted of testing twenty large-scale wall specimens featuring idealized-pinned support conditions. The specimens comprised four sets of tests that addressed all possible combinations of the two primary test variables: quasi-static vs. dynamic load, and low vs. high reinforcement ratio. The partially grouted wall specimens had nominal dimensions of 3 m high and 1 m wide and were constructed using standard 200 mm hollow concrete masonry blocks arranged in a running bond pattern. The dynamic load was generated using a 4th order autoregressive function to produce a series of realistic wind load time histories for varying wind intensities. The dynamic loads and the quasi-static loads were applied using a four-point loading setup.

Both the strength and deformation characteristics of the wall specimens were analyzed and compared. The results indicate that the wall specimens loaded under realistic dynamic loading conditions resisted slightly higher peak loads at higher levels of ductility compared to that of the wall specimens loaded under quasi-static loading conditions. Furthermore, the amount of reinforcement did not have significant impact on the general behaviour characteristics between the two types of loading conditions.

Acknowledgments

I would like to extend my sincere gratitude to Dr. Bruce Sparling for his support and guidance as my graduate supervisor. It was a pleasure to work with such a knowledgeable and supportive supervisor. I would further like to thank my graduate committee members Dr. Lisa Feldman and Dr. Leon Wegner for their support and suggestions during this study.

I would like to thank the Saskatchewan Masonry Institute (SMI), the Canadian Masonry Design Centre (CMDC) and the University of Saskatchewan College of Engineering for providing the funding necessary to complete this study.

Furthermore, I would like to thank Brennan Pokoyoway (Laboratory Technician at University of Saskatchewan), Sasha Kisin (CMDC) and Roy Nicolas (Gracom Masonry Ltd.) for all the assistance in the construction and testing of the experimental program.

To conclude, I would also like to thank my family, friends and fellow colleagues in the graduate program at University of Saskatchewan for all the support extended over the course of this study. I would especially like to mention my colleagues Henry Miranda, Kien Doan, Amir Rezeivahdati, Umesh Poudyal and Ryan Yakimoski.

Table of Contents

List of Figures

List of Tables

List of Symbols

t	Current time step used in autoregressive function
$\Delta\tau$	Time step increment used to generate simulated wind turbulence
k	Increment number (1,2,3,4) used in autoregressive simulation
$u(t)$	Instantaneous fluctuating wind speed at current time step
$u(t-k\Delta\tau)$	Instantaneous wind speed at k^{th} previous time step
ϕ_k	Weighting factors for the previous time steps used in autoregressive function
ϕ_ω	Weighting factor of the random shock value at the current time step
$\omega(t)$	Random shock value at the current time step
$R^u(k\Delta\tau)$	Autocorrelation value at k^{th} previous time step
f	Frequency in Hz
$S^u(f)$	Wind speed power spectral density
z	Reference height above ground
z_0	Surface roughness parameter
$\overline{U}(z)$	Mean wind speed at an elevation of z above the ground surface
u_*	Friction velocity of wind
f_y	Yield strength of the reinforcement in MPa
ρ_{all}	Allowable reinforcement ratio of the wall specimens
ρ_b	Balance reinforcement ratio of the wall specimens
q	Wind pressure applied over the wall surface area
ρ	Density of air
V_s	Wind speed
$f`_m$	Calculated effective compressive strength of wall specimens
f_{avg}	Average compressive strength wall specimens

Chapter 1: Introduction

1.1 Background

Masonry construction is one of the oldest and most widely used methods of construction. It is a type of construction where many small modular units are mortared together to produce a structure or a structural element. At present, concrete masonry block construction is commonly used for wall type structural elements, such as partition walls and in-fill walls, which accounts for much of masonry construction.

Historically masonry structures were massive, and the mass of the structure itself accounted for the primary loading of the structure. Therefore, these structures were constructed such that all the components would primarily be in, and resist, compression. In contrast, modern masonry structures, such as walls, are much lighter and slender, and are susceptible to out-of-plane loading. Therefore, many masonry wall structures require additional reinforcement to adequately resist flexural loads that result from out-of-plane loading conditions.

Wind loading is a primary source of out-of-plane loading. Wind loading generally consists of a steady mean component and a dynamic component that fluctuates randomly about the mean component of the wind. To account for both these components, the current design standards approximate an effective static pressure to represent the peak out-of-plane loading produced by the wind. However, this approximate static loading may not accurately represent the behaviour of masonry wall structures under real wind loading conditions as the dynamic interaction between the wind and the structure is not explicitly considered.

The current body of research and studies that have been carried out on steel reinforced masonry walls under wind loading conditions is limited. Furthermore, these studies primarily deal with wind loading under quasi-static loading conditions. Overall, the research carried out under

dynamic loading conditions generally pertain to earthquake and blast type loading conditions. Udey (2014) investigated the behaviour characteristics of unreinforced masonry walls under quasi static and dynamic loading conditions. The study indicated a slight increase in capacity under dynamic loading conditions, as compared to quasi-static loading conditions. Considering this, however, there is a lack of knowledge regarding the behaviour of reinforced masonry wall elements under realistic dynamic wind loading conditions. Therefore, this thesis is intended to address this gap in knowledge. In addition, the impact of the reinforcement ratio of reinforced masonry walls under dynamic loading conditions is also considered in this study. This is taken into consideration, as the amount of reinforcement has significant impact of the behavioural characteristics of reinforced masonry wall elements, such as stiffness, natural frequency and energy dissipation characteristics.

1.2 Objectives

The objective of this research was to investigate the flexural behaviour of reinforced masonry walls, with idealized pinned support conditions, subjected to realistic out-of-plane wind loads. Specifically, the research was intended to:

- Compare the differences in load resisting and displacement characteristics of reinforced masonry walls under quasi-static loading conditions and realistic dynamic wind loading conditions; and
- Compare the behavioural characteristics of reinforced masonry walls featuring different levels of steel reinforcement under both quasi-static and dynamic loading conditions.

In summary, the intent of the study was to provide insight as to whether the current quasi-static design approach for wind loading of masonry walls is appropriate.

1.3 Scope

The focus of this study was to determine the differences in strength and behaviour characteristics of reinforced masonry walls that had two different levels of reinforcement under quasi-static and dynamic loading, representative of steady uniform wind pressure and realistic wind storms, respectively. A laboratory based experimental study was conducted, in which wall specimens were

subjected to out-of-plane loading, similar to that experienced under wind loading conditions, and featured idealized pinned support conditions.

The wind loading conditions were applied to the wall specimens using two methods. A quasi-static loading was applied under displacement control during which the applied load was monotonically increased until failure. In addition, a dynamic loading was applied under load control during which the load was applied using predefined fluctuating patterns, or time histories, that were incrementally increased in intensity until failure.

The wall specimens featured two different levels of reinforcements, using No.10 bars and No.15 bars, respectively; however, both configurations were designed to be under-reinforced sections. The walls were partially grouted and measured 3 m high and 1 m wide. They were constructed using standard 200 mm concrete blocks arranged in a running bond pattern and were made using consistent mix designs for the mortar and grout. Therefore, each wall specimen was fundamentally the same, with the only differences between the test series being the different levels of reinforcement and the type of loading.

Chapter 2: Literature Review

2.1 Introduction

In the current body of literature, much of the research on out-of-plane loading of masonry walls has been carried out under static or quasi-static loading conditions. In addition, there has been a limited amount of research focusing on masonry walls under wind loading conditions. With regards to research pertaining to reinforced masonry walls, most recent research has dealt with FRP or other such composite reinforcement methods compared to traditional steel rebar reinforcement. Therefore, information on steel-reinforced masonry walls subjected realistic dynamic wind loading conditions is limited.

2.2 Out-of-Plane Loading of Reinforced Masonry Walls

The poor tensile resistance of masonry has been noted as the significant factor that leads to the failure of unreinforced masonry walls under out-of-plane loading conditions. In general, the failure of the bond between masonry units and mortar bedding due to the tension stress produced by flexural loading leads to the failure of the unreinforced masonry wall assemblage under out-of-plane loading conditions. Thus, reinforcement is frequently inserted into masonry walls to supplement their tensile resistance.

Abboud, Hamid, and Harris (1996) conducted a comprehensive study on steel-reinforced concrete-block masonry walls under static out-of-plane flexural loading conditions. The flexural behaviour characteristics of the masonry walls was investigated considering the parameters of the amount and location of reinforcement, extent of grouting and masonry unit size. The experimental program encompassed the testing of six concrete-block masonry walls that were 3 blocks wide and 13 courses high. The wall specimens spanned vertically under ideally-pinned support conditions and were monotonically loaded using a four-point loading system, in which two equal line loads were applied at the third points along the wall surface.

It was observed that cracking initiated along the horizontal masonry block and mortar interface of the tension face near the mid height of the wall specimen. Further flexural tension cracks propagated as the load was increased beyond the cracking load, which eventually led to the formation of flexural shear cracks closer to the supports. As the specimens reached their capacity, crack widths increased gradually until one of the cracks opened significantly, which was followed by spalling within the mortar joints and face shells on the compression side at failure.

Several of the key conclusions reached by Abboud et al. (1996), which are also generally stated in masonry design textbooks, are as follows.

- Reinforced masonry walls under out-of-plane loading conditions exhibit a ductile failure mode characterized by the yielding of reinforcement that results in spalling within mortar joints and face shells of the compression face at ultimate capacity.
- The extent of grouting has significant effect on the cracking load while the amount of reinforcement does not.
- The amount of reinforcement has a significant effect on the ultimate capacity.
- The amount of reinforcement has an influence on the shape of the load deflection curve, while the extent of grouting does not.
- The amount of reinforcement has a significant effect on the displacement and ductility ratio (i.e., ratio of displacement at ultimate loading over displacement at yield loading).

2.3 Dynamic Loading of Masonry Walls

There have been relatively few studies pertaining to out-of-plane loading of masonry walls under wind loading conditions; flexural loading, such as wind loading, is generally applied as quasi-static loading in most experimental programs. In contrast, there have been several studies pertaining to support motion-induced out-of-plane loading that have been carried out using dynamic loading conditions. Tomazevic, Lutman, and Petkovic (1996) and Griffith, Lam, Wilson, and Doherty (2004) were two such studies that subjected masonry walls to support motion-induced dynamic loading using a shake table apparatus. Tomazevic et al. (1996) subjected reinforced masonry walls to monotonic, cyclic and seismic type loading conditions. The study concluded that there were indications of possible behavioural differences between the different types of loading but recommended further investigation since the findings were not statistically significant. On the

other hand, Griffith et al. (2004) subjected brick masonry walls with different degrees of slenderness to static and dynamic support motion loading conditions. The study concluded that the static tests provided an adequate approximation for the dynamic loading conditions.

In terms of research on wind loading on masonry walls, Udey (2014) conducted tests on unreinforced masonry walls which were subjected to realistic dynamic wind loading conditions. The research was carried out to analyse the differences in behaviour characteristics of realistically-pinned and ideally-pinned unreinforced masonry walls under quasi-static and dynamic wind loading conditions. The experimental program encompassed the testing of 20 concrete-block masonry walls that were 2.5 blocks wide and 15 courses high. The wall specimens spanned vertically and were loaded using a four-point loading system, which applied two equal line loads using a spreader system. Both realistically-pinned and ideally-pinned wall specimens were tested using monotonically increasing quasi-static loading as well as realistic dynamic loading based on realistic wind time histories. The wind time histories used in the dynamic loading were generated using a mathematical formulation, which adequately approximated realistic wind loading conditions.

Udey (2014) concluded that the differences between quasi-static and dynamic loading were not conclusive in terms of the realistically-pinned wall specimens. In contrast, the ideally-pinned wall specimens displayed increased moment capacity under dynamic loading conditions. In addition, it was concluded that the failure of the wall specimens under dynamic loading conditions was due to sustained large amplitude “gusts” instead of the largest instantaneous peak loading of the wind time histories. On the other hand, the displacement behaviour of the wall specimens was found to be independent of the type of loading, but instead depended on the type of support conditions.

2.4 Masonry Material under Dynamic Loading

Masonry is a nonhomogeneous and anisotropic composite, which is an assemblage of masonry block units, mortar, grout and steel reinforcement. Furthermore, the behavioural characteristics of masonry walls are not perfectly elastic, even at small deformations, and become increasingly nonlinear at higher loading levels. The changes in overall stiffness and crack distributions over time can be observed during the testing of masonry wall specimens, which indicates the sensitivity of test results to load-time histories like that of realistic wind loading conditions.

The influence of rate of loading on the strength of cementitious materials used in masonry construction was investigated by Zielinski and Reinhardt (1982) and Burnett et al. (2007). These studies conducted tensile strength tests on mortar cylinders and brick-mortar prisms. Split Hopkinson Pressure Bar testing was carried out at different rates of loading. The studies concluded that the mortar specimens showed higher levels of tensile strength under higher rates of loading, than under quasi-static loading conditions. This apparent increase in strength was attributed to the failure mechanism of the mortar. The cracks through the mortar progressed from the micro-cracks that were already present under quasi-static loading conditions. The stresses in the mortar could redistribute under lower rates of loading, and the cracks formed along the path of least resistance. Under higher rates of loading, however, the stresses in mortar could not redistribute and the cracks could not form along the path of least resistance. As a result, this led to an increase in the strength of mortar by a factor of as much as three under higher rates of loading, as compared to quasi-static loading conditions.

Tomazevic et al. (1996) investigated the energy dissipation characteristics of reinforced masonry walls under dynamic loading conditions. The study investigated the behaviour of reinforced masonry walls under seismic loading conditions. Support motion type testing was carried out on wall specimens under monotonic, cyclic and earthquake loading conditions, both dynamically and statically. The findings indicated that, under dynamic loading types, the reinforced wall specimens generally showed higher lateral resistance and more rigid initial behaviour, as compared to static loading. However, similar levels of ultimate ductility were seen under both dynamic and static loading types. In general, rapidly applied monotonic loading resulted in much higher levels of capacity and ultimate displacement. Furthermore, the study indicated that more input energy from the dynamic loading was required to cause similar damage states in reinforced wall specimens that were subjected lower levels of axial loading, such as non-loadbearing walls. Williams and Scrivener (1974) and Tercelj et al. (1977) carried out similar testing on the influence of frequency of application of cyclic lateral loads on the shear strength and ductility of plain masonry walls.

2.5 Testing Methods for Out-of-Plane Loading of Masonry Walls

There have been several methods of testing masonry walls subjected to wind-type out-of-plane loading conditions mentioned in the literature. The provisions provided by

ASTM C1717-12 (2012) outlines a standard method of testing masonry walls using a four-point loading arrangement. In addition, ASTM E72-15 (2015) provides a standard method for testing masonry walls using an air-bag loading apparatus. In general, the testing methods that have been used in the literature fall under the two types of testing methods mentioned above.

In comparison to point loading methods, air-bag loading methods have generally produced better approximations of the moment distribution which would result from a uniform load similar to that of a uniform wind load. Hamoush, McGinley, Mlakar, Scott, and Murray (2001) and Hoeppner, Sparling, Wegner, and Sakr (2002) were studies pertaining to FRP strengthening of masonry walls in flexure that made use of air-bag loading methods. On the other hand, Abboud et al. (1996), Albert, Elwi, and Cheng (2001) and Udey (2014) made use of four-point loading arrangements in order to adequately approximate uniform out-of-plane loading. Bean Popehn, Schultz, Lu, Stolarski, and Ojard (2008) conducted research pertaining to slender unreinforced masonry walls using a six-point loading arrangement to better approximate a uniform out-of-plane loading. Additionally, out-of-plane loading tests have also been carried out using horizontally spanning wall specimens. Galal and Sasanian (2010) conducted research on GFRP-reinforced masonry walls where testing was carried out on both GFRP and steel reinforced masonry specimens using a four-point loading setup on horizontally spanning wall specimens.

Although the air-bag testing apparatus could better approximate the moment distribution of uniform loading conditions, it can only simulate increasing unidirectional loading conditions. Therefore, in cases of dynamic analysis, such as Udey (2014) where realistic wind time histories simulations were required, an air-bag testing apparatus is not appropriate. As wind is a highly dynamic and fluctuating load, a four-point loading system driven by a hydraulic actuator, similar to the test apparatus used in Udey (2014), would be a more appropriate approach to apply a realistic wind loading.

2.6 Simulation of Wind Loading

Wind is a random and dynamic load. As a result, the loading conditions produced by wind could be infinitely variable for any given situation. Nevertheless, it has been necessary to adequately simulate these load time histories in a realistic manner for research purposes. Although there has only been a limited number of studies done with regards to wind loading on masonry walls, there

have been an ample amount of research with regards to wind loading on structural systems in general. Therefore, multiple methods of generating wind loading conditions can be found in the current literature. Several such methods of generating wind time histories are outlined as follows.

Pressure profiles obtained from wind tunnel testing conducted on small-scale replicates of structures have been used to generate wind time histories. Surry et al. (2007), Morrison and Kopp (2011) and Kopp, Morrison, and Henderson (2012) were several such examples of studies that have used this method to generate the necessary wind time histories. These studies made use of the wind tunnel facility at Western University, Ontario. In general, wind tunnel testing provides realistic wind loading time histories, but modelling of complex structures can be difficult and costly.

Wind load time histories have been generated using in-situ measurements of real wind storms that were recorded for specific structures or locations of interest. Juhásová (1997) and Henderson and Ginger (2011) were a couple of examples of studies that have used in-situ measurements to generate the necessary wind time histories. According to Gani and Legeron (2010) there are several challenges in using this method. There are practical limitations in taking in-situ wind storm measurements of large-scale structures; in addition, the probability of being able to observe a design wind storm is low since they generally have long return periods.

Wind time histories have also been obtained through mathematical formulations. Sparling and Davenport (1998), Gani and Legeron (2010) and Udey (2014) were several studies that were carried out using mathematically generated wind time histories. Udey (2014) made comparisons between the power spectrum density plots of the mathematically generated wind loading and the theoretical wind loading specified by the National Building Code of Canada (2010). The comparisons concluded that the shapes of the power spectrum density plots were similar, although there were some shifts in the frequency content. Overall, it was concluded that the mathematical model adequately represented realistic wind loading conditions. In comparison to the above-mentioned methods, mathematical modelling can be efficiently applied to all cases to generate wind loading profiles regardless of type of structure or location.

2.7 Overview of Modelled Wind Time Histories

A fourth order autoregressive function was used to generate the realistic wind load time histories that were applied as dynamic loading in this experimental program. Overall, this mathematical procedure extrapolates the next time step in a wind speed time history by incorporating the previous time steps and a weighted random "shock" value. The weight factors were based on theoretical wind frequency distributions and gust intensities. Essentially, the model produces a random load time history with the general characteristics of a realistic wind storm. Sparling (1995) used a similar procedure, which was simplified and used in the experimental program of Udey (2014). This study used the same procedure that was used by Udey (2014) to generate the realistic wind time histories. While a more comprehensive description of the method can be found in Udey (2014), the following section gives a brief overview.

The fourth order function that generates the instantaneous wind speed at the current time step, t, was as follows:

$$u(t) = \phi_1 u(t - \Delta\tau) + \phi_2 u(t - 2\Delta\tau) + \phi_3 u(t - 3\Delta\tau) + \phi_4 u(t - 4\Delta\tau) + \phi_\omega \omega(t) \qquad (2.1)$$

where $u(t)$ is the instantaneous wind speed at current time step and $u(t - k\Delta\tau)$ is the wind speed at k^{th} previous time step, with each time step separated by the constant interval $\Delta\tau$. The weighting factors for the previous time steps are ϕ_k, while the weighting factor of the random shock value at the current time step, $\omega(t)$, is ϕ_ω. The random shock values were a set of random values with Gaussian distribution and a mean value of unity.

The weight factors for the fourth order autoregression were calculated using a set of Yule-Walker equations represented in matrix form as follows:

$$\begin{bmatrix} \phi_1 \\ \phi_2 \\ \phi_3 \\ \phi_4 \end{bmatrix} = \begin{bmatrix} R^u(0) & R^u(\Delta\tau) & R^u(2\Delta\tau) & R^u(3\Delta\tau) \\ R^u(\Delta\tau) & R^u(0) & R^u(\Delta\tau) & R^u(2\Delta\tau) \\ R^u(2\Delta\tau) & R^u(\Delta\tau) & R^u(0) & R^u(\Delta\tau) \\ R^u(3\Delta\tau) & R^u(2\Delta\tau) & R^u(\Delta\tau) & R^u(0) \end{bmatrix}^{-1} \begin{bmatrix} R^u(\Delta\tau) \\ R^u(2\Delta\tau) \\ R^u(3\Delta\tau) \\ R^u(4\Delta\tau) \end{bmatrix} \qquad (2.2)$$

where $R^u(k\Delta\tau)$ terms are the autocorrelation terms based on the power spectral density of theoretical wind time histories. The weighting factor of the random shock value was calculated as follows:

$$\phi_\omega^2 = R^u(0) - \phi_1 R^u(\Delta\tau) - \phi_2 R^u(2\Delta\tau) - \phi_3 R^u(3\Delta\tau) - \phi_4 R^u(4\Delta\tau) \quad (2.3)$$

The autocorrelation terms, which were used to calculate the weighting factors, were determined by applying Fourier transformation over a frequency domain of a power spectral density of a theoretical wind storm, which describes how the energy of the turbulent wind is distributed with frequency. The resulting formulation was as follows:

$$R^u(k\Delta\tau) = \int_0^\infty S^u(f) e^{i 2\pi f k \Delta\tau}\, df \quad (2.4)$$

where f is frequency and $S^u(f)$ is wind speed power spectral density. The theoretical wind speed power spectral density referenced in this study was proposed by Kaimal et al. (1972), which presents an elevation dependent expression as follows:

$$\frac{f S^u(z,f)}{u_*^2} = \frac{200\left(\frac{fz}{\bar{U}(z)}\right)}{\left[1+50\left(\frac{fz}{\bar{U}(z)}\right)\right]^{\frac{5}{3}}} \quad (2.5)$$

where z is the reference height above ground, $\bar{U}(z)$ is the mean wind speed at the specified reference height and u_* is the turbulent friction velocity, which is formulated as follows:

$$u_* = \frac{0.4\bar{U}_{10}}{ln\left(\frac{10}{z_0}\right)} \quad (2.6)$$

where z_0 is the surface roughness parameter and $\bar{U}_{10}$ is the wind speed at an elevation of 10 m. The values of the parameters $\Delta\tau$, z, z_0 and $\bar{U}_{10}$ that were used in this study are discussed in Chapter 3 (Section 3.4), along with the characteristics of the resulting wind time histories.

Chapter 3: Experimental Program

3.1 Overview

A total of twenty large-scale wall specimens were constructed for testing, all with the same geometric design and idealized pinned support conditions. The general parameters considered for this experimental design were based primarily on the previous research performed by Udey (2014).

The test program comprised four sets of masonry wall specimens, which addressed all possible combinations of the two primary test variables: quasi-static vs. dynamic wind loading conditions, and low vs. high reinforcement ratios. Therefore, the four sets of masonry wall specimens can be described as follows:

- Specimens with low reinforcement ratio tested under quasi-static loads;
- Specimens with low reinforcement ratio tested under dynamic loads;
- Specimens with high reinforcement ratio tested under quasi-static loads; and
- Specimens with high reinforcement ratio tested under dynamic loads

Each set consisted of five replicate specimens which were loaded beyond the yield load under both dynamic load time histories (representative of a realistic wind load) and quasi-static monotonically increasing loads (representative of a static pressure load). The testing was halted once the deformation of the specimen reached the feasible limits of the test setup. The number of replicated specimens for each set was limited to five due to constraints on available laboratory space and resources. It was judged to be an adequate number of replicated specimens based on a previous study done by Udey (2014).

Additional testing was carried out in conjunction with the out-of-plane load testing. Companion specimens were tested to correlate material and assemblage properties with the behaviour of the wall specimens. In addition, material tests were carried out on mortar, grout, rebar and masonry blocks to ensure quality and consistency between different batches that were used in construction.

Vibration tests were conducted on several wall specimens prior to the out-of-plane load testing to determine approximate natural frequencies of the undamaged wall specimens.

The construction and testing were carried out in two phases at the University of Saskatchewan Structures Laboratory. The first phase included the construction and testing of the specimens with the lower reinforcement ratio, while the second phase included the construction and testing of the specimens with the higher reinforcement ratio.

3.2 Materials

In accordance with CSA S304.1-14 (2014) Clause 3.4.1, the materials used in the construction of the masonry specimens satisfied the provisions laid out in CSA A371-04 (2004): Masonry Construction for Buildings. The materials were acquired from local suppliers recommended by the Saskatchewan Masonry Institute (SMI).

3.2.1 Concrete Masonry Blocks

Normal density 200 mm hollow concrete masonry blocks (390 x 190 x 190 mm) with a nominal strength of 15 MPa were used to construct all the masonry wall specimens. A combination of frog-ended and flat-ended blocks were used for construction due to the availability of mixed-block pallets from the supplier; the pallets consisted of approximately 60% frog-ended blocks and 40% flat-ended blocks. *Figure 3.1* represents the blocks that were used for the construction of the specimens.

Figure 3.1: Flat-ended (left) and frog-ended (right) concrete masonry blocks

To ensure consistency in material properties, some of the blocks were cut in half using a concrete saw, as shown in *Figure 3.2*, and used as the half-width units that were required at one end of each course of blocks. The cut-ends of the flat-ended blocks were oriented such that they faced the exterior end of the wall specimens, which ensured that they were not used in any of the head joints in the masonry assemblages.

Two batches of blocks were supplied by Expocrete Ltd. (Saskatoon, SK). The block pallets were stored in the University of Saskatchewan Structures Laboratory for approximately two weeks prior to the start of construction to equilibrate the masonry units to the laboratory environmental conditions. One batch was used for the first phase, while the second batch was used for the second phase. The blocks were delivered in mixed pallets consisting of both frog and flat ended blocks. The nominal compressive strength of the units was checked as per the procedure outlined in CSA A165-04 (2004).

Figure 3.2: Concrete saw used in cutting the masonry blocks

3.2.2 Mortar

In accordance with CSA S304.1-14 (2014), Type S mortar was used for construction. The mortar was batched using a 3:1 sand to cement ratio and a water to cement ratio of approximately 0.7. Whenever possible, a mortar batch used was not re-tempered as its workability decreased. Instead, a new batch was prepared once the workability of the batch no longer met the necessary requirements of the experienced mason. The quality assurance and the compressive strength of the mortar was checked as per the procedure outlined in CSA A179-14 (2014). Further details on the mortar mix is provided in Section 3.4.2.

3.2.3 Grout

It was important to ensure adequate workability and flowability of the grout to properly fill voids in the cells of the masonry assemblage. Therefore, a high-slump grout with a measured slump of 200 to 250 mm and a maximum aggregate size of 10 mm was used to construct the masonry specimens. For quality assurance purposes, a non-absorbent cylinder compressive strength test was conducted for each grout batch as per the procedure outlined in CSA A179-14 (2014). Two cylindrical samples were cast for each grout batch. In addition, one absorbent grout block was molded for each grout batch as per the procedure outlined in ASTM C1019-14 (2014). This absorbent grout block test was intended to provide a more realistic measure of the compressive strength of the in-situ grout, considering the water absorption of the concrete block units. Further details on the grout mix is provided in Section 3.4.3.

3.2.4 Reinforcement

Two sizes of CSA G30 18-09 400W reinforcement bars were used for the construction of the masonry specimens. The wall specimens were designed such that they were under-reinforced cross sections. In accordance with CSA S304.1-14 (2014), the allowable reinforcement ratio, ρ_{all}, for non-loadbearing reinforced wall specimens is as follows:

$$\frac{0.8}{f_y} < \rho_{all} < \rho_b \qquad (3.1)$$

where f_y (in MPa) is the yield strength of the reinforcement bars and ρ_b is the balanced reinforcement ratio of the wall specimens. Preliminary calculations, based on design values

provided by CSA S304.1-14 (2014), estimated that the allowable reinforcement ratio was between 0.2% and 1.3% (i.e., approximately between 76 mm^2 and 511 mm^2, respectively). Therefore, the wall specimens with lower reinforcement ratios included two No.10 bars and the wall specimens with the higher reinforcement ratios included two No.15 bars, thereby providing 200 mm^2 and 400 mm^2 reinforcement area per 1 m width, respectively (i.e., approximately 0.5% and 1.1% reinforcement ratio, respectively). The reinforcement was placed at mid-depth of the wall specimens along the entire height. Further details on the installation of rebar and grouting is provided in Section 3.4.3. The tensile strength of the reinforcement bars was determined as per the procedure outlined in ASTM A615-12 (2012).

3.3 Wall Specimen and Masonry Prism Description

3.3.1 Wall Specimens

Each of the twenty masonry wall specimens constructed was 15 courses high and 2.5 blocks wide. They were constructed using standard 200 mm hollow concrete blocks arranged in a half running bond pattern. The specimens featured face-shell mortar bedding with concave-tooled 10 mm mortar joints. Therefore, the nominal dimensions of a wall specimen were approximately 3000 x 1000 x 190 mm (height x width x depth). Ten of the specimens featured No.10 reinforcement bars, while the other ten specimens featured No.15 reinforcement bars. Within each specimen, the reinforcing bars were placed in two locations, namely the 2nd and 4th cells from the ends of the walls. The reinforcement was placed at mid-depth of the wall specimens, or approximately 95 mm from the face of the walls, with the aid of rebar positioners detailed in Section 3.4.1. Only the cells containing reinforcing bars were grouted; a mortar dam was used to prevent the grout from spilling out to the adjacent ungrouted cells. Therefore, all the wall specimens were partially grouted. *Figure 3.3* provides a basic overview of the wall specimens.

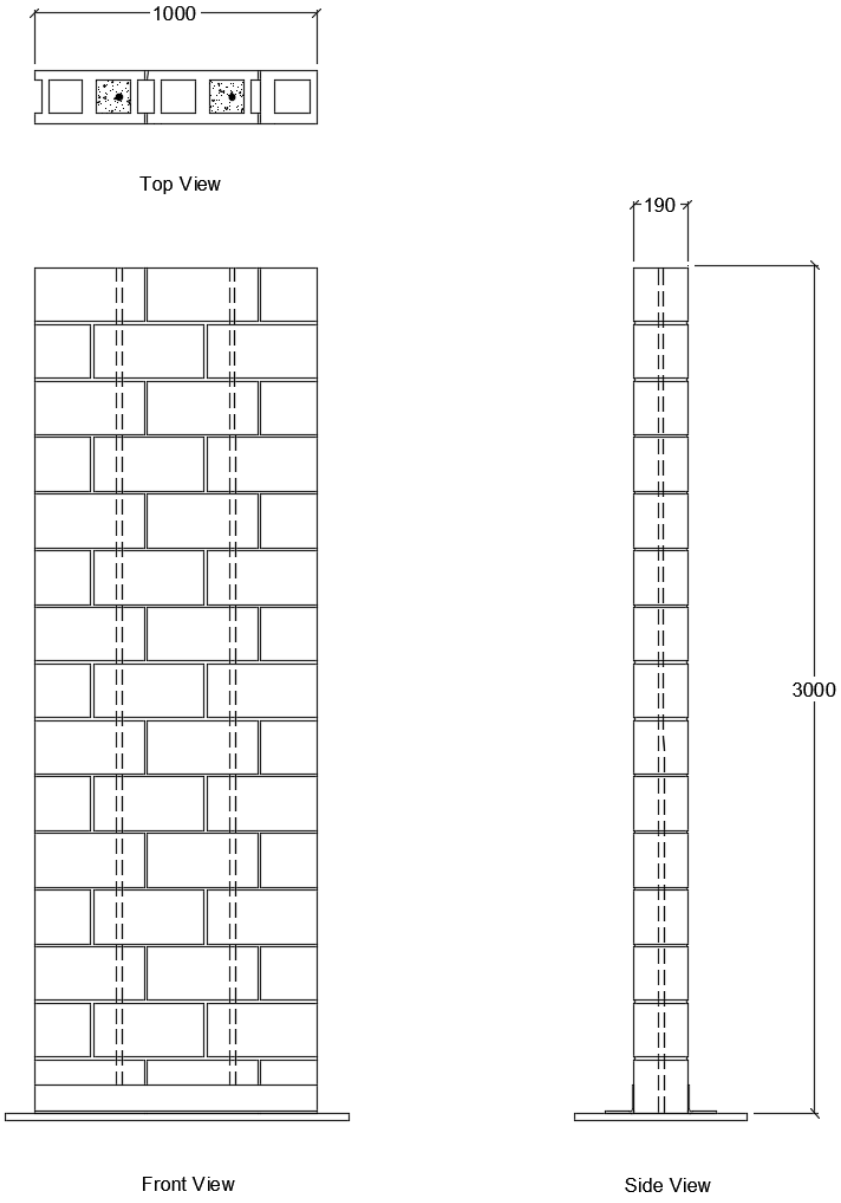

Figure 3.3: Wall specimen overview

3.3.2 Supporting Bases

The masonry wall specimens were constructed and mounted on a knife-edge support to approximate ideally pinned support conditions. As part of configuring the support conditions, the wall specimens were constructed on steel bases featuring slotted holes, as shown in *Figure 3.4*. The nominal dimensions of the steel plates were 1219 x 610 x 25 mm. To prevent sliding of the wall relative to the base plate under load, steel angles that spanned the full width of the wall specimens were positioned flush against both faces of the first course of the wall specimens and

bolted in place to the base plate through the six slotted holes. To prevent the lateral movement of the steel base relative to the knife-edge support, a grooved steel plate was bolted in place through the four groove plate holes as well. In addition, the bases featured lifting lugs, on either side, that enabled the specimens to be lifted by the 10-tonne crane in the Structural Lab and allowed them to be transported as necessary after being constructed.

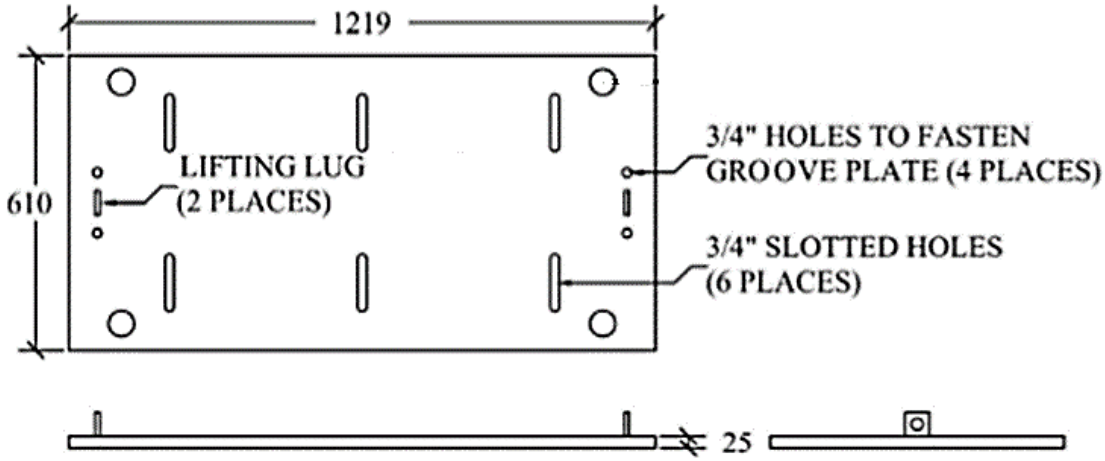

Figure 3.4: Steel base plate (Udey, 2014)

3.3.3 Masonry Prisms

Two masonry prisms were constructed for each masonry wall specimen; one ungrouted prism and one grouted prism. These prisms were constructed using the same batch of block, mortar and grout that was used in constructing the mid-height section of the specific masonry wall specimen, where the maximum moment was to be applied. The four-course prisms were one block wide and arranged in running bond pattern, as shown in *Figure 3.5*. The prisms were constructed as such, based on the feedback provided by the Saskatchewan Masonry Institute (SMI) to better represent the wall specimens being tested. The nominal dimensions of the four-course prisms were approximately 790 x 390 x 190 mm (height x width x depth). Whereas the ungrouted prisms were constructed using a mix of frog-ended and flat-ended blocks, the grouted prisms were strictly constructed using only flat-ended blocks. The grouted prisms were constructed, as such, to simplify the estimation of its cross-sectional area (i.e., cross-sectional area of the grouted masonry prisms was assumed to be the same as the gross cross-sectional area of the flat-ended blocks). As the masonry block tests that were carried out indicated similar properties between the frog-ended and flat-ended blocks, the decision to construct the masonry prisms in this manner did not seem to

have any negative impact on the prism test results. The masonry prisms cured alongside the masonry wall specimens under the same laboratory conditions and were used for compression strength testing of the masonry assemblage. The testing was carried out as per the procedure outlined in CSA S304.1-14 (2014). Further details on the masonry prisms test are presented in Section 3.7.

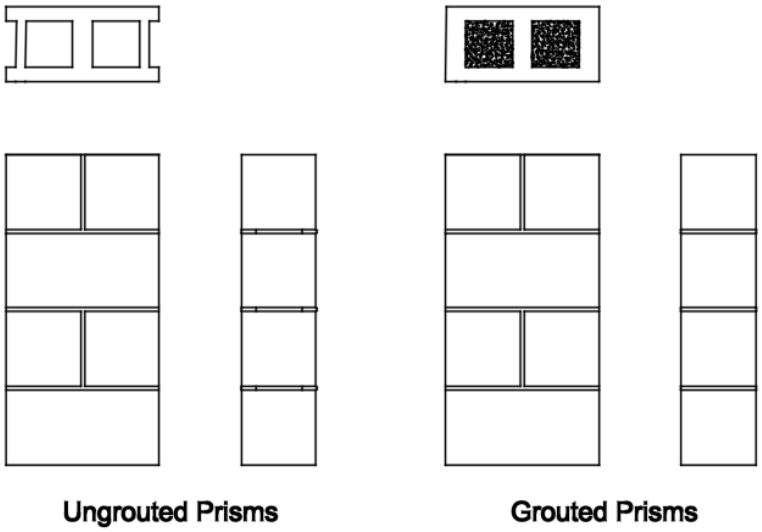

Figure 3.5: Masonry prisms

3.4 Construction

The construction of the twenty wall specimens and their companion specimens was carried out in two phases in the University of Saskatchewan Structures Laboratory. The first phase of construction, which spanned from March 14 to April 1, 2016, dealt with the specimens with the low reinforcement ratio. The second phase of construction, which spanned from June 20 to June 30, 2016, dealt with the specimens with the high reinforcement ratio. The construction of both phases was carried out by Roy Nicholas from Gracom Masonry Ltd. (Saskatoon, SK), a qualified masonry tradesman supplied by the Saskatchewan Masonry Institute (SMI).

3.4.1 Construction of the Wall Specimens

The 15 course high and 2.5 block wide wall specimens were constructed in two stages during each phase. Since a low lift grouting procedure was used in construction, the first stage consisted of the construction and grouting of the lower half of the wall specimens, up to the ninth course, while the

second stage consisted of the construction and grouting of the subsequent courses of the wall specimens. *Figure 3.6* shows the construction of the lower half of a wall specimen.

Figure 3.6: Construction of the first half of a wall specimen

To ensure proper alignment of the steel reinforcement, several makeshift positioners were used along the height of the wall specimen. They were made by cutting strips of wire mesh with the wire to wire spacing being approximately the same as the diameter of the reinforcement bars used. The wire gage was such that it was easy to cut and bend manually, but at the same time was strong enough to hold the bars in place during grouting. These positioners were installed in the 2nd and 4th cells from the ends of the walls, at courses 1, 8 and 14 from the bottom of the walls. They were held in place using a mortar dam. *Figure 3.7* shows the installation of the positioners after the first course had been laid.

Figure 3.7: Laying the first course and installing the rebar positioners

Additional care was taken when constructing the first course on the steel base. The blocks were laid directly on the steel base without a mortar bedding. The course was arranged to be as straight as possible and centered on the steel base. This was to ensure that the knife-edge support was aligned with the middle of the wall specimen, as well as to ensure proper contact between the wall surface and the steel angles that were placed to prevent the wall specimen from slipping on the steel base. Furthermore, the steel angles were installed after the completion of the first half of the wall specimen, as shown in *Figure 3.8*, to minimize any disturbance to the specimen due to the installation process.

Figure 3.8: Steel angles attached to the base of the wall specimens

The companion prisms for each specimen were constructed after the completion of the first half of the corresponding wall specimen, as shown in *Figure 3.9*. Once the first halves of all the wall specimens were constructed, the reinforcement bars were dropped in place, centered in the 2nd and 4th cells from the ends of the walls, and the grouting of the lower half was completed. The completed lower halves of the wall specimens, with the reinforcing bars installed, are shown in *Figure 3.10.*

Figure 3.9: Construction of companion prisms

Figure 3.10: The wall specimens after the first stage of construction

The remainder of the wall specimens, courses 10 through 15, were laid and the second grouting lift was completed during the second stage of construction, as shown in *Figure 3.11*. The wall specimens were then braced for safety reasons and left to cure under normal laboratory conditions, as shown in *Figure 3.12.*

Figure 3.11: Construction of the second half of a wall specimen

Figure 3.12: The completed wall specimens from phase 2

3.4.2 Mortar Preparation

The mortar was prepared under the close supervision of the mason using the mortar mixer that is available in the laboratory, as shown in *Figure 3.13.* The mixture consisted of three ten-gallon buckets (approximately 114 L) of mortar sand, one 34 kg bag of Lafarge Type S mortar cement and approximately one ten-gallon bucket (approximately 38 L) of water. The water content was adjusted as necessary by the mason to give the mortar the required workability. For each batch, six 50 mm mortar cube samples were cast using the molds available in the laboratory, as shown in *Figure 14.* The mason did re-temper the mortar when required during construction; however, whenever possible, a new batch was prepared once too much time had passed and the workability was no longer adequate as judged by the mason.

Figure 3.13: Mortar mixer

Figure 3.14: Mortar samples

3.4.3 Grouting

The grout batches were prepared under the close supervision of the mason using the concrete mixer that is available in the laboratory, as shown in *Figure 3.15*. The mixture consisted of nine five-gallon buckets (approximately 170 L) of grout aggregate mix with a maximum aggregate size of 10 mm, two 20 kg bag of Lafarge type GU cement and approximately 1.5 ten-gallon buckets (approximately 57 L) of water. The water content was adjusted as necessary by the mason to give the grout the required flowability with a high slump of about 20 to 25 cm. *Figure 3.16* depicts a slump test, which was carried out for each grout batch prepared. For each batch, two 100 mm diameter non-absorbent cylinder samples were cast, as shown in *Figure 3.17*, and one absorbent grout block was cast using a block arrangement, as shown in *Figure 3.18.*

Figure 3.15: Concrete mixer

Figure 3.16: Slump test for grout batch

Figure 3.17: Grout cylinder samples

Figure 3.18: Grout absorbent block samples

The wall specimens were partially grouted. The reinforcement was placed at two locations, at center depth in the 2nd and 4th cells from the ends of the walls, and only these cells were grouted. The grouting was carried out using a low lift grouting procedure. The first lift was placed after the completion of the first half of the wall specimens, up to the ninth course. The grout was only filled up to a height of approximately 8.5 courses to prevent creating a plane of weakness (i.e., prevent aligning the contact surface of the two grout lifts with a bed-joint). At this point, the same grout batch was used to fill in the grouted companion prisms of the corresponding wall specimen. The second lift was placed after the completion of the entire wall specimens. The high slump grout mixture was poured, and a concrete vibrator was used to properly compact the mixture. The rebar positioners did an adequate job at properly aligning the reinforcing bar, as observed during the examination of damaged wall specimens after the conclusion of testing. *Figure 3.19* shows a wall specimen after the completion of the first grout lift.

Figure 3.19: Partially grouted wall specimen after the first grout lift

3.5 Test Setup

3.5.1 Four-Point Loading Setup

Figure 3.20 illustrates an overview of the test setup used in the testing of all the wall specimens. A four-point loading setup was used to approximate the uniform loading condition of a wind load. All wall specimens featured idealized pinned support conditions. The load for both quasi-static and dynamic tests was applied using a horizontally oriented hydraulic actuator positioned at the mid-height and mid-width of the wall specimens. Two equal line loads were applied to the wall specimen using a spreader system, whose horizontal arms were located 800 mm apart vertically, at 1100 mm and 1900 mm along the height of the wall specimen measured from the base. The arrangement of displacement transducers and load cells that was used to acquire the necessary displacement and applied load readings is shown in *Figure 3.20*. *Figure 3.21* shows the test setup, while *Figure 3.22* shows the instrument setup used in the experimental program.

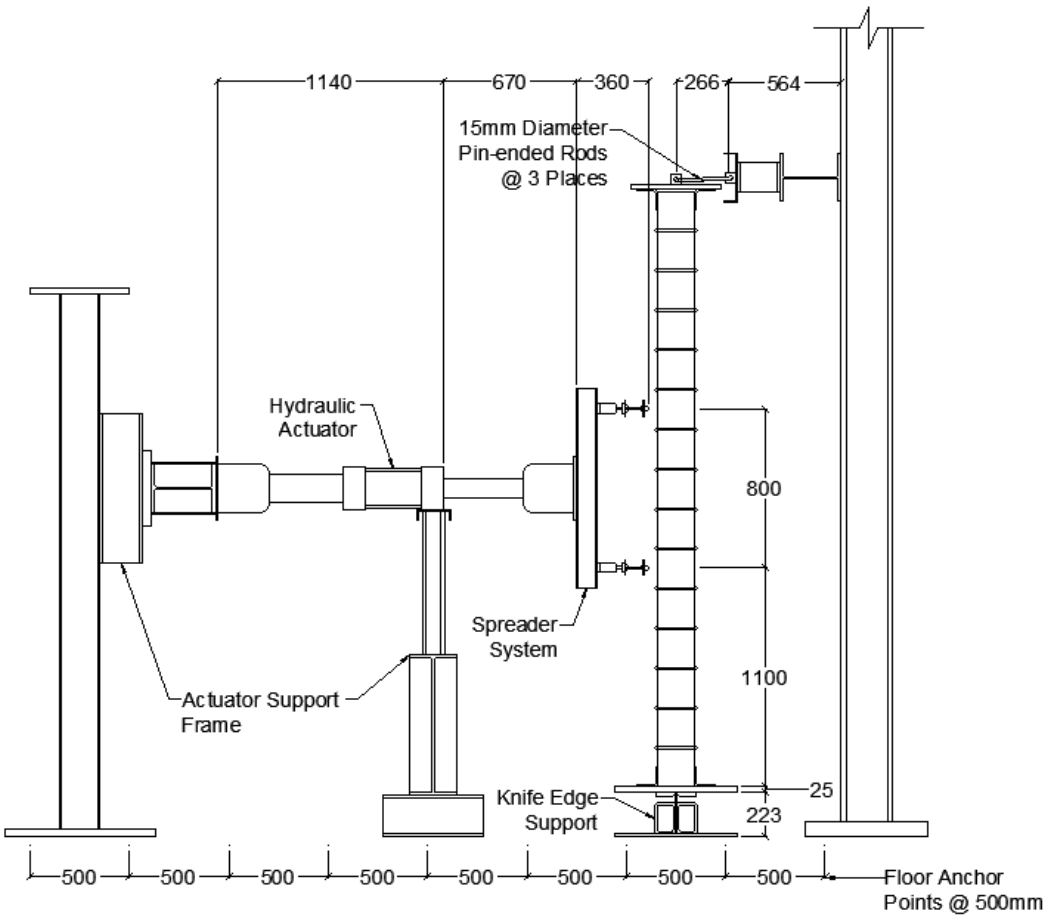

Figure 3.20: Test setup illustration

Figure 3.21: Test setup

An MTS® Series 244, Model 244.31, hydraulic actuator was used to apply the loading. The actuator had a load capacity of 250 kN and a maximum stroke of 254 mm. An MTS® controller system and software suite were used to control the actuator during both the quasi-static and dynamic testing. The actuator featured a built-in force transducer and displacement transducer. The precision of force transducer and displacement transducer were ±0.001 N and ±0.001 mm, respectively. The mid-height deflection measurements were taken using a Micro-Epsilon optoNCDT 1700-500 laser optical displacement measurement device, which had a precision of ±0.001 mm. The data from these instruments were captured by a National Instruments™ NI-SCXI-1305 acquisition card in a NI-SCXI-1001 chassis. Two additional Micro-Measurements HS100 100 mm LVDTs (Linear Variable Differential Transducer) were used to collect deflection measurements at 500 mm and 2500 mm along the height of the wall specimens. In addition, two Interface 110AF-10k load cells were used to measure the load applied by each spreader arm. The data were sampled at a rate of 100 Hz and was recorded using LabView© software suite for further processing.

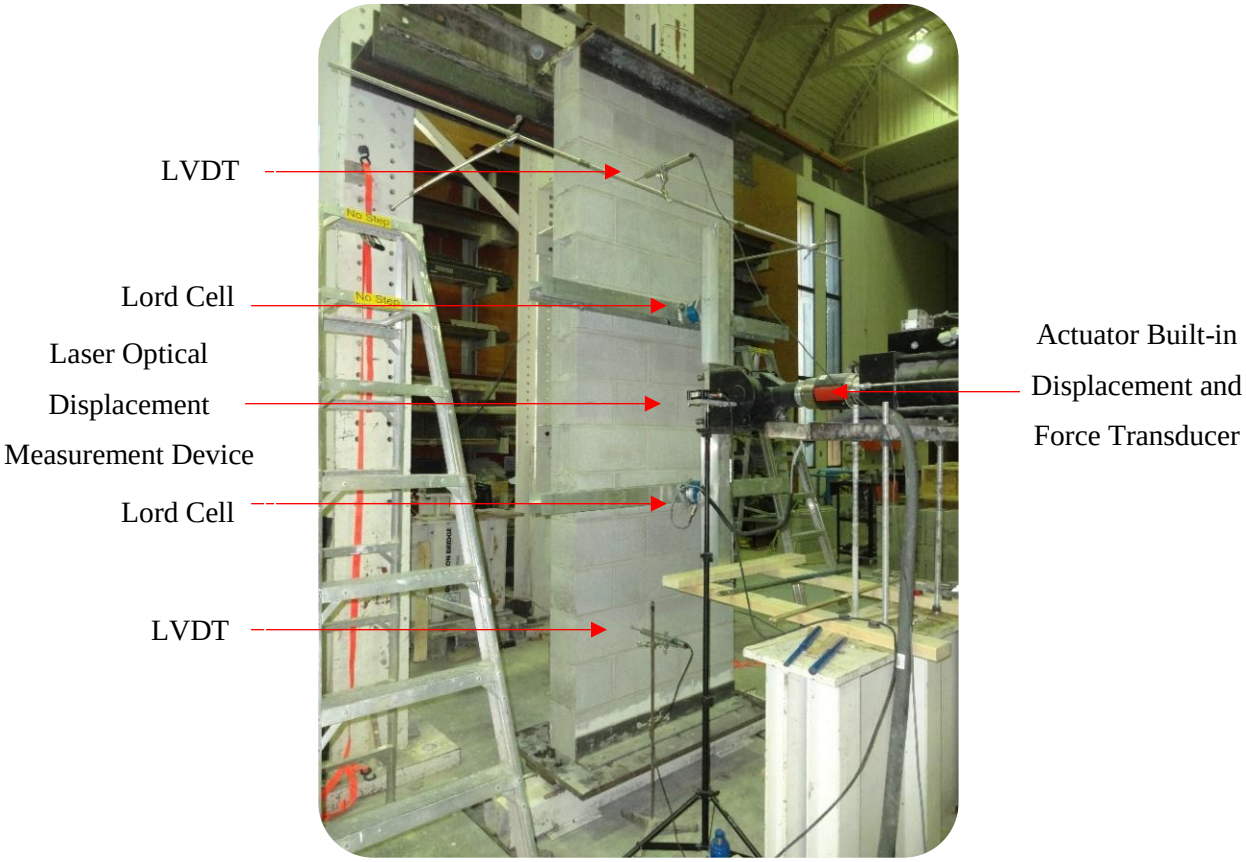

Figure 3.22: Instrument setup

3.5.2 Support Conditions

All the wall specimens were setup to have idealized pinned support conditions. The bottom support was designed as a knife-edge support, as shown in *Figure 3.23*. A steel plate with a full-width groove inscribed along the centre line of its bottom face was bolted to the underside of the steel base plate on which the wall specimens were constructed. It was then placed on the edge of a steel plate, which was oriented vertically. The bottom support restricted both horizontal and vertical motion, while allowing unrestrained rotation.

Figure 3.23: Bottom knife edge support

The top support consisted of a horizontal steel plate that rested on the top of the wall specimen and was connected to two full-width angles attached to its underside that were positioned to be flush against the two faces of the wall specimen. The angles were then clamped snug to the top course of the specimen. The top steel plate was connected to the test frame using three horizontal rods, which were pin-connected at either end to both the top of the steel plate and the test frame. The top support was designed to act like a roller support, with which horizontal motion was restricted while allowing limited vertical motion and free rotation. *Figure 3.24* shows the top support configuration used during testing.

Figure 3.24: Top support configuration

3.6 Wind Load Generation

The wind load time histories were generated using the same mathematical model used in the study conducted by Udey (2014). A 4th order autoregressive function was used to produce a dynamic wind speed time history that represented a gusty wind of a given mean wind speed. The general behaviour and the frequency content of the wind time history was based on the theoretical power spectrum density of a gusty wind proposed by Kaimal et al. (1972). The wind speed time history was then converted to a wind load time history and used in the load-controlled dynamic load testing.

However, it was uncertain as to what degree a specific load time history would affect the wall specimen, given that a generated wind time history was based on a specific mean wind speed. Therefore, a series of generated load time histories with increasing intensity had to be applied to the wall specimens prior to failure. Based on preliminary calculations, this series was selected such that the intensity of the first generated load time history would do no significant damage to the wall specimen. The intensity of the subsequent load time histories would then be increased in steady increments until the failure of the wall specimen occurred, or until displacement limitations of the test setup were reached. The increment in mean wind speed between successive time histories was chosen based on consideration for both the resolution of the gathered data and the time taken for the tests of one specimen to be carried out.

Preliminary static analyses indicated that the wall specimens would start experiencing significant damage at an equivalent mean wind speed of approximately 30 to 40 m/s. Therefore, the intensity of the first generated wind load time history was based on a mean wind speed of 30 m/s. The mean wind speeds of the subsequent load time histories were increased by 10 m/s, thereby successively increasing the intensity of the load time histories until the limitations of the test setup were reached.

The duration of a wind storm applied to the specimens was set to be 10 min based on the previous study conducted by Udey (2014). Several assumptions were made when generating the wind time histories. The reference height was taken to be z = 10 m above the ground. A surface roughness value of z_0 = 0.3 m was chosen as per Simiu and Scanlan (1986), assuming a typical suburban terrain surrounding. The wind speed time history was generated using a time-step of $\Delta\tau$ = 0.25 s, primarily due to the limitations of the available equipment. Thus, the Nyquist frequency of the

generated time history was 2 Hz (i.e., the frequency of the highest frequency components in the simulated wind), so that the modelled wind storm did not contain frequency content higher than that. Further discussion of the properties and the limitations of the generated wind is provided in Chapter 4 (Section 4.6.1). *Figure 3.25* is a sample wind time history generated by the model of a wind storm with mean wind speed of $\overline{U}_{10}$ = 40 m/s (at a reference height of 10 m above ground).

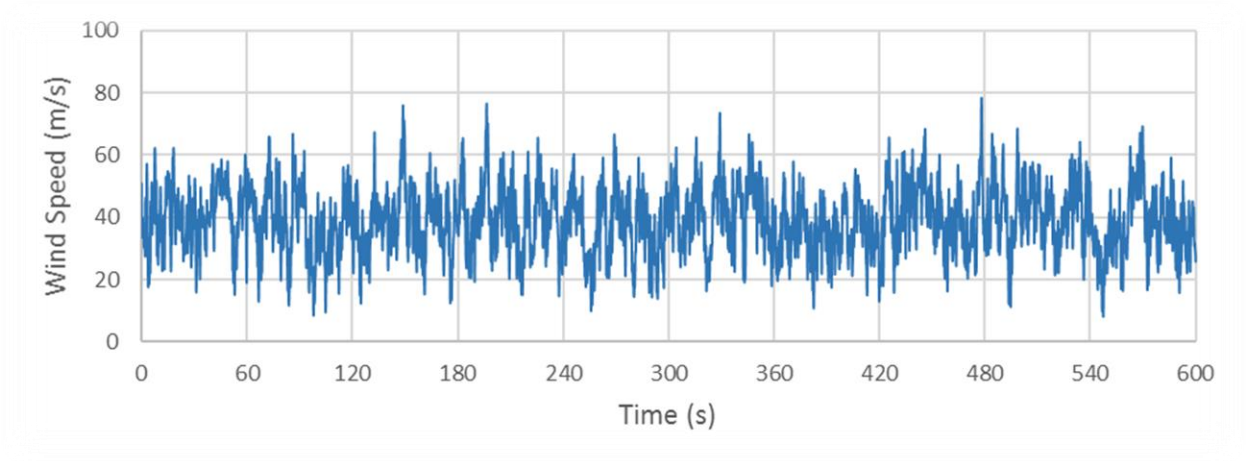

Figure 3.25: Sample wind time history with mean speed of 40 m/s

The dynamic tests were conducted under load control. Therefore, the generated wind speed time histories were converted to load time histories. The National Building Code of Canada (NBCC) provides the following relationship to convert the wind speed to a load:

$$q = \frac{1}{2}\rho V_s^2 \qquad (3.2)$$

where q (in kPa) is wind pressure applied over the wall surface area, ρ (in kg/m^3) is the density of air and V_s (in m/s) is the wind speed. Assuming the wind pressure was perfectly correlated over the wall specimen surface area, the pressure value was multiplied by the wall specimen's nominal surface area of 3 m^2 to calculate the load applied by the wind time histories. In addition, the value for the density of air was taken as 1.293 kg/m^3 as per NBCC (2010). To avoid the application of a sudden impact load at the start of a load cycle, an initialization period of 2 min was added to the beginning of a load time history. During this period, the load was gradually increased to the mean value of the wind time history after which the dynamic fluctuating component was gradually increased from zero to its full value. *Figure 3.26* is the load time history of the sample wind speed time history shown above.

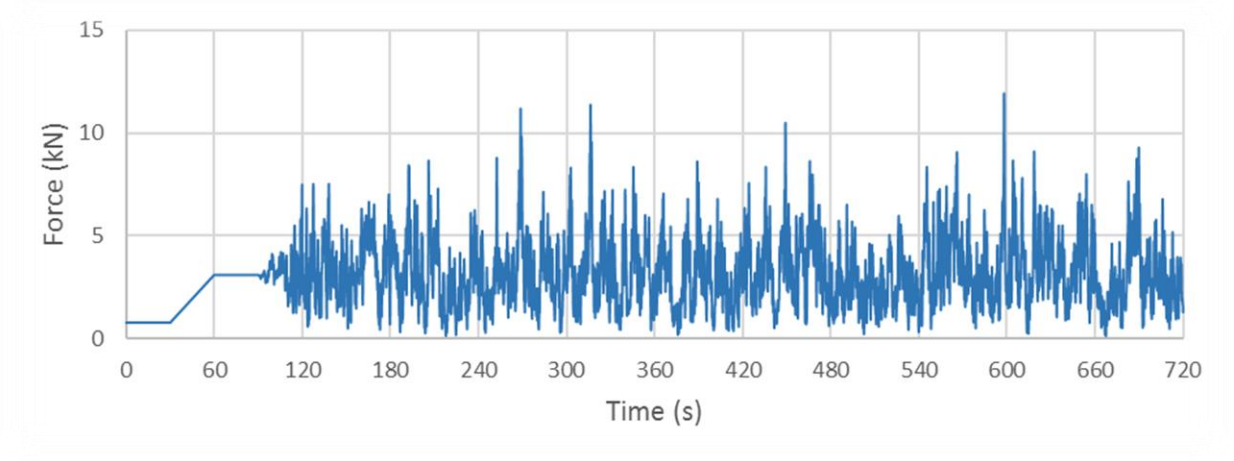

Figure 3.26: Sample load time history with mean wind speed of 40 m/s

3.7 Testing Wall Specimens

3.7.1 Curing and Transportation of Wall Specimens

In both phases, testing of the wall specimens was carried out following 5 to 8 weeks of curing. The 10-ton crane available in the laboratory was used to transport the wall specimens to the test setup; once positioned, the wall specimens were configured to be as plumb as possible. The partially grouted wall specimens were rigid and strong enough to be safely transported using the crane, at the time of testing, without the requirement of additional bracing or protection. The companion specimens of the corresponding wall specimen were tested immediately following the wall test. Further details on the setup for the companion specimen tests is described in Section 3.7. Additionally, for several specimens, vibration testing was carried out prior to the lateral load testing to determine the fundamental natural frequencies of the undamaged wall specimens.

3.7.2 Quasi-Static Wall Loading

The wall specimens that were tested under quasi-static loading conditions were tested under displacement control. They were loaded at a rate of 6 mm/s, based on consideration of time required to complete a test, as well as on the judgment of the laboratory technician; the testing was carried out until the wall specimens were loaded past the yield point, as indicated by a plateau in the measured load-deflection plot. The testing was stopped once the significantly large

deformation of the wall specimen was beyond the feasible limits of the test setup. Visual observations were made throughout the loading to correlate the behaviour of wall specimens, such as cracking and visible distress, with the collected displacement and load data.

3.7.3 Dynamic Wall Loading

The wall specimens that were tested under dynamic loading conditions were tested under load control. A series of load time histories with successively increasing intensity were applied to each wall specimen. A pair of specimens from the two sets of specimens loaded dynamically, one with a low reinforcement ratio and the other with a high reinforcement ratio, were subjected to the same series of load time histories. Thus, a total of five pairs of wall specimens were subjected to a different series of load time histories. Ultimately, the wall specimens were each subjected to load intensities high enough to cause significant deformation to occur. The testing was stopped when a load time history of high intensity began to significantly deform and damage the specimen, which pushed the test setup past its feasible limits. Visual observations were made to correlate the behaviour of wall specimens, such as cracking and visible distress, with the collected displacement and load data during each of the applied load time histories.

3.8 Masonry Prism Tests

The ungrouted and grouted masonry prisms were tested immediately following the wind load testing of the corresponding wall specimen. The prisms were loaded onto the Amsler beam bender, which was also used for the block tests. Fibre boards were placed at the top and bottom of the prisms to ensure even loading surfaces. The prisms were loaded to failure manually by the lab technician at a loading rate of approximately 1 kN/s. *Figure 3.27* shows the testing of a masonry prism. The compressive load applied was recorded, which was used to calculate the nominal compressive strength of the masonry assemblage. The results are summarized in Chapter 4 (Section 4.1).

Figure 3.27: Testing of a masonry prism

3.9 Companion Specimen Tests

Companion specimen tests were carried out in conjunction with lateral testing of the wall specimens. These tests were carried out to correlate material and assemblage properties with the behaviour of each wall specimen, as well as to check the quality and consistency of the material used in constructing the wall specimens.

3.9.1 Masonry Block Tests

Several masonry units from each of the two batches were tested for their compressive strength. Two frog ended blocks and two flat ended blocks were tested from each batch. The testing was carried out using the 1500 kN capacity Amsler beam bender that is available in the laboratory, as shown in *Figure 3.27*. The blocks were loaded until failure manually by the lab technician at a loading rate of approximately 1 kN/s. The compressive load applied was recorded, which was used to calculate the nominal compressive strength of the masonry blocks. The results are summarized in Chapter 4 (Section 4.1).

Figure 3.28: Masonry block test

3.9.2 Mortar Cube Tests

Six mortar cubes, as shown in *Figure 3.29,* were tested for each batch of mortar prepared during the construction. The tests were carried out using the Instron DX600 Universal Testing Machine that is available in the laboratory, as shown in *Figure 3.30.* The compressive strength of the mortar cubes was recorded to ensure the quality of the mortar used to construct the masonry wall specimens. The results of the mortar cube tests are summarized in Chapter 4 (Section 4.1).

Figure 3.29: Six masonry cubes that were cast per batch

Figure 3.30: Mortar cube testing

3.9.3 Grout Cylinder and Prism Tests

Figure 3.31 depicts the two cylinder samples and the block sample tested per batch of grout prepared during the construction. The ends of the cylinder samples were capped, while fiber boards were used on the top and bottom of the block samples to ensure even loading surfaces. The tests were carried out using the Instron DX600 Universal Testing Machine that is available in the laboratory as shown in *Figure 3.32.* The compressive strengths of the grout samples were recorded to ensure the quality of the grout used to construct the masonry wall specimens. The results of the cylinder samples and the block samples are summarized in Chapter 4 (Section 4.1).

Figure 3.31: Grout cylinder samples (left) and block sample (right)

Figure 3.32: Testing grout cylinder sample (left) and block sample (right)

3.9.4 Reinforcement Bar Tests

Tensile strength tests were carried out on both No.10 bars and No.15 bars that were used in the construction of the wall specimens. All the reinforcing bars of each bar diameter were taken from the same heat of steel. Six approximately 10-inch length samples were prepared for both No.10 and No.15 bars. The testing was carried out using the Instron DX600 Universal Testing Machine that is available in the laboratory. The stress-strain diagrams that were generated were used for calculating the yield strength and the ultimate strength of the reinforcing bars used. The results are summarized in Chapter 4 (Section 4.1). *Figure 3.33* shows the testing of a rebar sample.

Figure 3.33: Rebar test

3.10 Vibration Testing

Vibration tests were carried out on several wall specimens prior to carrying out the lateral load tests, from both the low and high reinforcement ratio specimens. The tests were carried out to determine the fundamental natural frequencies of the undamaged wall specimens.

Due to limited availability, four Kinemetrics EpiSensor Model ES-U accelerometers were used. They were calibrated to a maximum range of ±0.25g, where g = 9.81 m/s^2. The accelerometers were attached to the wall specimens, as shown in *Figure 3.34*, using metal tabs that were glued to the wall surface using a polymer adhesive. The accelerometers were then bolted onto the metal tabs. They were attached to the wall in the arrangement shown in *Figure 3.35*. Specifically, two accelerometers were attached along the mid-height of the wall specimen, at the centerline and 200 mm from the edge. The remaining two were attached along the centerline of the wall specimen, at a height of 700 mm and 2300 mm respectively from the base of the wall specimen.

Figure 3.34: Attaching accelerometers to the wall surface

Two types of vibration tests were carried out; impact tests and ambient tests. The impact tests were carried out by striking the wall specimen with a rubber mallet at its center, along the right side and at the top. A series of impacts at each of these locations was carried out and readings were taken for 3 to 5 min periods. The ambient tests were carried out by measuring the accelerometer data during a period where no overt external forces were being applied to the wall specimens. Several readings were taken for 5 min periods.

Figure 3.35: Accelerometer arrangement

Chapter 4: Results and Analysis

4.1 Overview

This chapter presents the results gathered from the testing carried out as described in the previous chapter. The results pertain to testing carried out on the twenty large scale wall specimens and their respective companion specimens, including masonry prism tests and material tests. The experimental program was carried out at the University of Saskatchewan Structures Laboratory during the period of April 2016 to October 2016.

For convenience, a set of abbreviations was used to referring to the specimen designation for the four sets of large-scale wall specimens tested as part of the experimental program. Each set of wall specimens consisted of five replicate specimens, which the number accompanying the abbreviations refers to. The four sets of wall specimens were:

- Low reinforcement ratio specimens tested under quasi-static loads (denoted by LS);
- Low reinforcement ratio specimens tested under dynamic loads (denoted by LD);
- High reinforcement ratio specimens tested under quasi-static loads (denoted by HS); and
- High reinforcement ratio specimens tested under dynamic loads (denoted by HD).

4.2 Material Test Results

Table 4.1 and *Table 4.2* provide the mean values and the coefficients of variation (CV) of the measured properties for materials used in the construction of the wall specimens tested under both types of loading conditions. Detailed results for all material specimen tests are provided in Appendix G.

Table 4.1: Masonry block, mortar and grout test results

Specimen Reinforcement Ratio	Block Strength		Mortar Compressive Strength		Grout Compressive Strength			
					Cylinder Sample		Absorbent Block	
	Mean (MPa)	CV (%)	Mean (MPa)	CV (%)	Mean (MPa)	CV (%)	Mean (MPa)	CV (%)
Low	17.0	16.9	19.6	24.5	28.3	13.8	22.4	14.0
High	18.1	9.2	20.7	12.7	28.5	6.8	20.5	11.2

Table 4.2: Wall specimen reinforcement test results

Specimen Reinforcement Ratio	Reinforcement Strength			
	Yield (MPa)	CV (%)	Ult. (MPa)	CV (%)
Low	440.7	12.4	665.6	14.2
High	436.8	7.6	659.2	8.3

As the construction and testing of the low and high reinforcement specimens were carried out in two phases, respectively, the material properties were checked to ensure consistency between the two phases. In addition, properties were also checked to ensure the quality of the material used in the construction of the wall specimens. Overall, the material properties conformed with the requirements of the necessary standards; also, the variability of the material used between the two phases was within acceptable levels as there was no significant difference at a 95% confidence interval.

Although the masonry block units were acquired from the same manufacturer, the blocks for the two phases of testing were ordered in two separate batches at different times. There were minor differences in the mould used and, therefore, in the resulting cross section; however, the overall nominal dimensions and the compressive strengths of the masonry block units from both batches were consistent and did not indicate a significant difference at a 95% confidence interval.

The same mix proportions of materials were used in the mixing of mortar and grout batches during both phases of testing, including sand, gravel and cement. The same experienced mason carried out the mixing of mortar and grout batches during both phases as well. Multiple batches of mortar and grout were generally used in constructing each wall specimen since a low lift grouting procedure was used. In general, two batches of mortar, and up to four batches of grout, were used to construct one wall specimen. There was some variability between the different batches used. In terms of mortar, the mean compressive strength of batches during phase one ranged from 13.6 MPa to 29.0 MPa; during phase two, they ranged from 16.9 MPa to 25.2 MPa. Additionally, the mortar pallets were sometimes tempered by the mason to ensure proper workability, which may not have been reflected in the sample test results. In terms of grout, the compressive strength of the absorbent grout blocks tested during phase one ranged from 17.5 MPa to 28.1 MPa; during phase two they ranged from 16.4 MPa to 24.2 MPa. Other than the material variability, the imperfections of the moulded blocks may have also had some impact on the variability of the test results. Overall, although there was some variability between batches, the mean strength of the samples tested indicated consistency between the mortar and grout batches used to construct the wall specimens. They did not indicate a significant difference between the two phases at a 95% confidence interval.

4.3 Masonry Prism Test Results

Table 4.3 provides the compressive strength test results of the ungrouted and grouted companion masonry prisms constructed for each respective large-scale wall specimen. The compressive strength of the ungrouted and grouted prisms constructed during each phase was calculated as per CSA S304.1-14 (2014):

$$f`_m = f_{avg}(1 - 1.64 \cdot CV) \qquad (4.1)$$

where $f`_m$ is the calculated effective compressive strength, $f_{avg}$ is the average compressive strength and $CV$ is the coefficient of variation. Additionally, the $Effective\ f`_m$ provided in *Table 2* is the effective compressive strength of the overall masonry wall assemblage, found by weighting the ungrouted and grouted strengths by their relative contribution to the net masonry area (Drysdale and Hamid, 2005).

Table 4.3: Masonry prism test results

Wall Specimen	Compressive Strength								
	Ungrouted				Grouted				Effective f`m
	Prism (MPa)	Avg (MPa)	CV (%)	f`m (MPa)	Prism (MPa)	Avg (MPa)	CV (%)	f`m (MPa)	(MPa)
LS1	13.4				-				
LS2	14.5				13.1				
LS3	13.9				11.3				
LS4	14.4				11.2				
LS5	13.8	13.9	5.8	12.6	11.8	11.2	8.8	9.6	**11.4**
LD1	15.2				11.8				
LD2	12.5				9.7				
LD3	13.1				10.0				
LD4	14.4				10.9				
LD5	-				11.0				
HS1	13.2				10.7				
HS2	12.8				11.0				
HS3	14.3				10.6				
HS4	13.2				8.6				
HS5	13.2	12.9	5.9	11.6	-	10.4	10.2	8.7	**10.4**
HD1	12.4				11.5				
HD2	12.7				12.0				
HD3	11.5				10.0				
HD4	-				9.4				
HD5	12.5				10.1				

Both an ungrouted and a grouted companion masonry prism were constructed for each wall specimen and tested immediately following the testing of the corresponding wall specimens. The prisms were constructed using the same mortar and grout batch that was used for constructing the mid-height section of the corresponding wall specimens. As the mid-height section of the wall specimens was subjected to the highest levels of bending moments, prisms with the same material composition were constructed to better reflect the overall strength of the wall specimens that were being tested.

The test results indicated that the low reinforcement ratio wall specimens had an effective compressive strength of 11.4 MPa. Similarly, the high reinforcement ratio wall specimens had an

effective compressive strength of 10.4 MPa. Although the effective compressive strengths show a slight difference between the low and high reinforcement ratio wall specimens, the difference was not statistically significant at a 95% confidence interval. Therefore, the specimens were determined to have similar assemblage properties overall.

4.4 Vibration Test Results

This section presents results from the vibration tests that were carried out on several wall specimens. The testing was carried out prior to the actual loading tests to estimate the natural frequency of the wall specimens in an undamaged state. Since the dynamic loading may induce a resonant response in cases where the frequency content of the applied load coincides with the natural frequency of the wall specimens that were tested, it was informative to get a general estimate of the natural frequency of the wall specimens to infer whether resonance would be a significant concern. However, it was recognized that, as the wall specimens were loaded and accumulated damage, the stiffness of the wall would deteriorate, and its natural frequency would shift to a lower value.

Figure 4.1 presents the Power Spectrum Density (PSD) plots of the ambient vibration tests carried out on a low reinforcement ratio specimen, LS5, and a high reinforcement ration specimen, HD1. The PSD plots were normalized using their respective root-mean-square values to mitigate the influence of the intensity of the impact excitation. The acceleration time histories measured were run through a Fast Fourier Transformation (FFT); using a peak picking method, the fundamental natural frequencies and the average mode shapes of the undamaged wall specimens were then extracted.

The analysis of the graphs depicted in *Figure 4.1* indicated a fundamental natural frequency of 9.8 Hz for the low reinforcement ratio specimen, and 9.6 Hz for the high reinforcement ratio specimen. The normalized average mode shapes at these natural frequencies are depicted in *Figure 4.1*. Overall, the fundamental natural frequency of both the low and high reinforcement ratio wall specimens was estimated to be approximately 10 Hz in an undamaged state. This was as expected, as both low and high reinforcement ratio wall specimens were under identical support conditions and their gross cross-sectional stiffness would be similar before being damaged. On the other hand, as the wall specimens deteriorate, the natural frequencies of the low and high

reinforcement ratio wall specimens would likely differ due to their different stiffness characteristics as the steel contribution become more significant.

The mode shapes depicted in *Figure 4.2* suggest some rigid body rotation about the bottom support, in addition to the flexural displacements seen for specimens LS5 and HD1. The rigid body rotation implies that the top support was not perfectly rigid, allowing some degree of horizontal displacement at the top end of the wall.

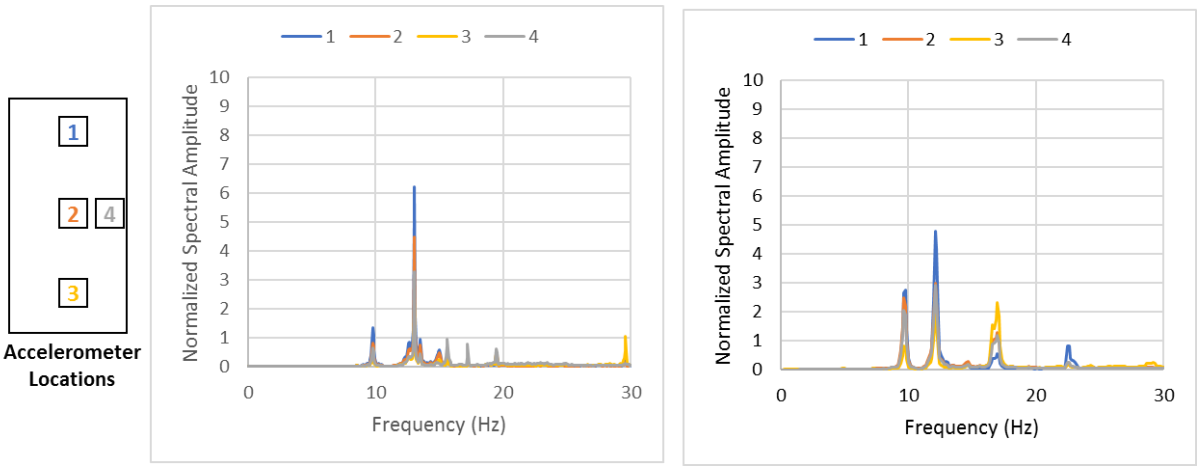

Figure 4.1: PSD diagrams of the vibration tests carried out on specimens LS5 (left) and HD1 (right)

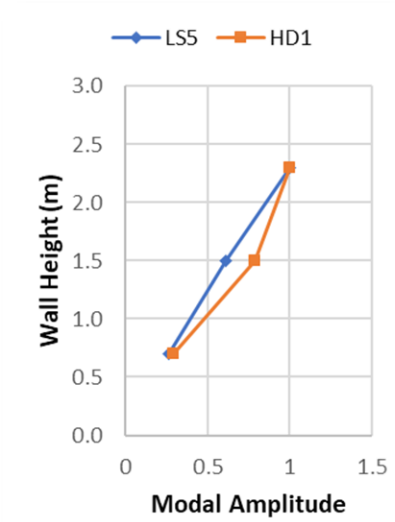

Figure 4.2: Averaged fundamental mode shapes of undamaged specimens LS5 and HD1

There were several setbacks when carrying out the vibration tests on the wall specimens. Primarily, there were limitations with recording the accelerometer data, where some sets of data were sampled at an irregular rate (i.e., the time between each recorded data point was not constant). In

addition, the high levels of background noise at all frequency ranges of the sampled data made it difficult to utilize the impact vibration test data to determine the natural frequencies and mode shapes. In conclusion, resonance likely was not a significant factor for undamaged specimens since the frequency content of the simulated wind storms was truncated below 10 Hz.

4.5 Wall Specimen Test Results

4.5.1 Overview

This section presents the out-of-plane loading test results of the twenty wall specimens tested under both quasi-static and dynamic loading conditions, which represents realistic wind loading conditions, respectively. The complete collection of the data gathered pertaining to the out-of-plane load tests can be found in the Appendices included at the end. Specifically:

- Appendix A: Load-deflection results of the quasi-static tests;
- Appendix B: Comparison of modelled and applied dynamic wind load time histories;
- Appendix C: PSD diagrams of the dynamic wind load time histories;
- Appendix D: Applied dynamic wind load time histories;
- Appendix E: Deflection time histories of the dynamic tests; and
- Appendix F: Load-deflection hysteresis plots of the dynamic tests.

Unless otherwise specified, the “Load” data referred to in this section is the total load applied to the wall specimens by the hydraulic actuator measured using the built-in force transducer throughout the entirety of the test run. The “Deflection” data refer to the mid-height out-of-plane deflection of the wall specimen measured using the laser optical displacement measurement device throughout the entirety of the test run.

Furthermore, although the nominal height of the wall specimens was 3.0 m, due to the top and bottom support configuration, a slight adjustment was made to the shear span from the supports to the points of load application when calculating the “Moment” data presented for the wall specimens tested under both quasi-static and dynamic loading conditions. This was done to more accurately calculate the moment carried by the wall specimens. *Figure 4.3* better illustrates this in the following section.

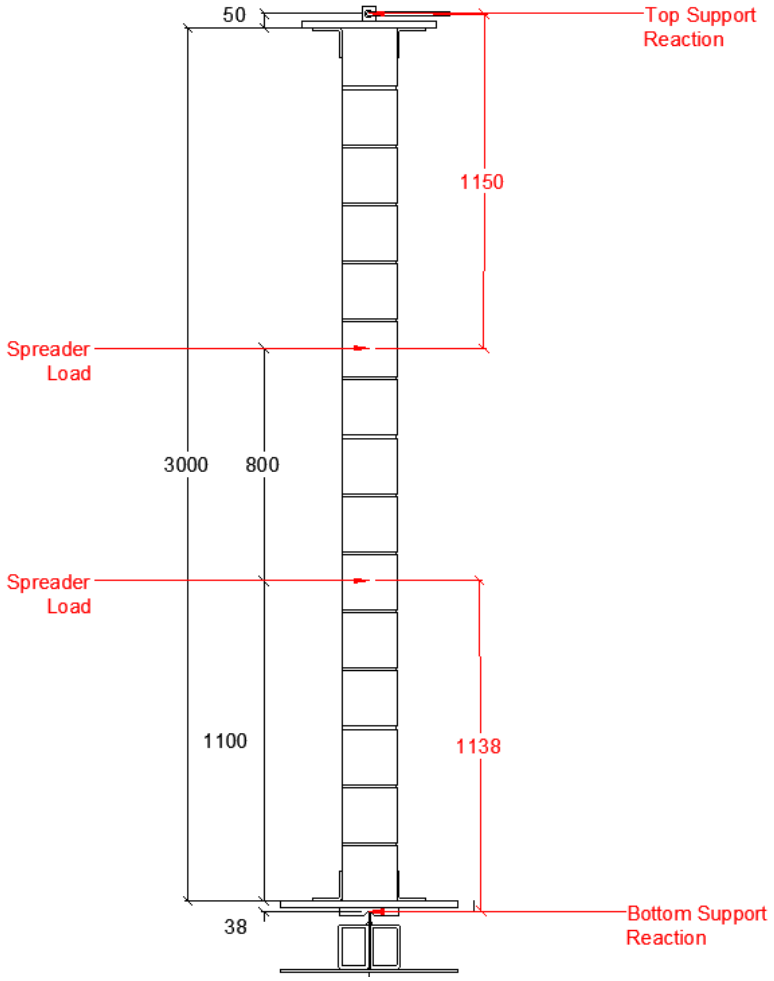

Figure 4.3: Shear span for calculating mid-height moment

The nominal height of the masonry wall specimens was 3000 mm. As such, if the support reactions were applied at the top and bottom ends of the wall specimens, the shear spans to the top and bottom spreader beams (i.e., the distance from the top support reaction to the top spreader load and the distance from the bottom support reaction to the bottom spreader load.) would be 1100 mm. However, due to the support configuration, an additional 50 mm and 38 mm was added to the top and bottom shear span, respectively, as illustrated in *Figure 4.3*. Therefore, an average value of 1144 mm for the shear span was considered when calculating the mid-height moment of the wall specimens. Furthermore, it was also assumed that the top and bottom spreader beams were applying equal line loads. The load data gathered by the two force transducers attached to the two spreader beams indicated approximately equal values throughout the testing. Further discussion on the limitations of this assumption is presented in Section 4.7.3.

4.5.2 Low Reinforcement Ratio Wall Specimens Under Quasi-Static Loading

Figure 4.4 depicts the load vs. deflection plots of the five low reinforcement ratio specimens tested under quasi-static load conditions. As noted previously, the load in the diagram represents the total load applied by the hydraulic actuator on the wall specimens and the deflection represents the deflection at mid-height of the wall specimens. Each of the plots are represented separately in Appendix A. The plots indicate that the results gathered across the five wall specimens were quite consistent.

The behavioural characteristics of all the low reinforcement ratio wall specimens tested under quasi-static load conditions were quite similar. They responded in a typical flexural ductile mode, as expected of lightly reinforced masonry wall members. The first distinct change in response was observed in the load vs. deflection diagrams at a mid-height deflection of approximately 5.5 mm, where a significant change, specifically a decrease, in the stiffness of the wall specimens occurred. The first signs of significant damage to the wall specimens were observed as the applied load reached approximately 6.5 kN, as cracks began to appear in the constant moment region near the mid-height of the wall specimens. *Figure 4.5* illustrates the typical damage patterns observed, showing a photograph of specimen LS5 taken at approximately the onset of cracking.

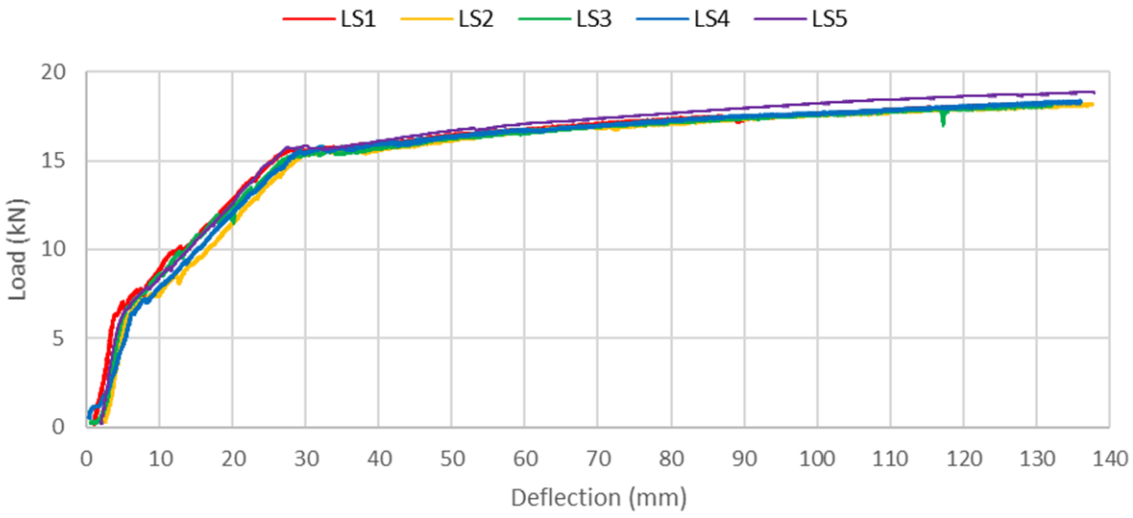

Figure 4.4: Load vs. deflection diagram for the low reinforcement ratio specimens

The illustrations of the wall specimen, as shown in *Figure 4.5*, give a clearer indication of the bed-joint numbers that will be referred to in the following sections when describing the damage

sustained by the wall specimens. Furthermore, the illustrations give an approximate qualitative indication of the magnitude of the cracks sustained by the wall specimens; bed-joints coloured in yellow indicate slight cracks, whereas bed-joints coloured in red indicate relatively much wider cracks. The width of the cracks represented in orange were approximately wider than the cracks represented in yellow, but narrower than the cracks represented in red. The "constant moment region" referred to in the illustrations represent the mid-height region of the wall specimens between the two spreader loads that sustain the highest moment along the height of the wall specimens.

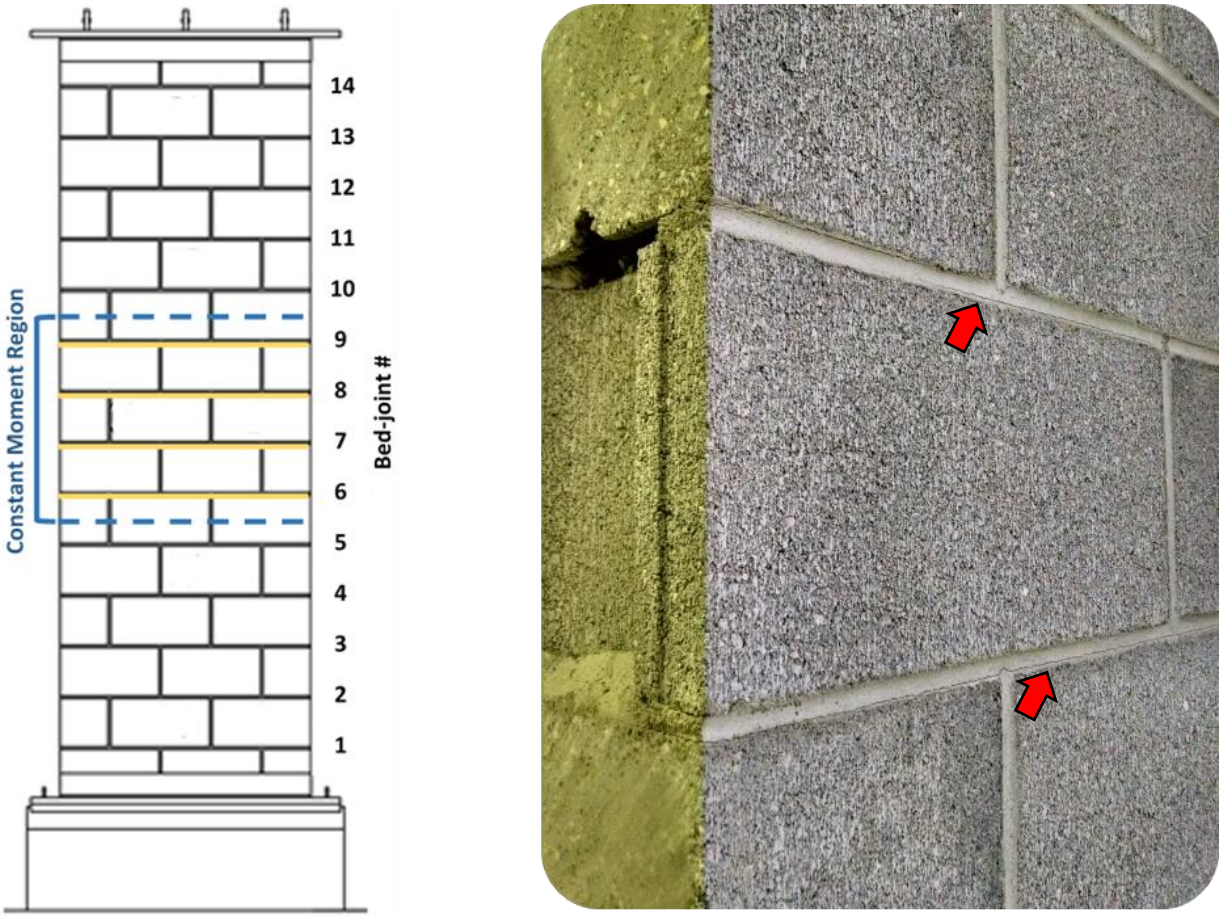

Figure 4.5: Illustration and photograph of the tension face of specimen LS5 just after cracking load

The onset of bed-joint cracks occurred in the mid-height constant moment region of the wall specimens. Cracks formed in the 6th, 7th, 8th and 9th bed-joints as the block-mortar interface separated over the entire width of the wall specimens. The load vs. deflection diagram indicates a significant change in stiffness of the wall specimens corresponding to the formation of flexural

cracks at the cracking load. With further loading, the wall specimens steadily accumulated more damage, which was observed as further flexural cracks propagated along the bed-joints adjacent to the mid-height constant moment region.

The next distinct change in response was observed in the load vs. deflection diagrams at a mid-height deflection of approximately 28.6 mm. As the load applied to the wall specimens reached approximately 15.5 kN, the wall specimens began to show significant plastic deformation. *Figure 4.6* illustrates the typical damage patterns observed, showing a photograph of specimen LS5 taken just after the onset of significant plastic deformation. The existing bed-joint cracks in the mid-height constant moment region of the wall specimens exhibited a significant increase in their width. The flexural cracks formed in the 6^{th}, 7^{th}, 8^{th} and 9^{th} bed-joints widened significantly. In addition, bed-joint cracks were observed in the 4^{th}, 5^{th}, 10^{th} and 11^{th} bed-joints, but these were not as wide as the bed-joint cracks that formed in the mid-height constant moment region. Correspondingly, the load vs. deflection diagram indicates a significant change in stiffness of the wall specimens with the onset of significant plastic deformation due to yielding of the reinforcement.

Beyond the onset of significant plastic deformation, the rate at which the total applied load increased was drastically reduced with further increases in the deflection of the wall specimens. The load vs. deflection diagram indicates that the total load carried by the wall specimens was gradually reaching an upper bound value. However, the test was terminated before the ultimate capacity of the wall specimens was reached due to excessive deformation that resulted due significant plastic deformation. Specifically, additional rotation at supports and deflection of wall specimens could not be accommodated by the test setup that was used past a mid-height deflection of about 135 mm. This limitation is discussed further in Section 4.7.2.

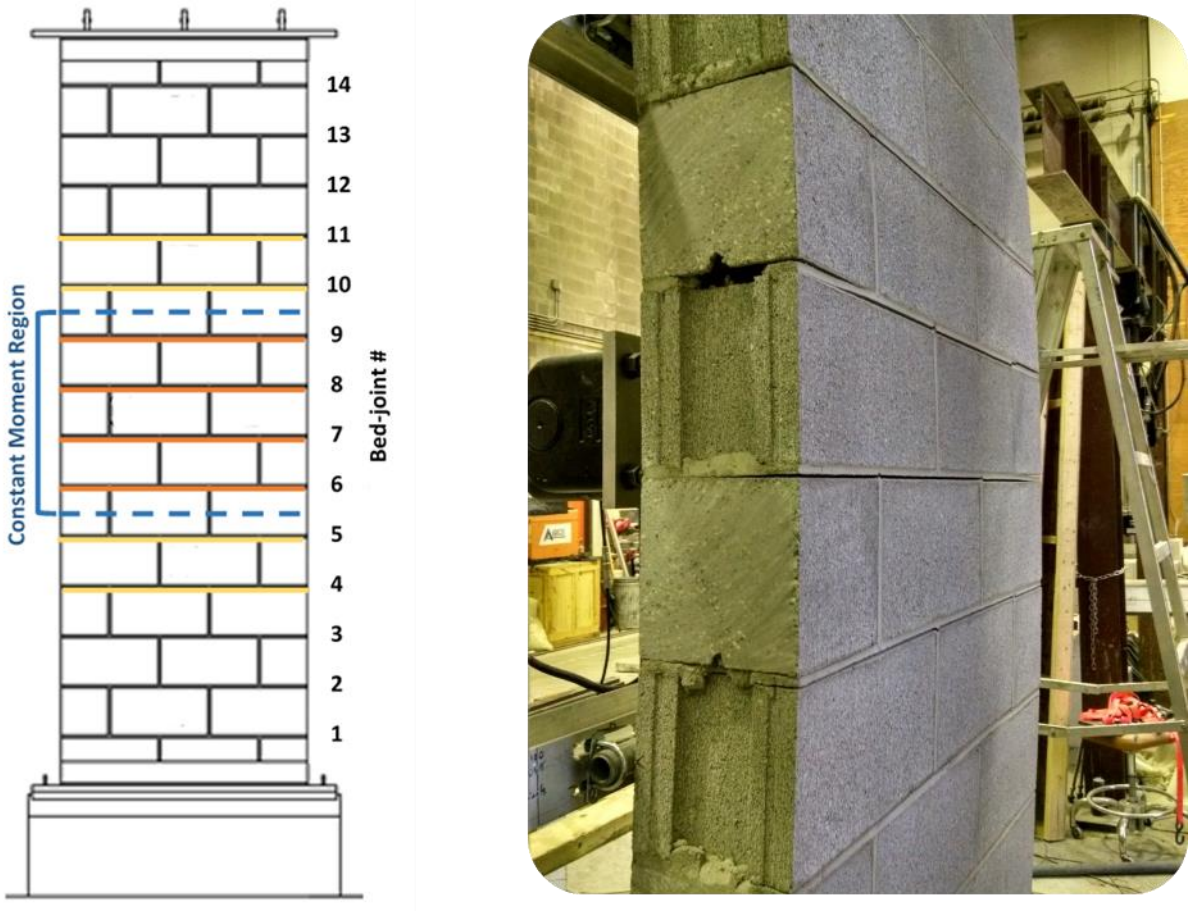

Figure 4.6: Illustration and photograph of the tension face of specimen LS5 just after yield load

The maximum load carried by the wall specimens at the termination of testing was approximately 18.4 kN. *Figure 4.7* illustrates the typical damage patterns observed, showing a photograph of specimen LS5 taken once the testing was halted and the loading removed. At the end of the testing, the wall specimens were significantly damaged. The flexural cracks, which formed in the mid-height constant moment region along the 6^{th}, 7^{th}, 8^{th} and 9^{th} bed-joints, widened further as compared to their state at the onset of significant plastic deformation. The cracks in the adjacent bed-joint, the 5^{th} and 10^{th} bed-joints, were also significant. Although not clearly seen in the photograph, slight cracks were observed in the 3^{rd}, 4^{th}, 11^{th} and 12^{th} bed-joints as well. However, there was no observable spalling or crushing of the mortar bed-joints or the masonry blocks on the compression side of the wall specimens, which indicated that the wall specimens had further capacity and had not reached the ultimate loading capacity at the end of the testing.

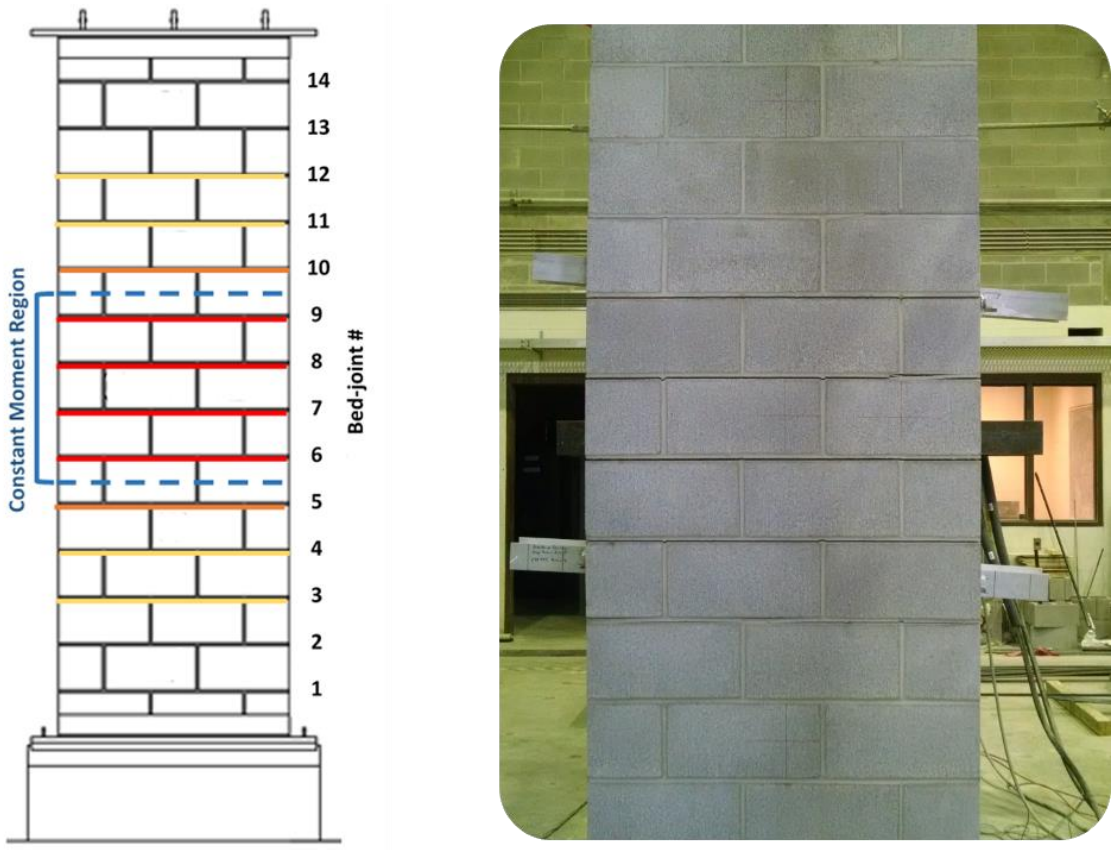

Figure 4.7: Illustration and photograph the tension face of specimen LS5 at conclusion of testing

4.5.3 High Reinforcement Ratio Wall Specimens Under Quasi-Static Loading

Figure 4.8 depicts the load vs. deflection plots of the five high reinforcement ratio specimens tested under quasi-static load conditions. The load in the diagram presents the total load applied by the hydraulic actuator on the wall specimens, while the deflection represents the deflection at mid-height of the wall specimens. Each of the plots are represented separately in Appendix A. The plots indicate some variability of the results across the five wall specimens, especially at larger deflections, more so than the results of the low reinforcement ratio wall specimens. This was likely due to the rebar positioners not being as effective in aligning the reinforcement bars of the high reinforcement ration wall specimens along the mid-depth of the wall specimens, as compared to the reinforcement bars of the low reinforcement ratio wall specimens. The No.15 bars that were used in the high reinforcement ratio wall specimens were much more rigid compared to the No.10 bars used in the low reinforcement ratio wall specimens. Therefore, it was likely more difficult to properly align them along the mid-depth of the wall specimens during construction using the rebar positioners.

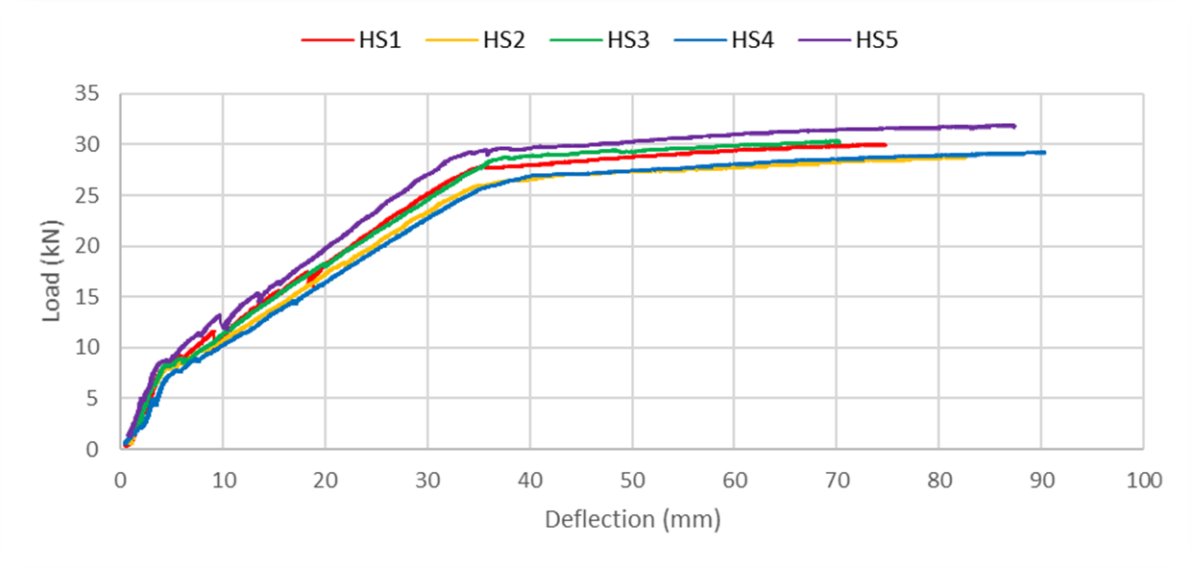

Figure 4.8: Load vs. deflection diagram for the high reinforcement ratio specimens

Overall, the high reinforcement ratio wall specimens tested under quasi-static load conditions showed similar behavioural characteristics. The wall specimens responded in a typical flexural ductile mode expected of reinforced masonry wall members. The first distinct change in response was at onset of cracking, where the first signs of significant damage to the wall specimens were observed. This was similar to what was observed for the low reinforcement ratio wall specimens at onset of cracking. At a mid-height deflection of approximately 4.4 mm, when the cracks were first observed, the load applied to the wall specimens was approximately 6.5 kN. Like that of the low reinforcement ratio specimens, cracks appeared in the mid-height constant moment region, which formed along the entire width of the 6^{th}, 7^{th}, 8^{th} and 9^{th} bed-joints of the high reinforcement ratio wall specimens. At the cracking load, the load vs. deflection diagram indicated a significant change in stiffness of the wall specimens. Further flexural cracks propagated along the bed-joints adjacent to the mid-height constant moment region as the monotonically increasing loading pushed the wall specimens towards the next distinct change in response, which was observed at the onset of significant plastic deformation.

At a mid-height deflection of approximately 36.0 mm, the load vs. deflection diagrams indicate a significant change in stiffness of the wall specimens corresponding to the onset of significant plastic deformation due to yielding of the reinforcement. The high reinforcement ratio wall specimens exhibited an applied load of approximately 27.9 kN at yield capacity. *Figure 4.9* illustrates the typical damage patterns observed, showing a photograph of specimen HS4 taken

just after the onset of significant plastic deformation. Like that of the low reinforcement ratio specimens, the width of the flexural cracks that had formed in the 6th, 7th, 8th and 9th bed-joints increased significantly at the onset of significant plastic deformation. Additionally, bed-joint cracks were observed in the 5th and 10th bed-joints, which were not as wide as the bed-joint cracks in the mid-height constant moment region. Slight cracks were observed in the 3rd, 4th, 11th and 12th bed-joints as well.

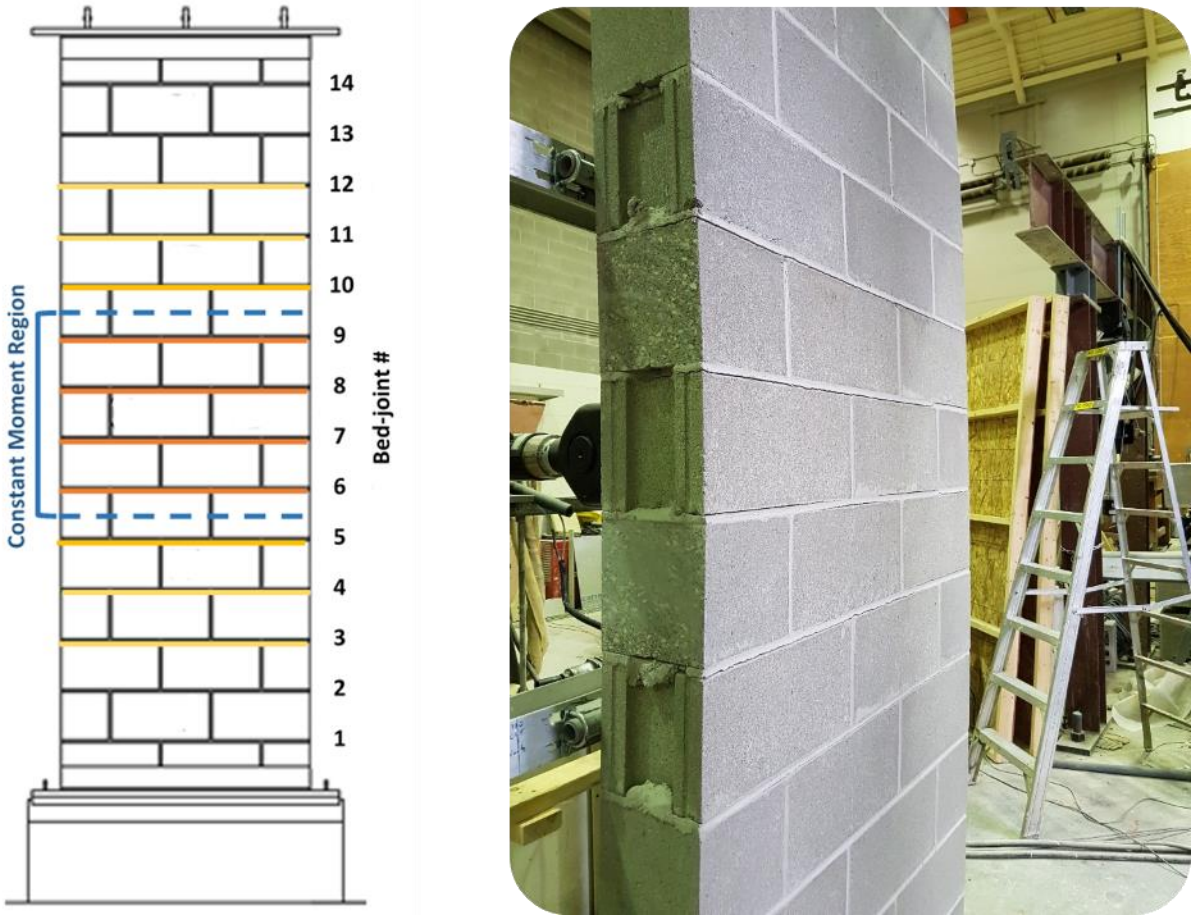

Figure 4.9: Illustration and photograph of the tension face of specimen HS4 just after yield load

The rate at which the total load carried by the wall specimens increased was drastically reduced beyond the onset of significant plastic deformation. Subsequently, the load vs. deflection diagrams indicate a gradual increase in the load carried by the wall specimens, which appeared to be reaching an upper bound value. However, the test was terminated before the ultimate capacity of the wall specimens was reached due to limitations with the test setup used, which is discussed further in Section 4.7.2.

The test was stopped at a mid-height deflection of approximately 81 mm. On average, the maximum load carried by the wall specimens at the point that the testing was stopped was approximately 30.1 kN. *Figure 4.10* illustrates the typical damage patterns observed, showing a photograph of specimen HS4 taken just prior to the termination of the test. The flexural cracks that formed in the mid-height constant moment region, along the 6th, 7th, 8th and 9th bed-joints, widened further as compared to the onset of significant plastic deformation. The cracks in the adjacent bed-joint, the 4rd, 5th, 10th and 11th bed-joints, were also significant. Slight indications of cracks were observed in the 3th and 12th bed-joints as well. Although the wall specimens were significantly damaged at the termination of the testing, there was no observable spalling or crushing of the mortar bed-joints or the masonry blocks on the compression face of the wall specimens. This indicated that the wall specimens had further capacity and had not yet reached the ultimate loading capacity prior to the termination of the testing.

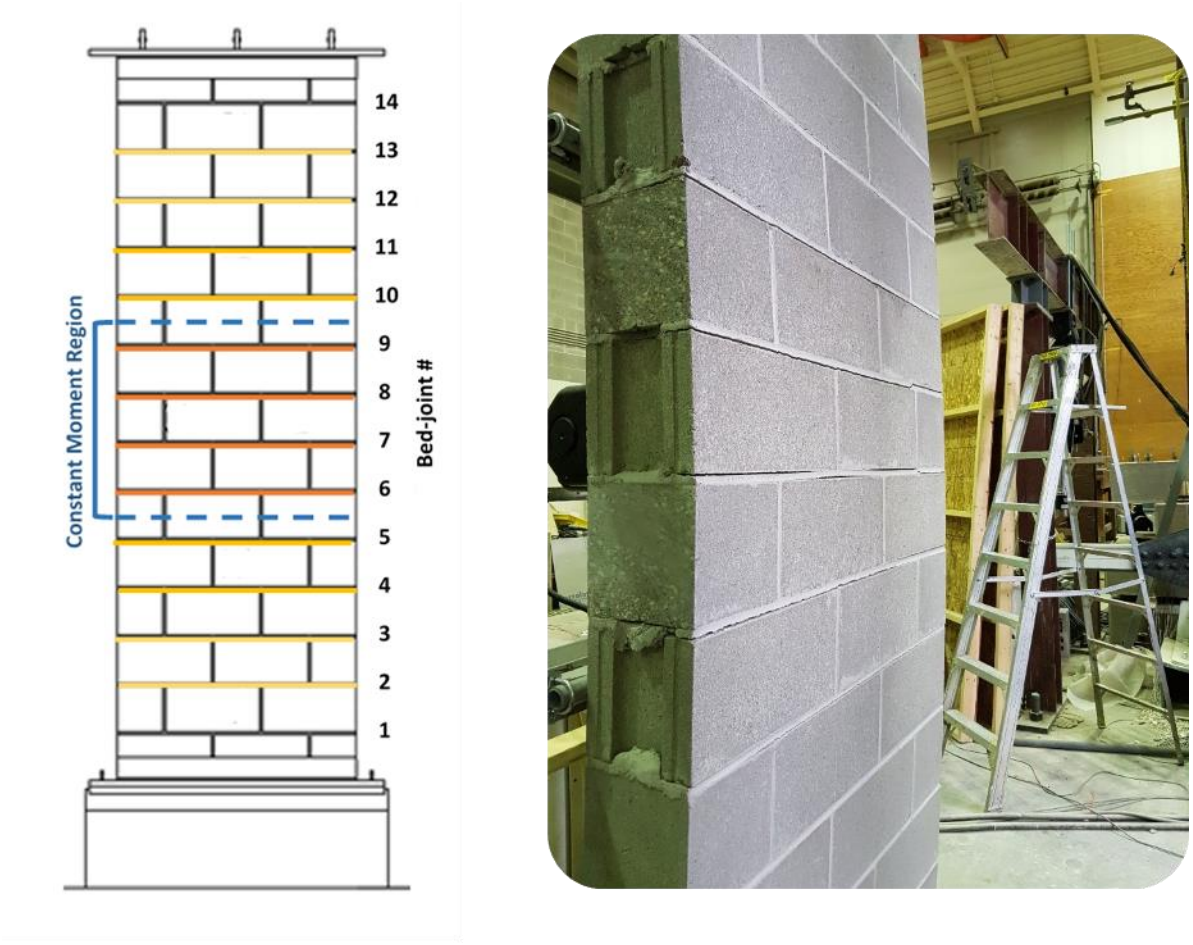

Figure 4.10: Illustration and photograph of the tension face of specimen HS4 prior to conclusion of test

4.5.4 Summary of Quasi-Static Loading Test Results

Table 4.4 lists the results obtained from the wall specimens tested under quasi-static loading conditions. The calculated moments were based on values within the mid-height constant moment region, while the deflections represent the corresponding mid-height deflections. When the first signs of cracking were observed in the mid-height region, the low and high reinforcement ratio wall specimens displayed a cracking load of approximately 3.7 kNm at a deflection 5.5 mm, and 4.6 kNm at 5.9 mm, respectively. Subsequently, when the wall specimens began to exhibit significant plastic deformation, the low and high reinforcement ratio wall specimens displayed a yield capacity of approximately 8.9 kNm at a deflection of 28.6 mm, and 15.8 kNm at 36.0 mm, respectively.

Table 4.4: Moment and deflection results of the quasi-static loading tests

Specimen		Cracking		Yielding		Maximum Applied	
		Moment (kNm)	**Deflection (mm)**	**Moment (kNm)**	**Deflection (mm)**	**Moment (kNm)**	**Deflection (mm)**
Low Reinforcement Ratio	**LS1**	3.6	4.2	8.9	28.2	10.5	132.1
	LS2	3.6	5.7	8.8	30.0	10.4	137.7
	LS3	3.8	5.8	8.7	27.9	10.4	132.1
	LS4	3.7	6.3	8.9	29.3	10.5	136.2
	LS5	3.8	5.2	9.0	27.5	10.8	137.9
Mean		**3.7**	**5.5**	**8.9**	**28.6**	**10.5**	**135.2**
CV (%)		2.8	14.5	1.4	3.6	1.5	2.2
High Reinforcement Ratio	**HS1**	4.3	3.8	15.9	35.5	17.2	74.9
	HS2	4.7	4.6	14.9	35.2	16.5	82.8
	HS3	4.9	4.6	16.3	36.9	17.4	70.4
	HS4	4.1	4.8	15.1	38.0	16.8	90.4
	HS5	5.0	4.1	16.8	34.3	18.3	87.5
Mean		**4.6**	**4.4**	**15.8**	**36.0**	**17.2**	**81.2**
CV (%)		8.2	9.5	5.1	4.1	4.0	10.4

The maximum applied moment and deflection listed in *Table 4.4* refer to the values measured at the termination of testing for each wall specimen. At the end of testing, the maximum loads applied to the low and high reinforcement ratio wall specimens were approximately 10.5 kN and 17.2 kN, respectively. The maximum mid-height deflections of the low and high reinforcement ratio wall specimens were approximately 135.2 mm and 81.2 mm, respectively. Nevertheless, the wall specimens had not yet reached their ultimate capacity at the end of testing, as indicated by the absence of compressive crushing. Assuming that the maximum deflection value represented the mid-height deflection at ultimate capacity, while recognising the fact that this is a conservative approximation made due to limitations of the experimental setup, the average ductility ratios for the low and high reinforcement ratio wall specimens were approximately 4.7 and 2.3, respectively (i.e., the ratio of the deflection at ultimate capacity over the deflection at yield capacity).

4.5.5 Determining Behavioural Characteristics Under Dynamic Loading Conditions

The damage patterns and the general behavioural characteristics of the wall specimens tested under the realistic dynamic wind loading conditions were comparable to that of the wall specimens tested under quasi-static loading conditions. Therefore, the two distinct changes in response observed under quasi-static loading conditions were likewise observed with the wall specimens tested under dynamic loading conditions. These responses included the following: the onset of cracking at the cracking load, and the onset of significant plastic deformation at the yield load. However, a different set of criteria had to be followed when determining the load and deflection values at these damage states with the dynamic loading test results, as compared to those used for the quasi-static loading test results. The quasi-static loading tests were carried out under displacement control, whereas the dynamic loading tests were carried out under load control. Therefore, the wall specimens tested under dynamic loading conditions were subjected to a series of wind load time histories with increasing load intensity.

Initially, the intensity of the wind load time histories at which these specific damage states occurred was determined through visual observation. Both cracking and yielding damage states were accompanied by a significant deterioration in the stiffness of the wall specimens, which resulted in a notable change in the mean displacement. Thus, the deflection time histories were analysed for notable changes in the mean deflection; the load-deflection hysteresis diagrams were then

analysed to confirm the load and deflection at which these distinct changes in the wall specimen stiffness occurred. The corresponding instances of the peak load which resulted in these changes in the mean deflection and the stiffness of the wall specimens were defined as being when the specific damage states occurred. Examples illustrating the application of these procedures are provided in the subsequent sections.

4.5.6 Low Reinforcement Ratio Wall Specimens Under Dynamic Loading

As described in Chapter 3, the construction and testing of the wall specimens were conducted in two phases. However, there were technical limitations with the loading system during the first phase, in which the low reinforcement ratio specimens were tested, which prevented it from properly simulating most of the high frequency content and peak loads modelled in the dynamic loading time histories. This is addressed in detail in Section 4.7.1.

The five low reinforcement ratio wall specimens tested under dynamic loading conditions were subjected to five different series of dynamic load time histories, with each subsequent load time history characterized by increasing intensity. Each series consisted of five dynamic load time histories, with mean wind speed ranging from 30 m/s to 70 m/s, at 10 m/s mean wind speed increments. Loading of intensities higher than those with a 70 m/s mean wind speed were not applied due to limitations of the test setup relative to the large resulting displacements of the wall specimens. The wind load time histories were 12 minutes in length, of which the first two minutes were applied gradually to ramp up initial loads to prevent sudden impacts at the start of loading. *Table 4.5* and *Table 4.6* list the mean and maximum values of the total load applied by the hydraulic actuator, along with the mid-height deflection of the wall specimens at each intensity of wind loading time history that was applied. The values that are presented in the following tables do not consider the initialization loading of the first two minutes, as the initializing load was much lower than the intensity of the modelled 10-minute wind storm. Furthermore, the mean mid-height deflection values presented in *Table 4.6* at 30 m/s and 70 m/s mean wind speed intensities represent the mean deflection before the onset of first cracking and the onset of significant plastic deformation, respectively.

Overall, the low reinforcement ratio wall specimens that were tested under dynamic loading conditions behaved in a typical ductile flexural mode, which was comparable to that of the wall

specimens tested under quasi-static loading conditions. Moreover, they exhibited consistent behavioural characteristics across all five wall specimens that were tested. The results of one of the wall specimens (Specimen LD3) is presented in this section to provide a general overview of the behavioural characteristics of low reinforcement ratio wall specimens that were tested under dynamic wind loading conditions.

Table 4.5: Dynamic loading of low reinforcement ratio specimens at each wind load intensity

Specimen		Applied Load at Each Intensity of Wind Load (kN)				
		30 m/s	40 m/s	50 m/s	60 m/s	70 m/s
LD1	**Mean**	2.0	3.6	5.4	7.7	10.5
	Max	4.7	8.3	12.1	15.5	18.1
LD2	**Mean**	2.0	3.5	5.4	7.5	10.0
	Max	5.0	7.5	14.9	15.4	17.8
LD3	**Mean**	2.0	3.5	5.4	7.7	10.4
	Max	4.7	7.6	14.9	15.6	18.6
LD4	**Mean**	2.0	3.3	5.6	7.7	10.4
	Max	4.6	7.9	11.6	15.5	18.7
LD5	**Mean**	2.0	3.6	5.4	7.7	10.8
	Max	4.9	7.6	11.0	15.8	18.6

Table 4.6: Dynamic deflections of low reinforcement ratio specimens at each wind load intensity

Specimen		Mid-Height Deflection at Each Intensity of Wind Load (mm)				
		30 m/s	40 m/s	50 m/s	60 m/s	70 m/s
LD1	**Mean**	1.7	2.4*	11.9	18.6	23.5*
	Max	2.3	9.6	19.1	29.8	123.4
LD2	**Mean**	1.8	2.6*	10.7	19.3	27.6*
	Max	2.7	7.3	24.8	29.7	90.8
LD3	**Mean**	3.9	6.1*	13.5	20.6	29.8*
	Max	5.0	10.4	27.5	31.1	141.8
LD4	**Mean**	9.0	9.6*	16.6	23.9	27.1*
	Max	9.7	12.8	23.0	33.5	136.5
LD5	**Mean**	2.7	3.5*	10.5	18.9	29.3*
	Max	3.3	7.8	15.7	30.3	111.0

**Prior to significant change in response (Cracking load/ Yield load)*

The lowest intensity dynamic load time histories that were applied to the wall specimens were not intended to do any significant damage. *Figure 4.11* presents the deflection time history and the

load vs. deflection diagram for the 30 m/s mean wind speed intensity dynamic load that was applied to specimen LD3. The load and deflection refer to the total load applied by the hydraulic actuator and the mid-height deflection of the wall specimen, respectively. For this load intensity, the wall specimens did not sustain any significant damage and behaved in an essentially linear elastic manner. The deflection time histories indicated that there were no notable changes in the mean deflection; similarly, the hysteresis diagrams indicated that there were no notable changes in stiffness of the wall specimens. The "mean deflection" refers to the central deflection value about which the vibrations occurred, which is indicated by the red line in the deflection time history in *Figure 4.11*. Furthermore, the "stiffness" refers to the slope of the stable hysteresis loop, which is indicated by the dashed red line in the hysteresis diagram bellow. In the case of specimen LD3, a mean load of 2.0 kN was applied over this load time history with the peak load being 4.7 kN. The wall specimen exhibited a mean mid-height deflection of 3.9 mm with a maximum mid-height deflection of 5.0 mm.

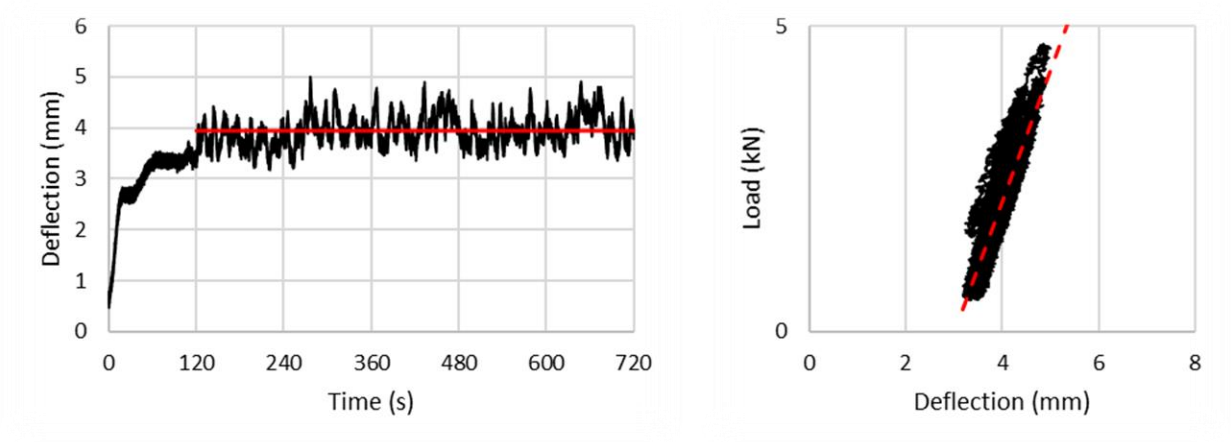

Figure 4.11: The 30 m/s deflection time history (left) and hysteresis diagram (right) of specimen LD3

Figure 4.12 presents the results of the 40 m/s mean wind speed intensity dynamic load that was applied to specimen LD3. The low reinforcement ratio wall specimens indicated the first signs of flexural cracks during the 40 m/s mean wind speed intensity loading. This first change in response was observed as bed-joint cracks appeared in the mid-height constant moment region of the wall specimens, similar to those observed during the quasi-static load testing at cracking load. The deflection time histories indicated a notable change in instantaneous mean deflection with a corresponding change in stiffness in the hysteresis diagrams. The low reinforcement ratio wall specimens indicated a cracking load of approximately 6.6 kN at a mid-height deflection of

approximately 4.6 mm under dynamic loading conditions. In the case of specimen LD3, a mean load of 3.5 kN was applied over this load time history with the peak load being 7.6 kN. The specimen LD3 initially had a mean mid-height deflection of 6.1 mm at the start of the wind storm, but then exhibited a notable change at approximately 150 s with a corresponding change in stiffness. This notable change in instantaneous mean deflection is indicated by the shift in the 1st red line to the 2nd red line in the deflection time history diagram below. Similarly, the change in slope of the stable hysteresis loops indicated by the 1st and 2nd dashed red lines in the hysteresis diagram below is the corresponding change in stiffness at the onset of cracking. A similar procedure, as illustrated here, was carried out to identify the changes in response of all the wall specimens tested under dynamic loading conditions. Using this approach, the cracking load of specimen LD3 was estimated to be 6.4 kN at a mid-height deflection of 6.5 mm. By the end of this wind loading time history, specimen LD3 exhibited a maximum mid-height deflection of 10.4 mm. The 3rd red lines indicate the stable hysteresis loop of specimen LD3 at the end of this wind load time history, suggesting that further cracking had taken place by this time.

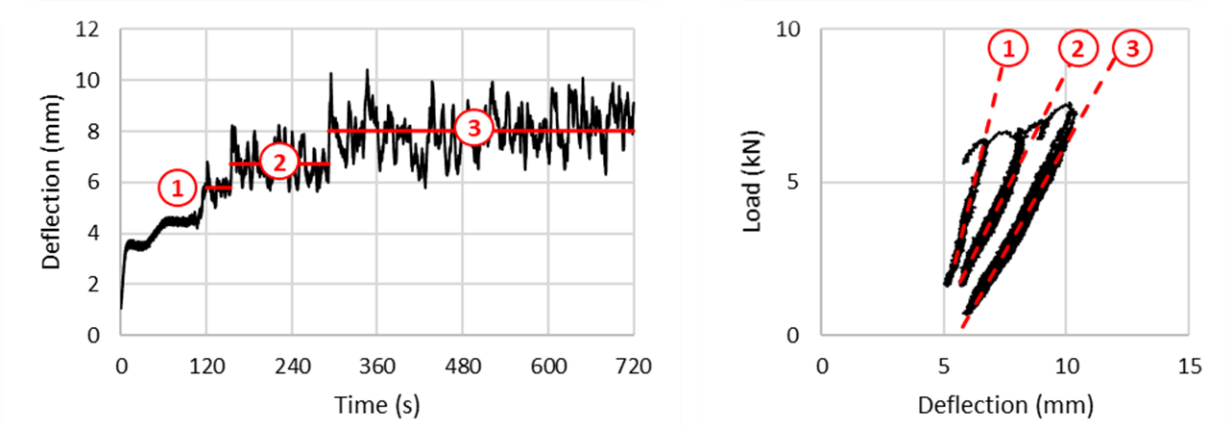

Figure 4.12: The 40 m/s deflection time history (left) and hysteresis diagram (right) of specimen LD3

Figure 4.13 and *Figure 4.14* presents the results of the 50 m/s and 60 m/s mean wind speed intensity dynamic loads that were applied to specimen LD3, respectively. The wall specimens sustained gradual damage during the 50 m/s and 60 m/s mean wind speed load time histories. Additional flexural cracks propagated along the bed-joints adjacent to the mid-height constant moment region of the wall specimens. The hysteresis diagrams indicated the gradual deterioration of stiffness of the wall specimens during these load intensities. However, the low reinforcement ratio wall specimens did not reach a damage state where they displayed the onset of significant

plastic deformation. During the 50 m/s mean wind speed intensity loading, the deflection time history of specimen LD3 showed a gradual increase in mean mid-height deflection that corresponded to the gradual deterioration of stiffness indicated by its hysteresis diagram. Similarly, specimen LD3 showed an overall increase in mean mid-height deflection in the 60 m/s mean wind speed intensity loading. However, there was no indication of a significant change in the mean mid-height deflection and stiffness at the end of this loading intensity.

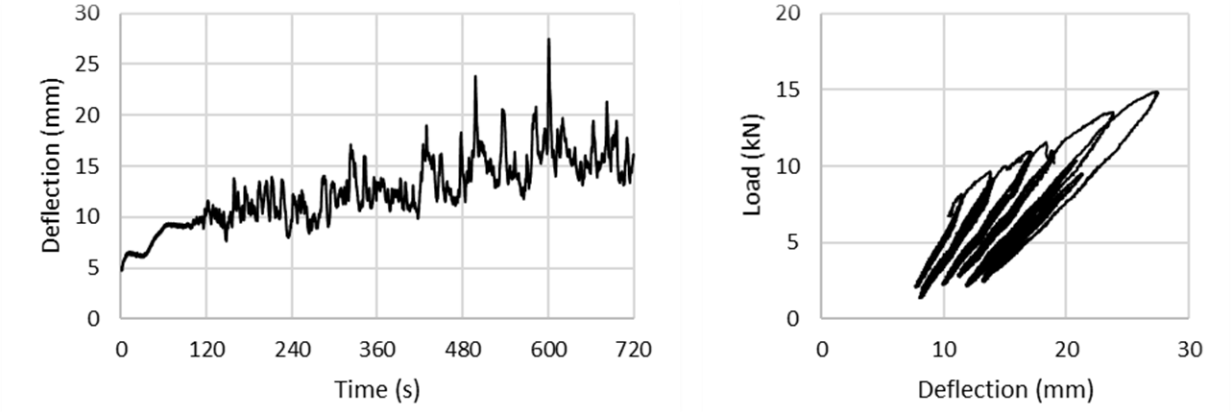

Figure 4.13: The 50 m/s deflection time history (left) and hysteresis diagram (right) of specimen LD3

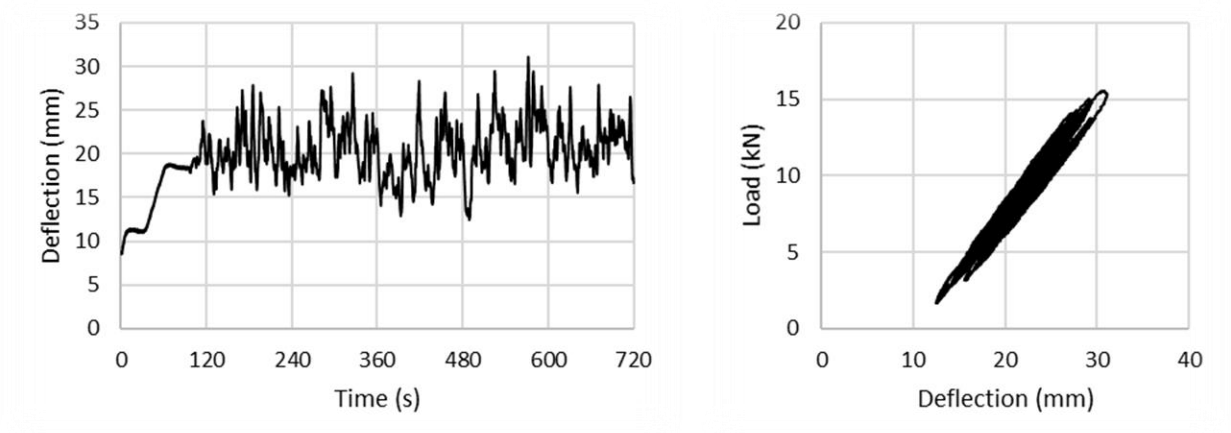

Figure 4.14: The 60 m/s deflection time history (left) and hysteresis diagram (right) of specimen LD3

Figure 4.15 presents the results of the 70 m/s mean wind speed intensity dynamic load that was applied to specimen LD3. The low reinforcement ratio wall specimens indicated the first signs of significant plastic deformation due to yielding of the reinforcement during the 70 m/s mean wind speed intensity loading. This change in response was observed as bed-joint cracks that formed in the mid-height constant moment region of the wall specimens widened significantly, similar to

that observed during the quasi-static load testing at the yield capacity. The deflection time histories indicated notable changes in mean deflection with corresponding changes in stiffness in the hysteresis diagrams. The low reinforcement ratio wall specimens exhibited a yield capacity of approximately 16.0 kN at a mid-height deflection of approximately 34.0 mm under dynamic loading conditions. In the case of specimen LD3, this load-time history applied a mean load of 10.4 kN with the peak load being 18.6 kN. The specimen LD3 initially exhibited a mean mid-height deflection of 29.8 mm; at the early stages of loading, the wall specimen exhibited a notable change at approximately 130 s, with a corresponding change in stiffness as seen in the hysteresis diagram. The yield capacity of specimen LD3 was estimated to be 16.1 kN at a mid-height deflection of 35.9 mm. By the end of this wind loading time history, specimen LD3 exhibited a maximum mid-height deflection of 111.0 mm.

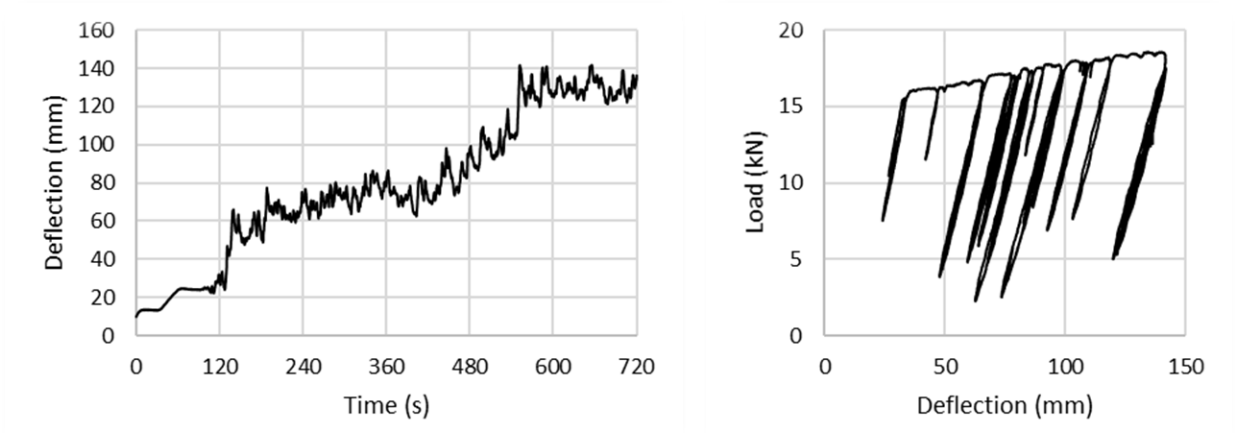

Figure 4.15: The 70 m/s deflection time history (left) and hysteresis diagram (right) of specimen LD3

Further loading, beyond the 70 m/s mean wind speed intensity, was not applied due limitations of the test setup, which is discussed further in the Section 4.7.2. After the onset of significant plastic deformation, the wall specimens were increasingly compliant due to the deterioration of stiffness. Therefore, they required increasingly higher deformation to achieve the peak loads at the highest intensity loading. The maximum load applied to the wall specimens at the end of testing was approximately 18.4 kN, which resulted in a maximum mid-height deflection of approximately 120.7 mm.

Figure 4.16 presents the load envelope of specimen LD3 (i.e., the load vs. deflection results of the entire series of load time histories applied to specimen LD3). Additionally, the plot in red

represents the mean static response of the low reinforcement ratio wall specimens tested under quasi-static loading conditions. Overall, the trends were similar to the load vs. deflection diagrams of the wall specimens tested under quasi-static loading conditions. At the end of testing, the wall specimens were significantly damaged with flexural crack patterns similar to those seen in the low reinforcement ratio wall specimens that were tested under quasi-static loading. However, as in the quasi-static tests, there was no observable spalling or crushing of the mortar bed-joints or the masonry blocks on the compression side of the wall specimens, which indicated that the wall specimens had not yet reached the ultimate loading capacity at the end of testing.

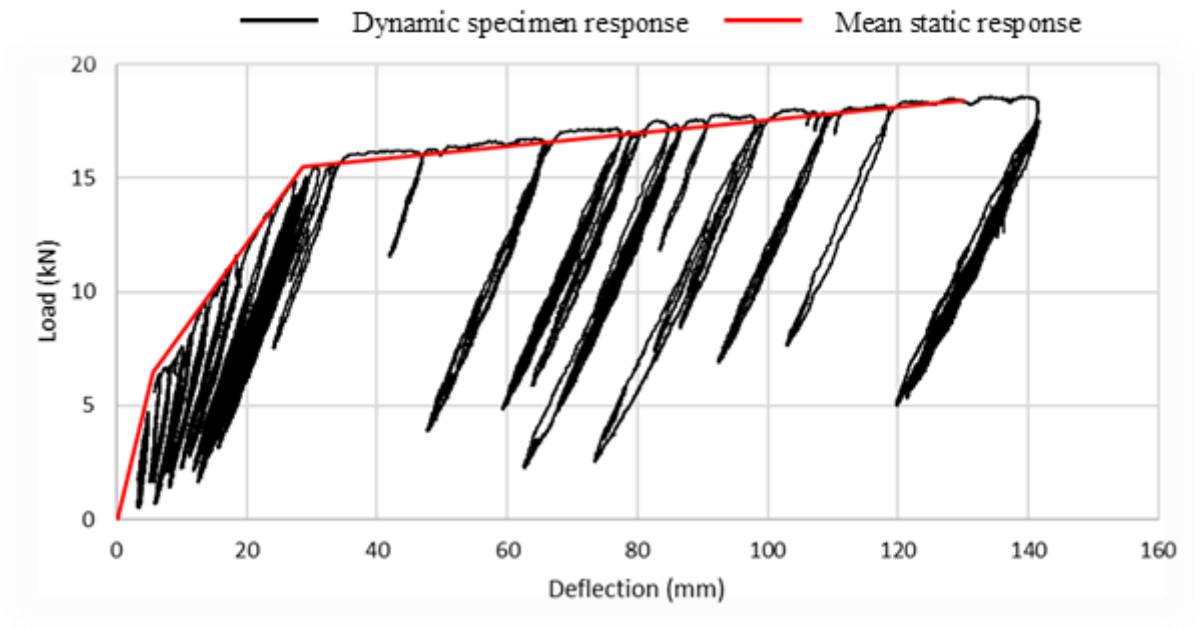

Figure 4.16: Load envelope of specimen LD3

4.5.7 High Reinforcement Ratio Wall Specimens Under Dynamic Loading

Each of the five high reinforcement ratio wall specimens tested under dynamic loading conditions was subjected to one of the five different series of dynamic load time histories that were used in the dynamic testing of the five low reinforcement ration wall specimens. However, the technical limitation during the testing of low reinforcement ratio wall specimens was resolved prior to the high reinforcement ratio wall specimen tests; as a result, a much better simulation of the target generated wind time histories was achieved. Further discussion is provided in Section 4.7.1. The loading series for each wall specimen consisted of five dynamic load time histories, which ranged

from a mean wind speed of 30 m/s up to 70 m/s, at 10 m/s mean wind speed increments. Loading of higher intensities than the 70 m/s mean wind speed were not applied due to limitations of the test setup. *Table 4.7* and *Table 4.8* list the mean and maximum values of the total load applied by the hydraulic actuator, as well as the mid-height deflection of the wall specimens at each intensity of wind loading that was applied. Furthermore, the mean mid-height deflection values presented in *Table 4.8* at 30 m/s and 70 m/s mean wind speed intensities represent the mean deflection before the onset of first cracking and the onset of significant plastic deformation, respectively.

Table 4.7: Dynamic loading of high reinforcement ratio specimens at each wind load intensity

Specimen		Applied Load at Each Intensity of Wind Load (kN)				
		30 m/s	40 m/s	50 m/s	60 m/s	70 m/s
HD1	**Mean**	2.0	3.6	5.5	7.8	10.6
	Max	6.5	12.3	17.7	24.9	29.1
HD2	**Mean**	2.1	3.6	5.5	7.6	10.1
	Max	6.7	10.4	21.3	22.7	30.4
HD3	**Mean**	2.1	3.6	5.4	7.8	10.5
	Max	5.9	11.4	21.4	22.3	31.9
HD4	**Mean**	2.1	3.5	5.6	7.8	10.5
	Max	6.1	11.8	17.6	21.2	31.1
HD5	**Mean**	2.1	3.7	5.5	7.8	10.9
	Max	7.5	11.3	15.5	25.3	29.9

Table 4.8: Dynamic deflections of high reinforcement ratio specimens at each wind load intensity

Specimen		Mid-Height Deflection at Each Intensity of Wind Load (mm)				
		30 m/s	40 m/s	50 m/s	60 m/s	70 m/s
HD1	**Mean**	6.1	7.0*	14.9	19.4	23.1*
	Max	7.1	17.8	26.8	40.4	101.7
HD2	**Mean**	2.9	4.2*	9.6	13.7	17.1*
	Max	4.5	9.6	25.0	28.1	69.2
HD3	**Mean**	5.3	7.0*	11.0	14.4	19.0*
	Max	6.2	11.9	24.3	25.8	64.4
HD4	**Mean**	4.0	4.6*	10.0	14.1	18.1*
	Max	5.3	11.8	20.4	26.7	82.2
HD5	**Mean**	2.5	3.4*	9.2	14.2	19.2*
	Max	3.7	9.8	17.5	31.8	47.4

**Prior to significant change in response (Cracking load/ Yield load)*

Overall, the high reinforcement ratio wall specimens that were tested under dynamic loading conditions behaved in a typical ductile flexural mode, which was comparable to that of the wall specimens tested under quasi-static loading conditions. All five wall specimens that were tested exhibited consistent behavioural characteristics. Therefore, the results of one of the wall specimens (specimen HD2) is presented in this section to provide a general overview of the behavioural characteristics of high reinforcement ratio wall specimens that were tested under dynamic wind loading conditions.

The lowest intensity dynamic load time histories applied to the wall specimens did not do any significant damage to them, as intended. *Figure 4.17* presents the deflection time history and the load vs. deflection diagram of the 30 m/s mean wind speed intensity dynamic load that was applied to specimen HD2. The deflection time histories indicated that there were no notable changes in the mean deflection, while the hysteresis diagrams indicated that there were no notable changes in stiffness of the wall specimens during this load time history. The wall specimens behaved in a fairly linear elastic manner as they did not sustain any significant damage. In the case of specimen HD2, a mean load of 2.1 kN was applied over this load time history with the peak load being 6.7 kN. The specimen exhibited a mean mid-height deflection of 2.9 mm with a maximum mid-height deflection of 4.5 mm.

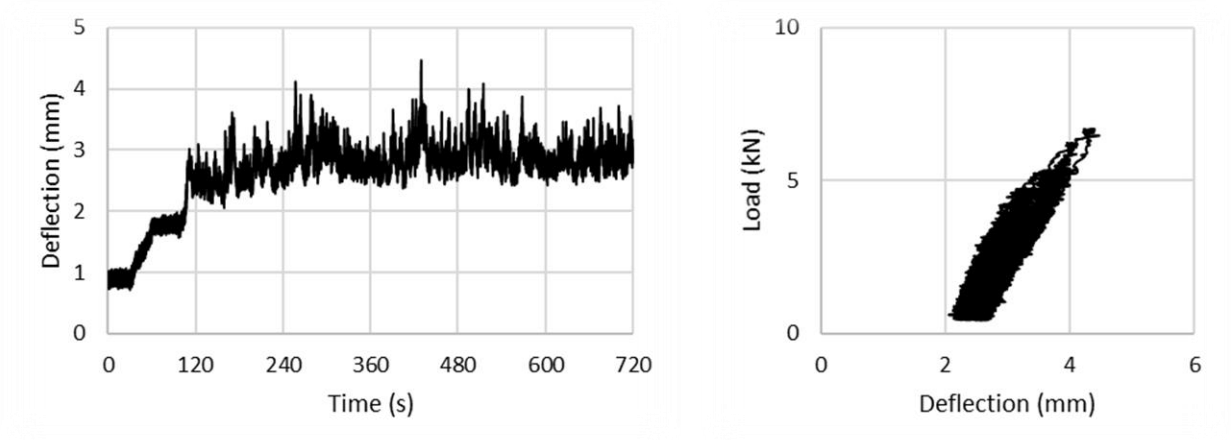

Figure 4.17: The 30 m/s deflection time history (left) and hysteresis diagram (right) of specimen HD2

Figure 4.18 presents the results of the 40 m/s mean wind speed intensity dynamic load that was applied to specimen HD2. The first signs of flexural cracks were observed during the 40 m/s mean wind speed intensity loading. Like that observed during the quasi-static load testing at cracking

load, bed-joint cracks appeared in the mid-height constant moment region of the wall specimens. The deflection time histories indicated a notable change in mean deflection, with a corresponding change in stiffness in the hysteresis diagrams. The load and the mid-height deflection at the onset of cracking of the high reinforcement ratio wall specimens was approximately 8.1 kN and 6.4 mm, respectively. In the case of specimen HD2, a mean load of 3.6 kN was applied over this load time history with a peak load of 10.4 kN. The wall specimen HD2 initially had a mean mid-height deflection of 4.2 mm, but then showed a notable change at approximately 270 s with a corresponding change in stiffness, as seen in the hysteresis diagram. The cracking load of specimen HD2 was estimated to be 7.9 kN at a mid-height deflection of 5.8 mm. At the end of this wind loading intensity, specimen HD2 showed a maximum mid-height deflection of 9.6 mm.

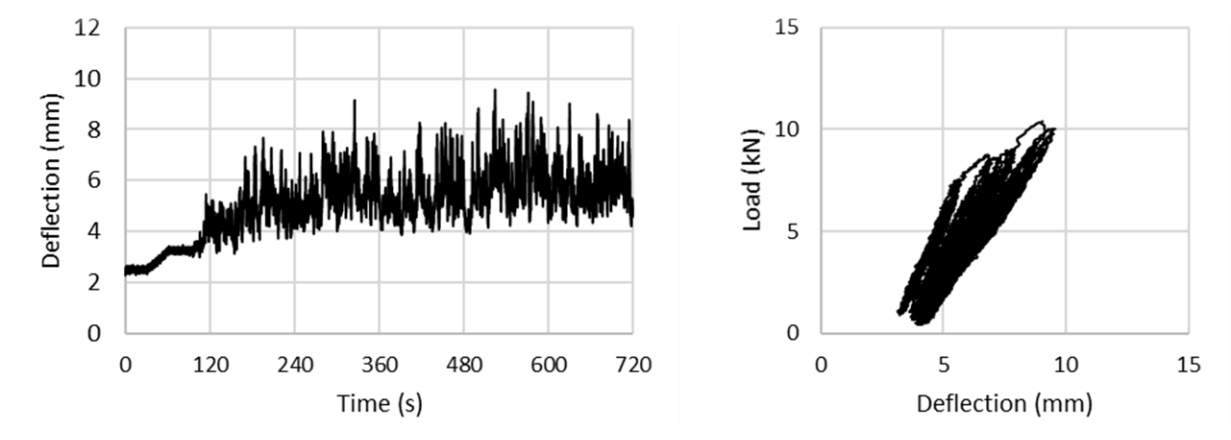

Figure 4.18: The 40 m/s deflection time history (left) and hysteresis diagram (right) of specimen HD2

Figure 4.19 and *Figure 4.20* present the results of the 50 m/s and 60 m/s mean wind speed intensity dynamic loads that were applied to specimen HD2, respectively. Over the next two load intensities the wall specimens sustained gradual damage, which resulted in additional flexural cracks that propagated along the bed-joints adjacent to the mid-height constant moment region. The hysteresis diagrams indicated the gradual deterioration of stiffness of the wall specimens during these load intensities; however, the high reinforcement ratio wall specimens did not reach a damage state where they displayed the onset of significant plastic deformation during these load time histories. The gradual deterioration of stiffness of the wall specimen was indicated by the deflection time history of specimen HD2, which showed a gradual increase in mean mid-height deflection during the 50 m/s mean wind speed intensity loading. The mid-height deflection in the 60 m/s mean wind speed intensity loading showed a gradual increase as well, although not to the same degree.

However, the wall specimens did not indicate a notable, abrupt change in its mean mid-height deflection and stiffness by the end of these loading intensities.

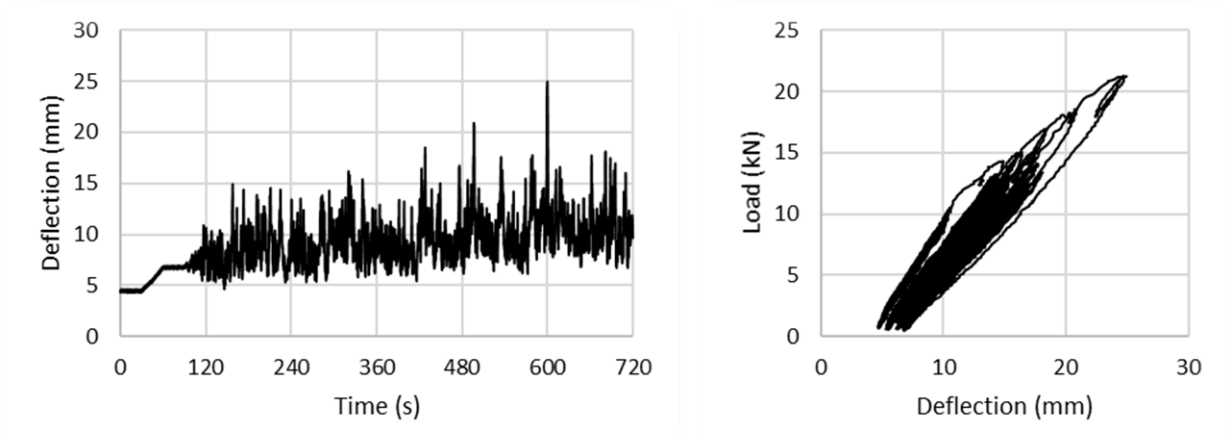

Figure 4.19: The 50 m/s deflection time history (left) and hysteresis diagram (right) of specimen HD2

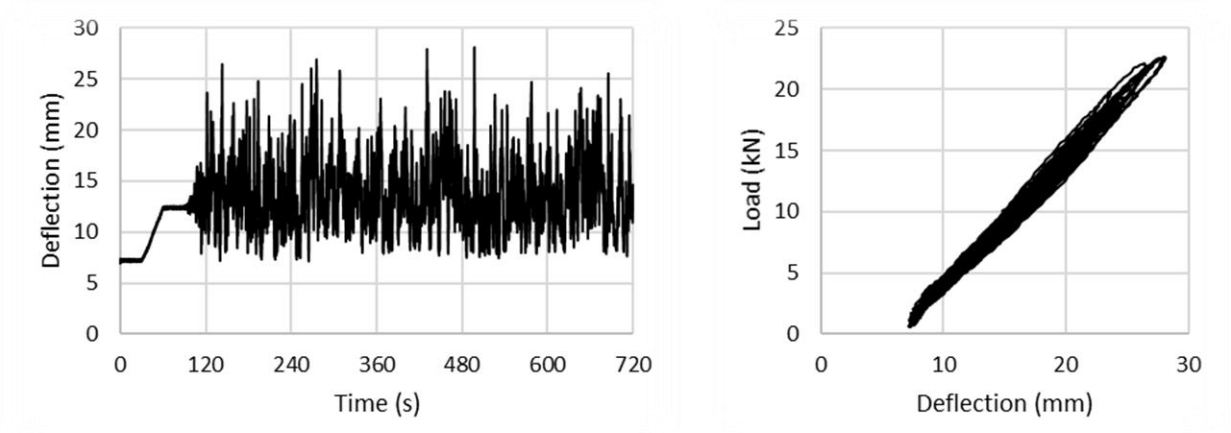

Figure 4.20: The 60 m/s deflection time history (left) and hysteresis diagram (right) of specimen HD2

Figure 4.21 presents the results of the 70 m/s mean wind speed intensity dynamic load that was applied to specimen HD2. The high reinforcement ratio wall specimens exhibited the onset of significant plastic deformation due to yielding of the reinforcement during the 70 m/s mean wind speed intensity loading. As was observed during the quasi-static load testing at yield capacity, the bed-joint cracks that formed in the mid-height constant moment region of the wall specimens widened significantly. The deflection time histories indicated notable changes in the mean deflection with corresponding changes in stiffness in the hysteresis diagrams. The high reinforcement ratio wall specimens exhibited a yield capacity of approximately 28.9 kN at a mid-height deflection of approximately 39.4 mm under dynamic loading conditions. In the case of

specimen HD2, this load time history featured a mean load of 10.1 kN with a peak load of 30.4 kN. The wall specimen HD2 initially had a mean mid-height deflection of 17.1 mm, but then showed a notable change at approximately 250 s with a corresponding change in stiffness, as seen in the hysteresis diagram. The yield capacity of specimen HD2 was estimated to be 29.0 kN at a mid-height deflection of 37.9 mm. At the end of this wind loading intensity, specimen HD2 showed a maximum mid-height deflection of 69.2 mm.

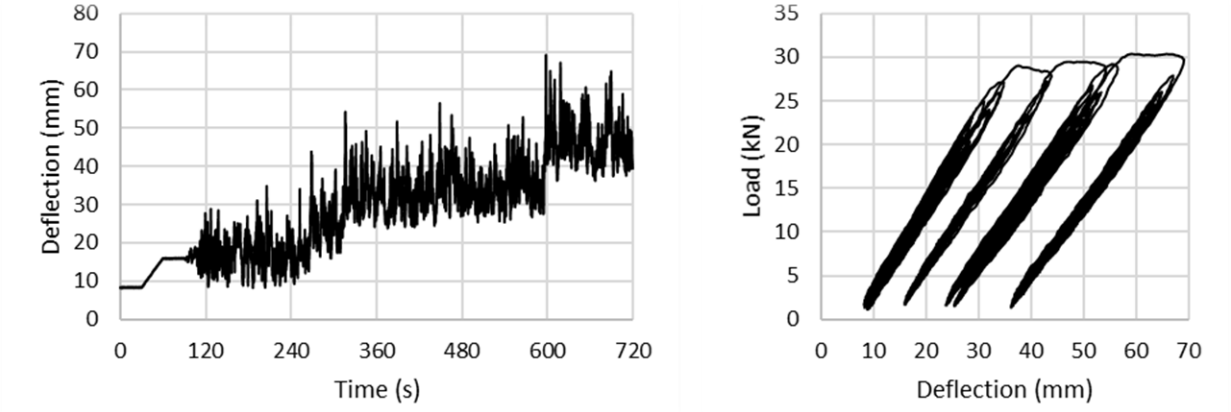

Figure 4.21: The 70 m/s deflection time history (left) and hysteresis diagram (right) of specimen HD2

The 70 m/s mean wind speed intensity was the highest intensity loading applied to the high reinforcement ratio wall specimens. Higher intensity loading was not applied due limitations of the test setup, which is discussed further in the following sections (Section 4.7.2). The wall specimens were increasingly compliant due to the deterioration of stiffness after the onset of significant plastic deformation due to yielding of the reinforcement. This resulted in high levels of deformation to achieve the peak loads of the highest intensity loading that were applied to the wall specimens. The maximum load applied to the wall specimens at the end of testing was approximately 30.5 kN, which resulted in maximum mid-height deflection of approximately 73.0 mm.

Figure 4.22 presents the load envelope of specimen HD2. Additionally, the plot in red represents the mean static response of the high reinforcement ratio wall specimens tested under quasi-static loading conditions. Overall, the load vs. deflection diagrams of the wall specimens tested under quasi-static loading conditions exhibited similar trends to that of the wall specimens tested under dynamic loading conditions; however, the envelop of the dynamic response is seen to plot above

the static response over the plastic response range. At the end of testing, the wall specimens were significantly damaged with flexural crack patterns similar to those of the high reinforcement ratio wall specimens that were tested under quasi-static loading. However, there was no observable spalling or crushing of the mortar bed-joints or the masonry blocks on the compression side of the wall specimens, which suggested that the wall specimens had not yet reached the ultimate loading capacity at the end of testing.

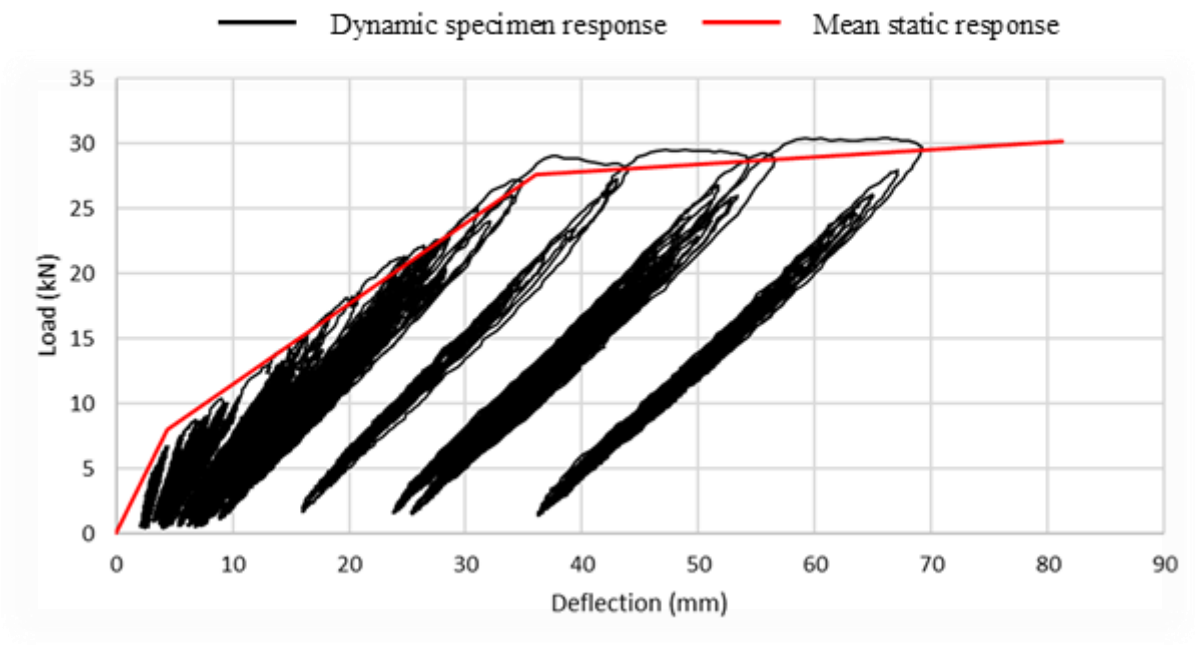

Figure 4.22: Load envelope of specimen HD2

4.5.8 Summary of Dynamic Loading Test Results

Table 4.9 provides the results obtained from the wall specimens tested under dynamic loading conditions. The calculated moments were based on values within the mid-height constant moment region, while the deflections represent the corresponding mid-height deflections. When the first signs of cracking were observed in the mid-height region, the low and high reinforcement ratio wall specimens displayed a cracking load of approximately 3.8 kNm at a deflection of 4.6 mm and 4.6 kNm at 6.4 mm, respectively. Subsequently, when the wall specimens began to show significant plastic deformation, the low and high reinforcement ratio wall specimens displayed a yield capacity of 9.1 kNm at a deflection of 34.0 mm and 16.5 kNm at 39.4 mm, respectively.

Table 4.9: Moment and deflection results of the dynamic loading tests

Specimen		Cracking		Yielding		Maximum Applied	
		Moment (kNm)	Deflection (mm)	Moment (kNm)	Deflection (mm)	Moment (kNm)	Deflection (mm)
Low Reinforcement Ratio	**LD1**	3.8	3.7	9.1	32.9	10.4	123.4
	LD2	3.7	4.0	9.2	34.3	10.2	90.8
	LD3	3.6	6.5	9.2	35.9	10.6	141.8
	LD4	4.2	-	9.0	35.6	10.7	136.5
	LD5	3.5	4.2	9.2	31.5	10.6	110.9
Mean		**3.7**	**4.6**	**9.1**	**34.0**	**10.5**	**120.7**
CV (%)		6.7	27.6	0.7	5.5	2.1	17.0
High Reinforcement Ratio	**HD1**	4.4	7.6	15.5	43.5	16.6	101.7
	HD2	4.5	5.8	16.6	37.9	17.4	69.2
	HD3	4.7	7.3	17.4	37.8	18.3	64.4
	HD4	4.5	6.1	16.3	38.5	17.8	82.2
	HD5	5.1	5.4	16.9	39.4	17.1	47.4
Mean		**4.6**	**6.4**	**16.5**	**39.4**	**17.4**	**73.0**
CV (%)		6.3	15.0	4.3	6.0	3.6	27.9

The maximum applied moments and deflections listed refer to the maximum values measured during the highest intensity dynamic loading time history applied to each respective wall specimen. At the end of testing, the low reinforcement ratio wall specimens were subjected to a maximum loading of approximately 10.5 kNm, while the high reinforcement ratio wall specimens were subjected to a maximum loading of approximately 17.4 kNm. Since the dynamic loading was carried out under load control, the maximum deflection of the wall specimens at highest intensity loading varied depending on the different wind storms applied. Overall, both the low and high reinforcement ratio wall specimens were damaged past the yield capacity at highest intensity loading. However, they still had not reached their ultimate capacity at the end of testing.

Taking the maximum deflection value to represent the mid-height deflection at ultimate capacity, while recognising the fact that this is a conservative approximation made due to limitations of the experimental program, the average ductility ratios for the low and high reinforcement ratio wall specimens tested under dynamic loading conditions were approximately 3.6 and 1.9, respectively.

4.6 Specific Observations of the Wall Specimen Test Results

Overall, the wall specimens of each set exhibited similar behaviour characteristics. However, there were several specimens that showed notably different behaviours during the testing, which is discussed in this section.

4.6.1 Specimen LS5

Specimen LS5 was the first wall specimen that was tested in the experimental program using the test setup. As such, there were a couple of issues that were observed during the testing that could not be addressed until after the testing was finished. However, they were minor issues which had no significant bearing on the test results.

The first issue was with the data acquisition system. Due to a programming error, the data were sampled at an irregular frequency. The target sampling rate was set at 100 Hz; however, during the testing of specimen LS5 the data was sampled at a slightly lower and irregular rate. However, this specimen was being tested under quasi-static loading conditions. Therefore, it did not have significant impact on the test results.

Secondly, the four-point loading system that was used in the test setup incorporated two load cells to measure the load applied by each spreader arm. This was to ensure that two equal line loads were applied by the spreader system. Due to an error in setup, these load cells ran out of enough actuation distance to measure the loading throughout the entire test. However, based on the readings up to that point, it was concluded that the load spreader system was functioning as intended so that the loads at the load points could be reliably inferred from the readings from the actuator force transducer.

4.6.2 Specimen LD4

At the start of the test for specimen LD4, a sudden significant horizontal movement in the direction of loading was observed due to improper configuration of the supports. The wall specimen was not properly restrained by the support configuration. There was some minor horizontal movement of the supports, initially at the start of the testing, due to limitations of the test setup. However, at the start of the first dynamic loading profile, specimen LD4 showed a significantly higher initial horizontal movement. *Figure 4.23* presents the mid-height deflection time history of the 30 m/s mean wind speed intensity dynamic load profile applied to the wall specimen, which indicates a significant jump in mean displacement at the start of loading, specifically during the initial loading from 0 to 60 s. Although the issue was addressed at the higher intensity load time histories, the deflection results at cracking load were dismissed due to the large error.

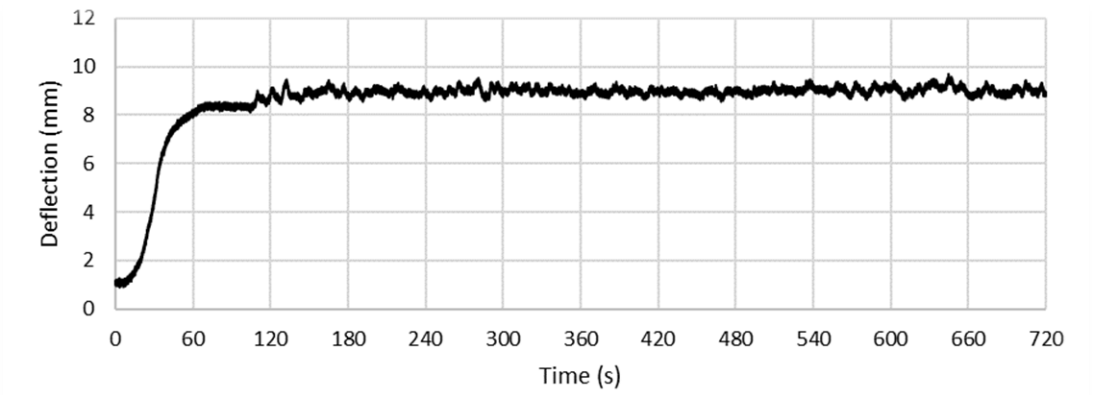

Figure 4.23: The 30 m/s deflection time history of specimen LD4

4.6.3 Specimen HS1

Figure 4.24 presents the load vs. mid-height deflection diagram of specimen HS1. The testing cycle of specimen HS1 was suddenly interrupted by the actuator control system. After some displacement past the cracking load, the loading abruptly stopped, and the actuator retracted due to an internal error registered by the actuator control system. The wall specimen had to be reconfigured and loaded a second time.

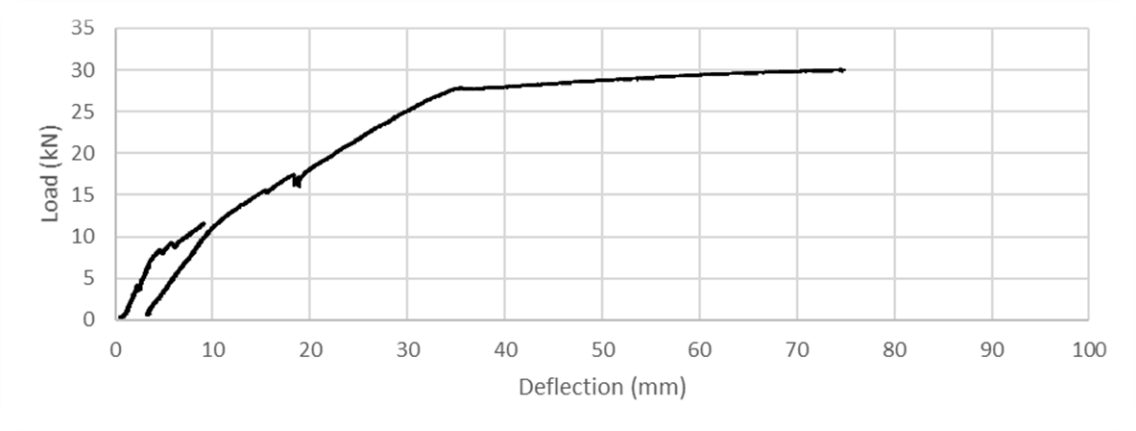

Figure 4.24: Load vs. deflection diagram for specimen HS1

4.6.4 Specimen HD1

Prior to testing specimen HD1, the actuator control system had to be reconfigured due to a malfunction. Several settings needed to be adjusted to properly simulate the dynamic wind load time histories; however, due to miss-adjustments, the actuator loading became unstable. *Figure 4.25* presents the load time history and the PSD diagrams of specimen HD1 for the 40 m/s mean wind speed intensity dynamic loading. At the beginning of this load intensity trial, the load was being properly applied; once past the cracking load, though, the loading became unstable, likely due to the wall becoming more compliant after cracking. The PSD diagram indicates the unusual high frequency content, at approximately 10 to 100 Hz, due to this instability. Furthermore, the applied load time history indicates that the actuator repeatedly lost contact with the wall surface (i.e., the negative load readings from 360 s to 720 s). This behaviour persisted through the next load intensity trial, after which the proper adjustments were made. Overall, the wall specimen did not indicate any anomalous results at the end of testing, as the issue was corrected before the application of higher intensity load time histories.

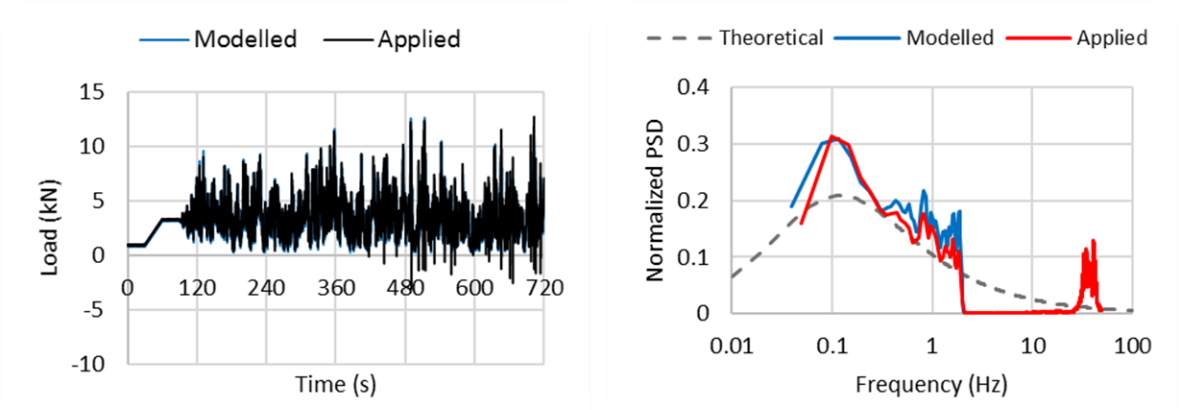

Figure 4.25: Load time history (left) and PSD (right) plots of HD1 for 40 m/s wind intensity

4.6.5 Cracking at Spreader Contact Points

Figure 4.26 shows the side view of a wall specimen that showed cracking at the contact point between the wall surface and the spreader system. These bearing cracks only occurred in several of the wall specimens at high loading beyond the yield capacity of the walls. In addition, these bearing cracks only occurred on the cut face of the half blocks that were used in the construction of the wall specimens. It was likely that the cut webs of the masonry block units were somewhat damaged during the cutting process and created a plane of weakness which cracked under the bearing load of the spreader system at higher load levels. Although several wall specimens showed similar cracks, there was no other observable damage to the wall specimens due to the bearing load applied by the spreader system to suspect any significant impact on the test results.

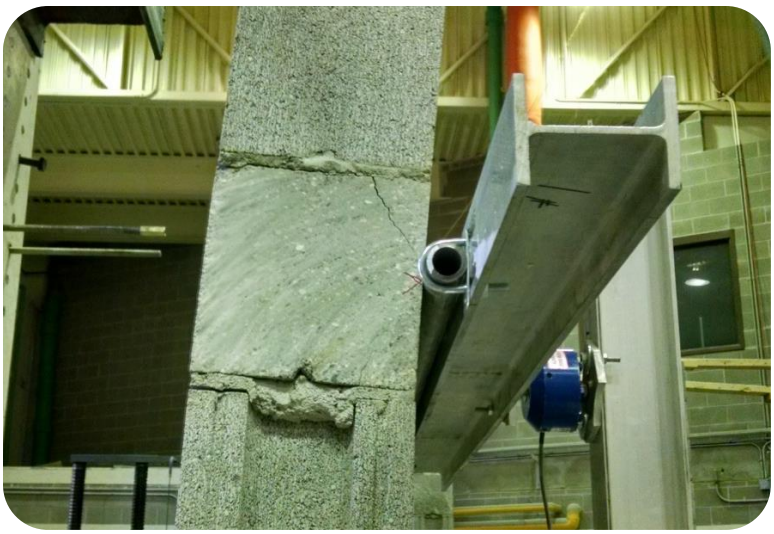

Figure 4.26: Cracking at the spreader contact point

4.7 Limitations of the Experimental Program

There were several limitations with the experimental program, which may have had some influence on the overall test results that were collected. These limitations could be generally categorized into two categories: limitations in simulating the dynamic wind loading conditions and limitations in the test setup. These limitations are addressed in this section.

4.7.1 Simulating the Dynamic Wind Loading Conditions

The limitations with simulating the dynamic wind loading conditions were primarily due to the limitations of the hydraulic actuator and its control system. *Figure 4.27* presents the load time histories and PSD diagrams of the same 70 m/s mean wind speed intensity dynamic load time history applied to specimens LD2 and HD2. There was poor agreement between the target wind time history and the actual dynamic load time histories applied to the wall specimens due to technical limitations with the actuator control system during the first phase of the testing program in which the low reinforcement ratio wall specimens were tested. This persisted throughout the testing of all the low reinforcement ratio wall specimens. The load time history and PSD diagram of specimen LD2 indicates that much of the high frequency content and the corresponding high peak loads were not applied as intended. Regardless of the intensity of the wind load time history, most of the target frequency content beyond 1 Hz was not applied to the low reinforcement wall specimens; the PSD of the applied loads were similar to that shown in *Figure 4.27* at all loading intensities. Nevertheless, this issue with the actuator control system was rectified during the second phase of testing in which the high reinforcement ratio wall specimens were tested. Thus, the load time history and PSD diagram of specimen HD2 indicates much better agreement between the target and applied dynamic load time histories.

The technical limitations during the first phase had other additional consequences. Due to the limitations with the actuator in applying higher frequency loading, the time-step of the generated wind time histories was limited to 0.25 s. The sudden drop in frequency content at 2 Hz observed in the PSD plots for both the modelled and applied loading time histories of specimen HD2 was because that was the Nyquist frequency (i.e., upper limit for a process with a given sampling rate) of the generated wind time histories. However, the generated wind time histories contained most of the frequency content of a theoretical wind load to adequately simulate realistic wind loading

conditions. Furthermore, the inability to apply the high peak dynamic (or gust) loads, as intended by the modelled load time histories, meant that much higher mean (or sustained) intensity wind loads had to be used to subject the low reinforcement wall specimens to the higher total (sustained plus dynamic) levels of loading. *Figure 4.28* presents the average mean and maximum loads of the modelled wind time histories, as well as the loading applied to the low and high reinforcement ratio wall specimens (LD and HD specimens, respectively) at each wind load intensity. As indicated, both the low and high reinforcement ratio wall specimens were subjected to similar levels of mean loading at all wind load intensities. On the other hand, the low reinforcement ratio wall specimens had to be subjected to much higher mean wind load intensities to be subjected to the same higher levels of the maximum loading levels. This also had an impact in selecting the increment of consecutive wind intensities, which had some effect on the resolution of the test results.

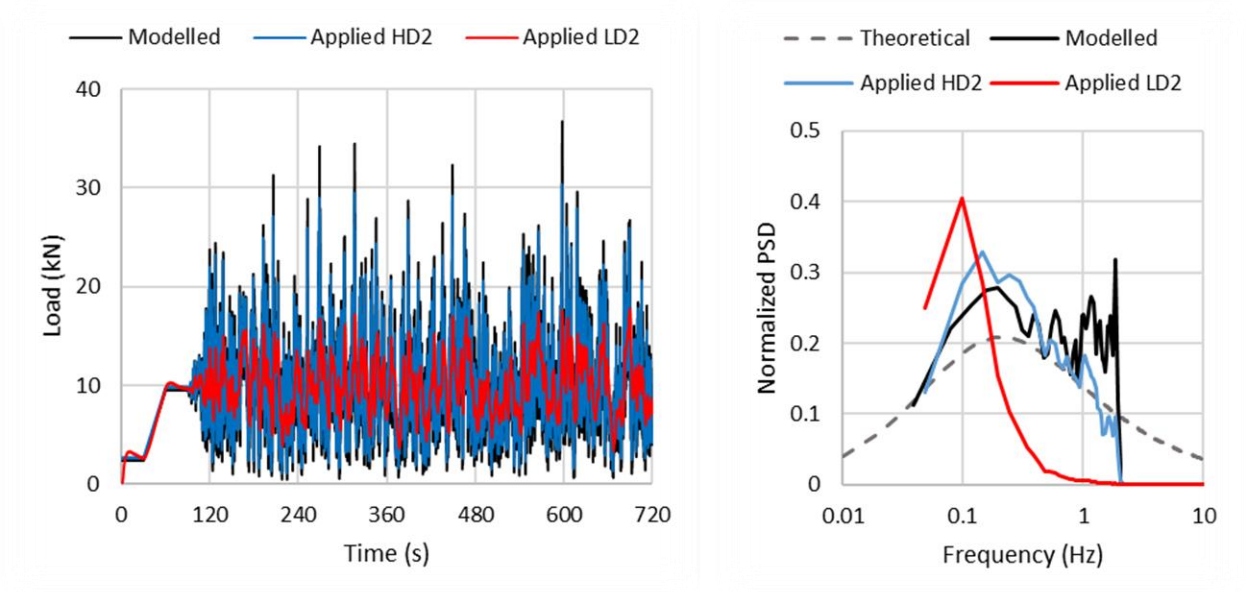

Figure 4.27: Load time histories (left) and PSD (right) plots of LD2 and HD2 for 70 m/s wind intensity

In general, it became more difficult to maintain high peak loads of the higher intensity loading time histories due to the increasing displacement required by the actuator to achieve the target loading as the wall specimens accumulated more damage and became more compliant. This was particularly the case with reinforced masonry wall specimens at higher load levels past the yield capacity of the walls due their high ductility. Overall, during the second phase, the applied loading showed much better agreement to the modelled dynamic loading time histories than during the

first phase. However, this discrepancy between the applied dynamic loading between the low and high reinforcement ratio wall specimens may have had some impact on the experimental results.

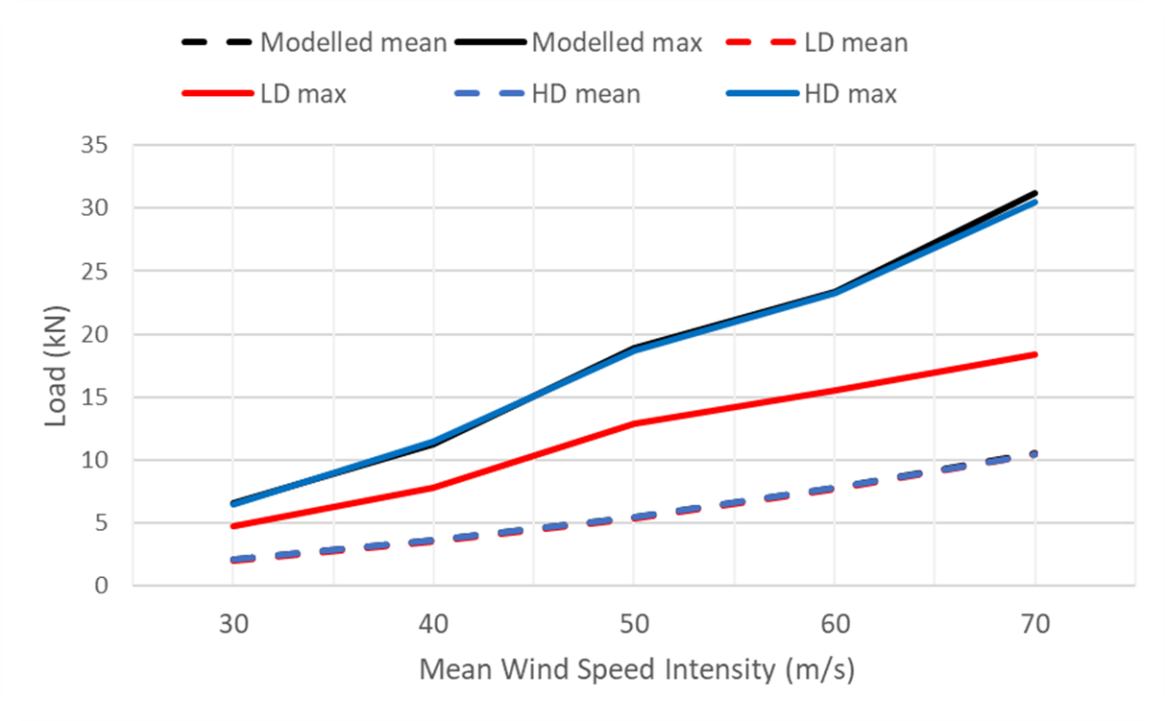

Figure 4.28: Average mean and maximum loading at each wind load intensity

4.7.2 Limitations of the Support Conditions at Higher Load Levels

It was not feasible to load the wall specimens to their ultimate loading capacity due to limitations of the support configuration. The reinforced wall specimens were relatively ductile, which caused high levels of displacement at load levels past yield capacity of the walls. The top support configuration only allowed limited amounts of support rotation, which was found not to be enough to permit loading of the wall specimens to their ultimate loading capacity, defined as either the onset of significant compressive crushing in the blocks or instability effects due to large displacement, while maintaining the idealized pinned support conditions. *Figure 4.29* shows an instance where specimen HD5 was loaded past the feasible limit of the test setup. The limitation of the support configuration caused a catastrophic failure of the wall specimen prior to reaching ultimate loading capacity.

Figure 4.29: Specimen HD5 loaded past feasible limits of the test setup

Both low and high reinforcement ratio wall specimens could not be loaded to their ultimate capacity as mentioned in the previous section. Therefore, limitations were placed on the maximum allowable deflection to mitigate unintended catastrophic failure of the wall specimen prior to reaching their ultimate loading capacity. However, the maximum allowable deflection of the high reinforced wall specimens, during the second phase of testing, was lower than the maximum allowable deflection of the low reinforced wall specimens, during the first phase of testing (i.e., the maximum deflection of the low reinforcement ratio wall specimens under quasi-static loading was approximately 135 mm, whereas for the high reinforcement ratio wall specimens it was approximately 81 mm). This was due to safety concerns with regards to the removal of the high reinforcement ratio wall specimens from the test setup after the termination of testing. At the conclusion of testing, a damaged wall specimen needed to be pushed back into, roughly, its plumb position (close to that of its undamaged state) to be safely removed from the test setup. However, as the high reinforcement ratio wall specimens were much more rigid as compared to the low reinforcement ratio wall specimens, this process became difficult to achieve safely once the maximum deflections of the high reinforcement ratio wall specimens were closer to what was achieved during the testing of the low reinforcement ratio wall specimens. Therefore, the maximum deflections of the high reinforcement ratio wall specimens were lower than the maximum deflections of the low reinforcement ratio wall specimens at the termination of testing.

4.7.3 Uneven Loading of Spreader Arms at Lower Load Levels

The loading applied by the top and bottom spreader arms were slightly uneven at low loading levels during the testing of a few of the wall specimens. *Figure 4.30* presents one such case where the top and bottom spreader arm loads were slightly different at the start of loading. The figure shows that the top spreader loading was higher than bottom spreader loading at the beginning stage of loading from 0 to 130 s. This was due to the weight of the spreader system bearing on the wall specimen at early stages of loading. The case presented was one of the worst examples and, as soon as the loading increased to a certain point, the issue resolved itself. The uneven loading generally occurred at load levels below the cracking load; therefore, this occurrence was deemed not to have a significant impact on the acquired experimental results.

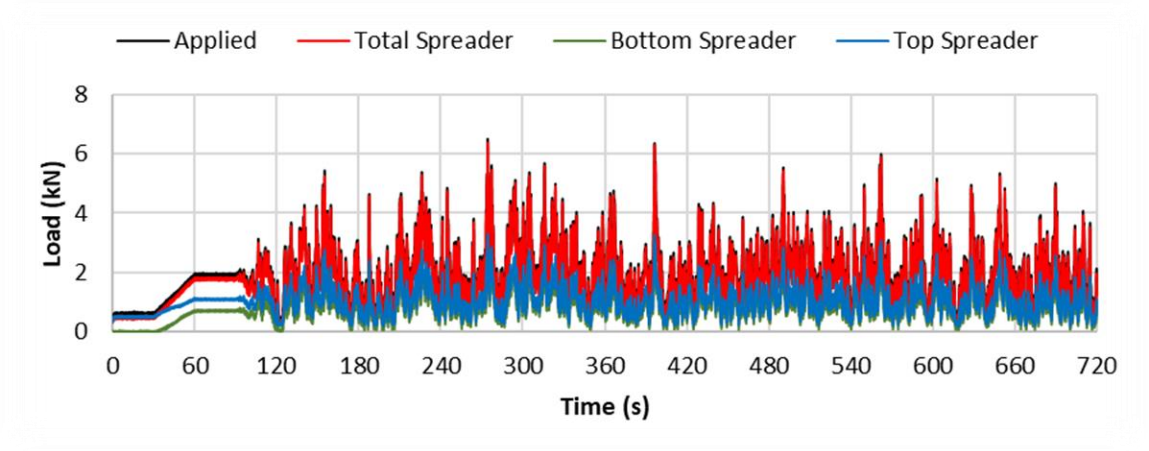

Figure 4.30: Spreader loading of specimen HD1 during 30 m/s intensity loading

4.7.4 Initial Horizontal Displacement at the Beginning of Loading

The deflection results of the wall specimens indicated a slight horizontal displacement at the start of loading. This horizontal displacement was due to limitations with the support configuration. There was a displacement of few millimeters due to the sliding of the base plate over the bottom knife edge support and the "play" in the rod connections at the top support. Although the resulting error in deflection measurements was minor, at cracking load there may have been a more significant impact as the deflection measurements at cracking load were relatively low. Therefore, further consideration may need to be given when considering the deflection results at the cracking load.

4.8 Summary of the Wall Specimen Test Results

Table 4.10 provides the mean values and the coefficients of variation (CV) of the moment and the mid-height deflection at cracking and yielding damage states of all four sets of reinforced masonry wall specimens that were tested under quasi-static and realistic dynamic wind loading conditions.

Table 4.10: Summary of moment and deflection results

Specimens		Mean Cracking				Mean Yielding			
Reinforcement Ratio	**Loading Type**	**Moment (kNm)**	**CV (%)**	**Deflection (mm)**	**CV (%)**	**Moment (kNm)**	**CV (%)**	**Deflection (mm)**	**CV (%)**
Low	**Static**	3.7	2.8	5.5	14.5	8.9	1.4	28.6	3.6
	Dynamic	3.7	6.7	4.6	27.6	9.1	0.7	34.0	5.5
High	**Static**	4.6	8.2	4.4	9.5	15.8	5.1	36.0	4.1
	Dynamic	4.6	6.3	6.4	15.0	16.5	4.3	39.4	6.0

4.8.1 General Behavioural Characteristics

Overall, the wall specimens exhibited similar flexural ductile modes of failure under both quasi-static and dynamic wind loading conditions. As the quasi-static testing was conducted under displacement control and the dynamic testing was conducted under load control, though, establishing direct comparisons of the behavioural characteristic between the two types of loading was difficult. However, meaningful comparisons could be made of the changes in response over the progression of damage states of the wall specimens under both types of loading conditions.

The first change in response was observed at the onset of flexural cracks at the cracking load of the wall specimens. Slight bed-joint cracks formed along the mortar and masonry block interface along the entire width of the wall specimens. These flexural cracks formed in the mid-height region of the wall specimens, which were subjected to the maximum constant moment. Further flexural cracks formed in the adjacent bed-joints as the loading progressed.

The next distinct change in response was observed at the yield capacity of the wall specimens, with the onset of significant plastic deformation. At the onset of yielding of the reinforcement, the bed-joint cracks in the mid-height region of the wall specimens widened significantly. Beyond this damage state, both low and high reinforcement ratio wall specimens exhibited significantly higher levels of plastic deformation at a much lower rate of increase in load carrying capacity. This was observed under both types of loading conditions.

The testing was halted once the large deformations of the wall specimens caused the test setup to reach its feasible limits. At the end of testing, the low reinforcement ratio wall specimens indicated much higher levels of ductility (i.e., defined as the ratio of peak midspan deflection to those at cracking load) than the high reinforcement ratio wall specimens. The wall specimens exhibited significant levels of damage at the end of testing. However, the specimens had not reached their ultimate loading capacity, as there were no visible signs of spalling or crushing of the mortar joint or masonry blocks on the compression face of the wall specimens. Overall, the wall specimens exhibited behaviour that was broadly similar to that observed under quasi-static loading conditions.

4.8.2 Load Capacity Comparison between Quasi-static vs. Dynamic Loading

Figure 4.31 summarises the loading results of the wall specimens at the specific damage states of cracking and yield capacity. There was insufficient evidence to make statistically significant conclusions at a 90% confidence interval due to the variability of the results and the low sample size. However, both the low and high reinforcement ratio wall specimens indicated slightly higher levels of load bearing capacity at higher loading levels under dynamic wind loading conditions, as compared to quasi-static loading conditions.

At yield capacity, in particular, the wall specimens indicated slightly higher capacity under dynamic loading conditions. The low reinforcement ratio wall specimens showed an increase in capacity of 3%, whereas the high reinforcement ratio wall specimen showed a slightly higher increase in capacity of 5%. As the wall specimens could not be loaded to their ultimate loading capacity, comparison of higher loading levels beyond yield capacity could not be made directly between the wall specimens tested under quasi-static loading conditions, as compared to dynamic loading conditions. Specifically, an adequate distinction of the damage state of the wall specimens

could not be established to make direct comparison of loading closer to, but not at, the ultimate capacity of the wall specimens, due to the difference in the two types of loading.

For example, the maximum moment applied to the high reinforcement ratio wall specimens tested under quasi-static loading conditions was approximately 17.2 kNm. The testing was carried out under displacement control and the wall specimens were subjected to a maximum displacement of approximately 81.2 mm to achieve this maximum loading capacity. On the other hand, the maximum moment applied to the high reinforcement ratio wall specimens tested under dynamic loading conditions was approximately 17.4 kNm. The testing was carried out under load control, under which, at the maximum loading, the wall specimens exhibited maximum displacements that ranged from 47.4 mm (specimen HD5) to 101.7 mm (specimen HD1). Therefore, it was difficult to infer whether both the wall specimens tested under quasi-static and dynamic loading conditions were at similar damage states at the termination of testing to make direct comparisons.

However, comparisons of loading envelopes of both low and high reinforcement ratio wall specimens that were tested under dynamic loading conditions indicated slightly higher levels of loading closer to ultimate capacity as compared to the loading curves of the wall specimens tested under quasi-static loading conditions.

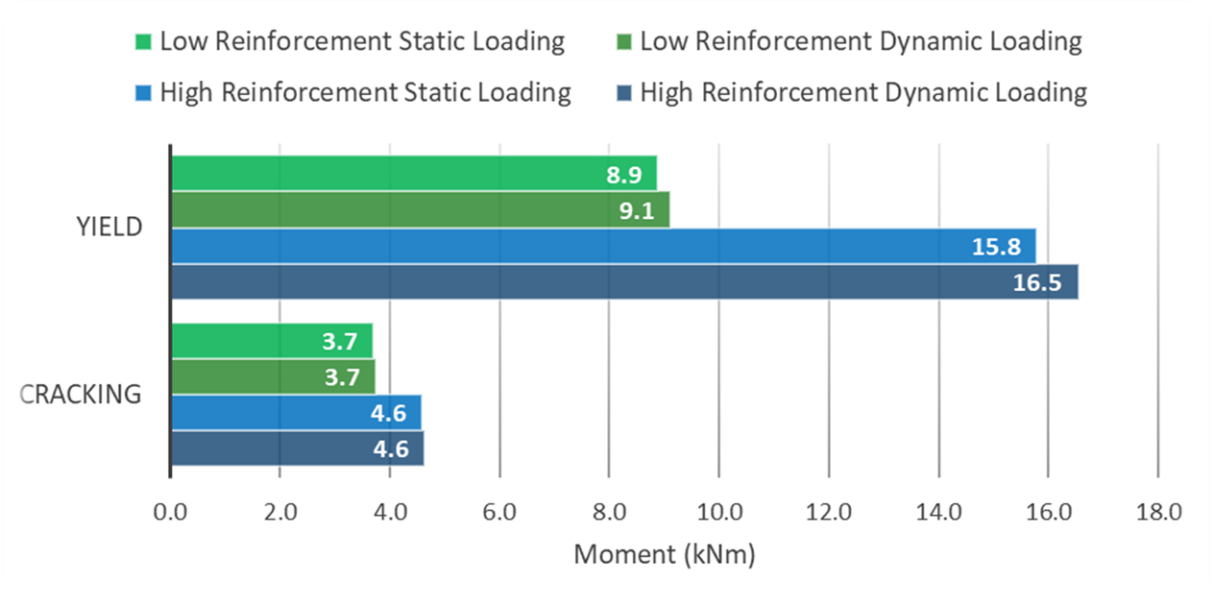

Figure 4.31: Summary of moment results at cracking and yielding conditions

On the other hand, both the low and high reinforcement ratio wall specimens exhibited similar cracking loads under both quasi-static and dynamic loading conditions. This difference in behaviour between the two damage states of the wall specimens may indicate the influence of different damage mechanisms under realistic wind loading conditions. The damage mechanism at yielding may be influenced by the rate of loading of the reinforcing steel, whereas cracking involves the loss of bond between the mortar and concrete block surface.

4.8.3 Deflection Comparison between Quasi-static vs. Dynamic Loading

Figure 4.32 summarises the mid-height deflection results of the wall specimens at the specific damage states of cracking and yield capacity. Both the low and high reinforcement ratio wall specimens indicated higher levels of deflection at higher intensity loading under dynamic wind loading conditions, as compared to quasi-static loading conditions.

There was enough evidence to indicate a statistically significant difference in the deflection at yield load between the wall specimens tested under quasi-static and dynamic loading conditions at a 90% confidence interval. The wall specimens indicated higher levels of deflection under dynamic loading conditions, as compared to quasi-static loading conditions at yield load. The low reinforcement ratio wall specimens showed an increase in mid-height deflection of 20%, whereas the high reinforcement ratio wall specimen showed an increase in mid-height deflection of 10% under dynamic loading conditions.

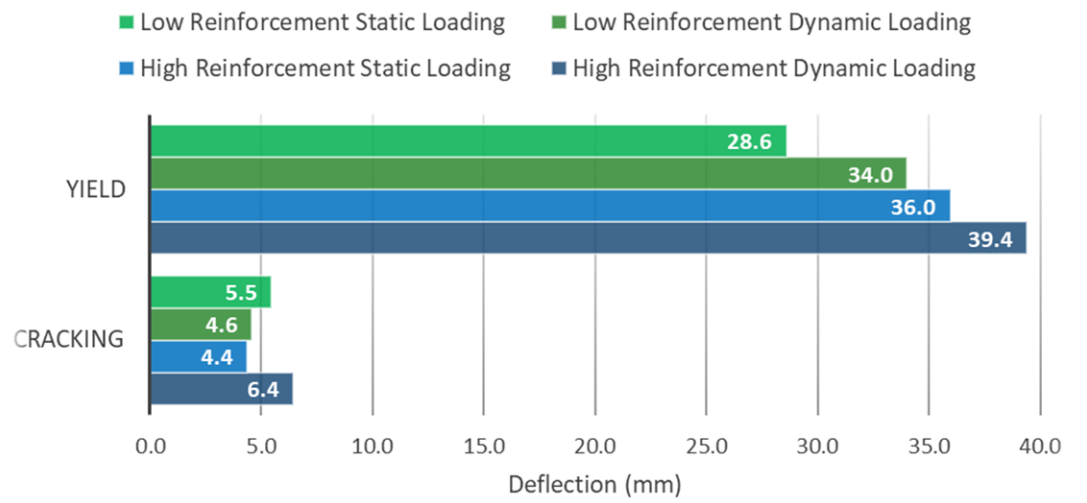

Figure 4.32: Summary of deflection results at cracking and yielding conditions

However, at cracking load, the low reinforcement ratio wall specimens indicated a slightly lower mid-height deflection under dynamic loading conditions, while the high reinforcement ratio wall specimen indicated a slightly higher mid-height deflection. These differences were not statistically significant at a 90% confidence interval and likely due to the deflection measurements being skewed due to unintended initial displacements of the test setup. Specifically, due to limitations of the support configuration, there was a slight horizontal movement at the start of loading. Although the resulting error was minor, as the deflection measurement at cracking itself was comparatively smaller, the initial horizontal displacement may have had significant impact on the overall deflection values at cracking load.

4.8.4 Low vs. High Reinforcement Ratio Wall Specimens

Overall, the relative performance under quasi-static and dynamic loading conditions was similar for both the low and high reinforcement ratio wall specimens. The results indicate that both low and high reinforced masonry walls resisted somewhat higher peak loads and higher levels of ductility under realistic wind loading conditions, as compared to those for quasi-static loading conditions. However, the low reinforcement ratio wall specimens did indicate higher overall levels of ductility compared to the high reinforcement ratio wall specimens under both types of loading conditions. On the other hand, the reinforcement ratio did not appear to influence first cracking behaviour, which was found to be similar under both quasi-static and dynamic loading conditions for both levels of reinforcement.

The high reinforcement ratio wall specimens indicated a slightly higher difference in yield capacity between the two types of loading than the low reinforcement ratio wall specimens. On the other hand, due to previously mentioned limitations with the load controller, the dynamic load applied to the lower reinforcement ratio wall specimens featured less high frequency content as compared to that applied to the higher reinforcement ratio wall specimens, which may also have contributed to this difference. On the other hand, the similarities in the behaviour between the low and high reinforcement ratio wall specimens, in view of the limitation in dynamic loading, may also indicate that the higher frequency content of the realistic wind loading had little influence on their overall behaviour. It may have also been the case that the difference in the level of reinforcement was not significant to a degree necessary to more clearly indicate a difference in behaviour characteristics.

To comply with design standard requirements, and to ensure under-reinforced sections, the two levels of reinforcement chosen for the wall specimens were the most feasible options.

Additionally, the wall specimens exhibited a difference in cracking load between the low and high reinforcement ratio wall specimens of 24%. This difference may likely be attributed to the difference in material used, as the low and high reinforcement ratio wall specimens were constructed during two separate phases. Specifically, a difference in the mortar used and in the curing conditions may have led to the difference in cracking load between the low and high reinforcement ratio wall specimens since the reinforcement would not have been effectively engaged at that point.

Chapter 5: Summary and Conclusions

5.1 Summary

Twenty large-scale wall specimens were tested under quasi-static and realistic dynamic wind loading conditions. The wall specimens had the same geometric design with the only difference being the level of reinforcement that was provided. As such, ten wall specimens had a lower reinforcement ratio (approximately 0.5%) and ten wall specimens had a comparatively higher reinforcement ratio (approximately 1.1%); both wall types were subjected to the two types of loading conditions. In summary, the experimental program consisted of testing four sets of wall specimens, each with five replicate wall specimens, comprising all possible combinations of the two primary test variables: quasi-static vs. dynamic wind load conditions, and low vs. high reinforcement ratios.

The wall specimens were tested under idealized pinned support conditions. A four-point loading arrangement was used to approximate the uniform loading conditions, with the load being applied to the wall specimens using a hydraulic actuator. The wall specimens were tested under both quasi-static monotonically increasing loads (representative of a static pressure load) and dynamic load time histories (representative of a realistic wind load). The quasi-static testing was carried out under displacement control, while the dynamic testing was carried out under load control. The wall specimens were loaded beyond their yield capacity, but the testing was halted once their deformation reached the feasible limits of the test setup.

The realistic wind loading was simulated using series of dynamic load time histories with increasing intensity, which were generated using a mathematical model. A 4^{th} order autoregressive function was used to generate the dynamic wind load time histories for a series of intensities. There were limitations in applying the dynamic loading to the wall specimens. Specifically, much of the high frequency content and the corresponding high peak loads were not applied as intended to the low reinforcement ratio wall specimens. Overall, though, the testing was carried out on both the

low and high reinforcement ratio wall specimens with adequate representation of both quasi-static and realistic dynamic wind loading conditions.

5.2 Conclusions

5.2.1 Quasi-static vs. Realistic Wind Loading Conditions

The reinforced masonry wall specimens exhibited similar flexural ductile modes of failure under both quasi-static and dynamic wind loading conditions. Both the low and high reinforcement ratio wall specimens indicated slightly higher levels of load bearing capacity and ductility at higher loading levels under dynamic wind loading conditions, as compared to quasi-static loading conditions. Although there was insufficient evidence to make statistically significant conclusions, the wall specimens indicated slightly higher strength and higher levels of deflection at yield capacity. The low reinforcement ratio wall specimens indicated a 3% increase in yield capacity at a 20% increase in deflection, while the high reinforcement ratio wall specimens indicated a 5% increase in yield capacity at a 10% increase in deflection, under dynamic wind loading conditions. On the other hand, both low and high reinforcement ratio wall specimens did not indicate a difference in load at the cracking load under the two types of loading conditions. The difference in the respective damage mechanisms may have had different influence on behavioural characteristics under realistic wind loading conditions. At higher loading capacities, the high rate of loading of the peak loads under dynamic loading conditions may have contributed to the apparent slight increase in load resistance of the reinforced wall specimens. Overall, though, the wall specimens tested under realistic wind loading conditions exhibited behavioural characteristics that were broadly similar to those observed under quasi-static loading conditions.

5.2.2 Low vs. High Reinforcement Ratio

Overall, both low and high reinforcement ratio wall specimens exhibited similar differences in behavioural characteristics under dynamic loading conditions, as compared to quasi-static loading conditions. However, the high reinforcement ratio wall specimens indicated a slightly higher increase in strength at yield capacity under dynamic wind loading conditions, compared to the low reinforcement ratio wall specimens. Likewise, the low reinforcement ratio wall specimens indicated higher increase in levels of ductility under dynamic wind loading conditions than the

high reinforcement ratio wall specimens. The difference in the levels of reinforcement may have accounted for this difference in behaviour between the low and high reinforcement ratio wall specimens. However, the observed differences may also be attributed to the limitations with the applied dynamic loading, as the dynamic load applied to the lower reinforcement ratio wall specimens featured less high frequency content and lower peak loads as compared that applied to the higher reinforcement ratio wall specimens. Overall, the results indicated that the levels of reinforcement did not have significant impact on the behavioural characteristics of reinforced masonry walls under realistic wind loading conditions.

5.3 Recommendations for Future Research

Additional gaps in knowledge were identified after this study. The following are several recommendations for future research that may help clarify the behaviour characteristics of reinforced masonry walls under realistic dynamic wind loading conditions.

Due to limitations with the test setup, the behaviour of reinforced masonry walls at ultimate loading capacity could not be adequately investigated. The study indicated differences in behaviour characteristics at different damage states of the wall specimens under realistic wind loading conditions. As such, further study into the behaviour of reinforced masonry walls at higher capacities is recommended.

Furthermore, the majority of masonry structures in practice are not supported under ideally pinned support conditions. Under realistic support conditions, which was not within the scope of this study, additional mechanisms such as arching may come into play. Therefore, behavioural characteristics of reinforced masonry walls under realistic support conditions would warrant further investigation under realistic wind loading conditions.

References

Abboud, B. E., Hamid, A. A., and Harris, H. G. (1996). Flexural behavior of reinforced concrete masonry walls under out-of-plane monotonic loads. *ACI Structural Journal, 93*(3), 327-335.

Albert, M. L., Elwi, A. E., and Cheng, J. J. R. (2001). Strengthening of unreinforced masonry walls using FRPs. *Journal of Composites for Construction, 5*(2), 76-84. doi:10.1061/(ASCE)1090-0268(2001)5:2(76)

ASTM International (ASTM). (2012). ASTM A615-12 Standard Specification for Deformed and Plain Carbon-Steel Bars for Concrete Reinforcement. ASTM, West Conshohocken, PA, United States.

ASTM International (ASTM). (2014). ASTM C1019-14 Standard Test Method for Sampling and Testing Grout. ASTM, West Conshohocken, PA, United States.

ASTM International (ASTM). (2012). ASTM C1717-12 Standard Test Methods for Conducting Strength Tests of Masonry Wall Panels. ASTM, West Conshohocken, PA, United States.

ASTM International (ASTM). (2015). ASTM E72-15 Standard Test Methods of Conducting Strength Tests of Panels for Building Construction. ASTM, West Conshohocken, PA, United States.

Bean Popehn, J. R., Schultz, A. E., Lu, M., Stolarski, H. K., and Ojard, N. J. (2008). Influence of transverse loading on the stability of slender unreinforced masonry walls. *Engineering Structures, 30*(10), 2830-2839. doi:10.1016/j.engstruct.2008.02.016

Burnett, S., Gilbert, M., Molyneaux, T., Tyas, A., Hobbs, B., and Beattie, G. (2007). The response of masonry joints to dynamic tensile loading. *Materials and Structures*, 40: 517-527.

Canadian Standards Association (CSA). (2004). CSA A165-04 CSA Standards on Concrete Masonry Units. Canadian Standards Association, Mississauga, ON Canada.

Canadian Standards Association (CSA). (2014). CSA A179-14 Mortar and Grout for Unit Masonry. Canadian Standards Association, Mississauga, ON Canada.

Canadian Standards Association (CSA). (2004). CSA A371-04 Masonry Construction for Buildings. Canadian Standards Association, Mississauga, ON Canada.

Canadian Standards Association (CSA). (2014). CSA S304.1-04 Design of masonry structures. Canadian Standards Association, Mississauga, ON Canada.

Drysdale, R. G., and Hamid, A. A. (2005). Masonry Structures: Behaviour and Design. Missisauga: Canadian Edition, Canadian Masonry Design Centre.

Galal, K., and Sasanian, N. (2010). Out-of- plane flexural performance of GFRP- reinforced masonry walls. *Journal of Composites for Construction, 14*(2), 162-174. doi:10.1061/(ASCE)CC.1943-5614.0000061

Gani, F., and Legeron, F. (2010). Dynamic response of transmission lines guyed towers under wind loading.(Report). *Canadian Journal of Civil Engineering, 37*(3), 450.

Griffith, M. C., Lam, N. T. K., Wilson, J. L., and Doherty, K. (2004). Experimental investigation of unreinforced brick masonry walls in flexure. *Journal of Structural Engineering, 130*(3), 423-432. doi:10.1061/(ASCE)0733-9445(2004)130:3(423)

Hamoush, S. A., McGinley, M. W., Mlakar, P., Scott, D., and Murray, K. (2001). Out-of- plane strengthening of masonry walls with reinforced composites. *Journal of Composites for Construction, 5*(3), 139-145. doi:10.1061/(ASCE)1090-0268(2001)5:3(139)

Henderson, D. J., and Ginger, J. D. (2011). Response of pierced fixed corrugated steel roofing systems subjected to wind loads. *Engineering Structures, 33*(12), 3290-3298. doi:10.1016/j.engstruct.2011.08.020

Hoeppner, C. R., Sparling, B. F., Wegner, L. D., and Sakr, K. (2002). CFRP reinforced masonry walls subjected to out-of-plane loading In Proceedings of 4th Structural Specialty Conference of the Canadian Society for Civil Engineering, Montreal, Quebec, Canada, 5-8 June 2002. (Vol. 2002, pp. 1889-1898).

Juhásová, E. (1997). Quasi-static versus dynamic space wind response of slender structures. *Journal of Wind Engineering and Industrial Aerodynamics, 69*, 757-766. doi:10.1016/S0167-6105(97)00203-1

Kaimal, J.C., Wyngaard, J.C., Izumi, Y., and Coté, O.R. (1972). Spectral characteristics of surface-layer turbulence. *Quarterly Journal of the Royal Meteorological Society*, 98: 563-589.

Kopp, G. A., Morrison, M. J., and Henderson, D. J. (2012). Full- scale testing of low- rise, residential buildings with realistic wind loads. *Journal of Wind Engineering and Industrial Aerodynamics, 104-106*, 25-39. doi:10.1016/j.jweia.2012.01.004

Morrison, M. J., and Kopp, G. A. (2011). Performance of toe- nail connections under realistic wind loading. *Engineering Structures, 33*(1), 69-76. doi:10.1016/j.engstruct.2010.09.019

National Research Council Canada (NRC). 2010. National Building Code of Canada. NRC, Ottawa, ON, Canada.

Simiu, E., and Scanlan, R.H. (1987). Wind Effects on Structures. John Wiley and Sons, Inc., Hoboken, N.J. USA.

Sparling, B.F., (1995). The dynamic behaviour of guys and guyed masts in turbulent winds. Ph.D. thesis, Deparment of Civil Engineering, The University of Western Ontario, London, Ontario.

Sparling, B., and Davenport, A. (1998). Three-dimensional dynamic response of guyed towers to wind turbulence. *Canadian Journal of Civil Engineering, 25*(3), 512-525.

Surry, D., Ho, T. C. E., Farquhar, S., Kopp, G. A., Sinno, R. R., and Nail, B. (2007). Structurally effective static wind loads for roof panels. *Journal of Structural Engineering, 133*(6), 871-885. doi:10.1061/(ASCE)0733-9445(2007)133:6(871)

Tercelj, S., Sheppard, P., and Tumsek, V. (1973). "The influence of frequency on the shear strength and ductility ofmasonry walls in dynamic loading tests." Proc.• 6th World Cont on Earthquake Engrg., Int. Assn. for Earthquake Engrg., 3, 2992-2999.

Tomazevic, M., Lutman, M., and Petkovic, L. (1996). Seismic behavior of masonry walls: experimental simulation. *Journal of Structural Engineering, 122*(9), 1040.

Williams, D., and Scrivener, J. C. (1974). "Response of reinforced masonry shear walls to static and dynamic cyclic loading." Proc.• 5th World Cont on Earthquake Engrg., Int. Assn. for Earthquake Engrg., 2, 1491-1494.

Zielinski, A.J., and Reinhardt, H.W. 1982. Stress-Strain behaviour of concrete and mortar at high rates of tensile loading. Cement and Concrete Research, 12(3): 309-319.

Appendix A: Load vs. Deflection Results of the Quasi-Static Tests

Appendix A contains the load vs. deflection diagrams of the wall specimens tested under quasi-static loading conditions. *Figure A.1* to *Figure A.5* depict the results of the wall specimens with the low reinforcement ratio, while *Figure A.6* to *Figure A.10* depict the results of the wall specimens with the high reinforcement ratio.

The load in the diagrams represents the total load applied by the MTS® Series 244 hydraulic actuator on the wall specimens. The load measurements were taken using the built-in force transducer of the actuator. The deflection in the diagrams represents the deflection at mid-height of the wall specimens. The deflection measurements were taken using the Micro-Epsilon optoNCDT 1700-500 laser optical displacement measurement device.

Load vs. Deflection Diagrams of the Low Reinforcement Ratio Specimens

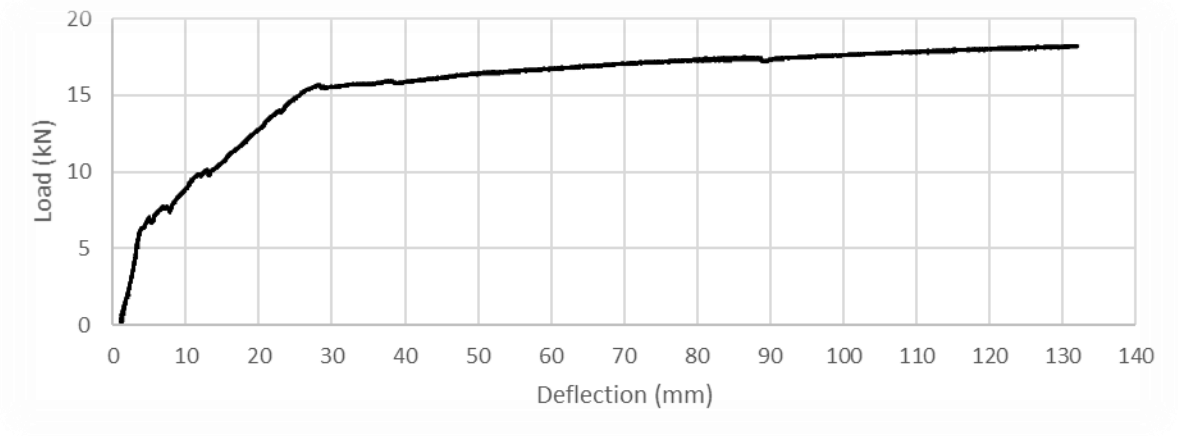

Figure A.1: Load vs. deflection diagram for specimen LS1

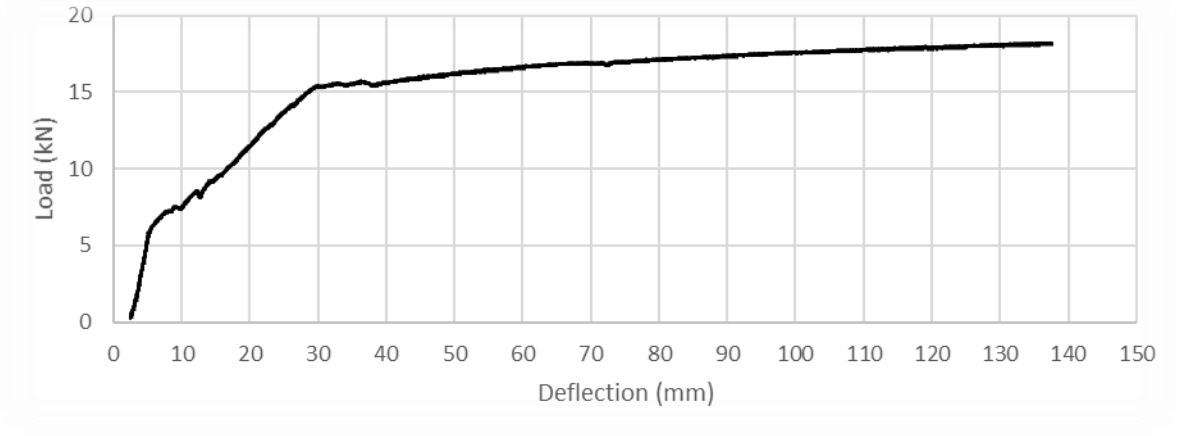

Figure A.2: Load vs. deflection diagram for specimen LS2

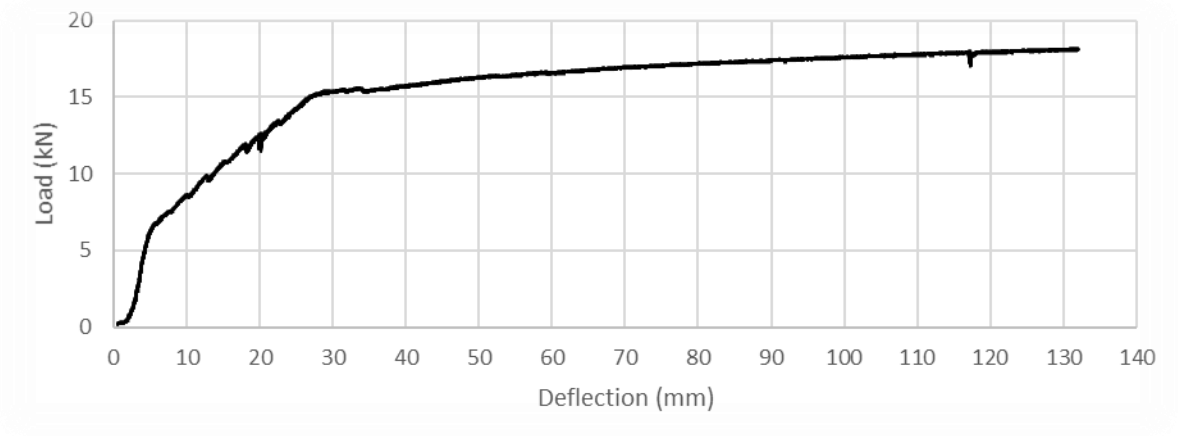

Figure A.3: Load vs. deflection diagram for specimen LS3

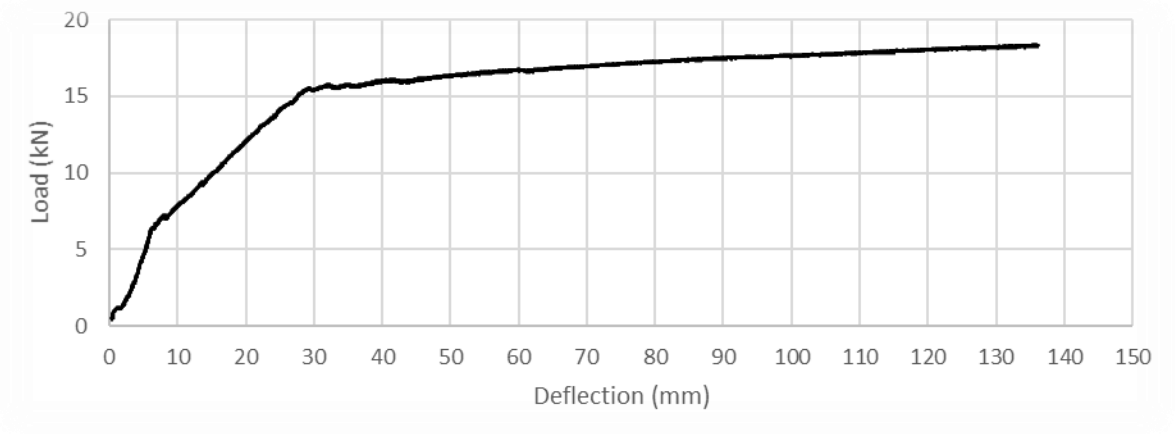

Figure A.4: Load vs. deflection diagram for specimen LS4

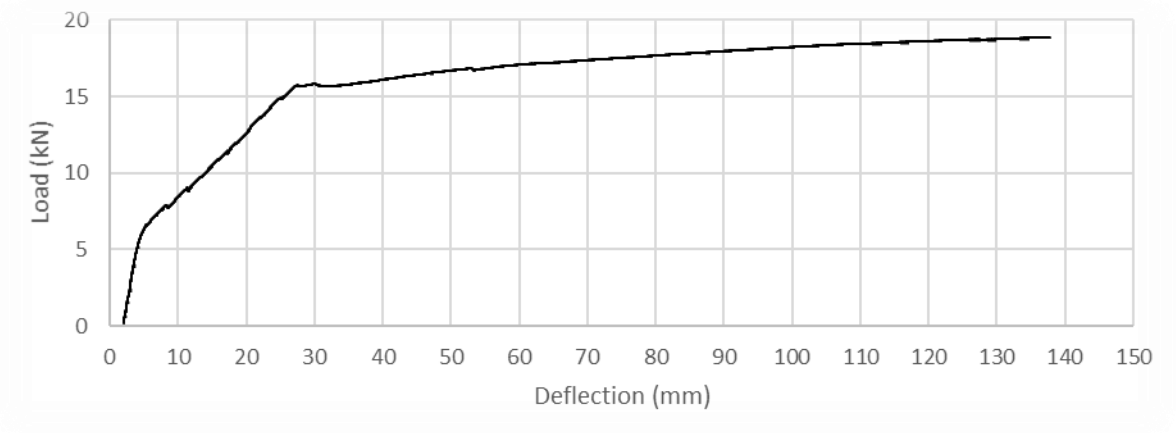

Figure A.5: Load vs. deflection diagram for specimen LS5

Load vs. Deflection Diagrams of the High Reinforcement Ratio Specimens

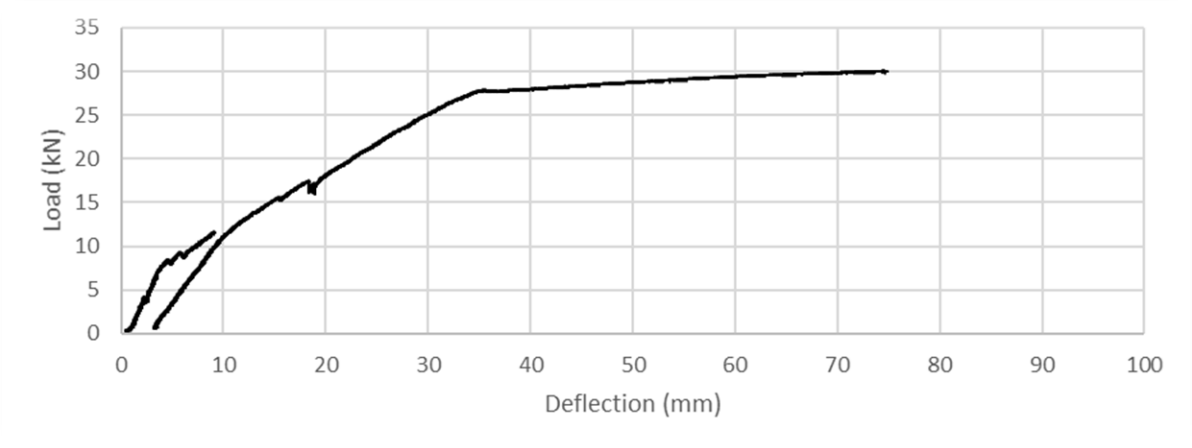

Figure A.6: Load vs. deflection diagram for specimen HS1

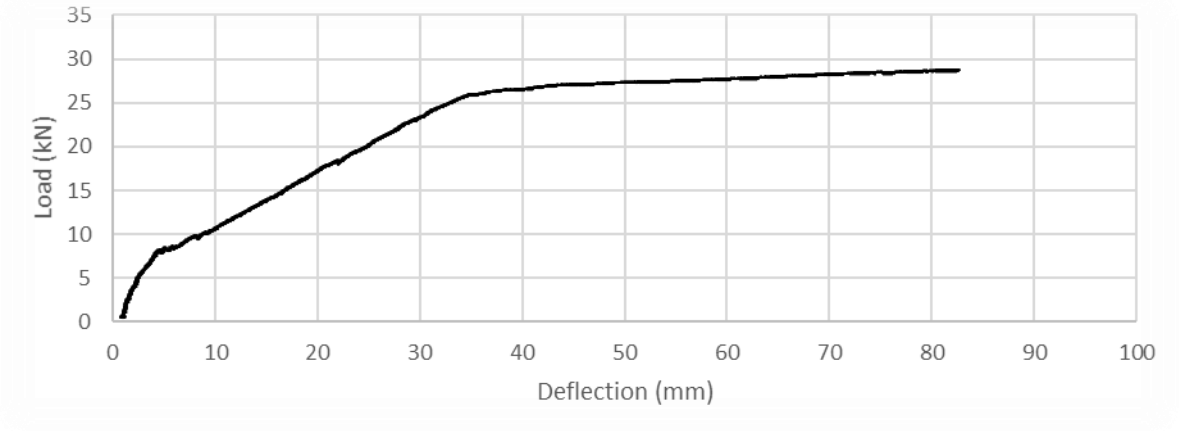

Figure A.7: Load vs. deflection diagram for specimen HS2

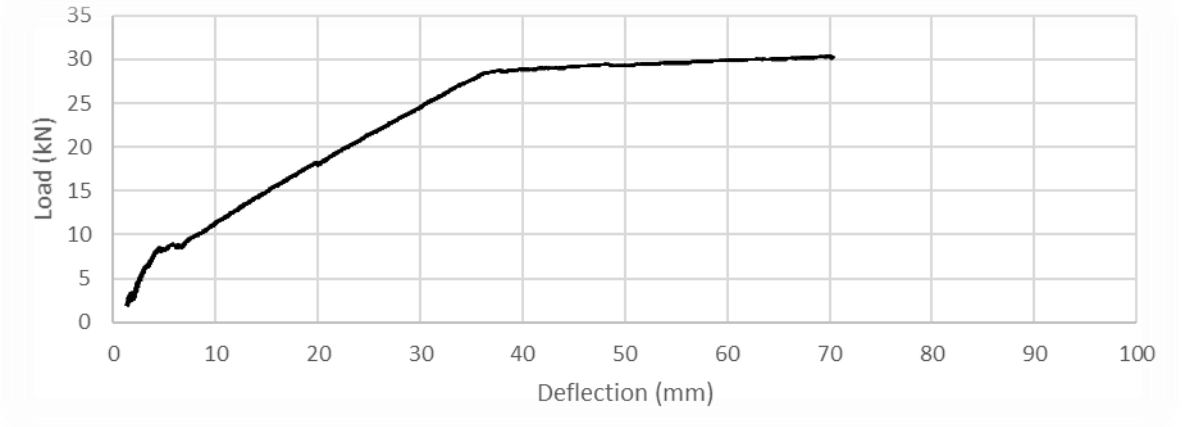

Figure A.8: Load vs. deflection diagram for specimen HS3

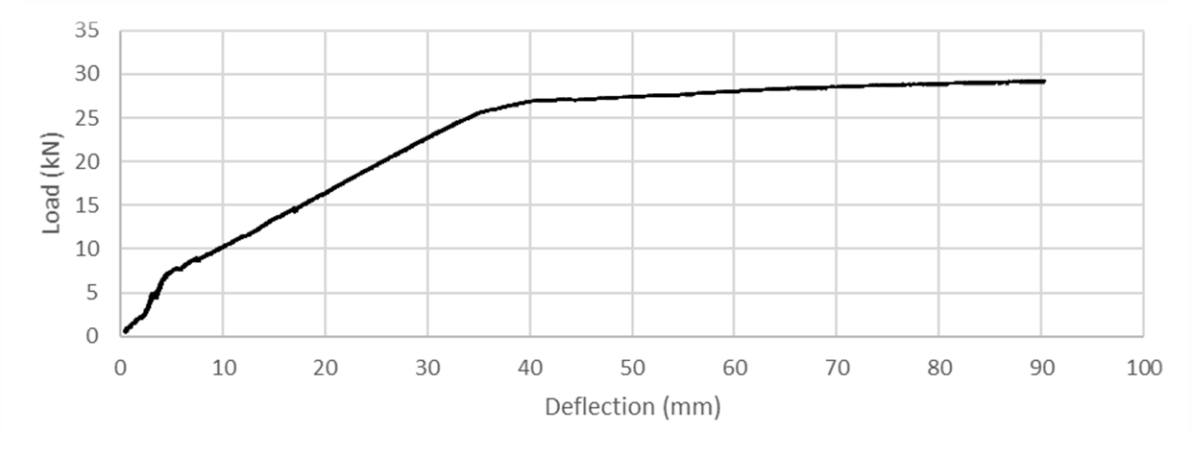

Figure A.9: Load vs. deflection diagram for specimen HS4

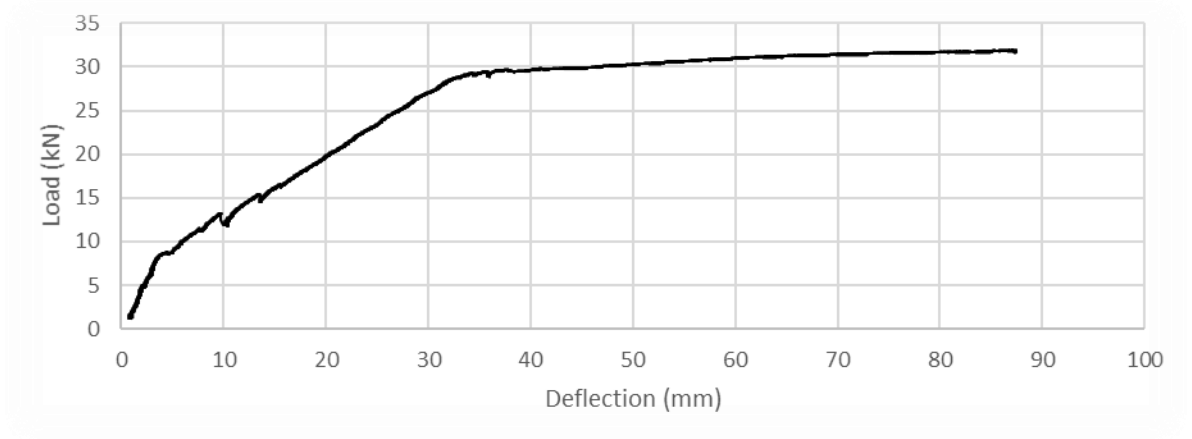

Figure A.10: Load vs. deflection diagram for specimen HS5

Appendix B: Modelled and Applied Dynamic Wind Load Time Histories

Appendix B contains the comparison between the modelled and applied load time histories of the wall specimens tested under dynamic loading conditions. *Figure B.1* to *Figure B.25* depict the plots for the wall specimens with the low reinforcement ratio, while *Figure B.26* to *Figure B.50* depict the plots for the wall specimens with the high reinforcement ratio.

The modelled load in the diagrams represents the wind load generated using the mathematical model described in Udey (2014). The applied load in the diagrams represents the total load applied by the MTS® Series 244 hydraulic actuator on the wall specimens. The measurements were taken using the built-in force transducer of the actuator.

Specimen LD1

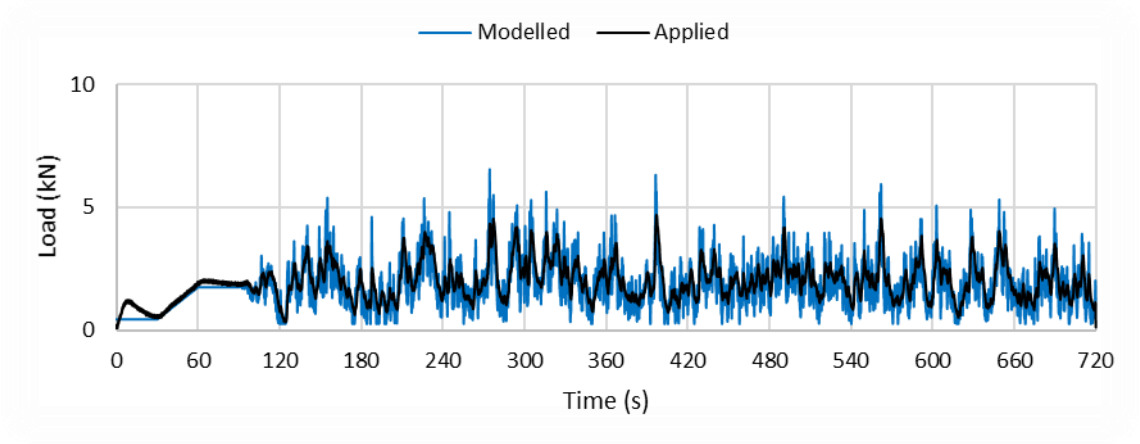

Figure B.1: Modelled and applied 30 m/s wind load time history for specimen LD1

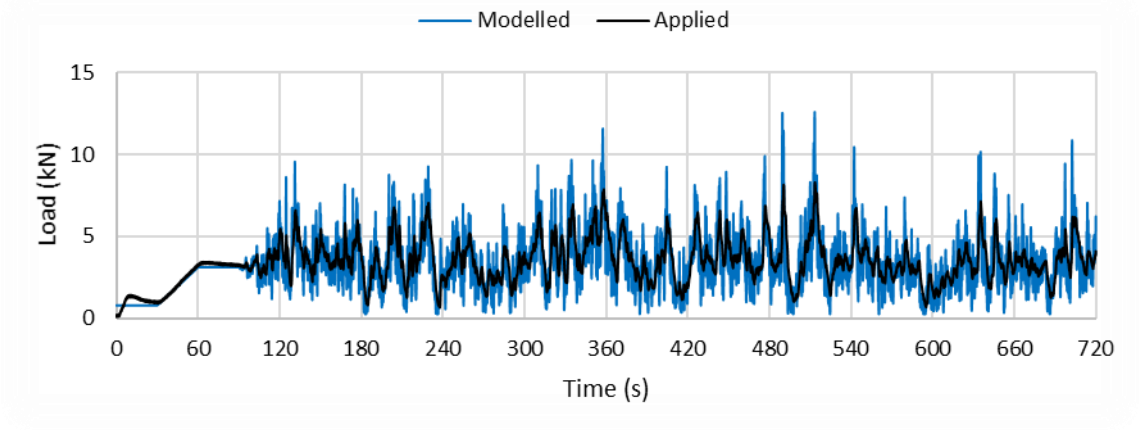

Figure B.2: Modelled and applied 40 m/s wind load time history for specimen LD1

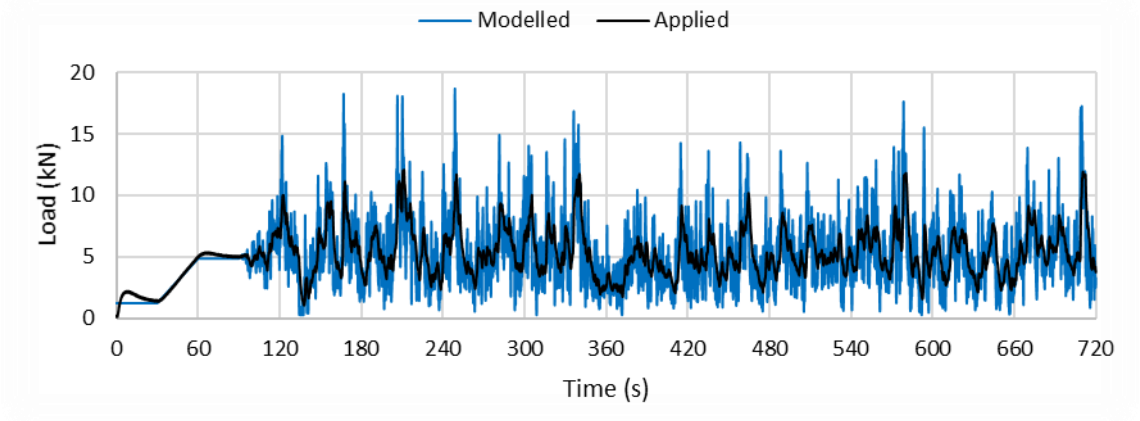

Figure B.3: Modelled and applied 50 m/s wind load time history for specimen LD1

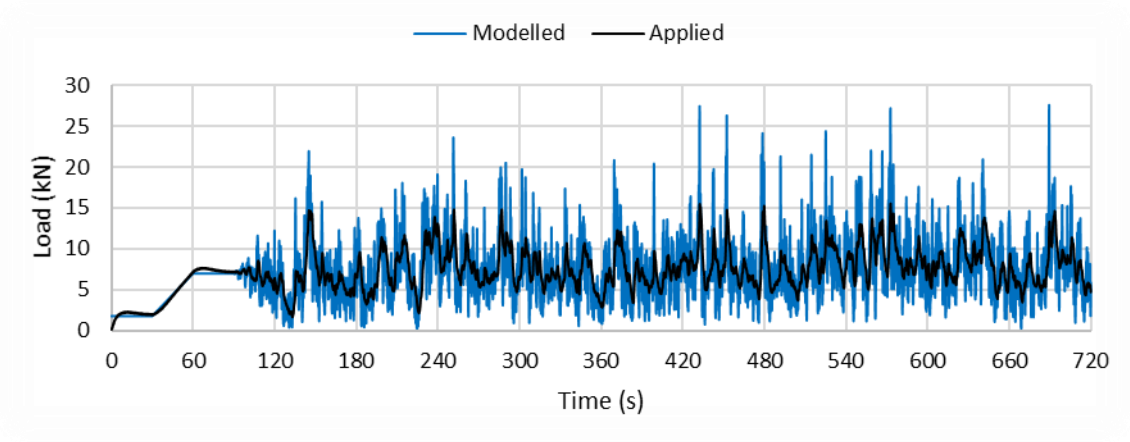

Figure B.4: Modelled and applied 60 m/s wind load time history for specimen LD1

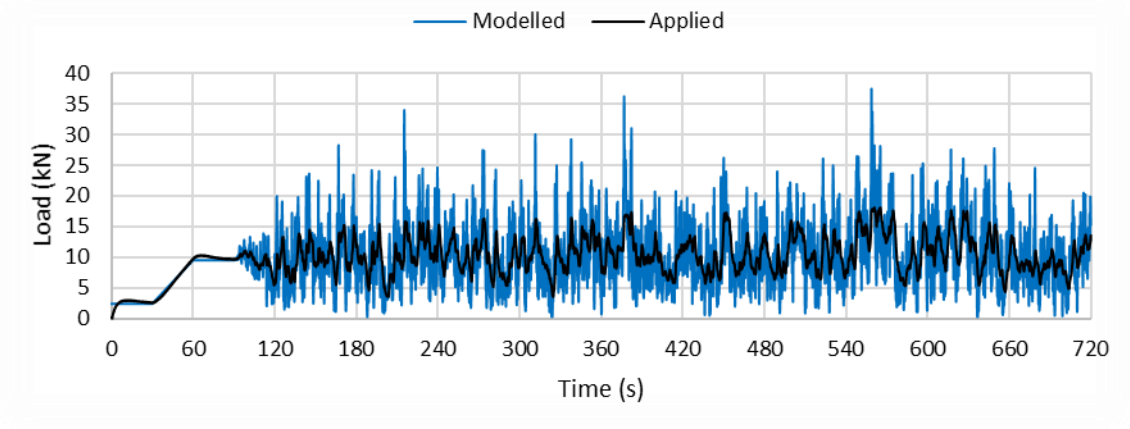

Figure B.5: Modelled and applied 70 m/s wind load time history for specimen LD1

Specimen LD2

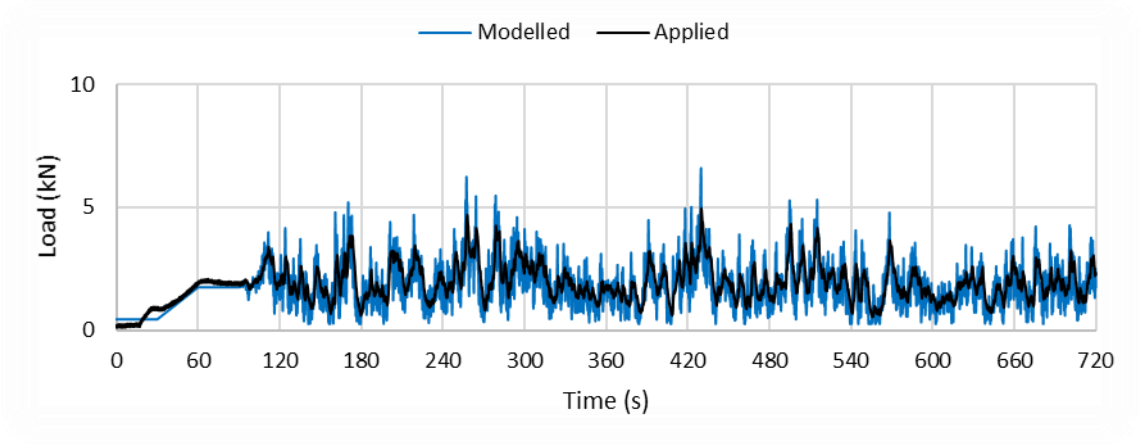

Figure B.6: Modelled and applied 30 m/s wind load time history for specimen LD2

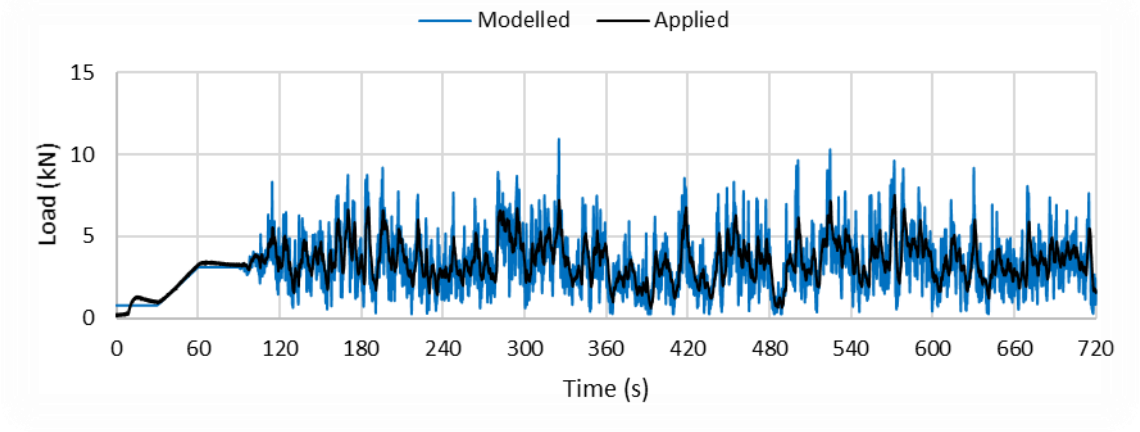

Figure B.7: Modelled and applied 40 m/s wind load time history for specimen LD2

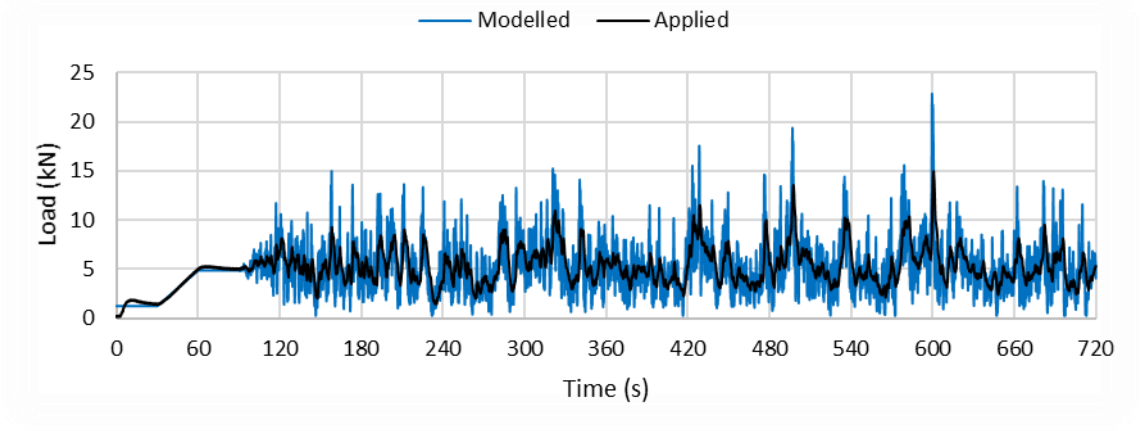

Figure B.8: Modelled and applied 50 m/s wind load time history for specimen LD2

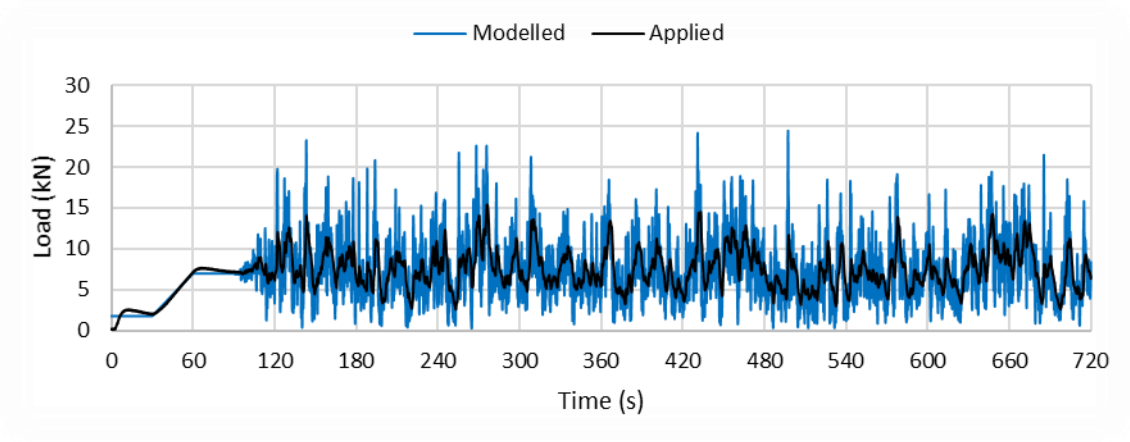

Figure B.9: Modelled and applied 60 m/s wind load time history for specimen LD2

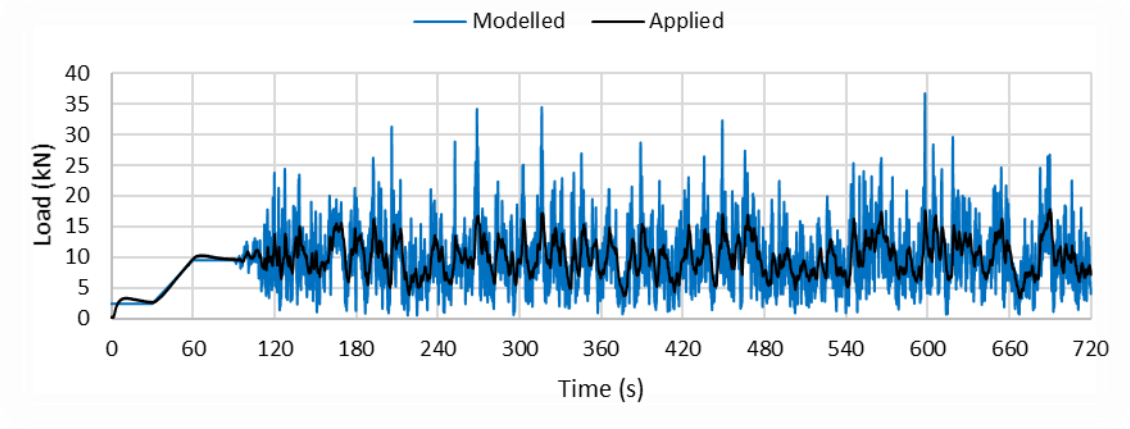

Figure B.10: Modelled and applied 70 m/s wind load time history for specimen LD2

Specimen LD3

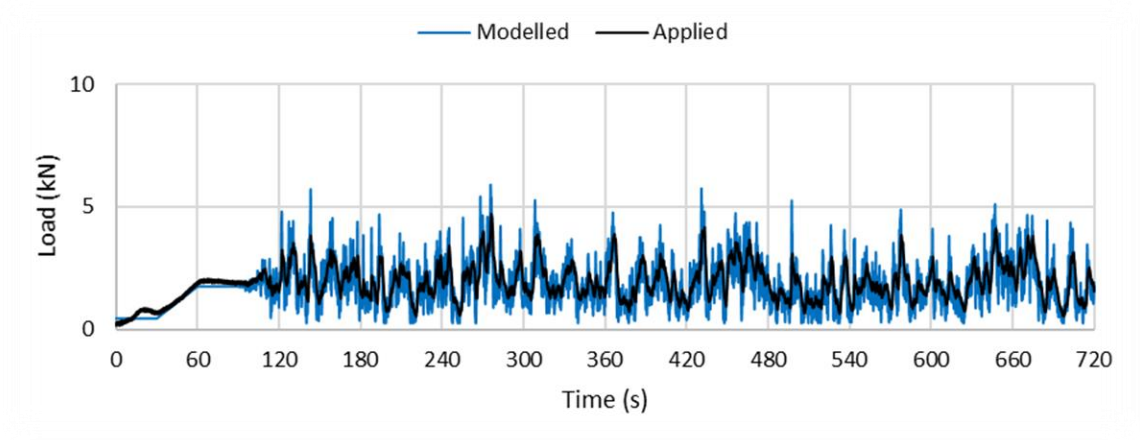

Figure B.11: Modelled and applied 30 m/s wind load time history for specimen LD3

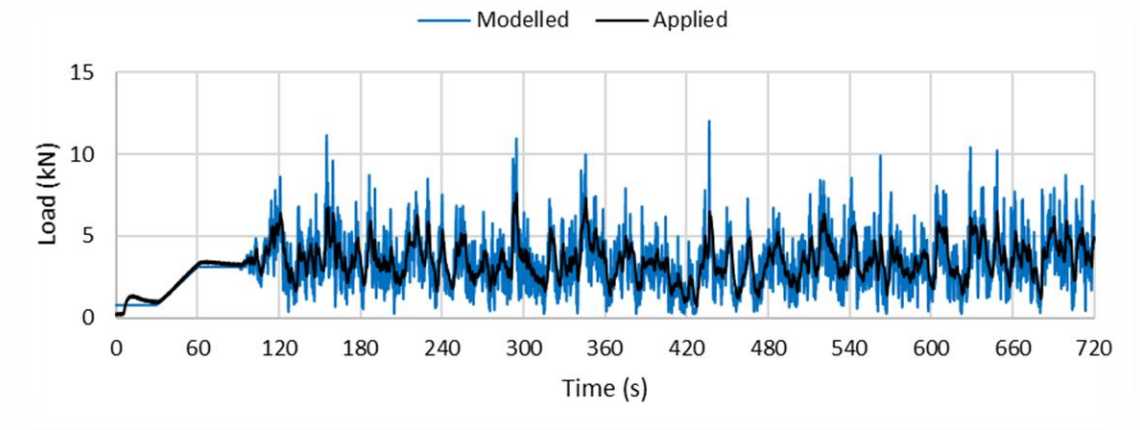

Figure B.12: Modelled and applied 40 m/s wind load time history for specimen LD3

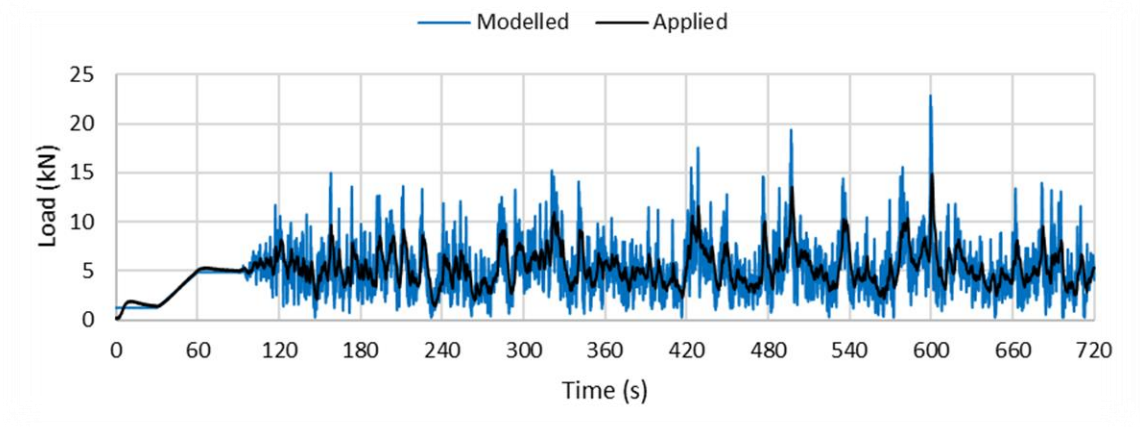

Figure B.13: Modelled and applied 50 m/s wind load time history for specimen LD3

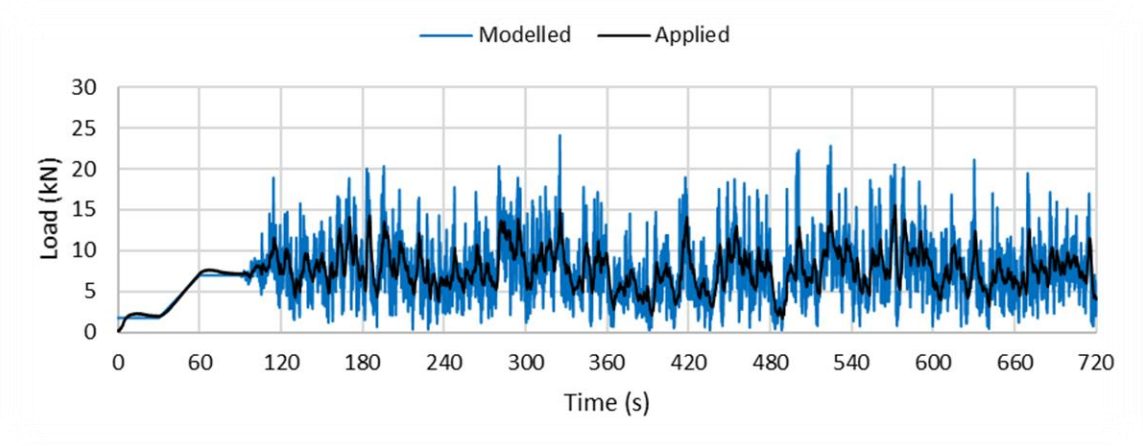

Figure B.14: Modelled and applied 60 m/s wind load time history for specimen LD3

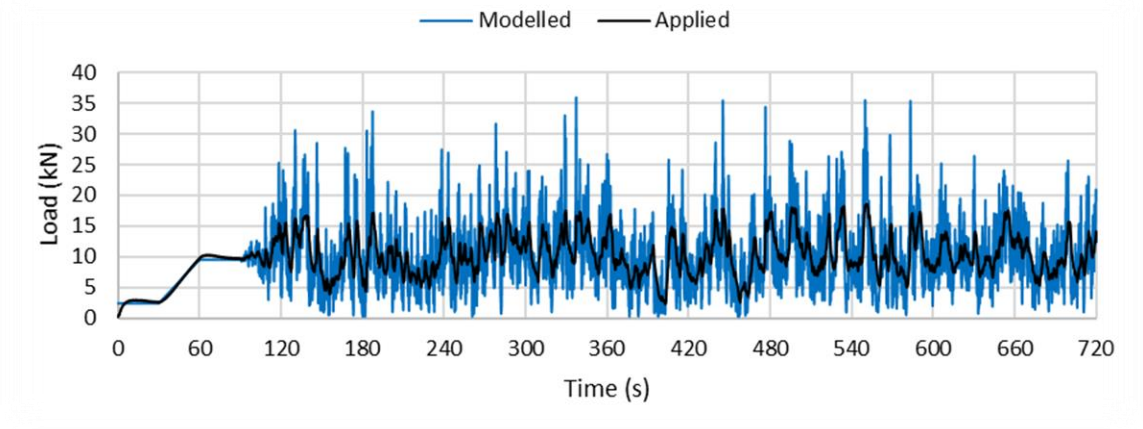

Figure B.15: Modelled and applied 70 m/s wind load time history for specimen LD3

Specimen LD4

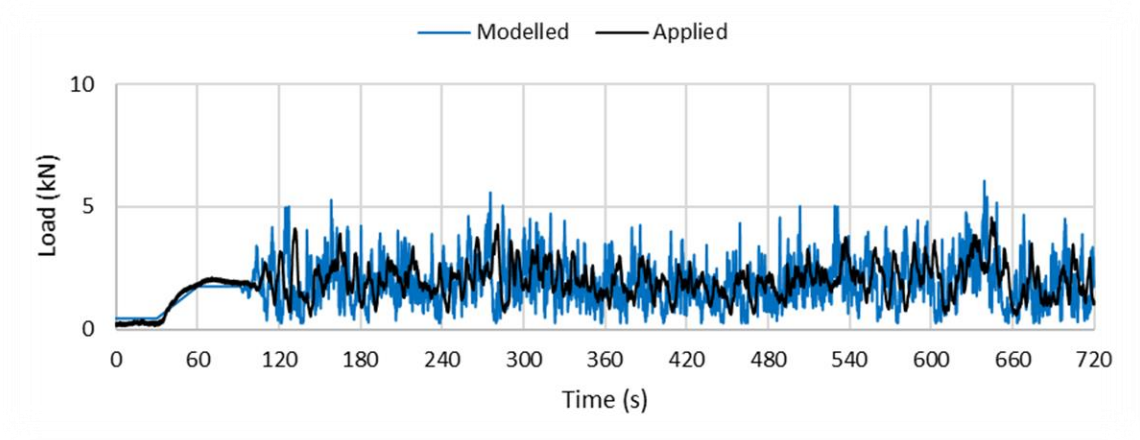

Figure B.16: Modelled and applied 30 m/s wind load time history for specimen LD4

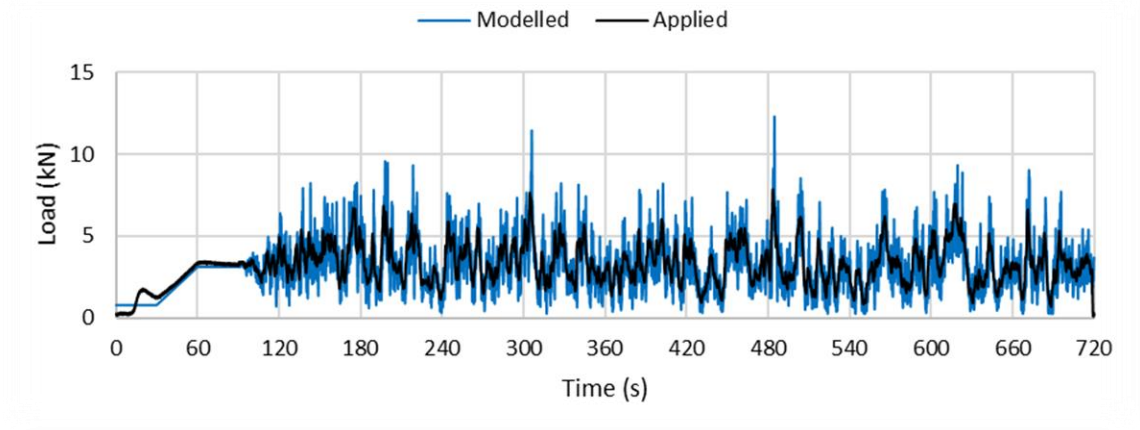

Figure B.17: Modelled and applied 40 m/s wind load time history for specimen LD4

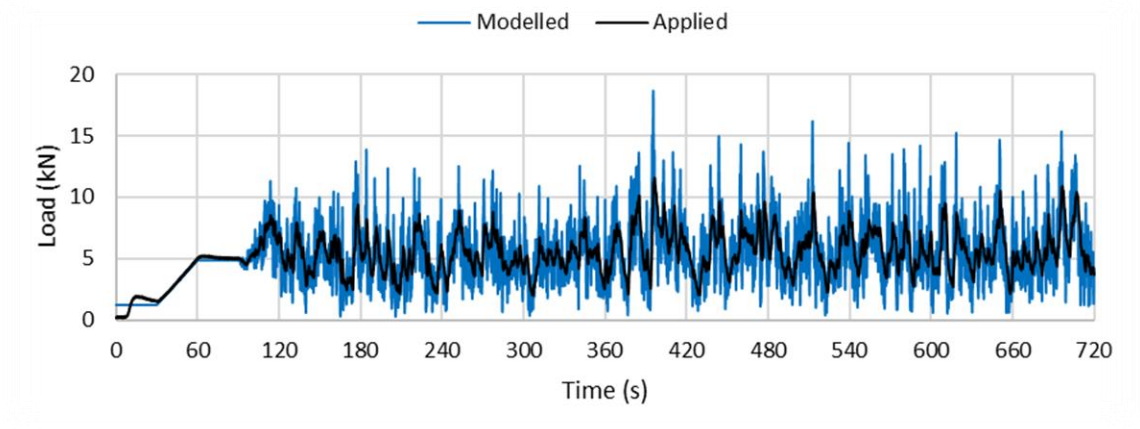

Figure B.18: Modelled and applied 50 m/s wind load time history for specimen LD4

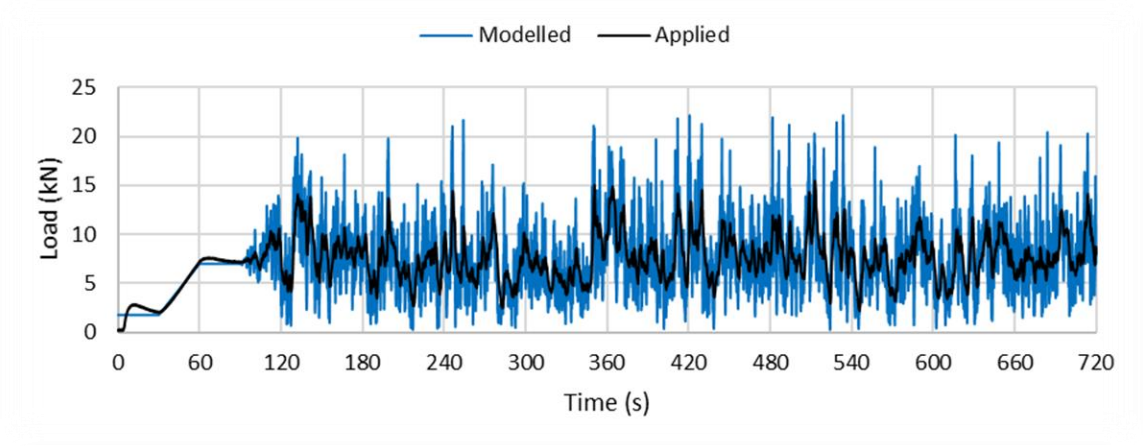

Figure B.19: Modelled and applied 60 m/s wind load time history for specimen LD4

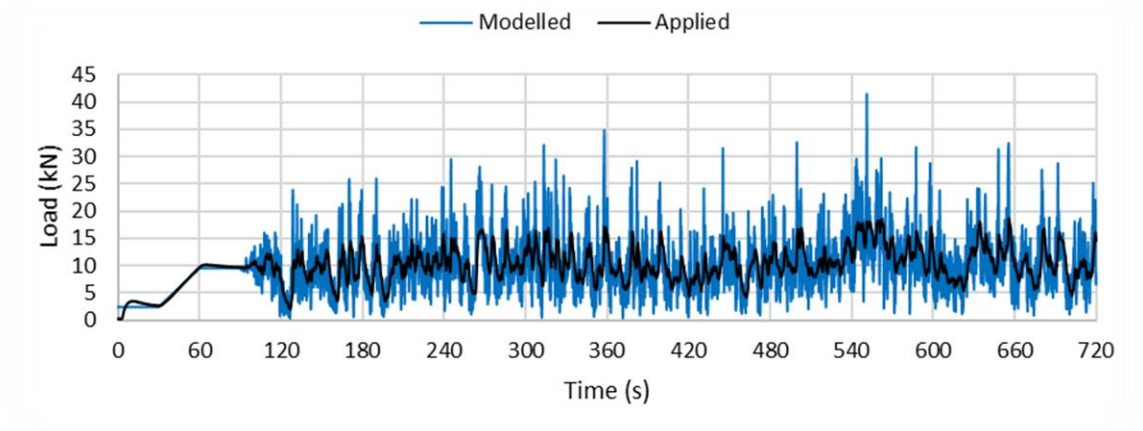

Figure B.20: Modelled and applied 70 m/s wind load time history for specimen LD4

Specimen LD5

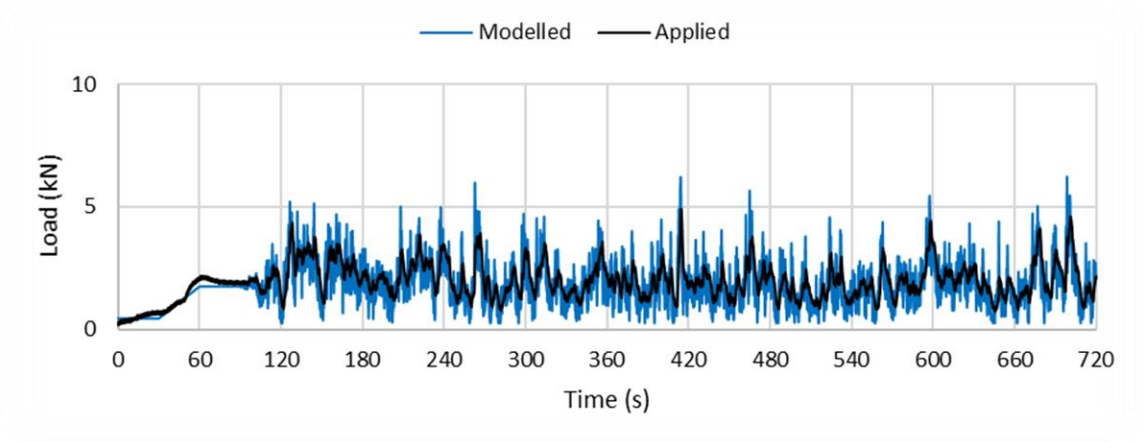

Figure B.21: Modelled and applied 30 m/s wind load time history for specimen LD5

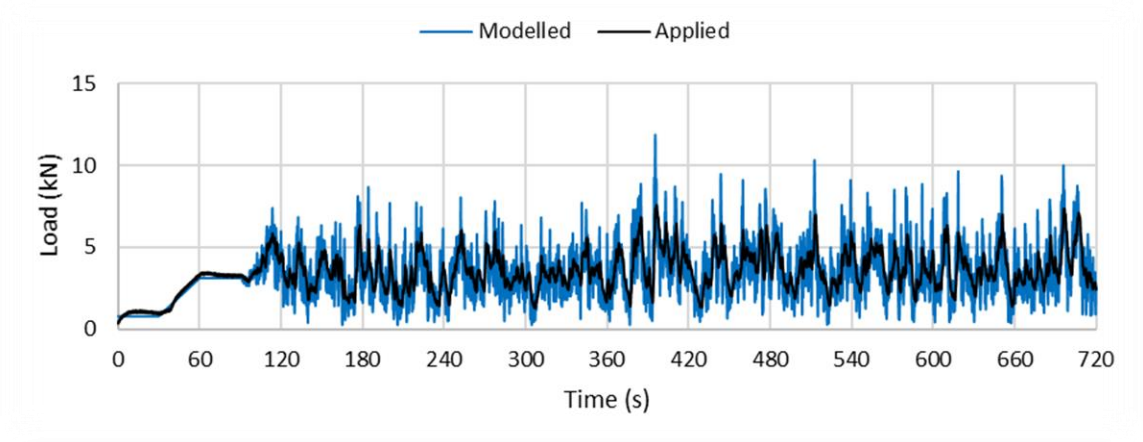

Figure B.22: Modelled and applied 40 m/s wind load time history for specimen LD5

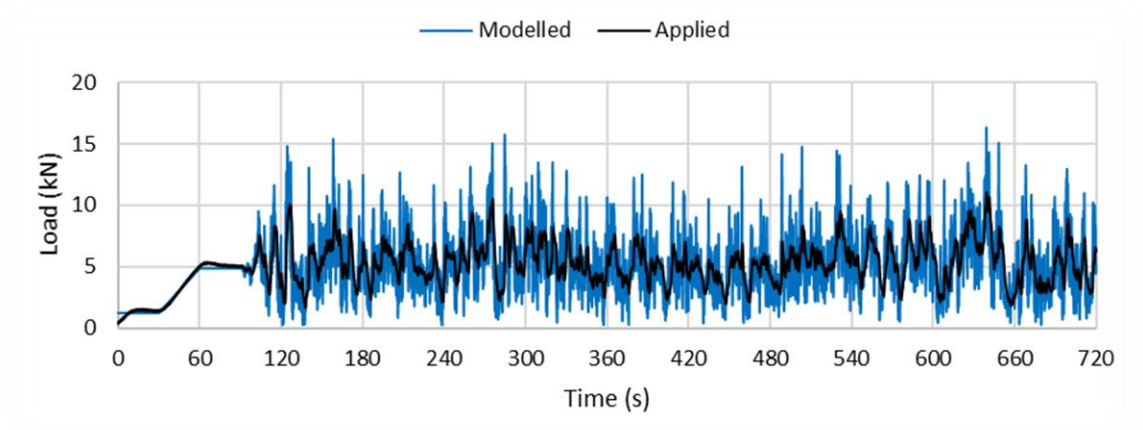

Figure B.23: Modelled and applied 50 m/s wind load time history for specimen LD5

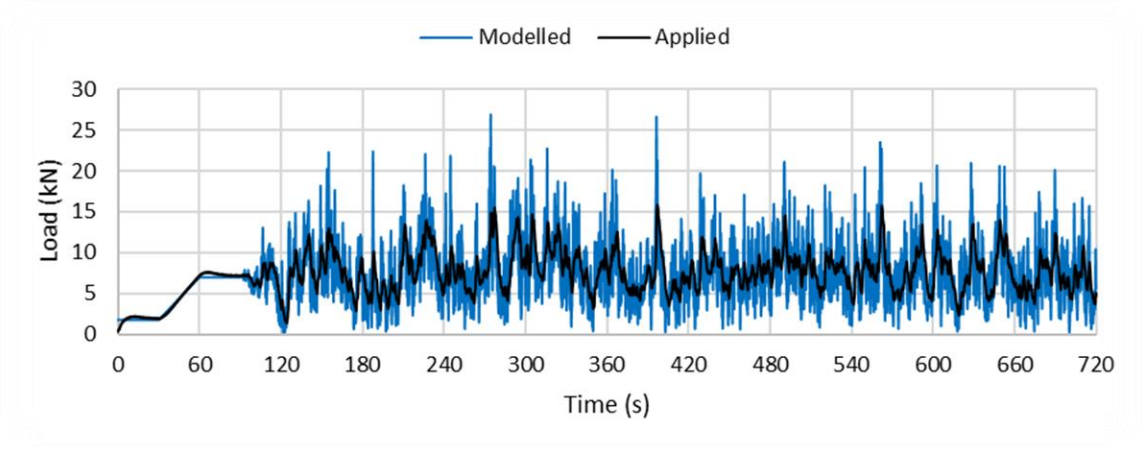

Figure B.24: Modelled and applied 60 m/s wind load time history for specimen LD5

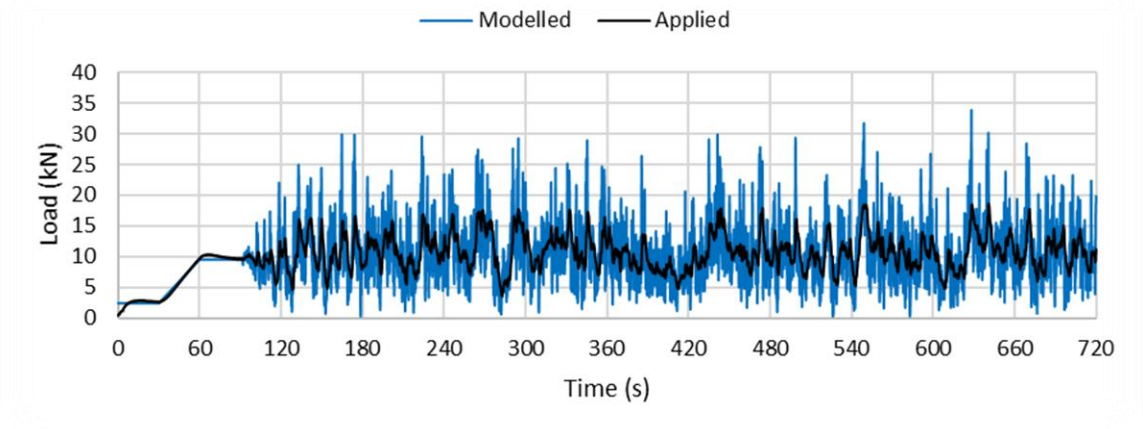

Figure B.25: Modelled and applied 70 m/s wind load time history for specimen LD5

Specimen HD1

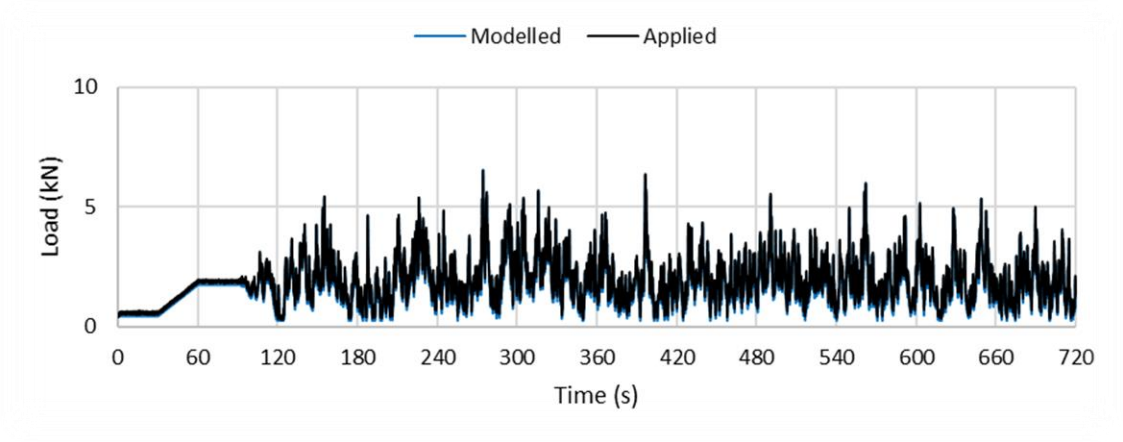

Figure B.26: Modelled and applied 30 m/s wind load time history for specimen HD1

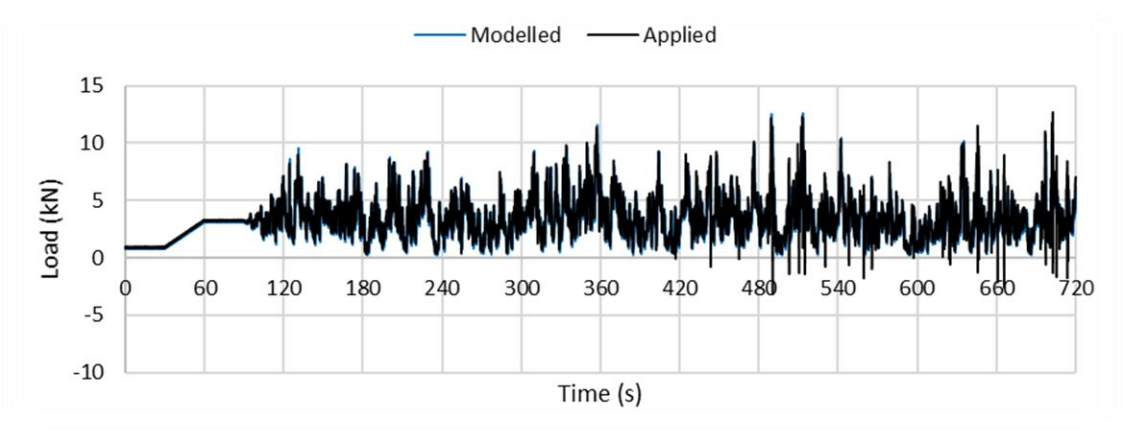

Figure B.27: Modelled and applied 40 m/s wind load time history for specimen HD1

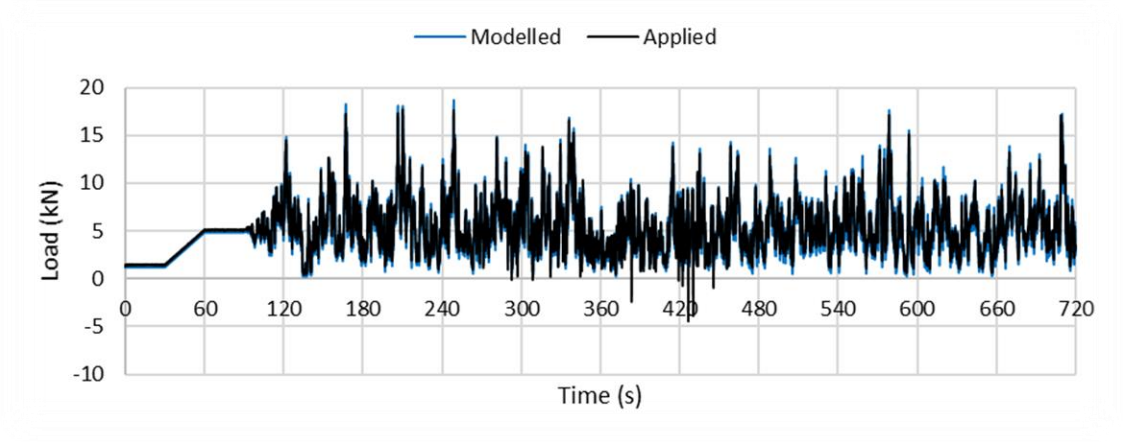

Figure B.28: Modelled and applied 50 m/s wind load time history for specimen HD1

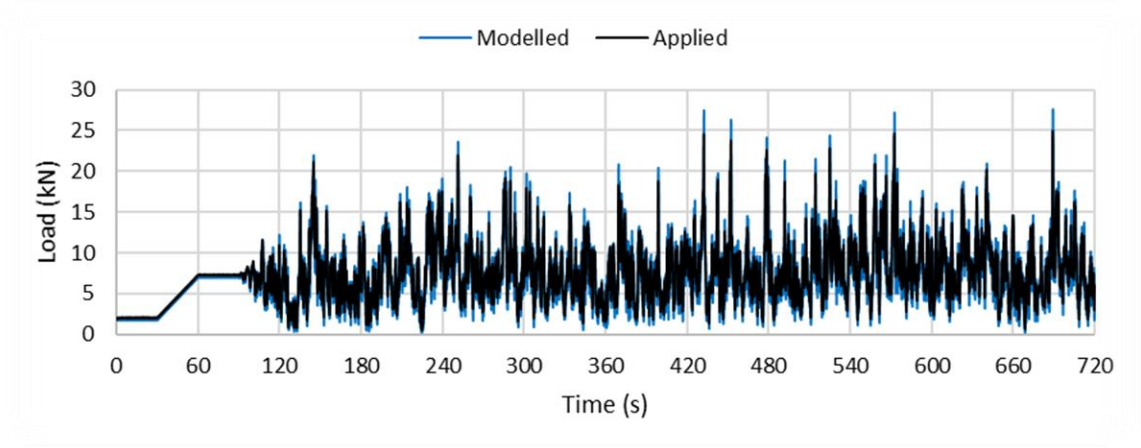

Figure B.29: Modelled and applied 60 m/s wind load time history for specimen HD1

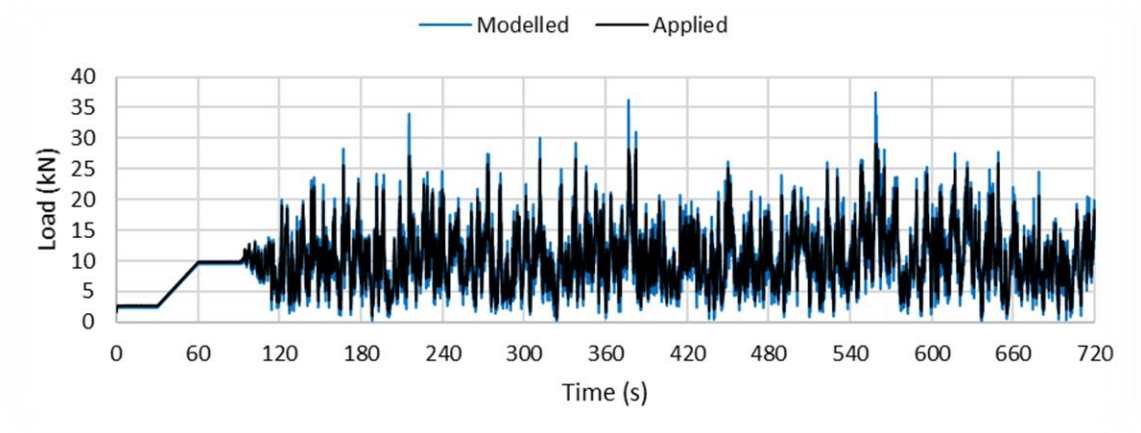

Figure B.30: Modelled and applied 70 m/s wind load time history for specimen HD1

Specimen HD2

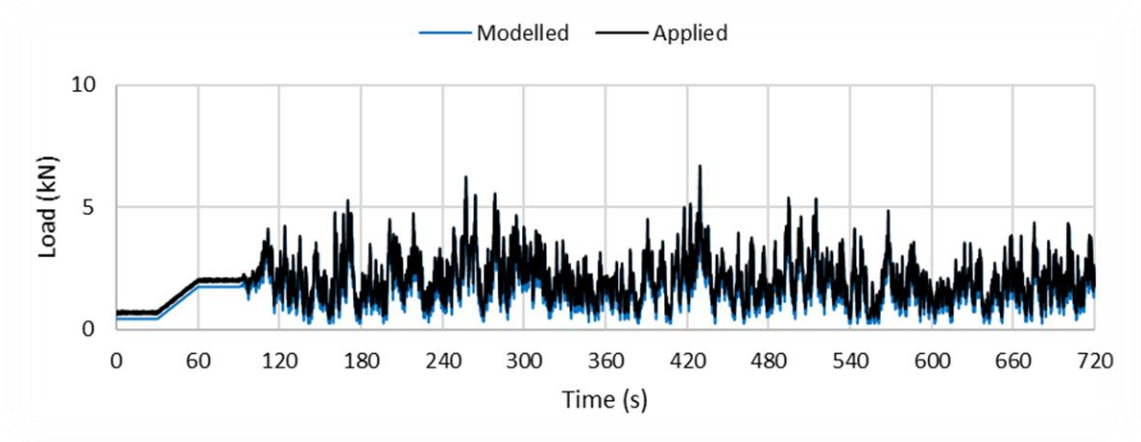

Figure B.31: Modelled and applied 30 m/s wind load time history for specimen HD2

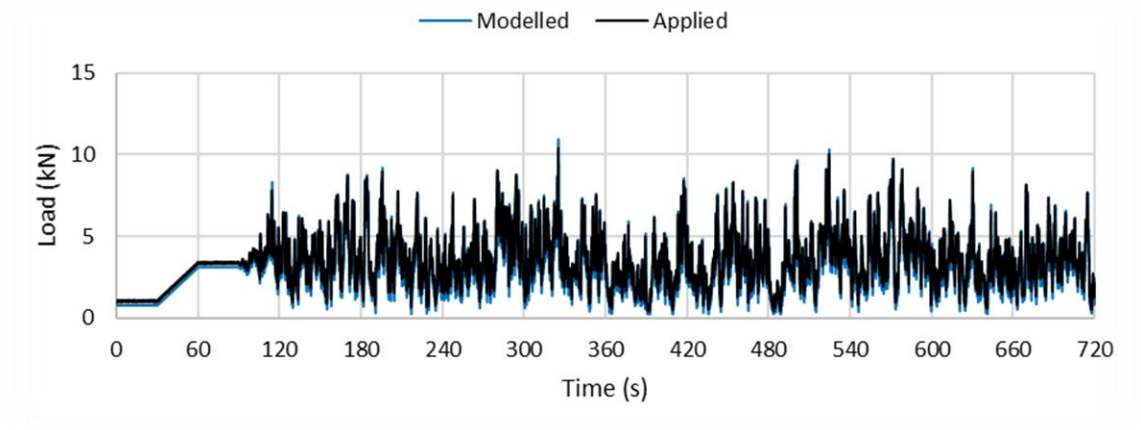

Figure B.32: Modelled and applied 40 m/s wind load time history for specimen HD2

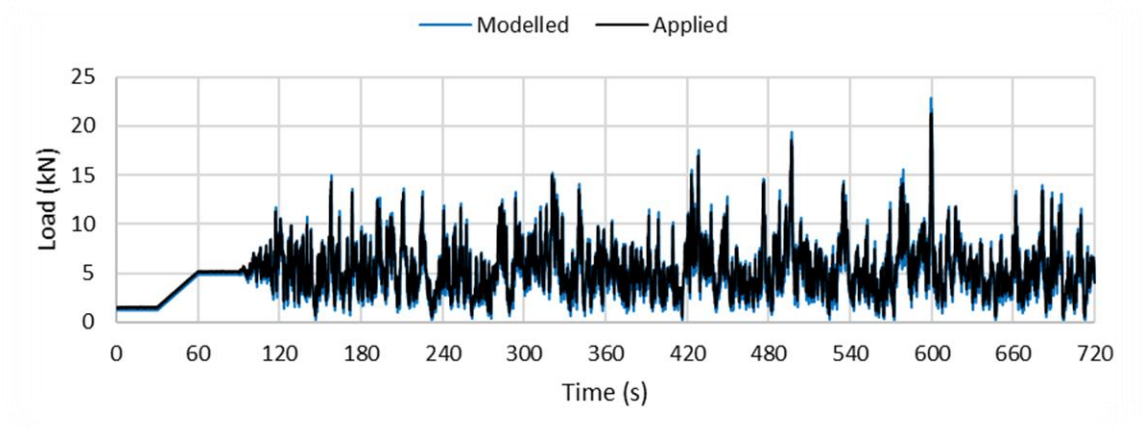

Figure B.33: Modelled and applied 50 m/s wind load time history for specimen HD2

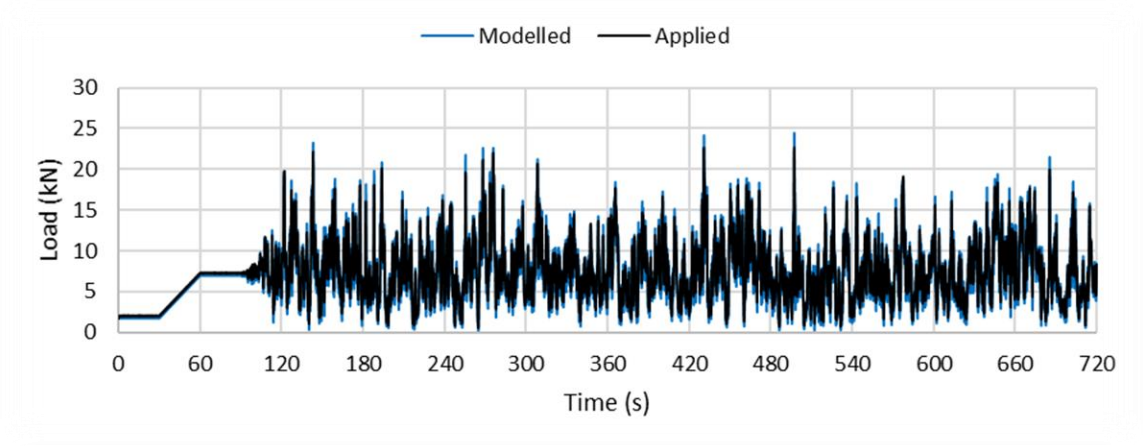

Figure B.34: Modelled and applied 60 m/s wind load time history for specimen HD2

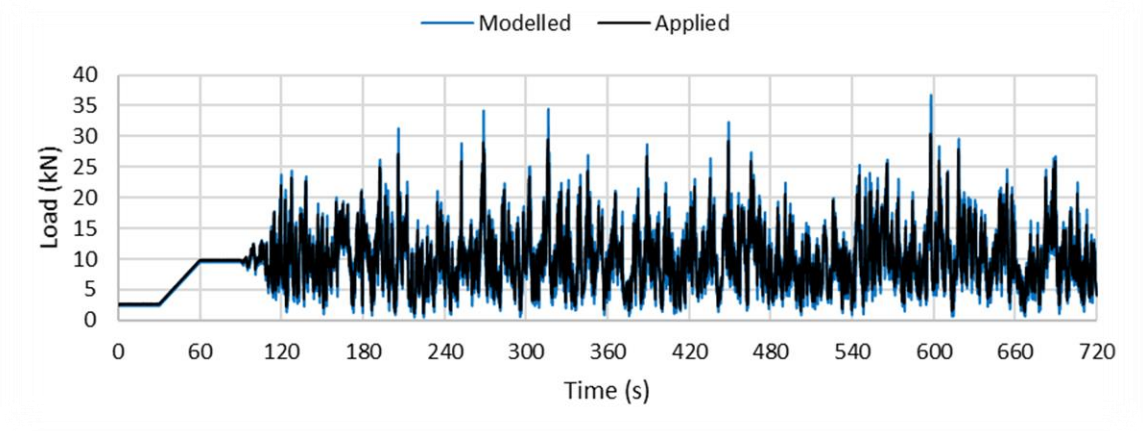

Figure B.35: Modelled and applied 70 m/s wind load time history for specimen HD2

Specimen HD3

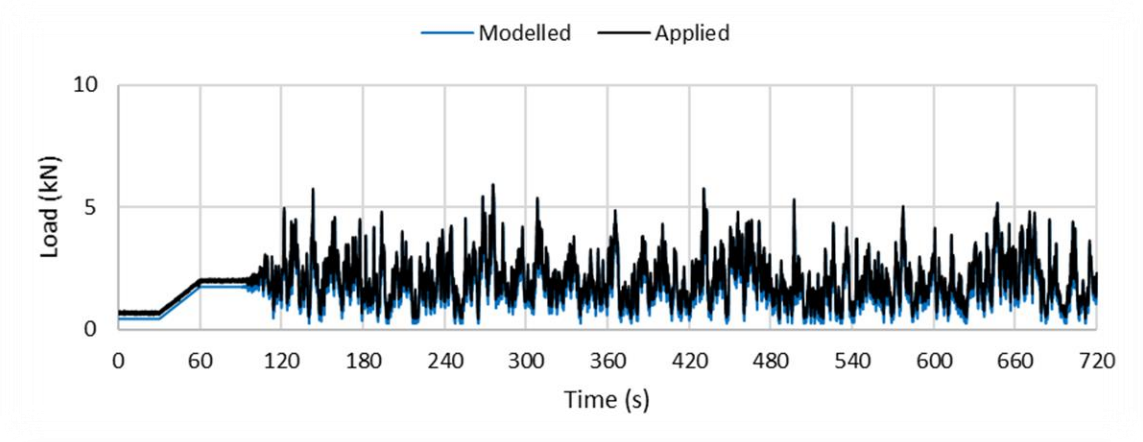

Figure B.36: Modelled and applied 30 m/s wind load time history for specimen HD3

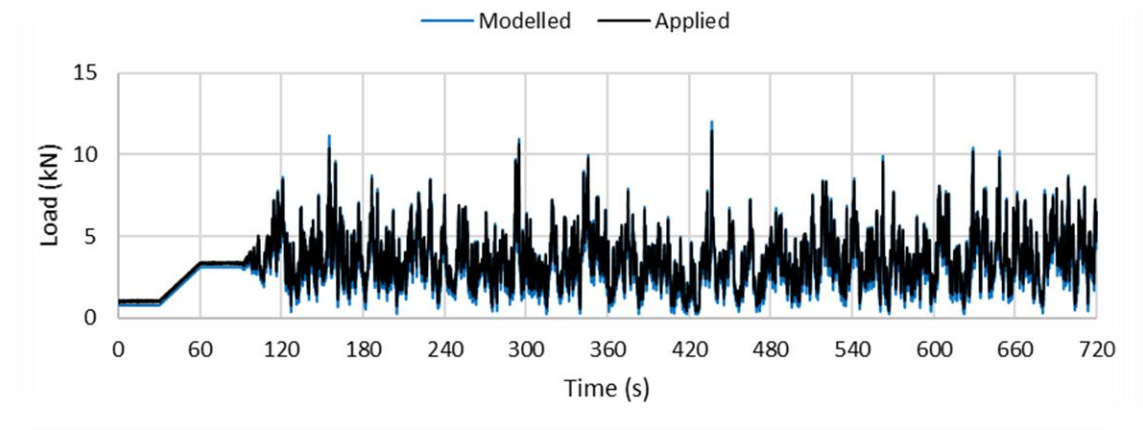

Figure B.37: Modelled and applied 40 m/s wind load time history for specimen HD3

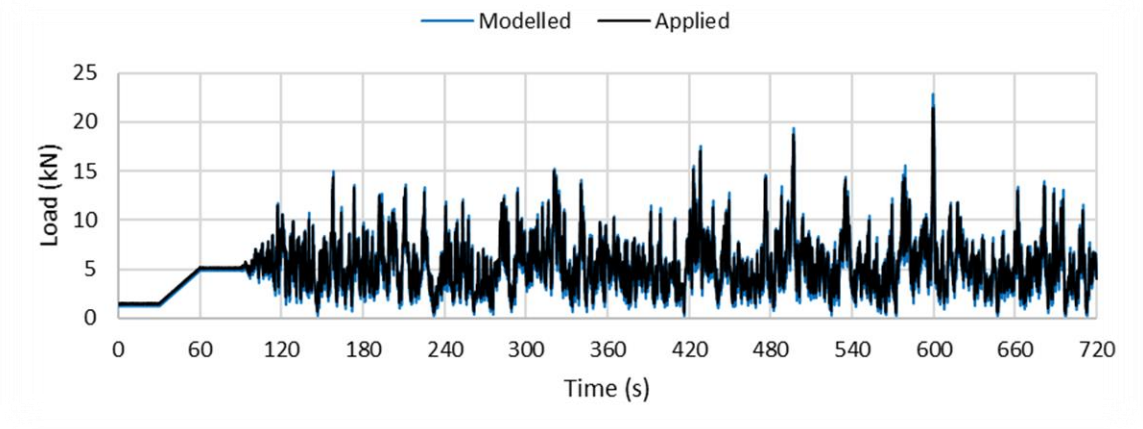

Figure B.38: Modelled and applied 50 m/s wind load time history for specimen HD3

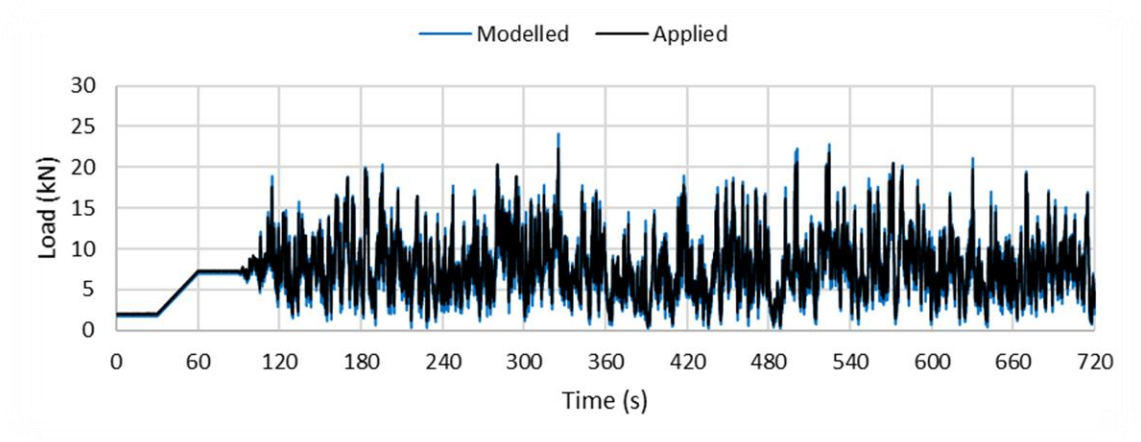

Figure B.39: Modelled and applied 60 m/s wind load time history for specimen HD3

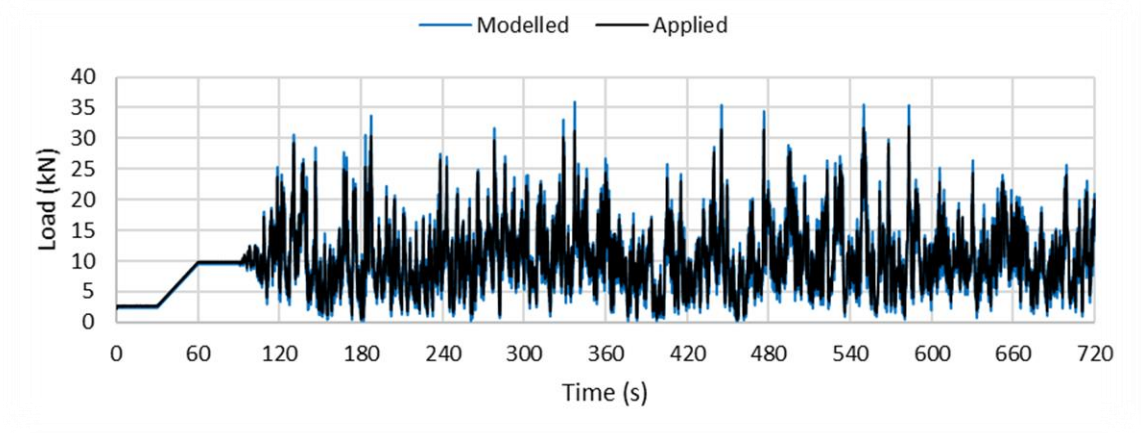

Figure B.40: Modelled and applied 70 m/s wind load time history for specimen HD3

Specimen HD4

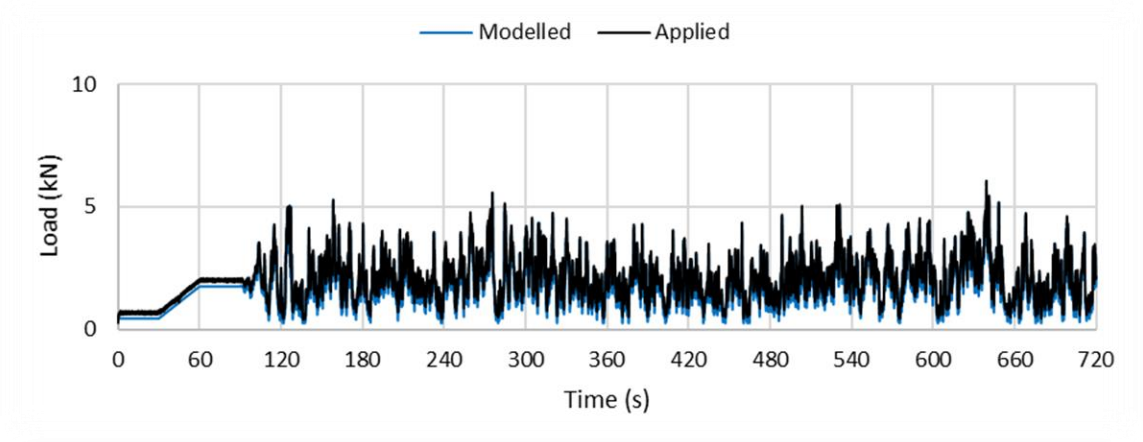

Figure B.41: Modelled and applied 30 m/s wind load time history for specimen HD4

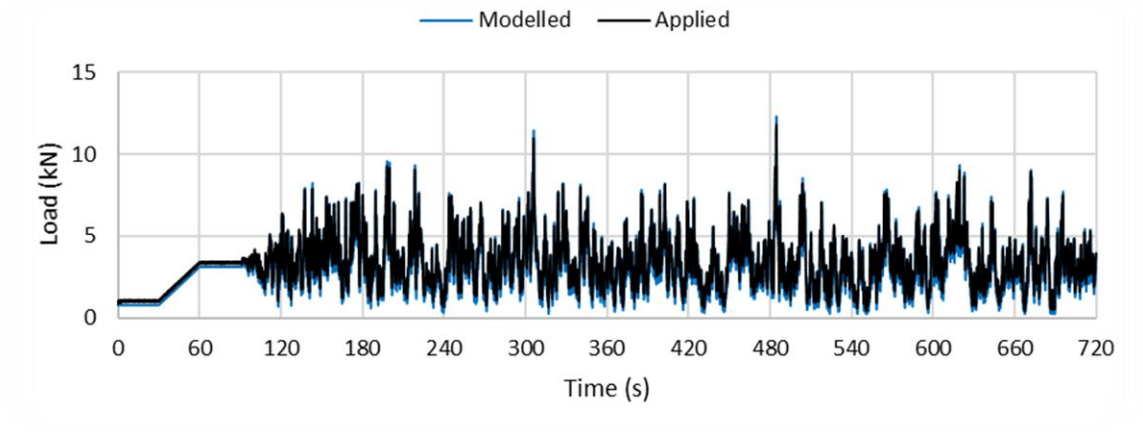

Figure B.42: Modelled and applied 40 m/s wind load time history for specimen HD4

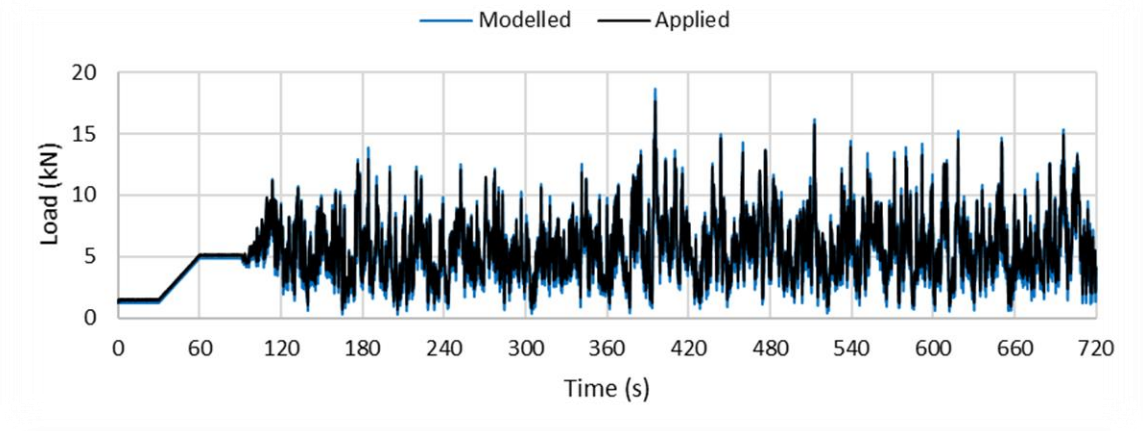

Figure B.43: Modelled and applied 50 m/s wind load time history for specimen HD4

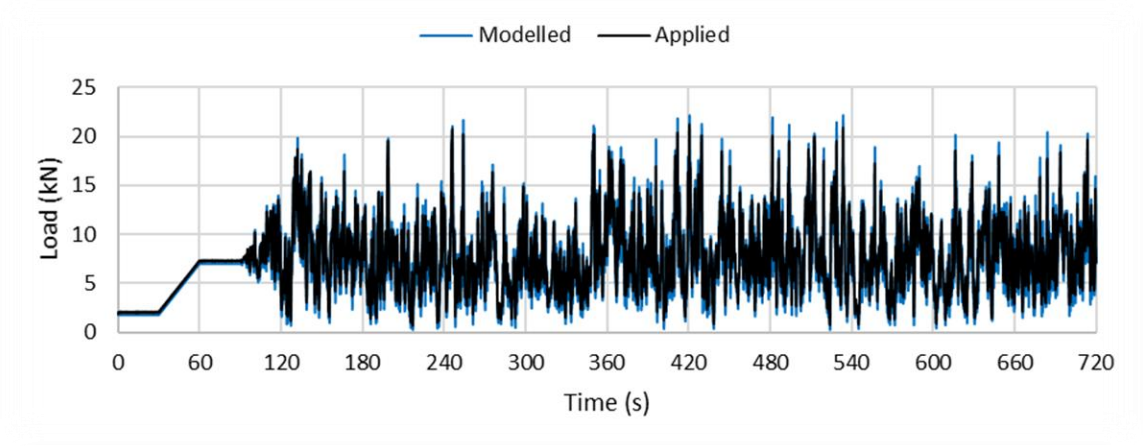

Figure B.44: Modelled and applied 60 m/s wind load time history for specimen HD4

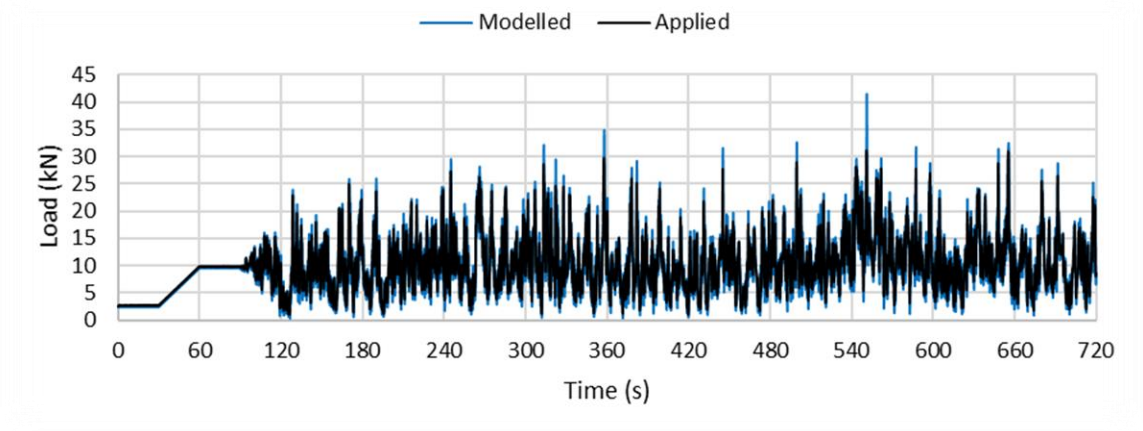

Figure B.45: Modelled and applied 70 m/s wind load time history for specimen HD4

Specimen HD5

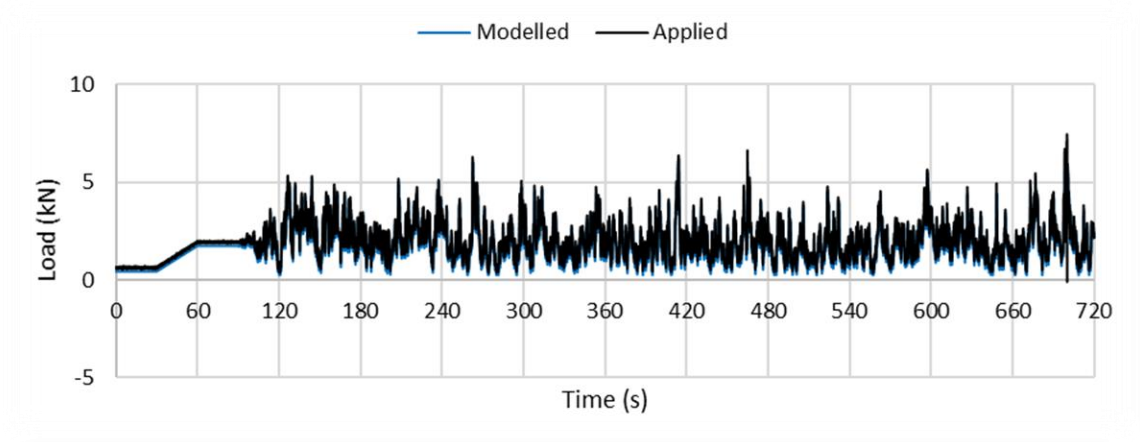

Figure B.46: Modelled and applied 30 m/s wind load time history for specimen HD5

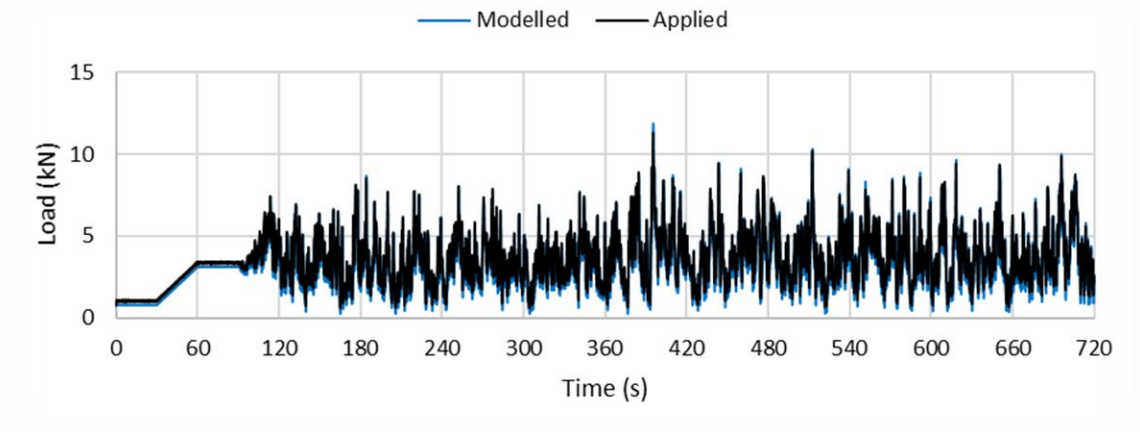

Figure B.47: Modelled and applied 40 m/s wind load time history for specimen HD5

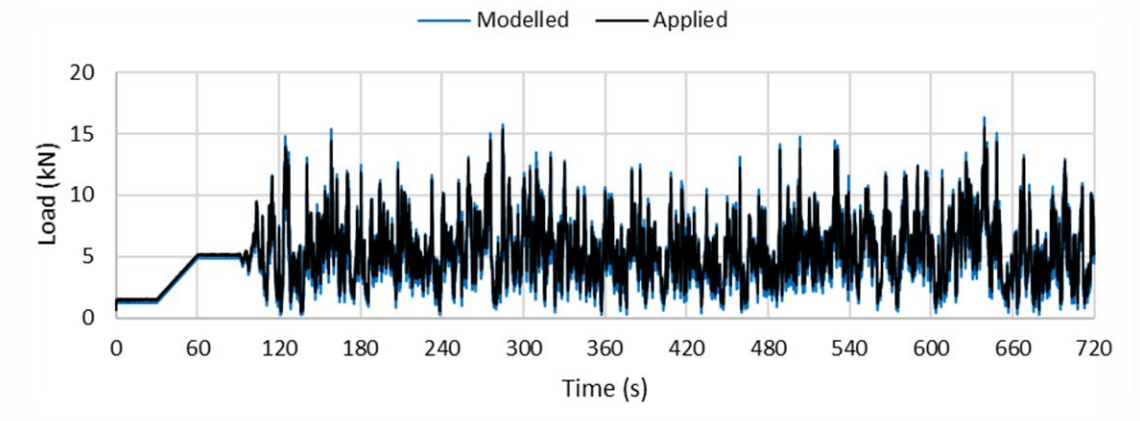

Figure B.48: Modelled and applied 50 m/s wind load time history for specimen HD5

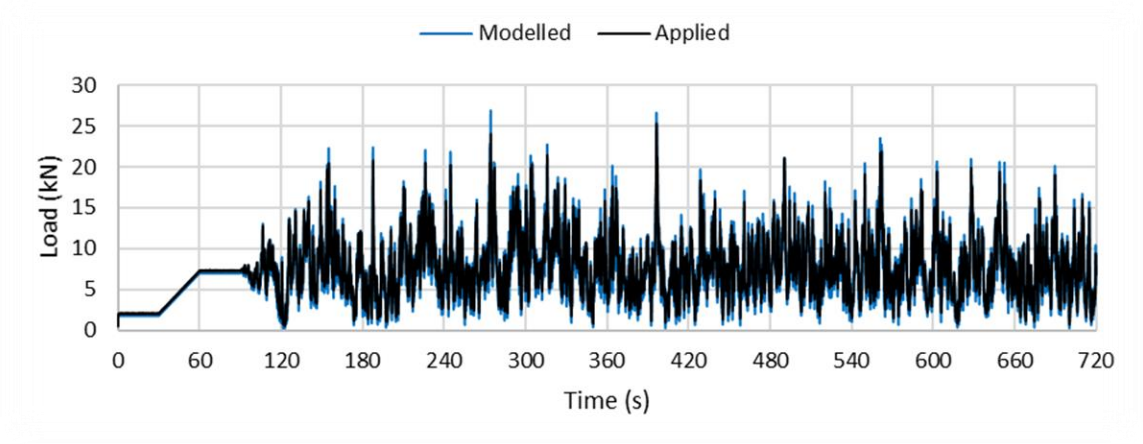

Figure B.49: Modelled and applied 60 m/s wind load time history for specimen HD5

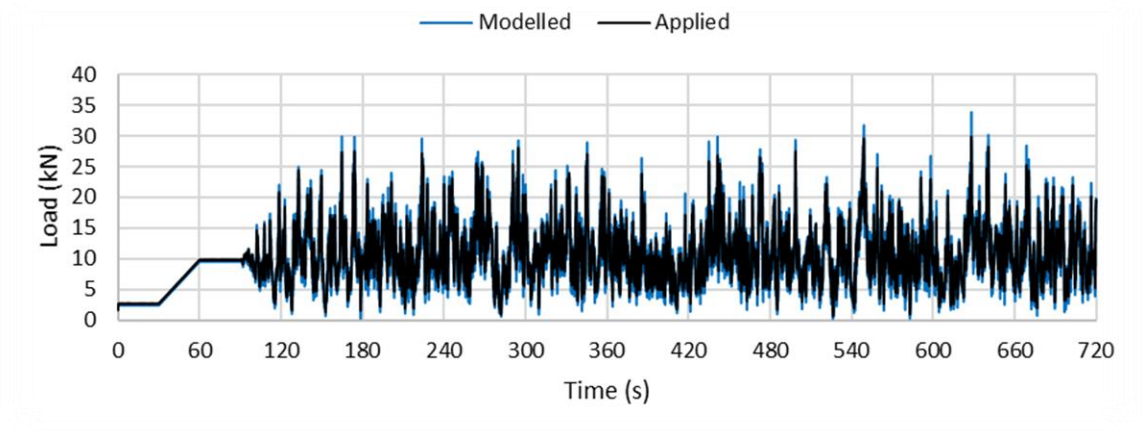

Figure B.50: Modelled and applied 70 m/s wind load time history for specimen HD5

Appendix C: PSD Diagrams of the Dynamic Wind Load Time Histories

Appendix C contains the PSD comparisons between the theoretical, modelled and applied load time histories of the wall specimens tested under dynamic loading conditions. *Figure C.1* to *Figure C.25* depict the plots for the wall specimens with the low reinforcement ratio, while *Figure C.26* to *Figure C.50* depict the plots for the wall specimens with the high reinforcement ratio.

The theoretical PSD diagrams were based on the theoretical wind time histories proposed by Kaimal et al. (1972). The modelled PSD diagrams were based on the generated wind time histories from the mathematical model described in Udey (2014). The applied PSD diagrams were based on the total load applied by the MTS® Series 244 hydraulic actuator on the wall specimens. The load measurements were taken using the built-in force transducer of the actuator.

Specimen LD1

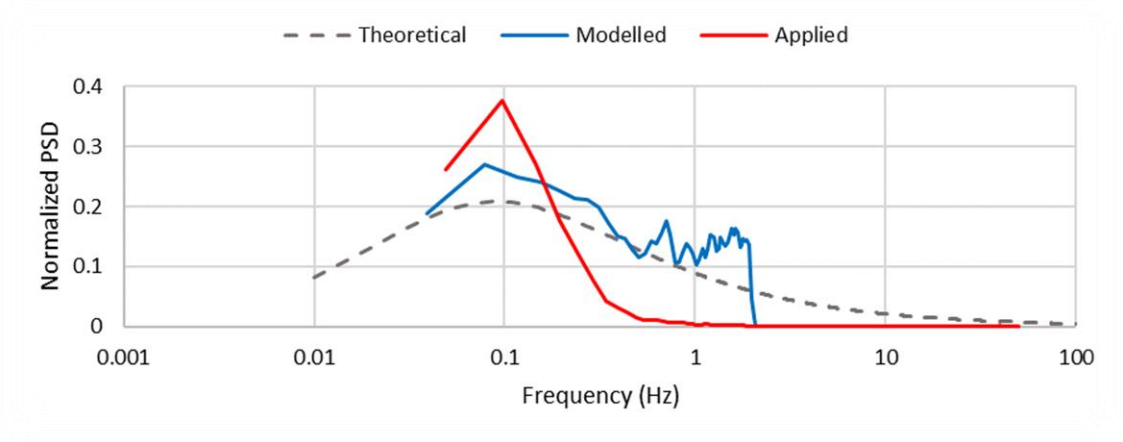

Figure C.1: PSD diagram for 30 m/s load time history of specimen LD1

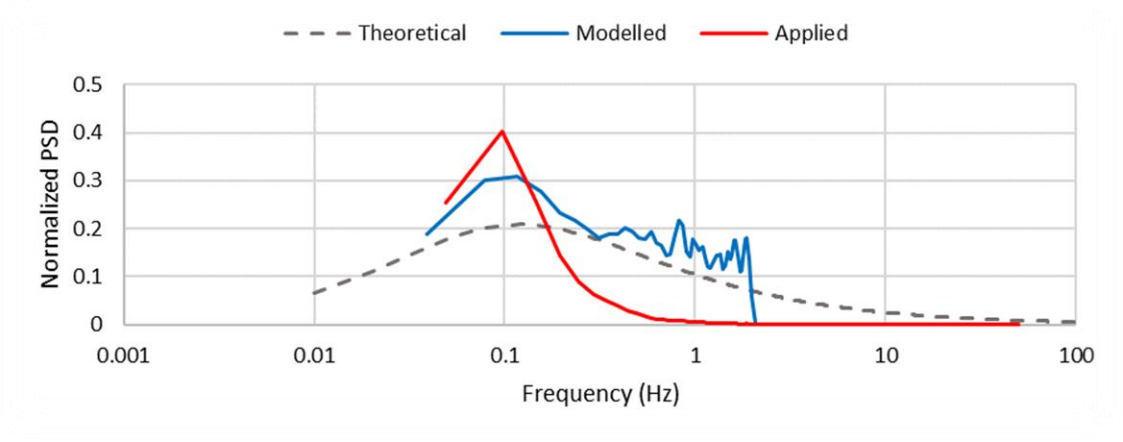

Figure C.2: PSD diagram for 40 m/s load time history of specimen LD1

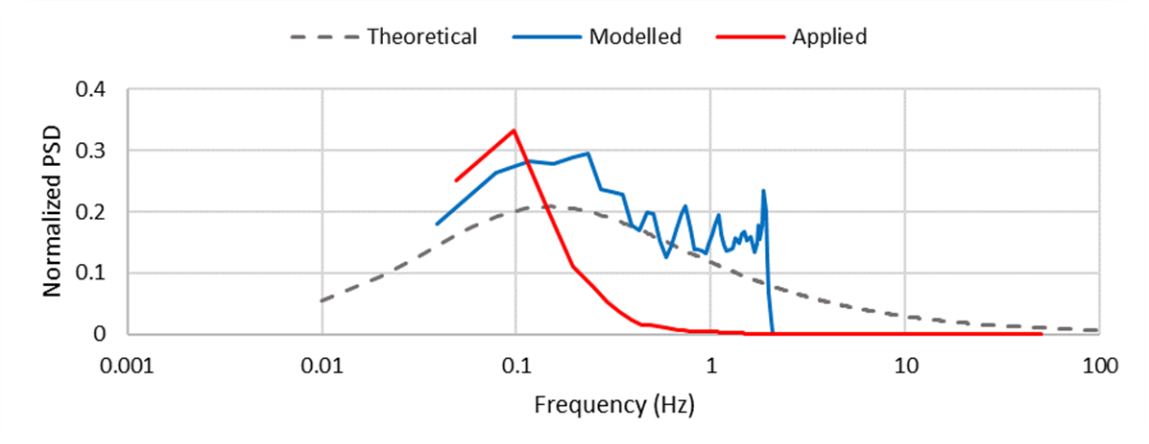

Figure C.3: PSD diagram for 50 m/s load time history of specimen LD1

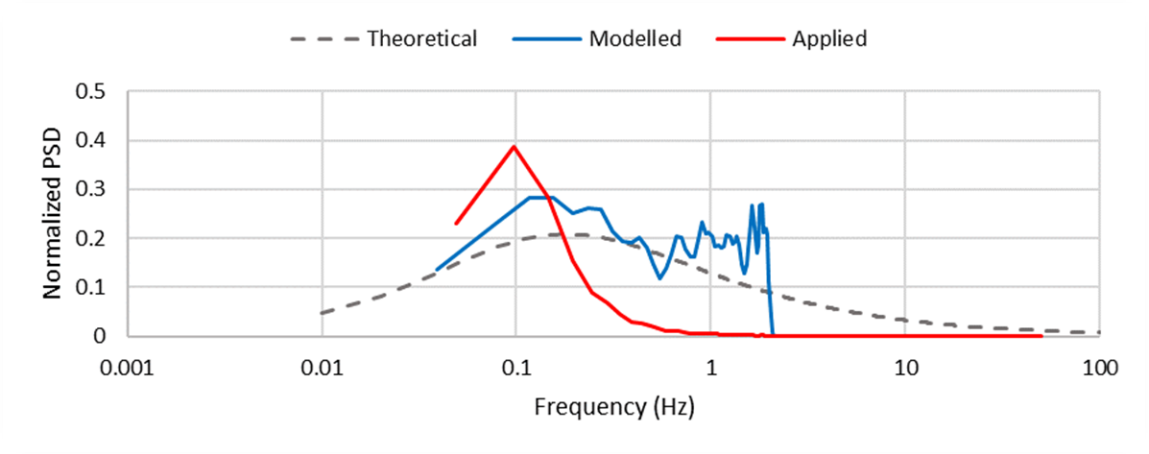

Figure C.4: PSD diagram for 60 m/s load time history of specimen LD1

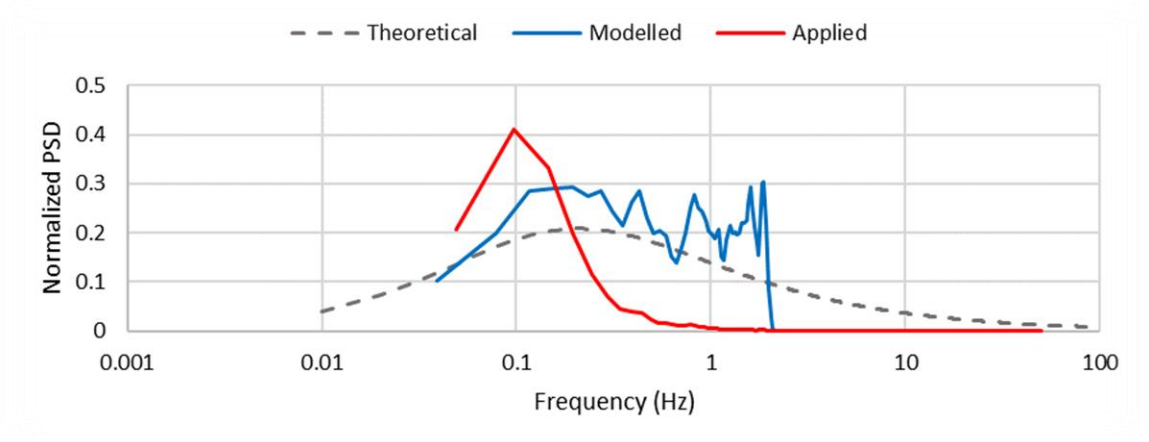

Figure C.5: PSD diagram for 70 m/s load time history of specimen LD1

Specimen LD2

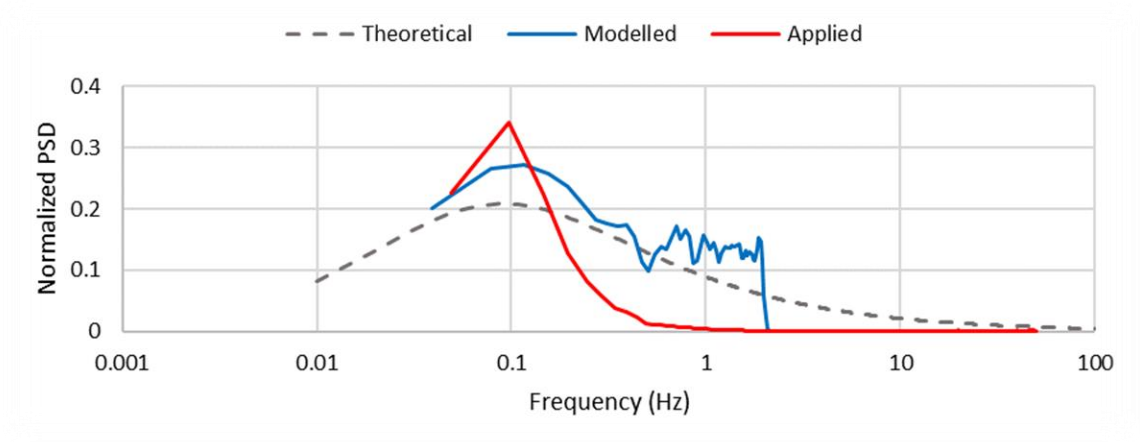

Figure C.6: PSD diagram for 30 m/s load time history of specimen LD2

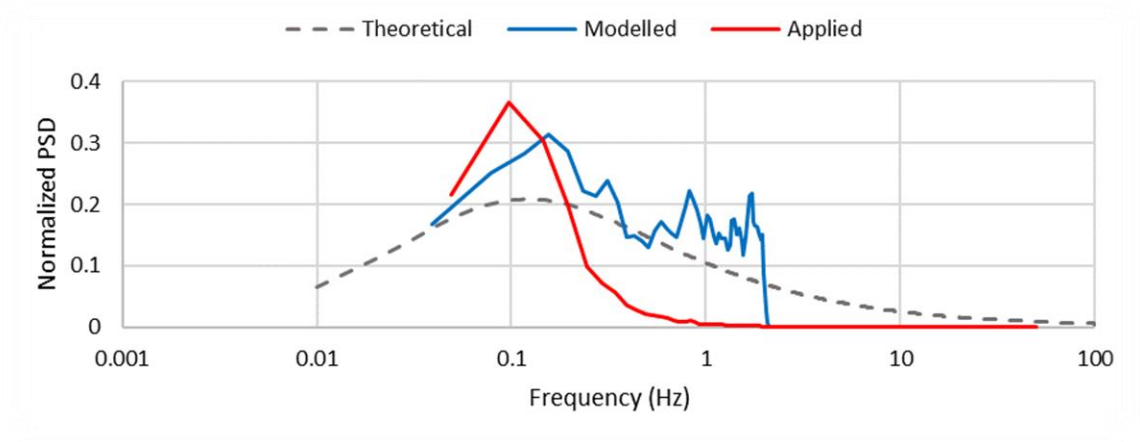

Figure C.7: PSD diagram for 40 m/s load time history of specimen LD2

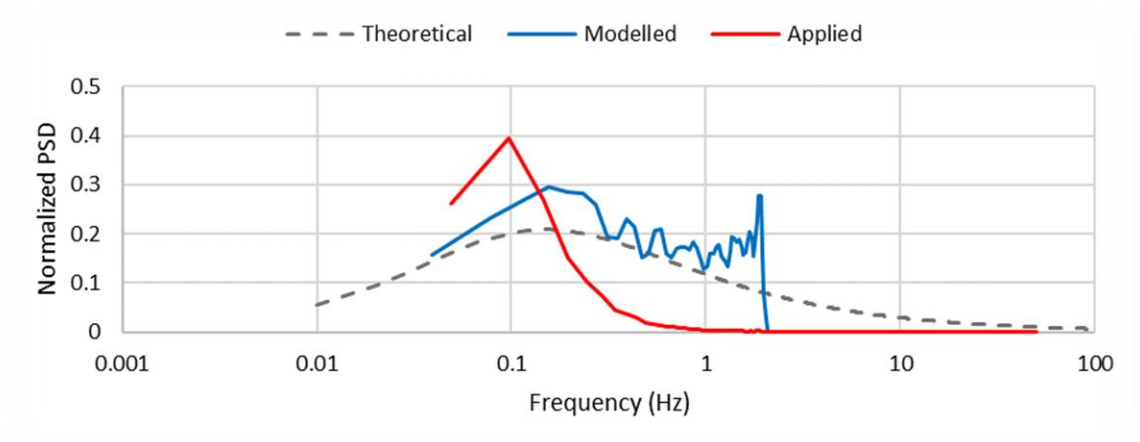

Figure C.8: PSD diagram for 50 m/s load time history of specimen LD2

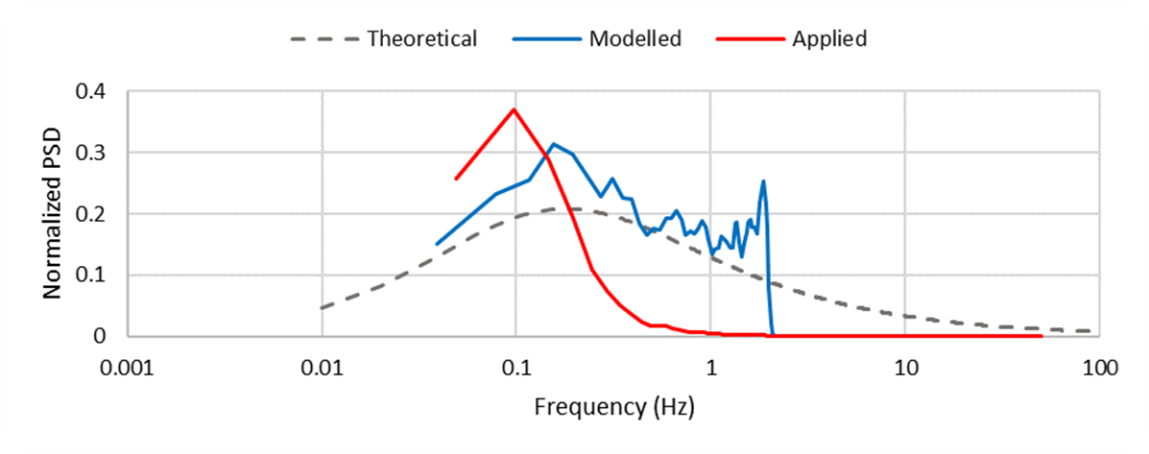

Figure C.9: PSD diagram for 60 m/s load time history of specimen LD2

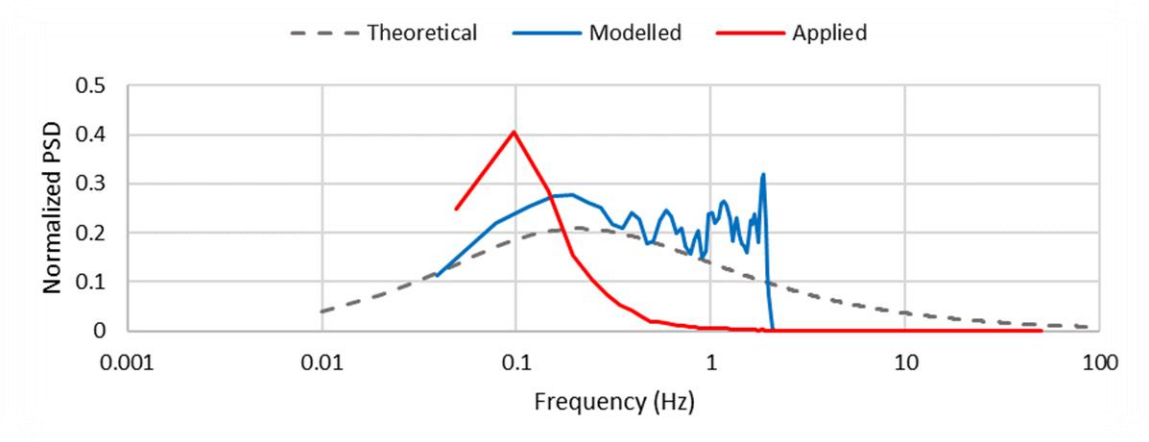

Figure C.10: PSD diagram for 70 m/s load time history of specimen LD2

Specimen LD3

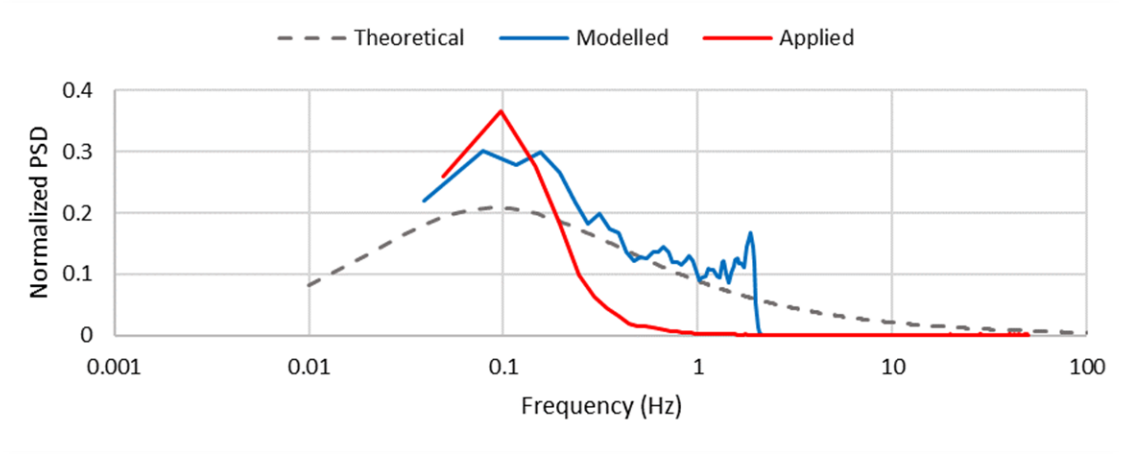

Figure C.11: PSD diagram for 30 m/s load time history of specimen LD3

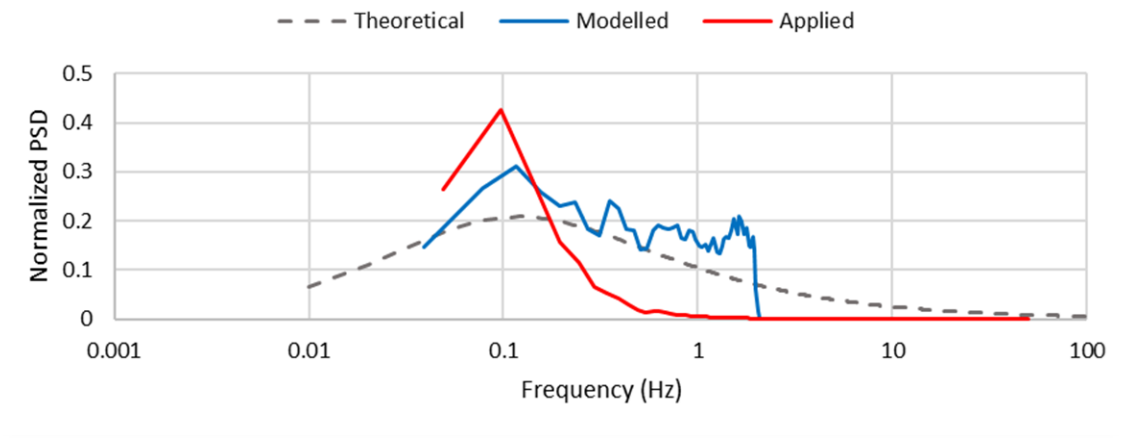

Figure C.12: PSD diagram for 40 m/s load time history of specimen LD3

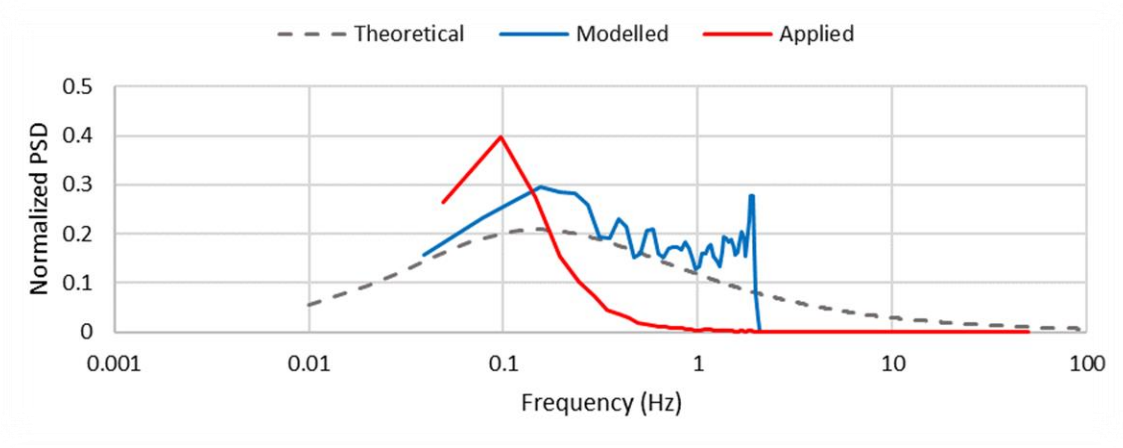

Figure C.13: PSD diagram for 50 m/s load time history of specimen LD3

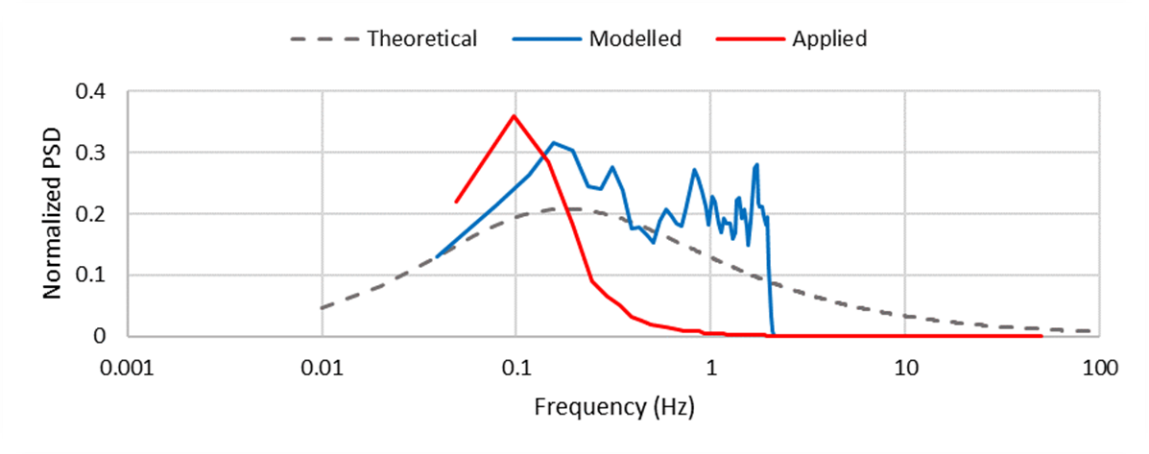

Figure C.14: PSD diagram for 60 m/s load time history of specimen LD3

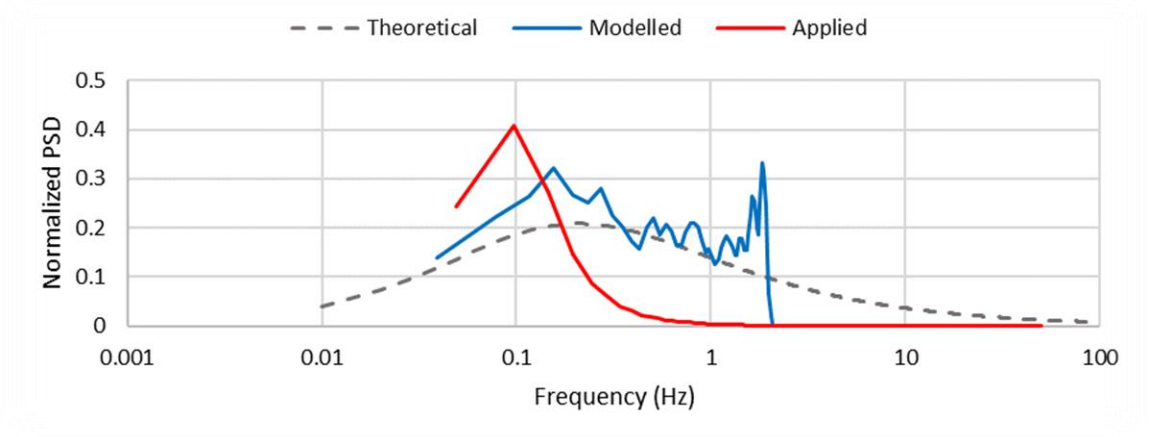

Figure C.15: PSD diagram for 70 m/s load time history of specimen LD3

Specimen LD4

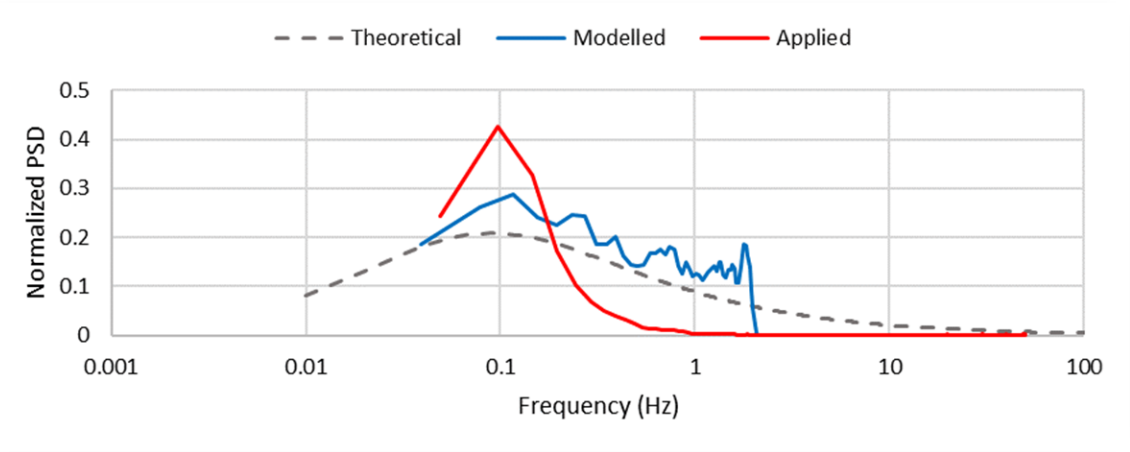

Figure C.16: PSD diagram for 30 m/s load time history of specimen LD4

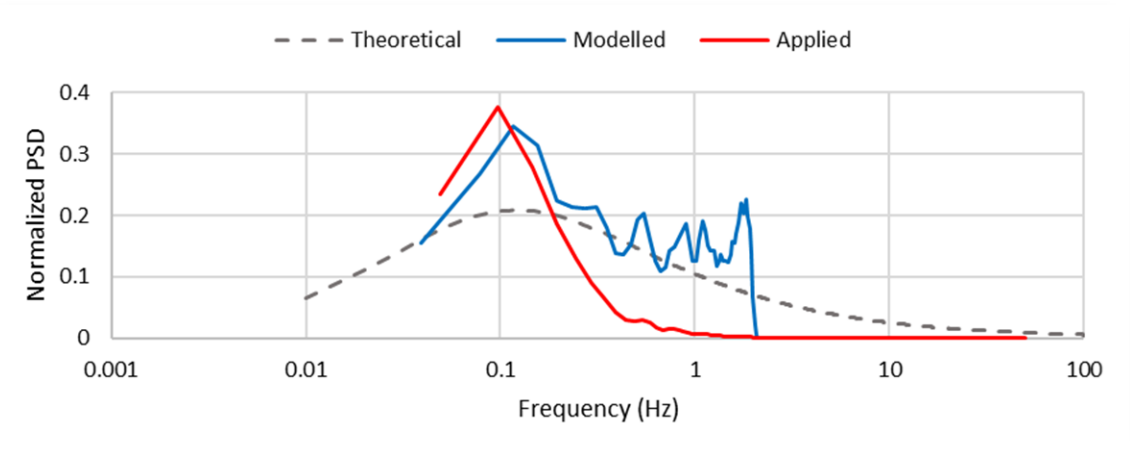

Figure C.17: PSD diagram for 40 m/s load time history of specimen LD4

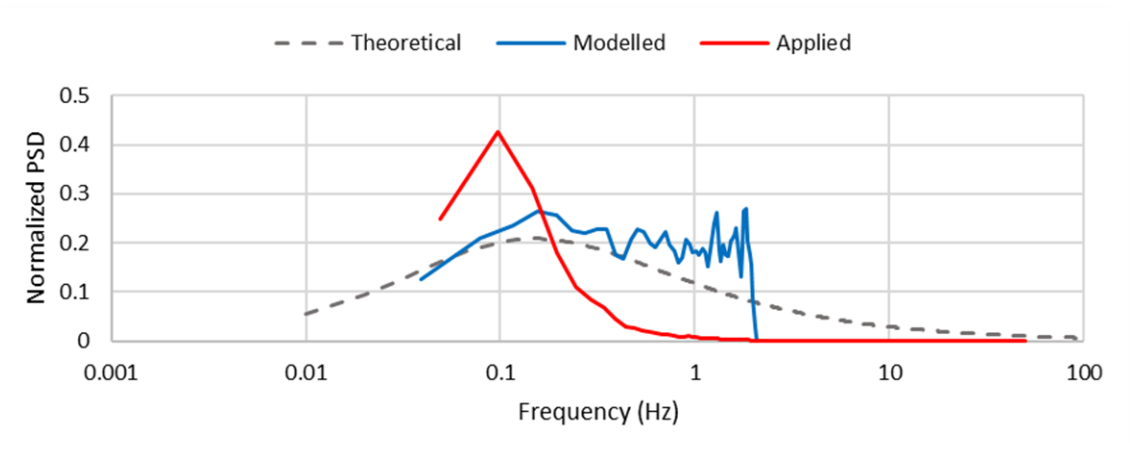

Figure C.18: PSD diagram for 50 m/s load time history of specimen LD4

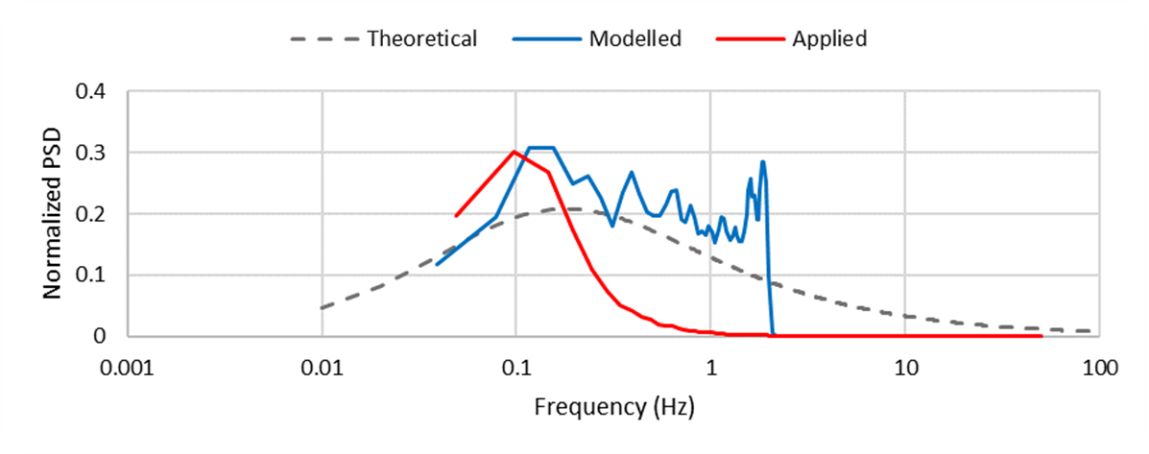

Figure C.19: PSD diagram for 60 m/s load time history of specimen LD4

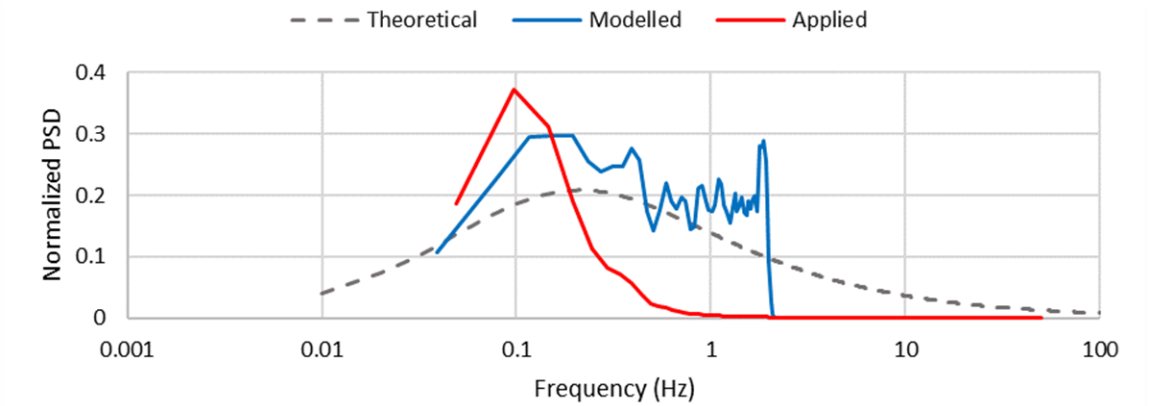

Figure C.20: PSD diagram for 70 m/s load time history of specimen LD4

Specimen LD5

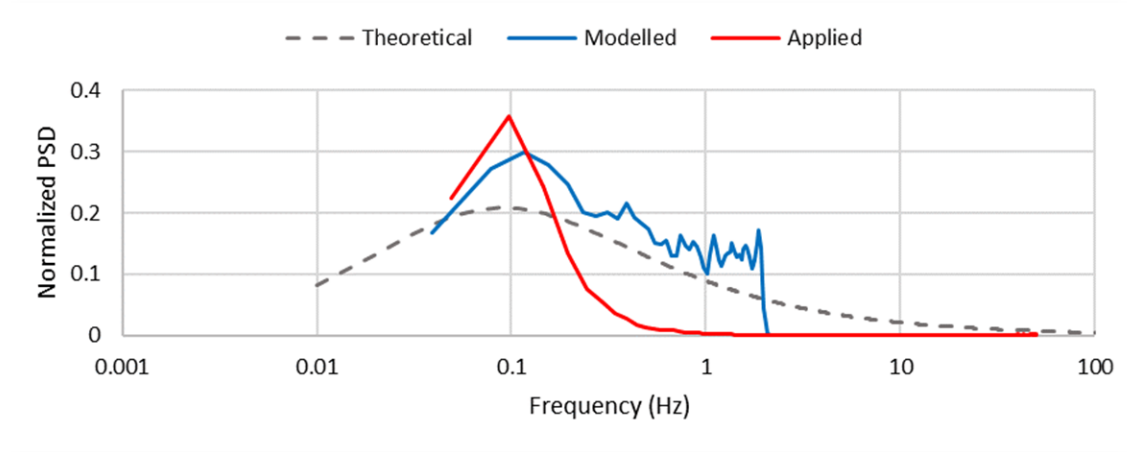

Figure C.21: PSD diagram for 30 m/s load time history of specimen LD5

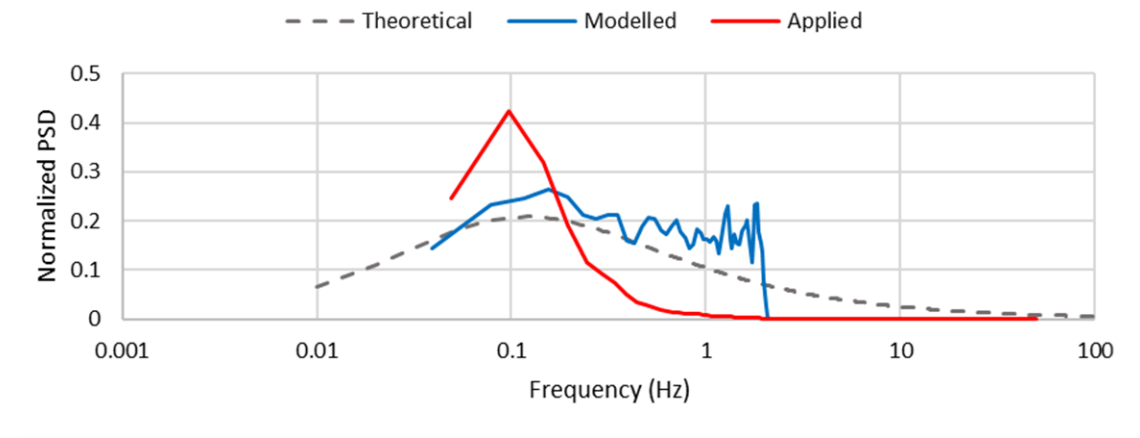

Figure C.22: PSD diagram for 40 m/s load time history of specimen LD5

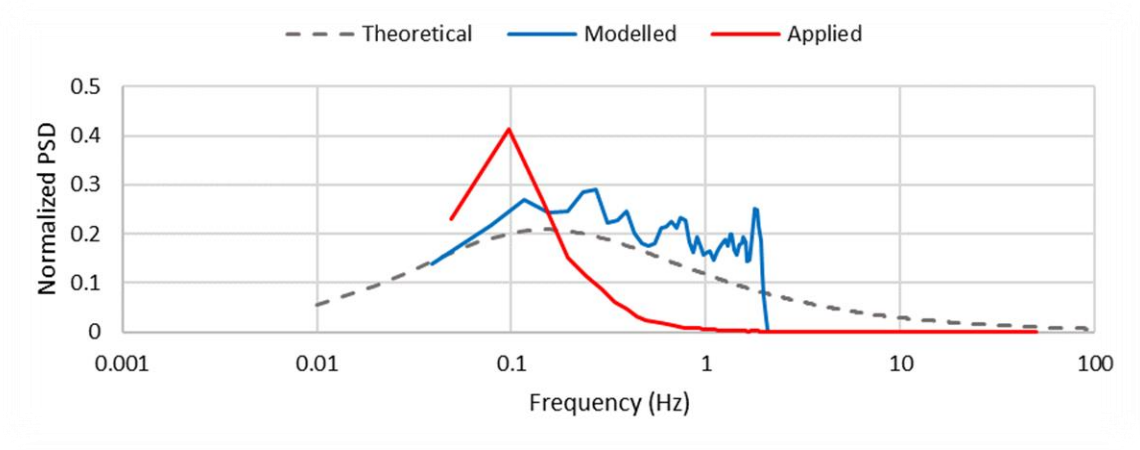

Figure C.23: PSD diagram for 50 m/s load time history of specimen LD5

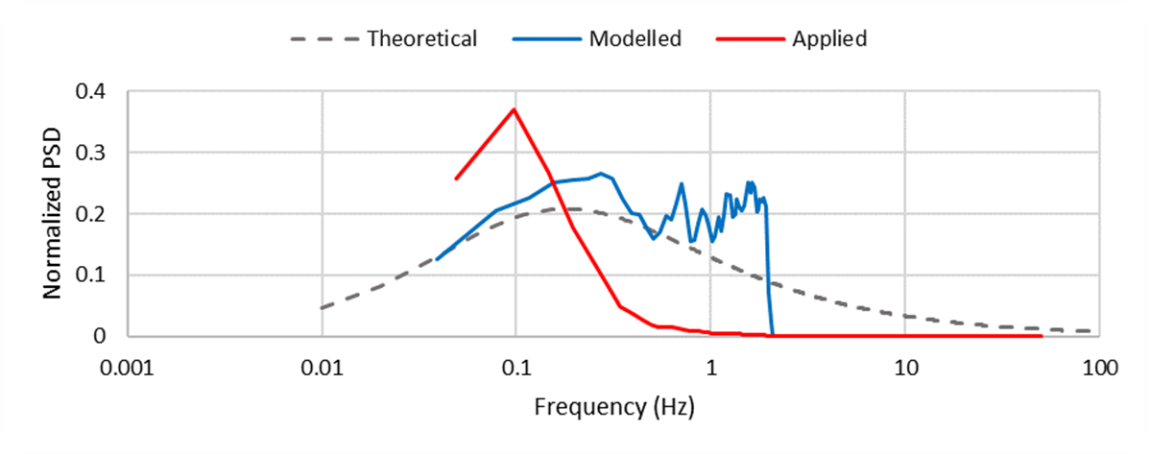

Figure C.24: PSD diagram for 60 m/s load time history of specimen LD5

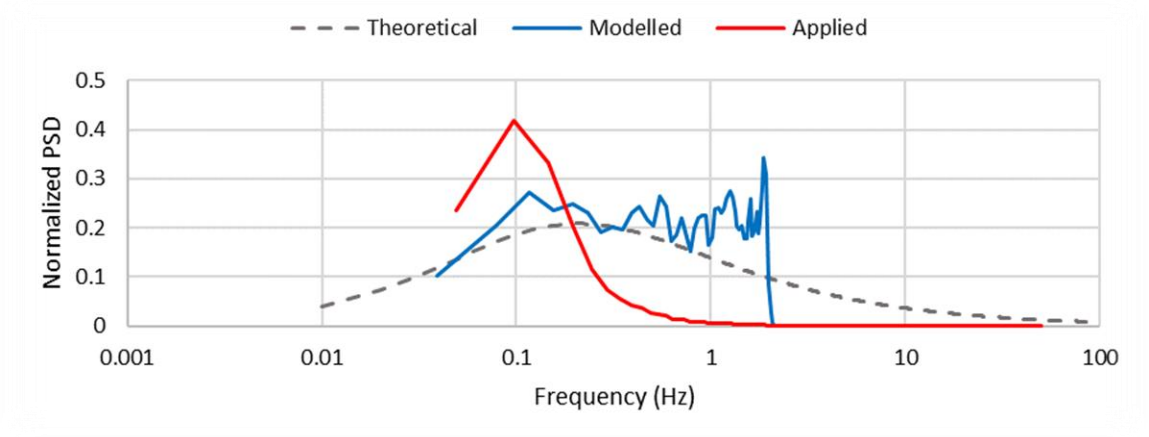

Figure C.25: PSD diagram for 70 m/s load time history of specimen LD5

Specimen HD1

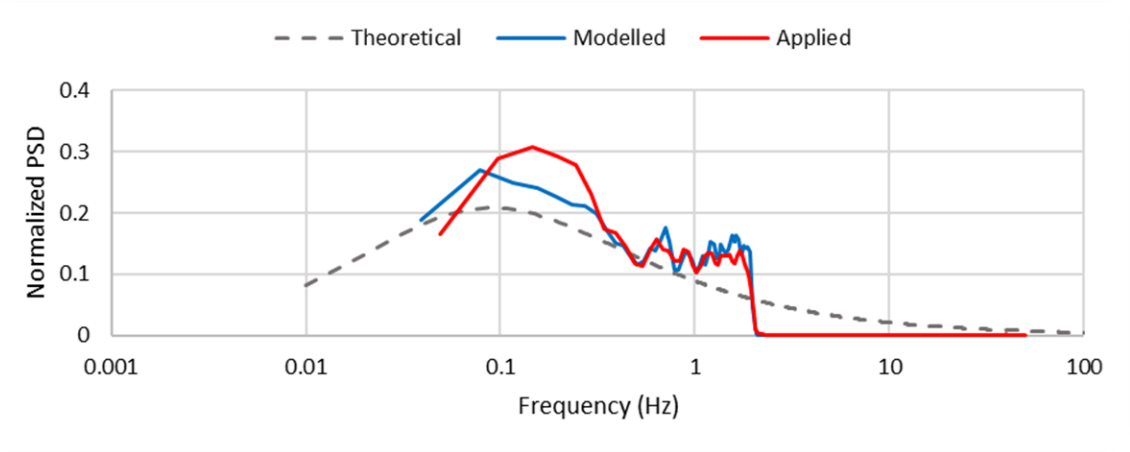

Figure C.26: PSD diagram for 30 m/s load time history of specimen HD1

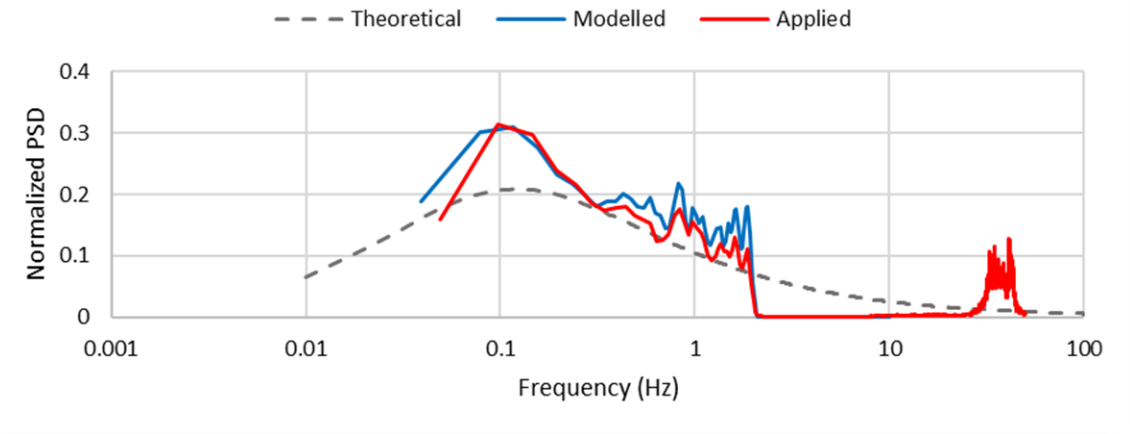

Figure C.27: PSD diagram for 40 m/s load time history of specimen HD1

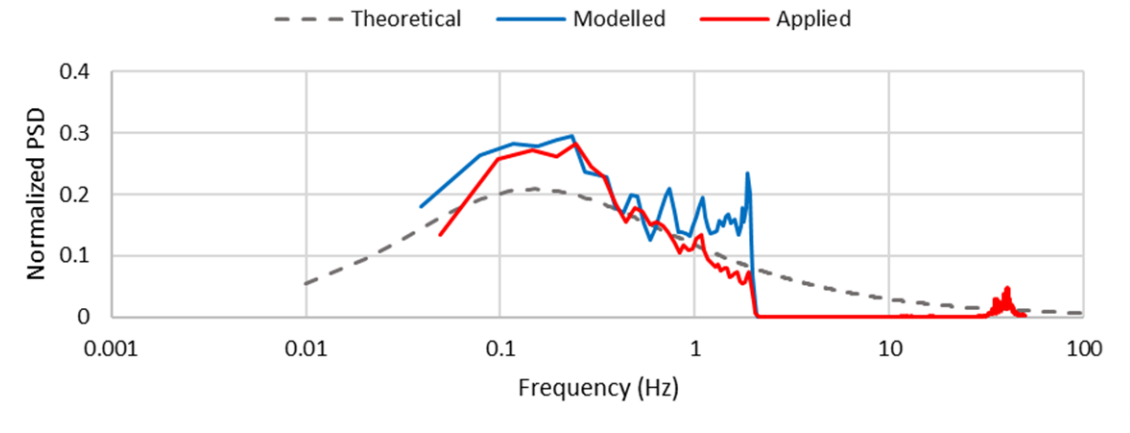

Figure C.28: PSD diagram for 50 m/s load time history of specimen HD1

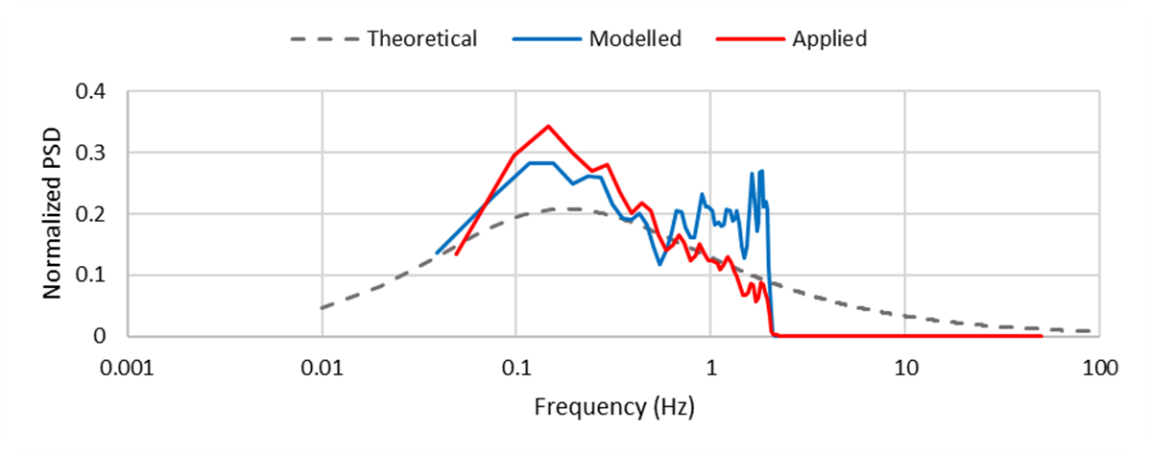

Figure C.29: PSD diagram for 60 m/s load time history of specimen HD1

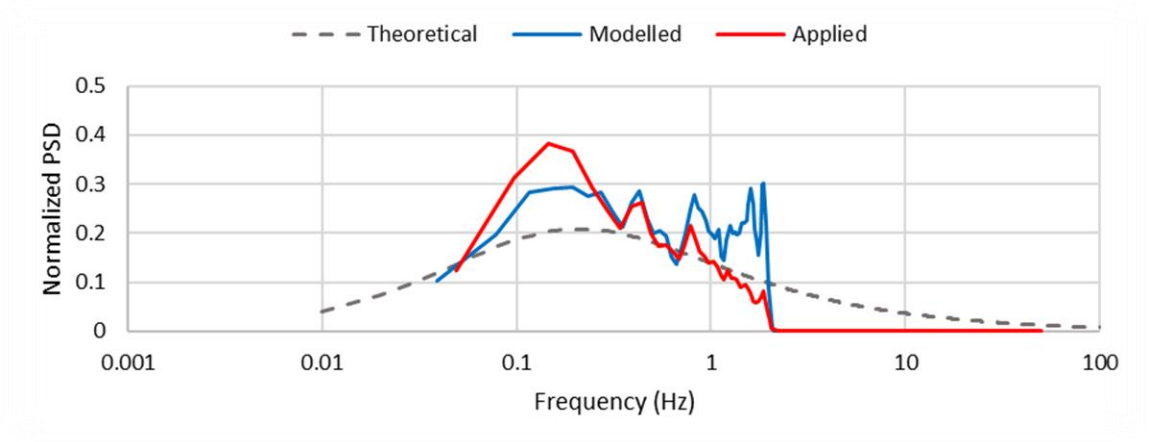

Figure C.30: PSD diagram for 70 m/s load time history of specimen HD1

Specimen HD2

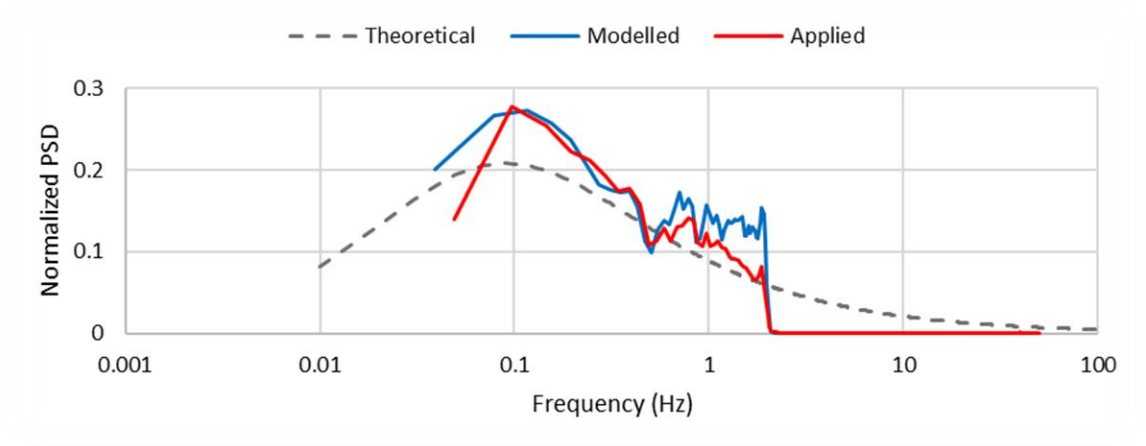

Figure C.31: PSD diagram for 30 m/s load time history of specimen HD2

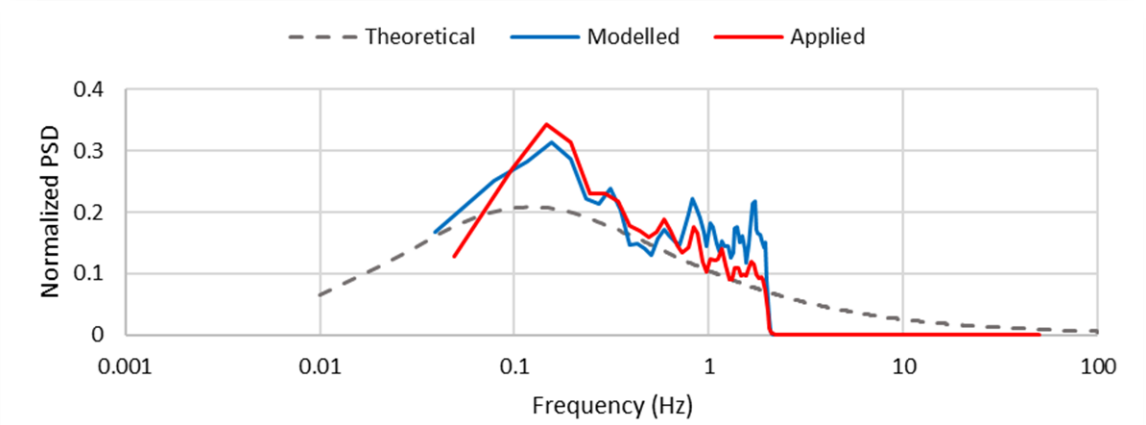

Figure C.32: PSD diagram for 40 m/s load time history of specimen HD2

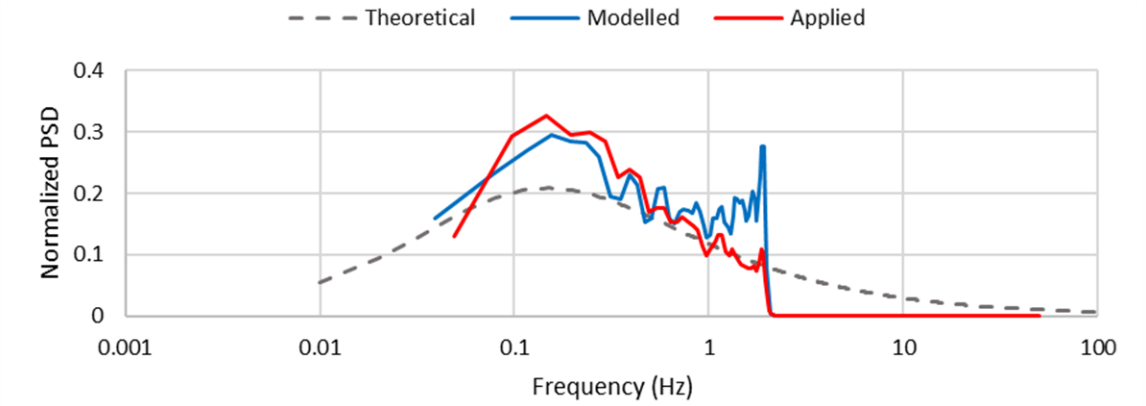

Figure C.33: PSD diagram for 50 m/s load time history of specimen HD2

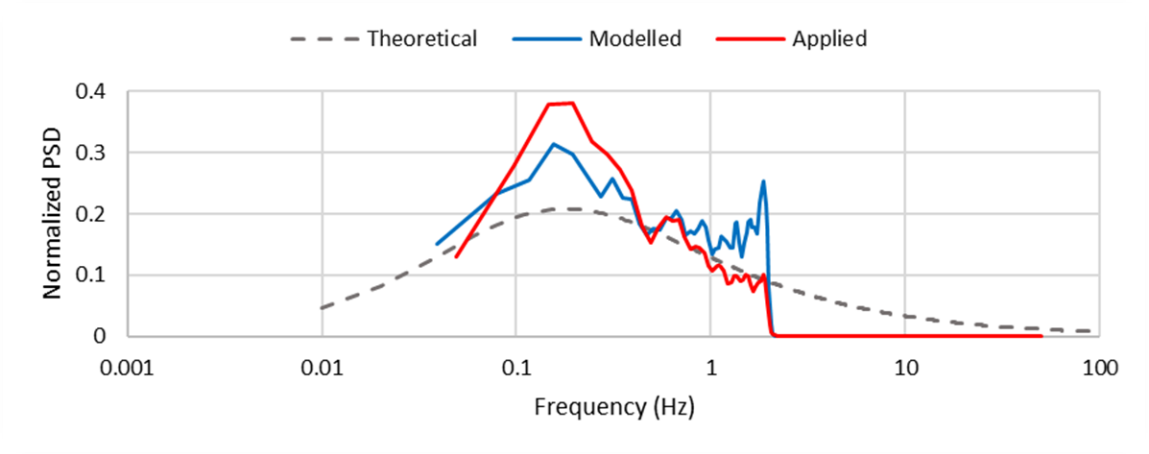

Figure C.34: PSD diagram for 60 m/s load time history of specimen HD2

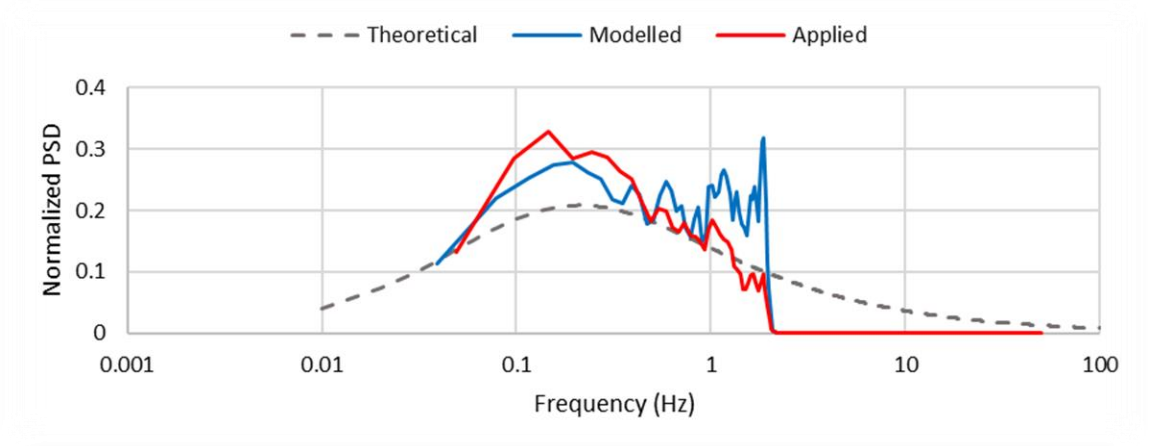

Figure C.35: PSD diagram for 70 m/s load time history of specimen HD2

Specimen HD3

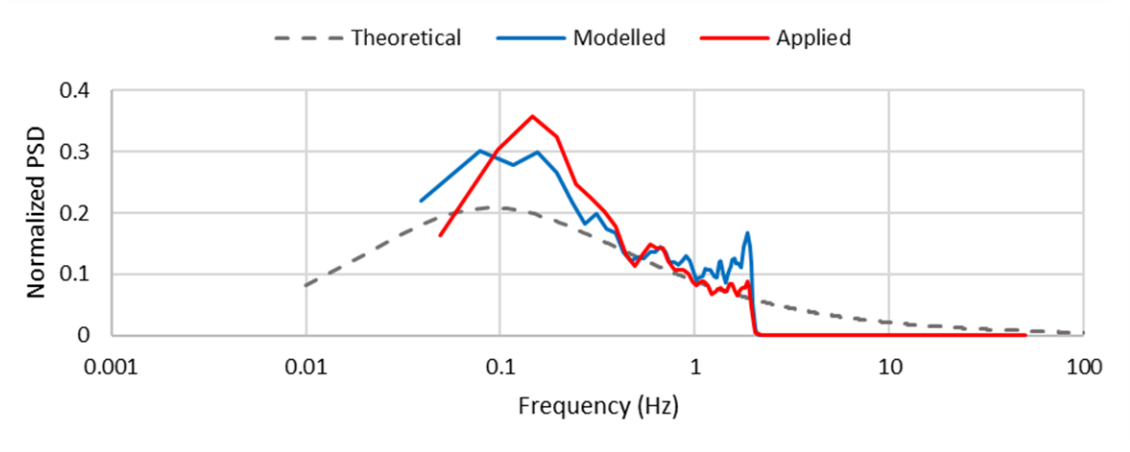

Figure C.36: PSD diagram for 30 m/s load time history of specimen HD3

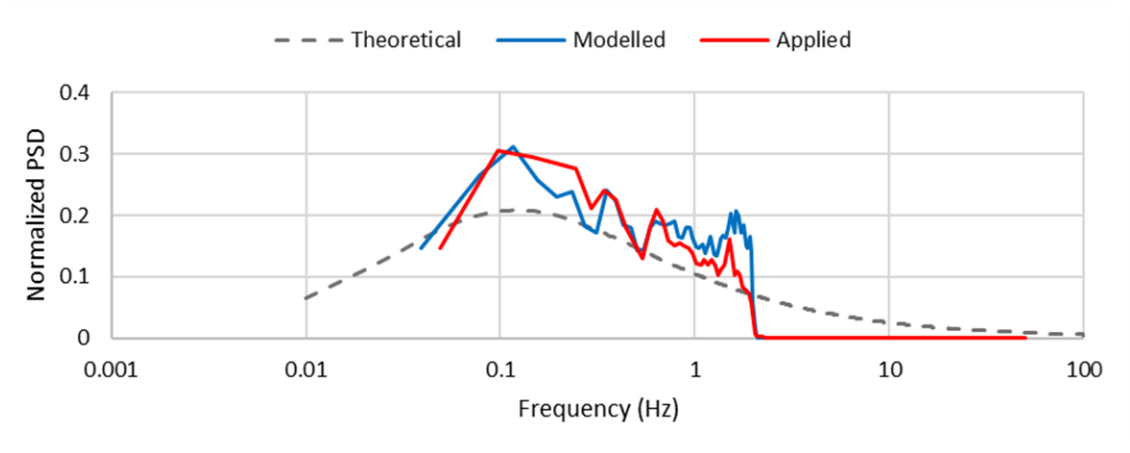

Figure C.37: PSD diagram for 40 m/s load time history of specimen HD3

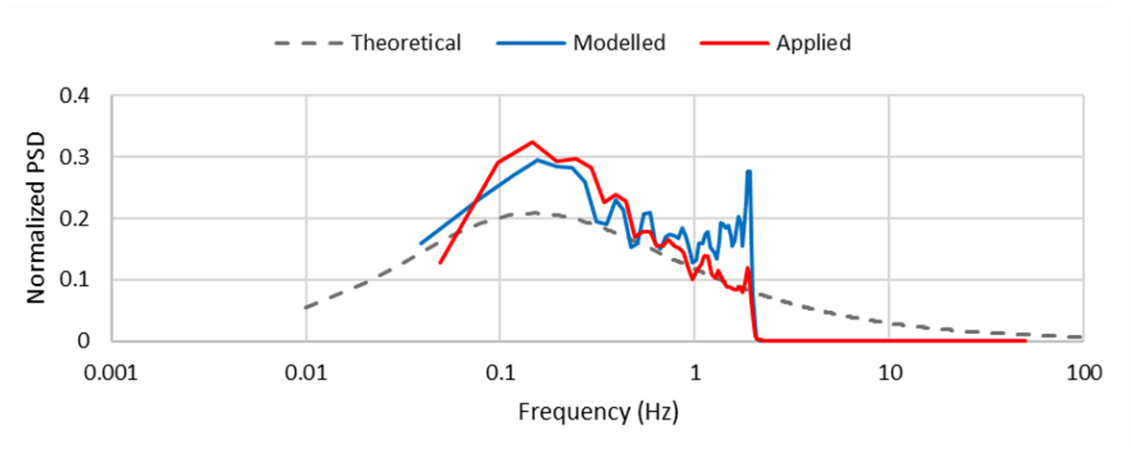

Figure C.38: PSD diagram for 50 m/s load time history of specimen HD3

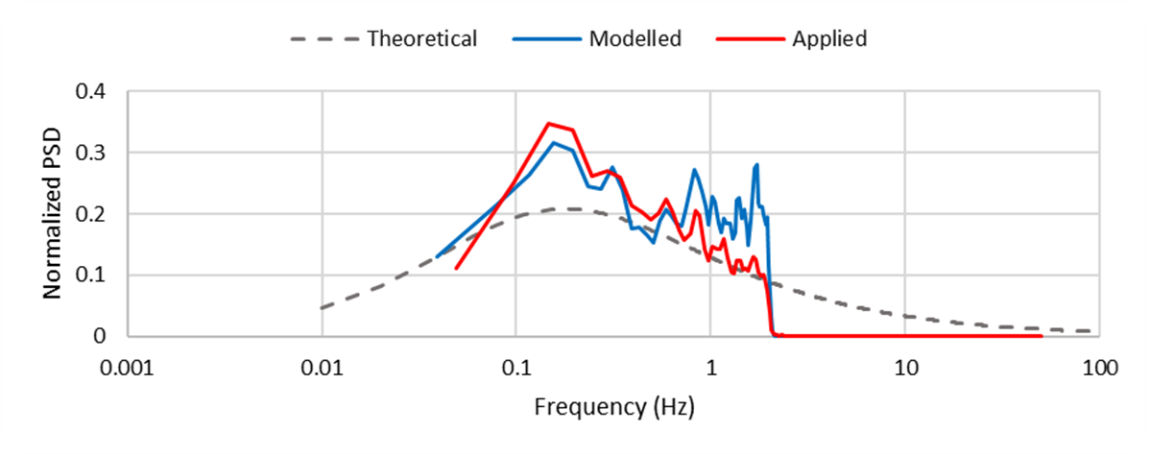

Figure C.39: PSD diagram for 60 m/s load time history of specimen HD3

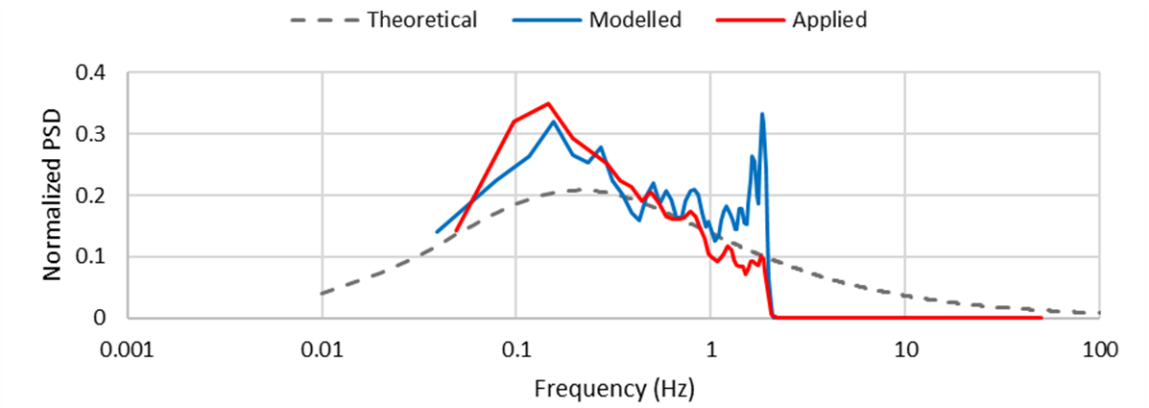

Figure C.40: PSD diagram for 70 m/s load time history of specimen HD3

Specimen HD4

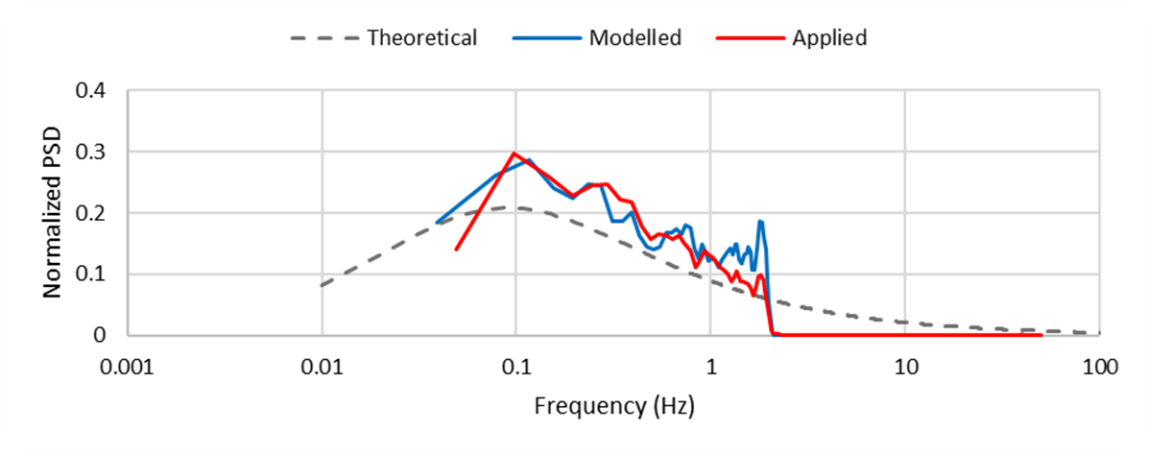

Figure C.41: PSD diagram for 30 m/s load time history of specimen HD4

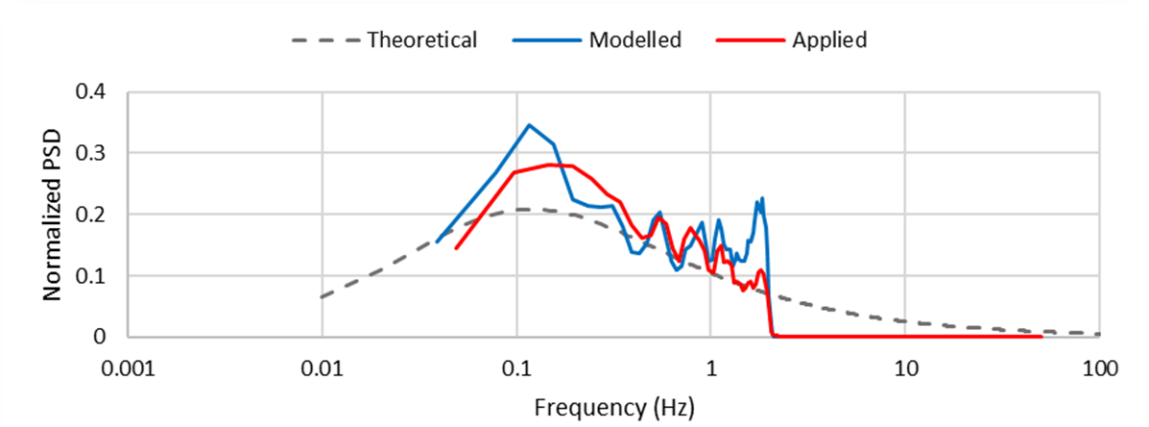

Figure C.42: PSD diagram for 40 m/s load time history of specimen HD4

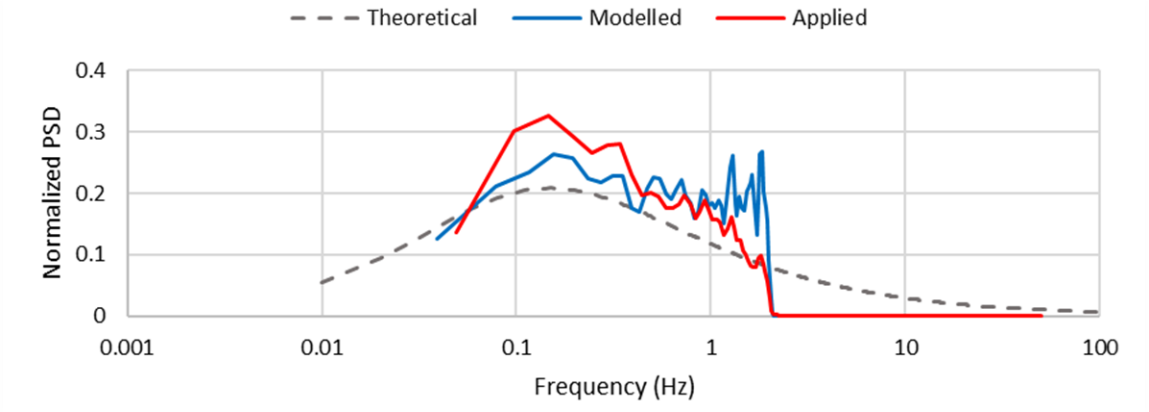

Figure C.43: PSD diagram for 50 m/s load time history of specimen HD4

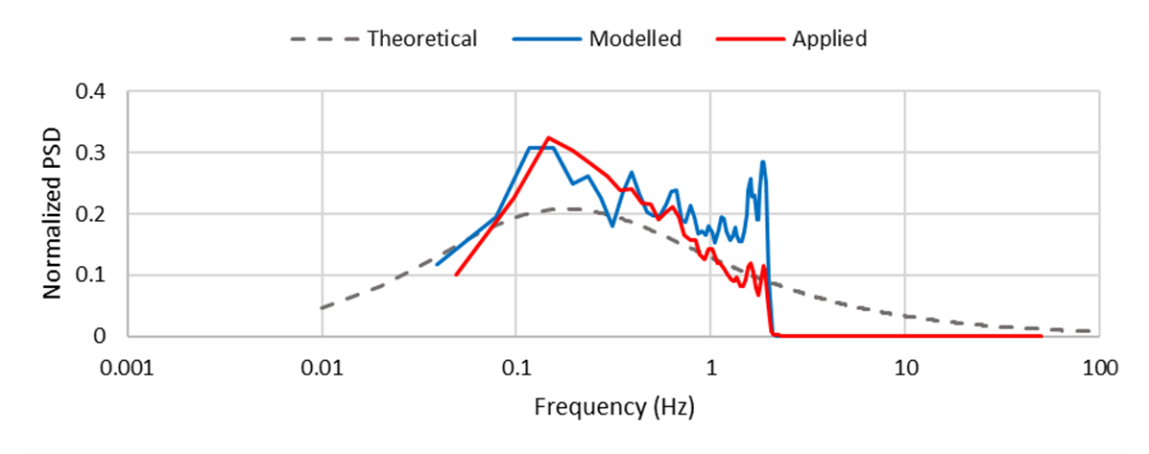

Figure C.44: PSD diagram for 60 m/s load time history of specimen HD4

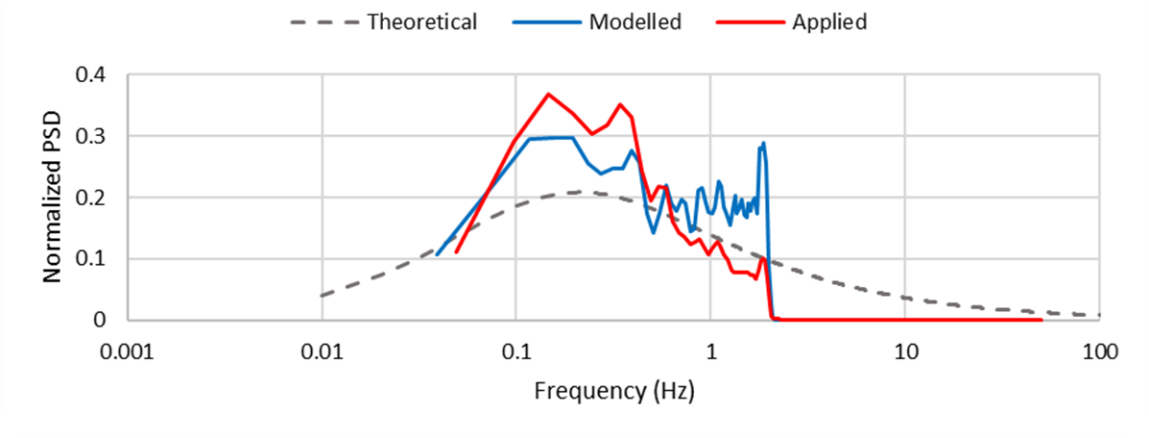

Figure C.45: PSD diagram for 70 m/s load time history of specimen HD4

Specimen HD5

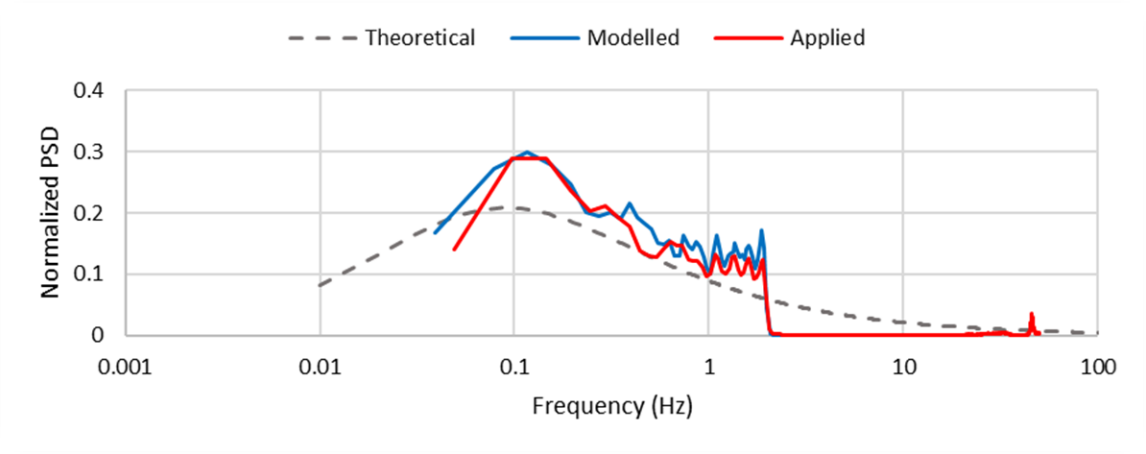

Figure C.46: PSD diagram for 30 m/s load time history of specimen HD5

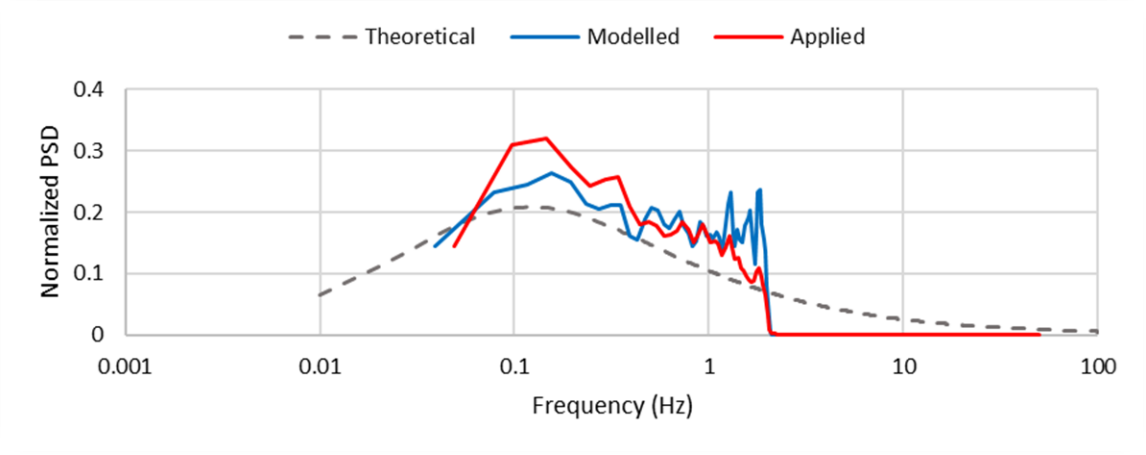

Figure C.47: PSD diagram for 40 m/s load time history of specimen HD5

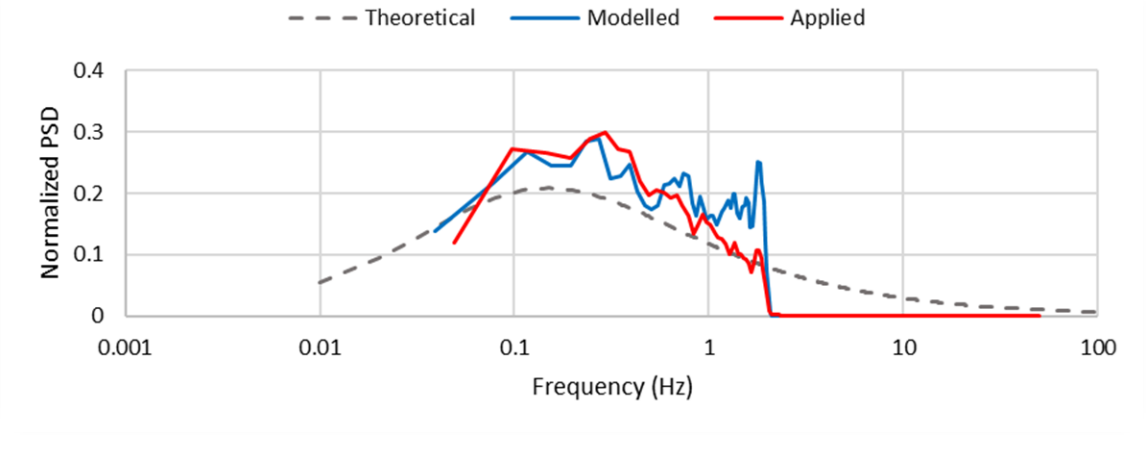

Figure C.48: PSD diagram for 50 m/s load time history of specimen HD5

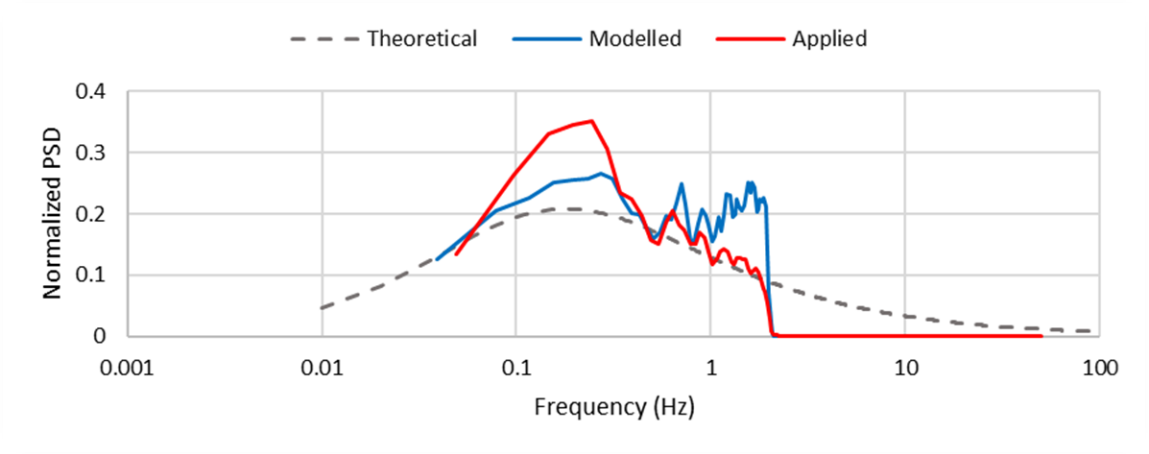

Figure C.49: PSD diagram for 60 m/s load time history of specimen HD5

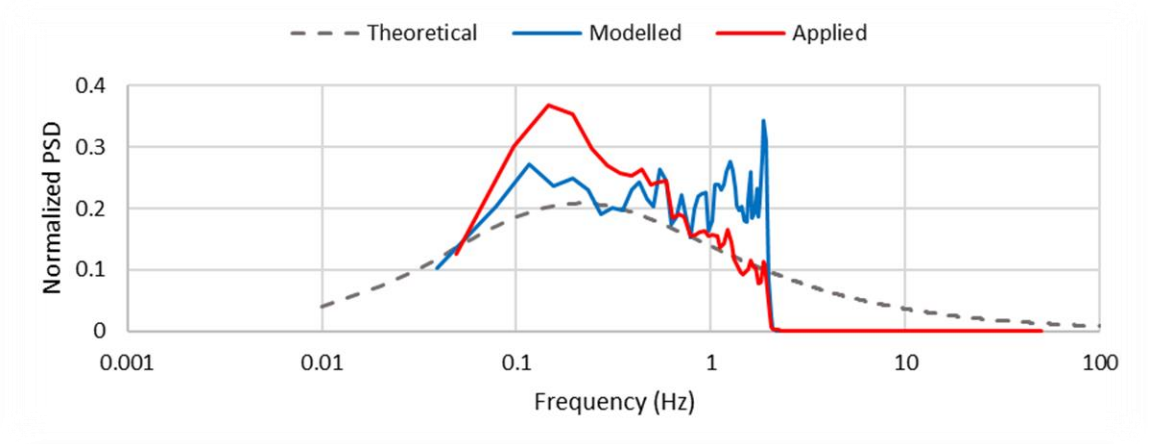

Figure C.50: PSD diagram for 70 m/s load time history of specimen HD5

Appendix D: Applied Dynamic Wind Load Time Histories

Appendix D contains the load time histories that were applied to the wall specimens tested under dynamic loading conditions. *Figure D.1* to *Figure D.25* depict the plots for the wall specimens with the low reinforcement ratio, while *Figure D.26* to *Figure D.50* depict the plots for the wall specimens with the high reinforcement ratio.

The applied load in the diagrams represent the total load applied by the MTS® Series 244 hydraulic actuator on the wall specimens. The measurements were taken using the built-in force transducer of the actuator.

Specimen LD1

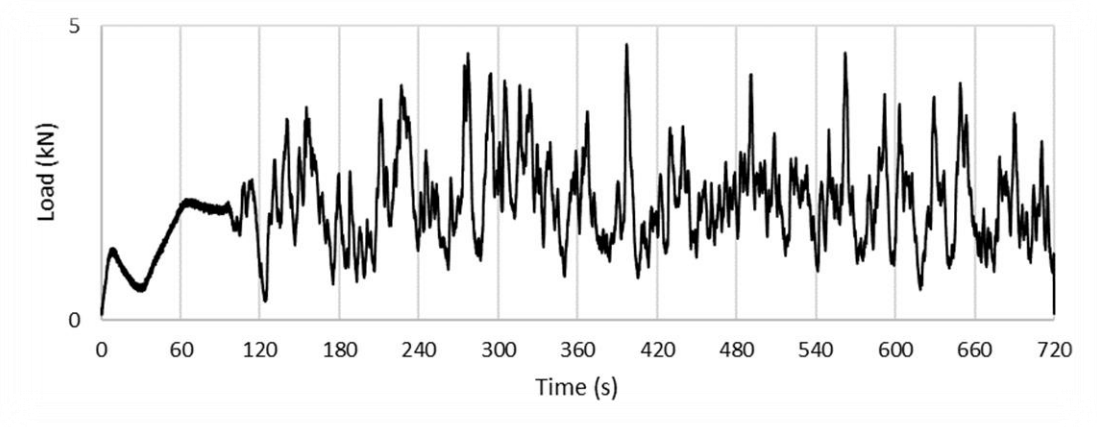

Figure D.1: The 30 m/s load time history of specimen LD1

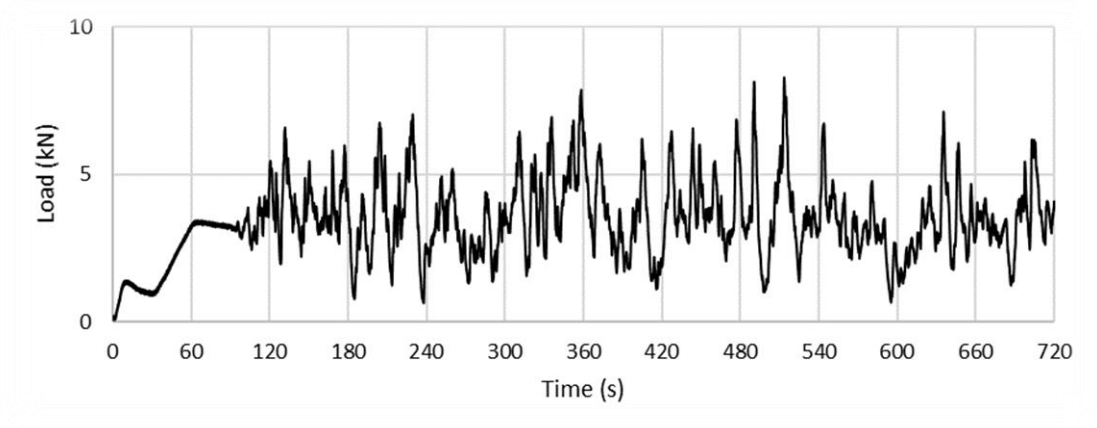

Figure D.2: The 40 m/s load time history of specimen LD1

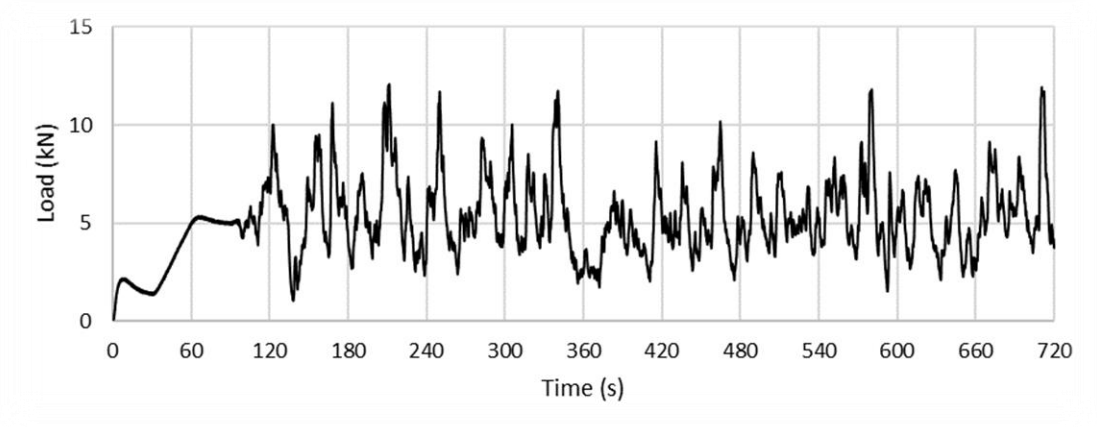

Figure D.3: The 50 m/s load time history of specimen LD1

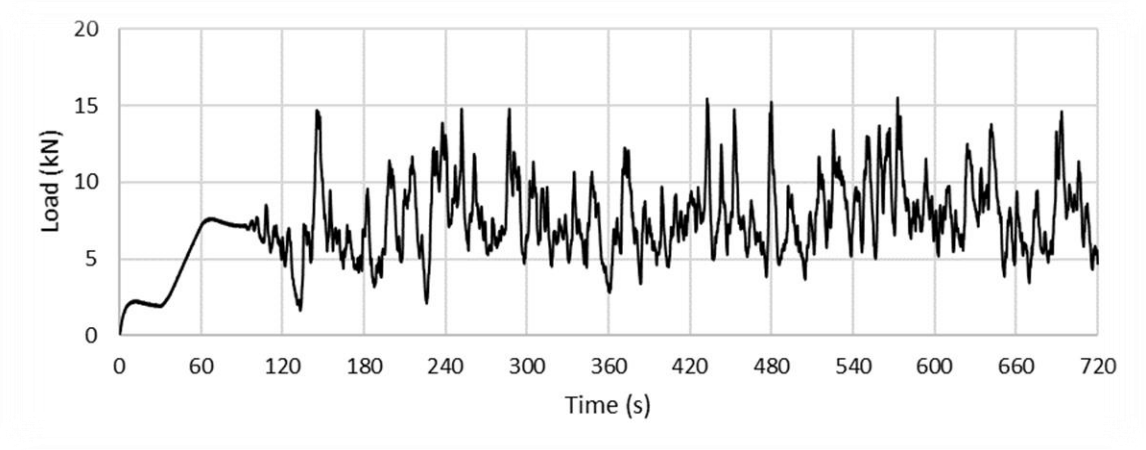

Figure D.4: The 60 m/s load time history of specimen LD1

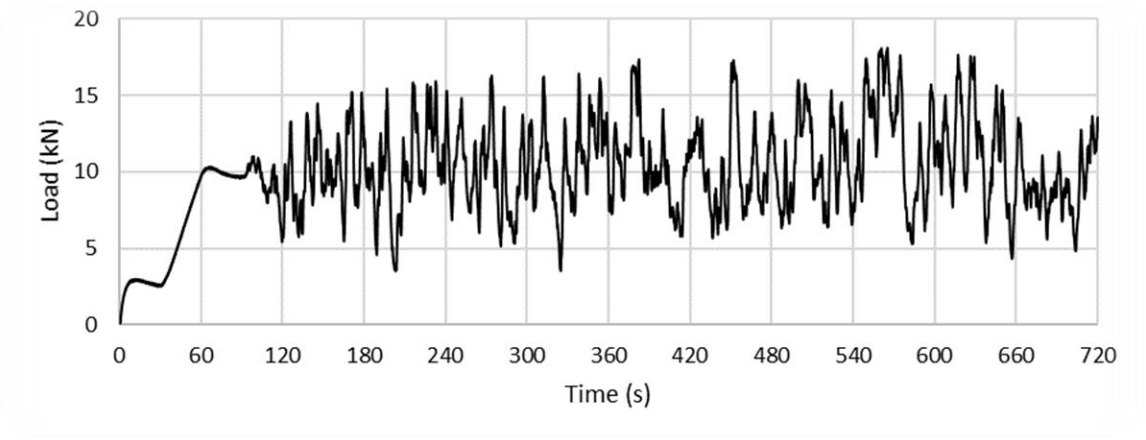

Figure D.5: The 70 m/s load time history of specimen LD1

Specimen LD2

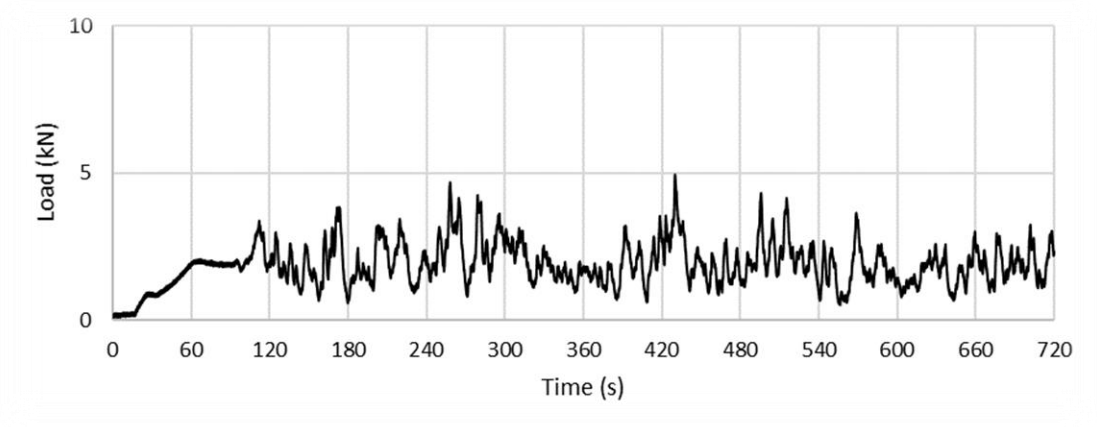

Figure D.6: The 30 m/s load time history of specimen LD2

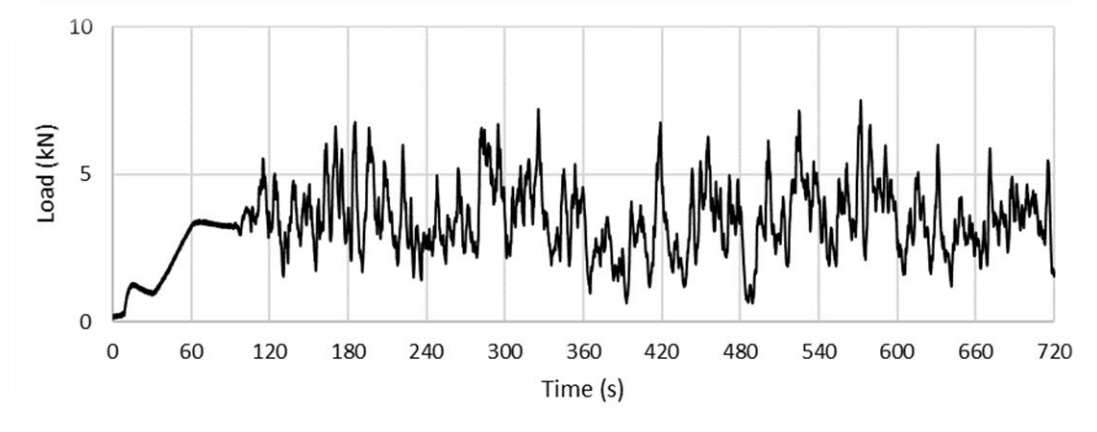

Figure D.7: The 40 m/s load time history of specimen LD2

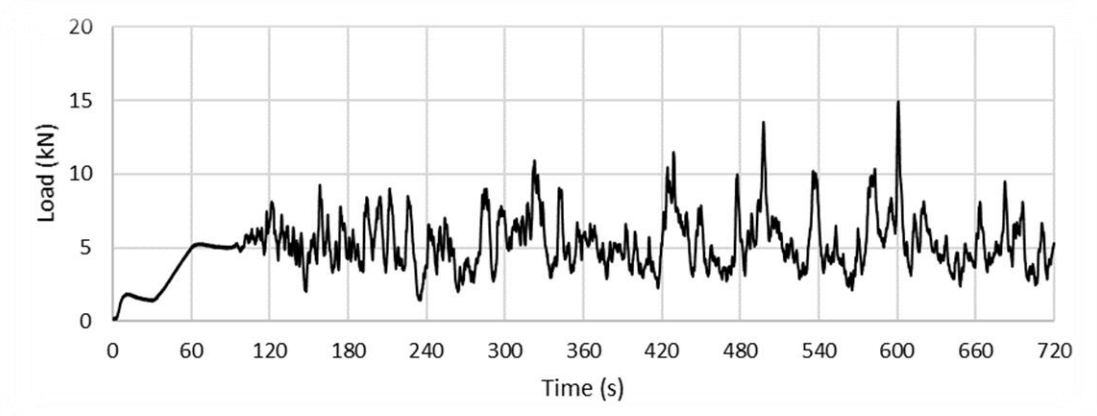

Figure D.8: The 50 m/s load time history of specimen LD2

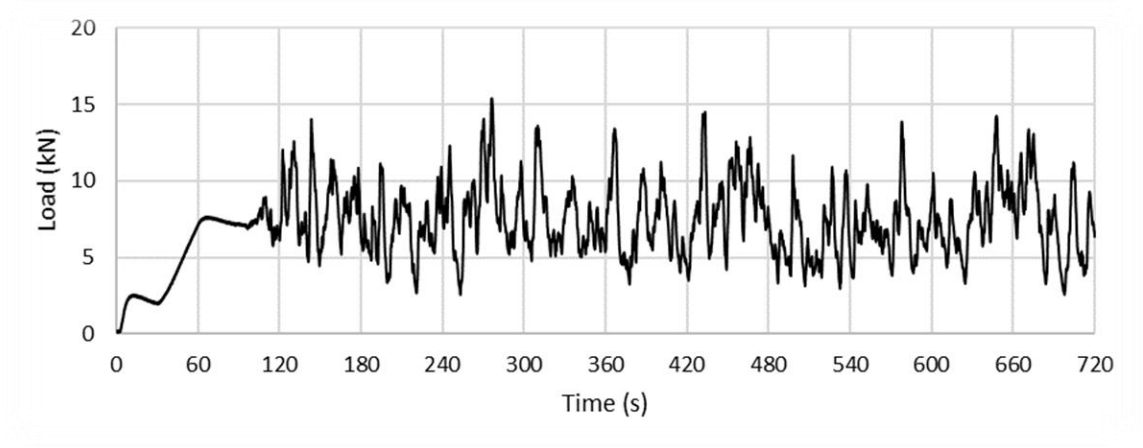

Figure D.9: The 60 m/s load time history of specimen LD2

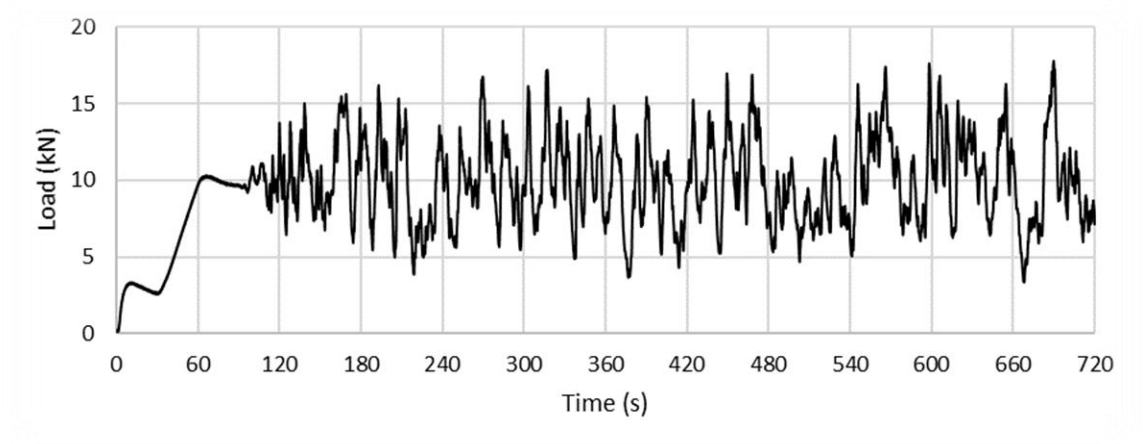

Figure D.10: The 70 m/s load time history of specimen LD2

Specimen LD3

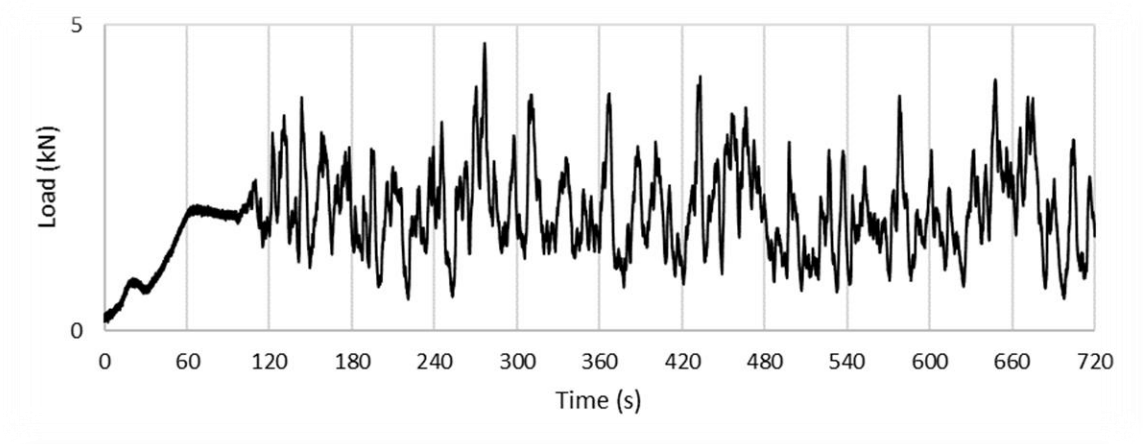

Figure D.11: The 30 m/s load time history of specimen LD3

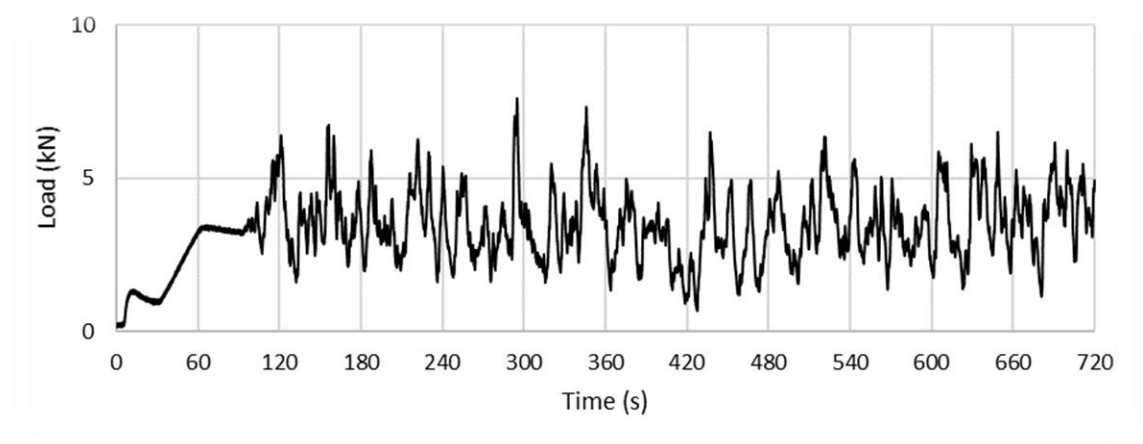

Figure D.12: The 40 m/s load time history of specimen LD3

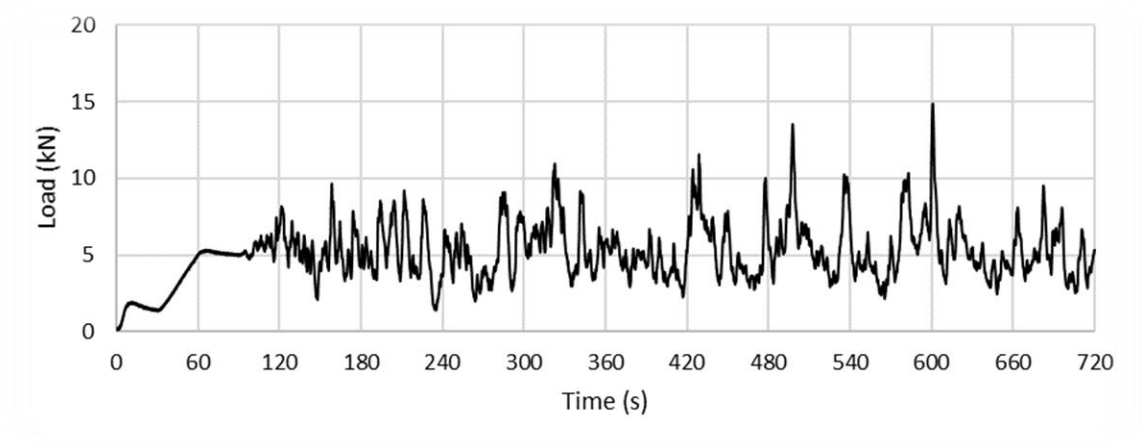

Figure D.13: The 50 m/s load time history of specimen LD3

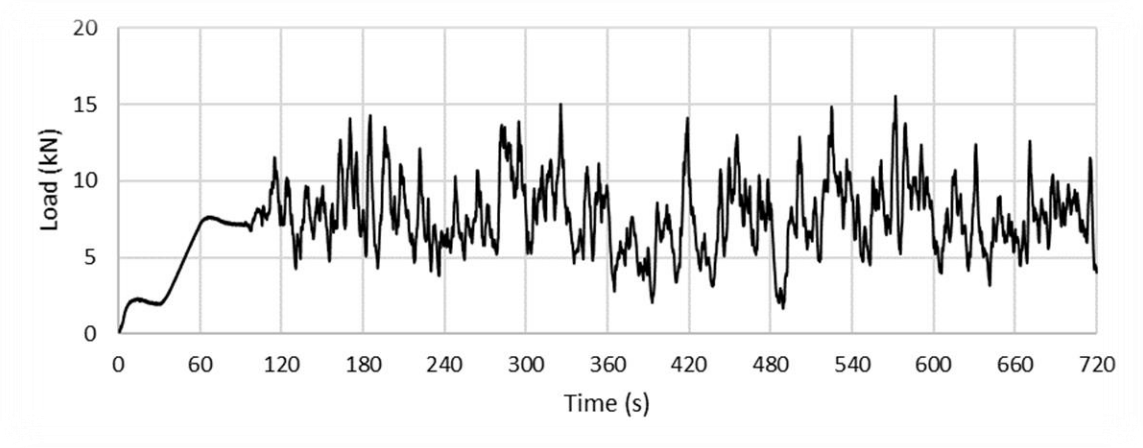

Figure D.14: The 60 m/s load time history of specimen LD3

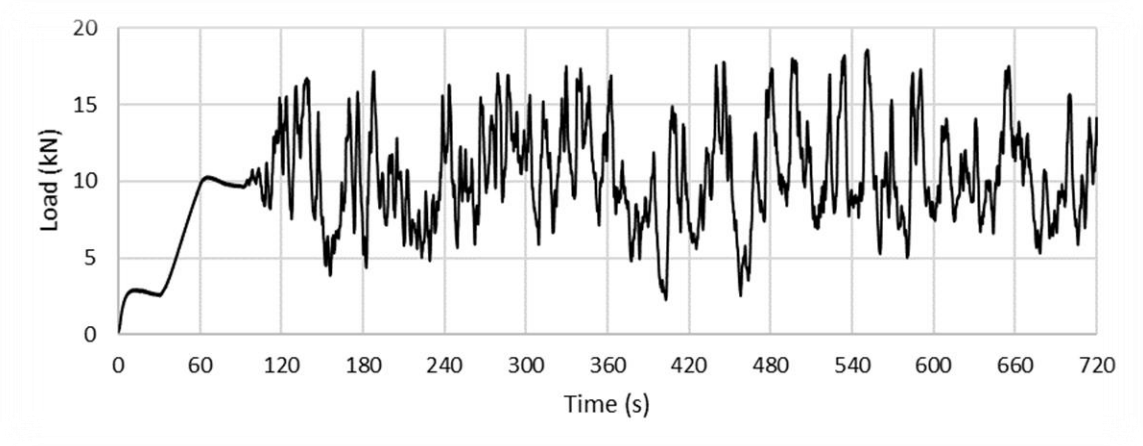

Figure D.15: The 70 m/s load time history of specimen LD3

Specimen LD4

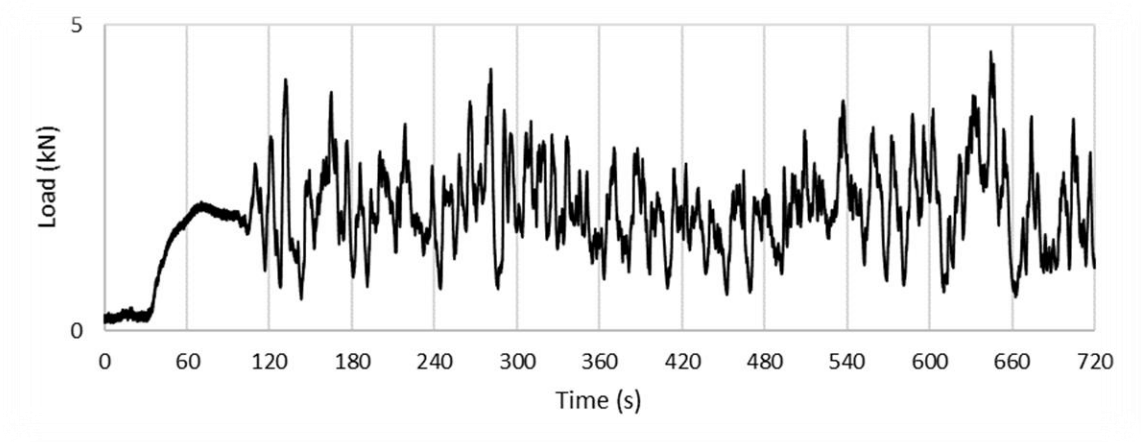

Figure D.16: The 30 m/s load time history of specimen LD4

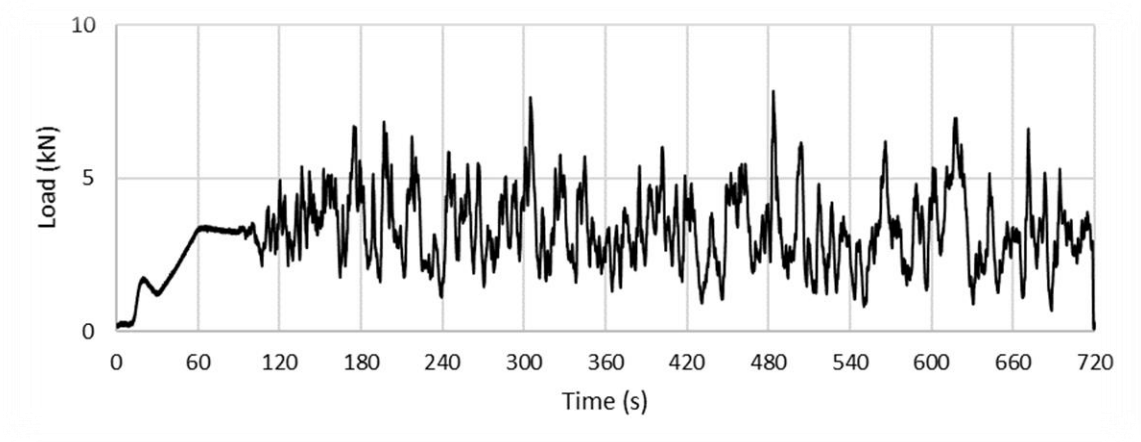

Figure D.17: The 40 m/s load time history of specimen LD4

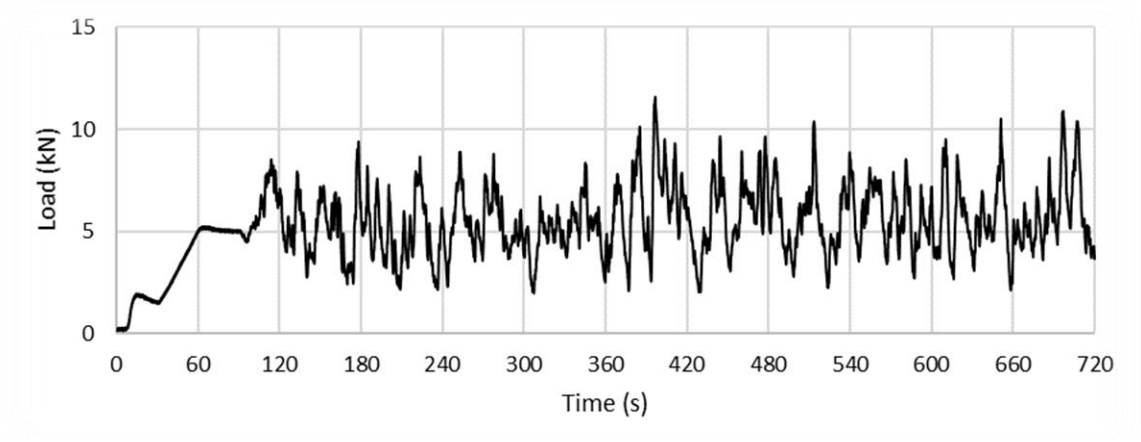

Figure D.18: The 50 m/s load time history of specimen LD4

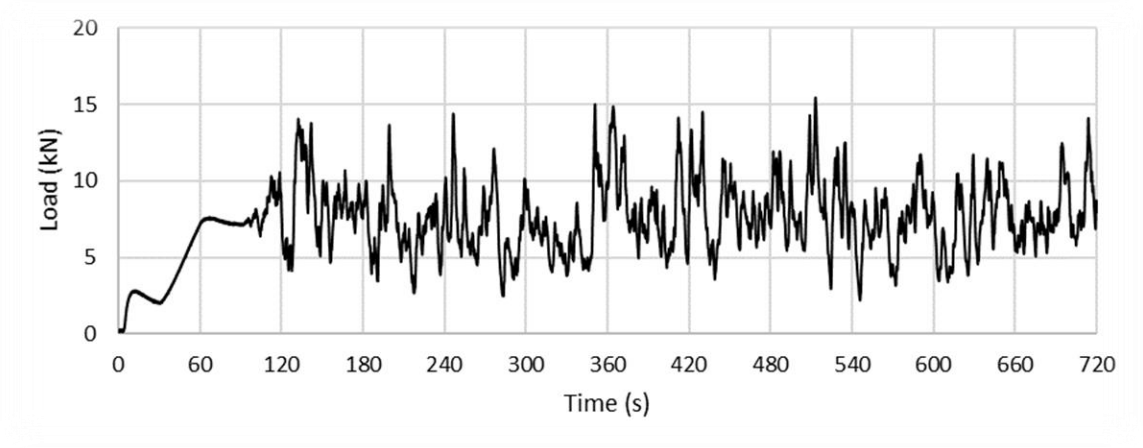

Figure D.19: The 60 m/s load time history of specimen LD4

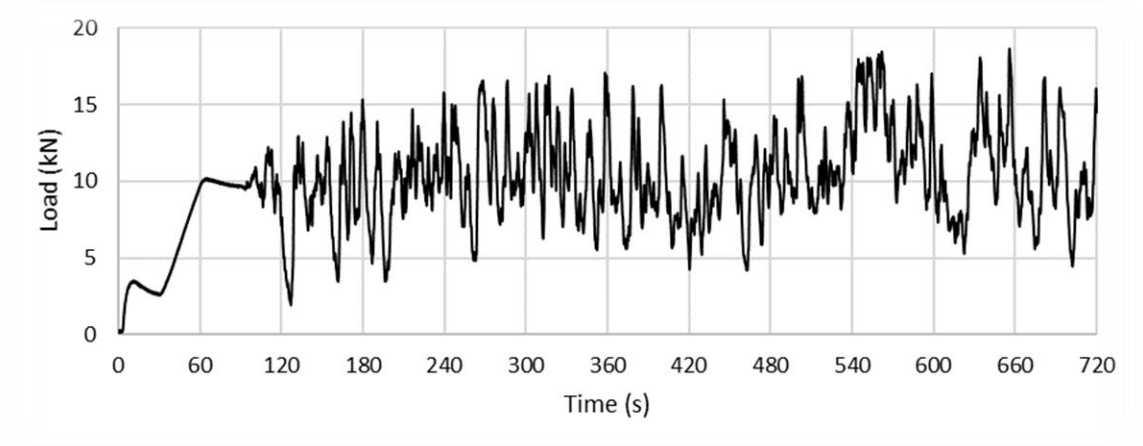

Figure D.20: The 70 m/s load time history of specimen LD4

Specimen LD5

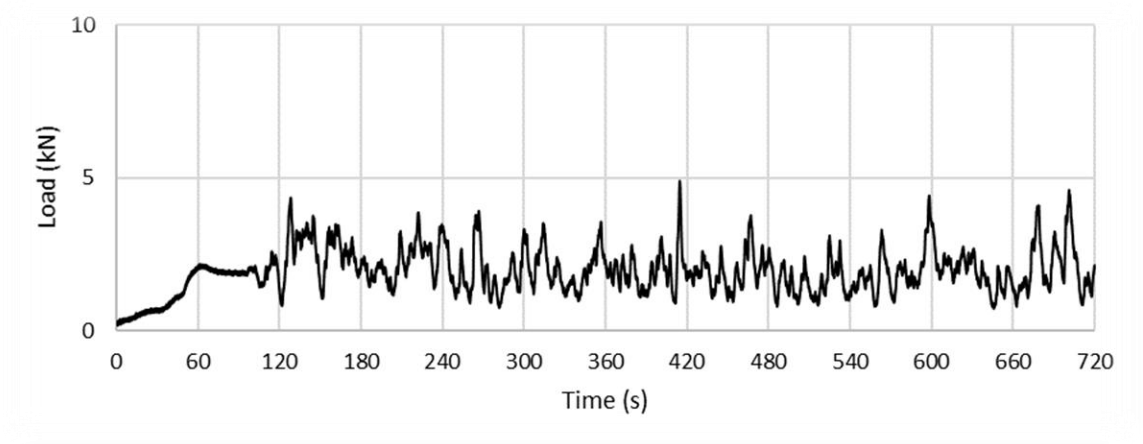

Figure D.21: The 30 m/s load time history of specimen LD5

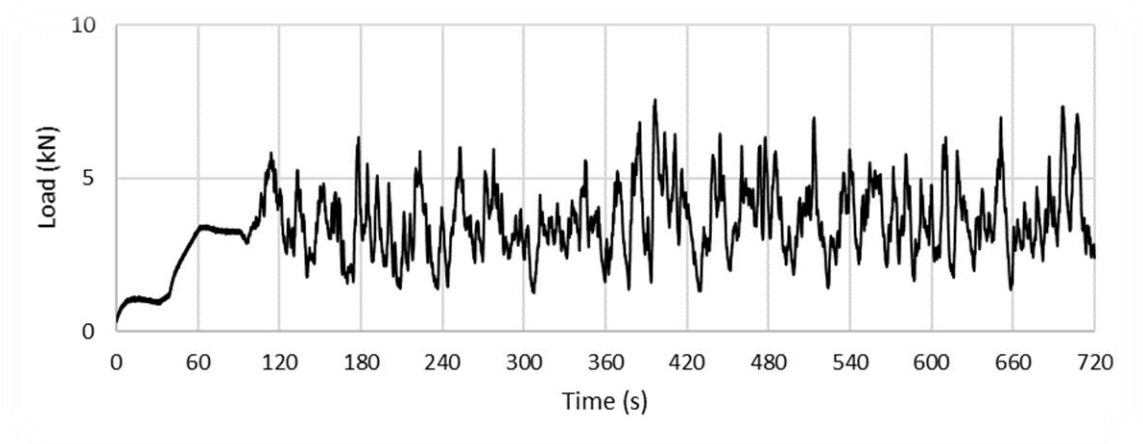

Figure D.22: The 40 m/s load time history of specimen LD5

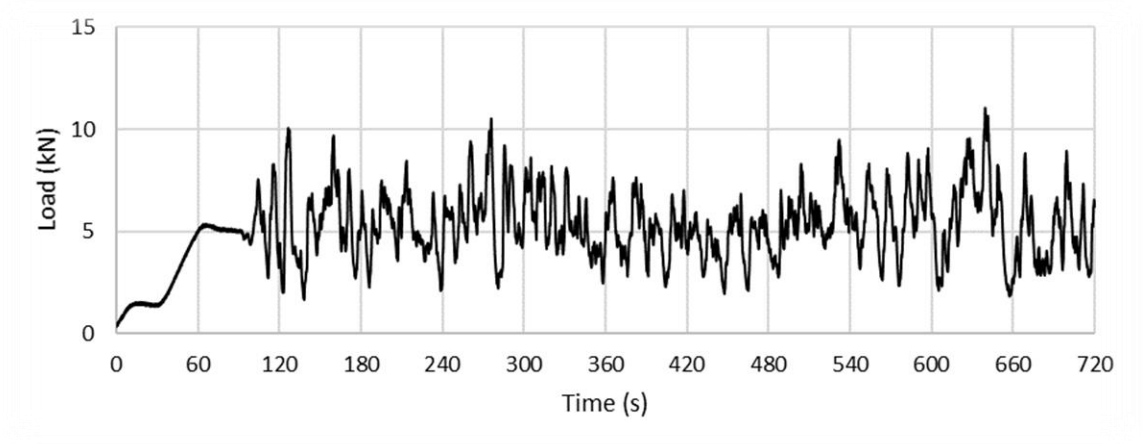

Figure D.23: The 50 m/s load time history of specimen LD5

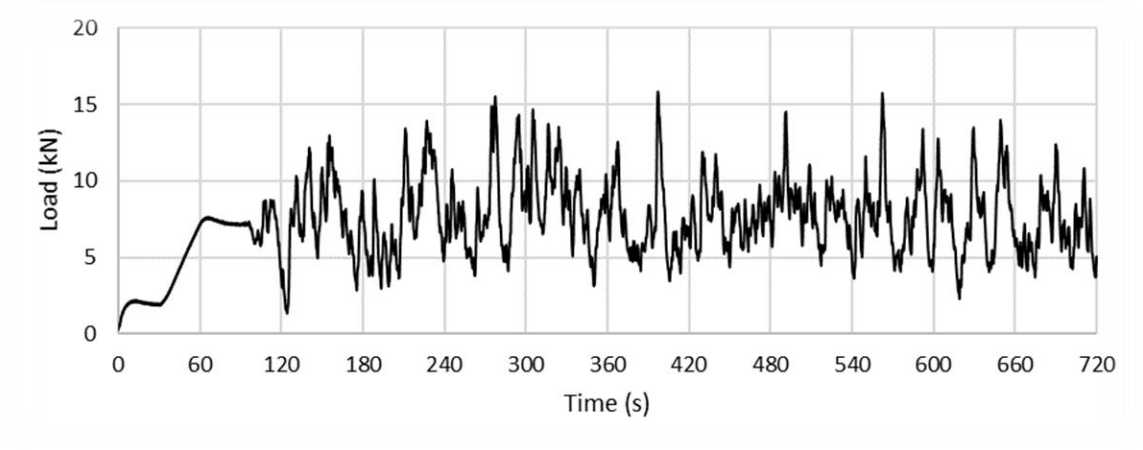

Figure D.24: The 60 m/s load time history of specimen LD5

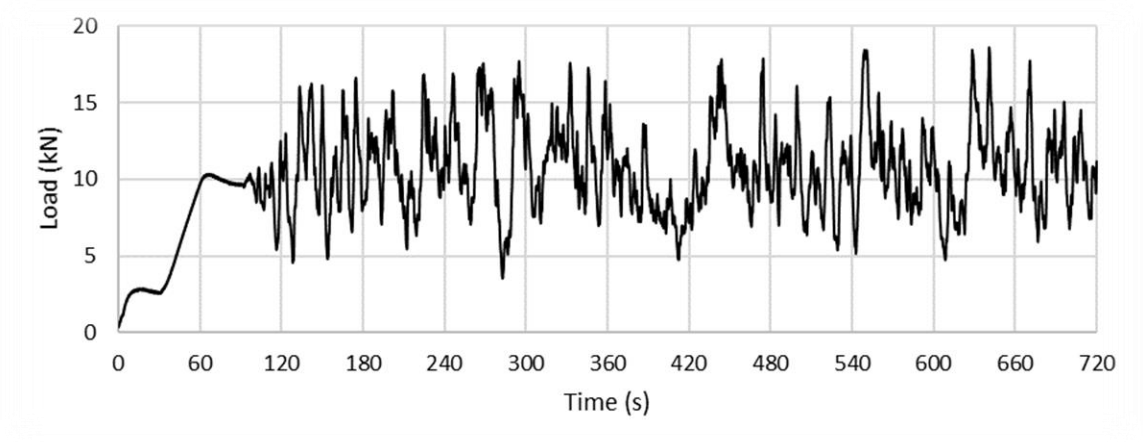

Figure D.25: The 70 m/s load time history of specimen LD5

Specimen HD1

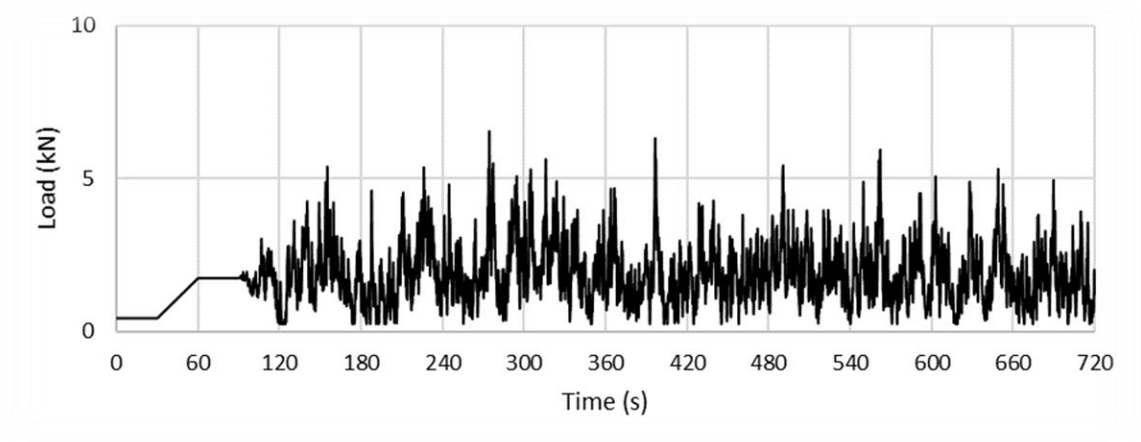

Figure D.26: The 30 m/s load time history of specimen HD1

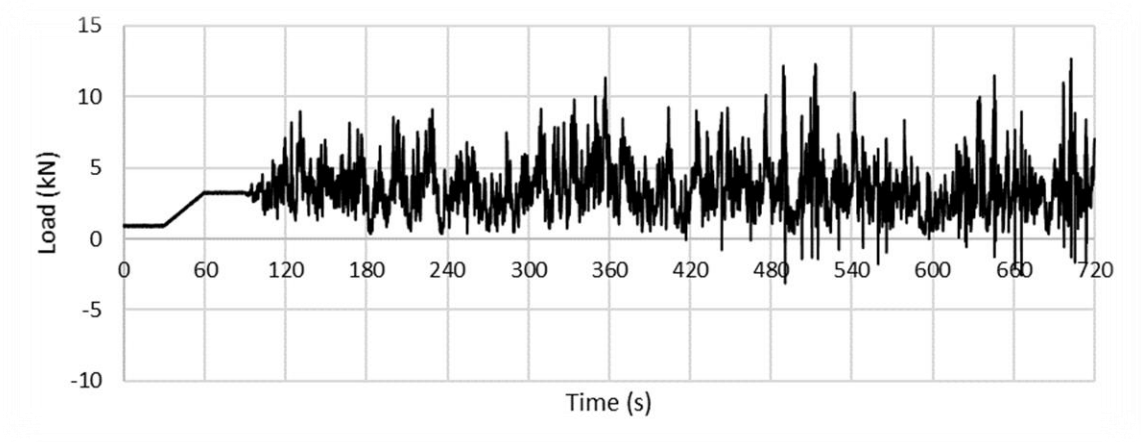

Figure D.27: The 40 m/s load time history of specimen HD1

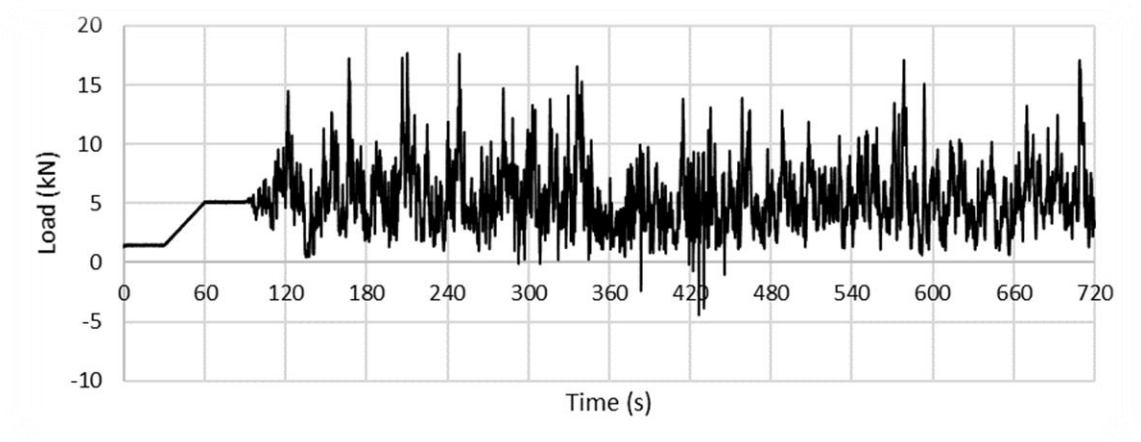

Figure D.28: The 50 m/s load time history of specimen HD1

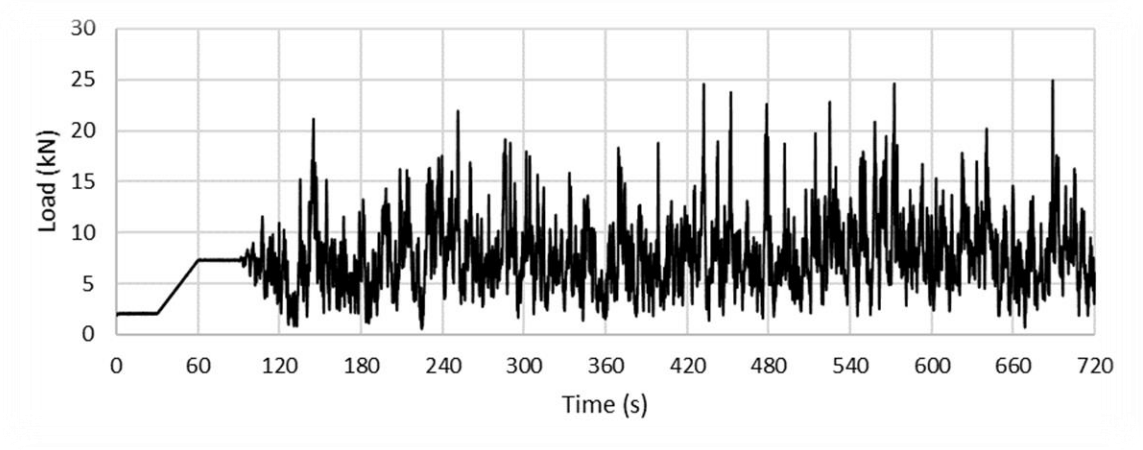

Figure D.29: The 60 m/s load time history of specimen HD1

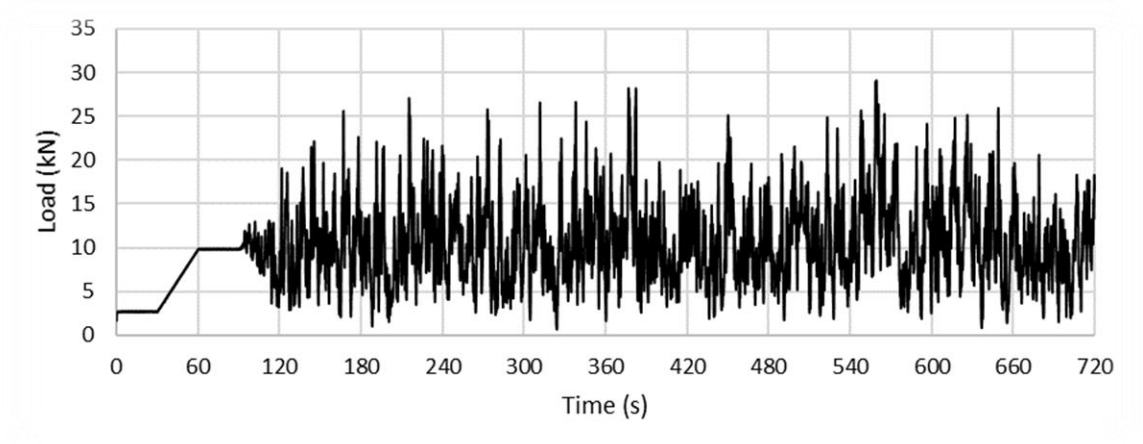

Figure D.30: The 70 m/s load time history of specimen HD1

Specimen HD2

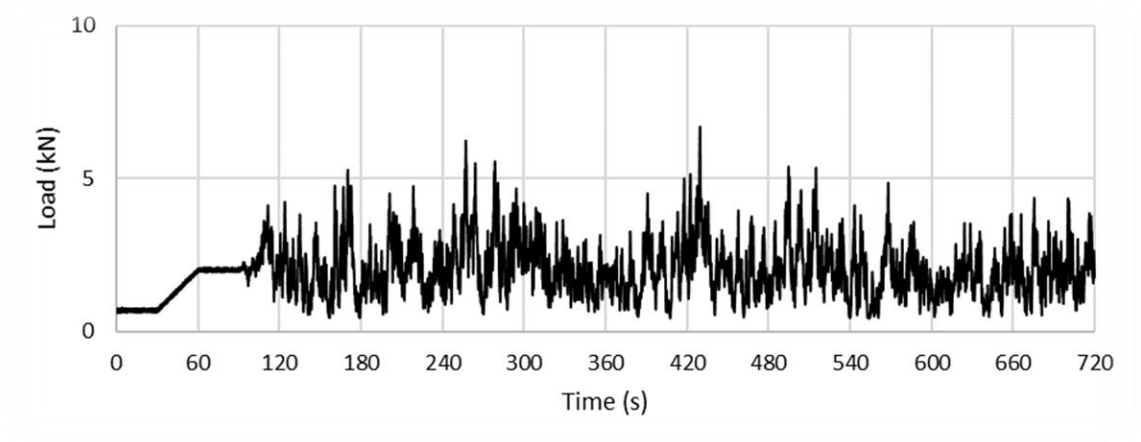

Figure D.31: The 30 m/s load time history of specimen HD2

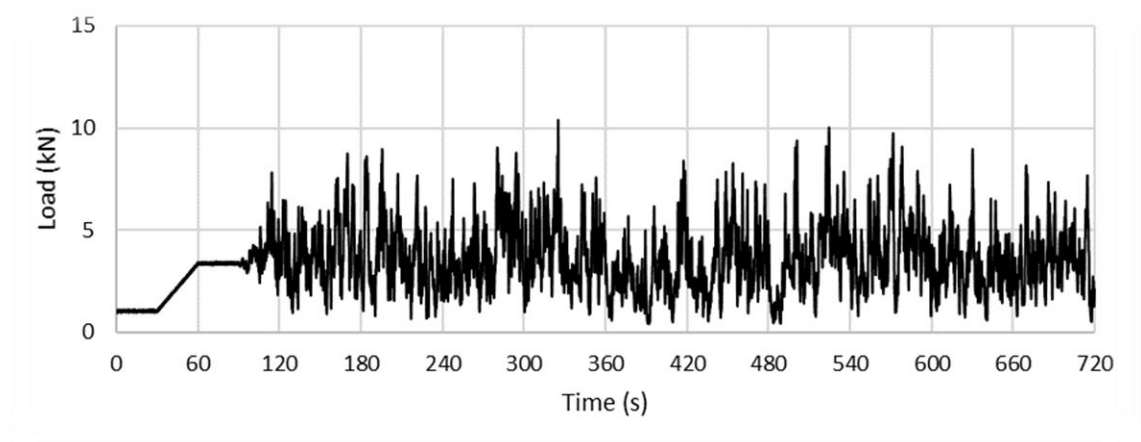

Figure D.32: The 40 m/s load time history of specimen HD2

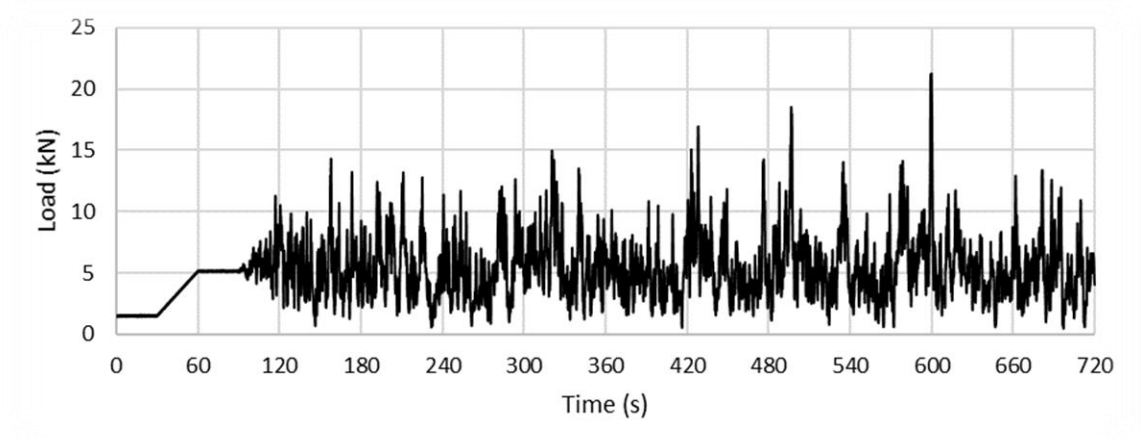

Figure D.33: The 50 m/s load time history of specimen HD2

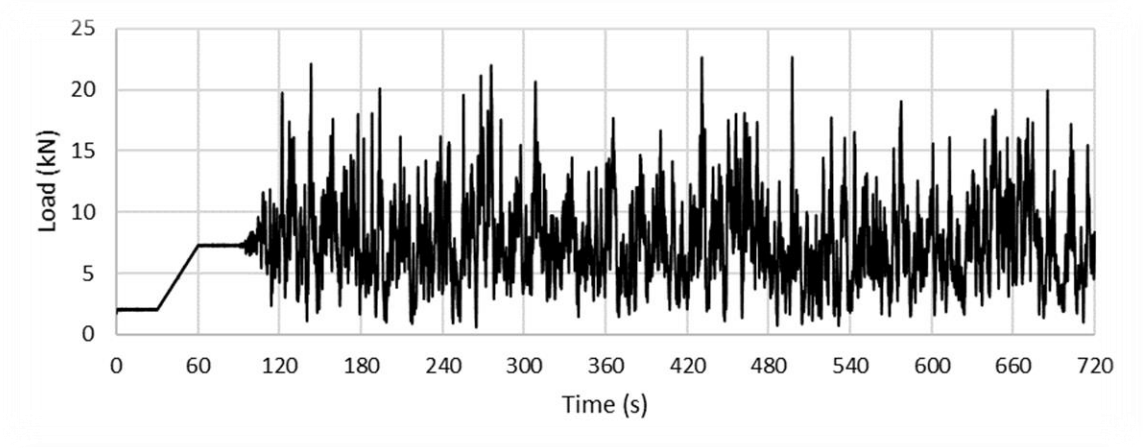

Figure D.34: The 60 m/s load time history of specimen HD2

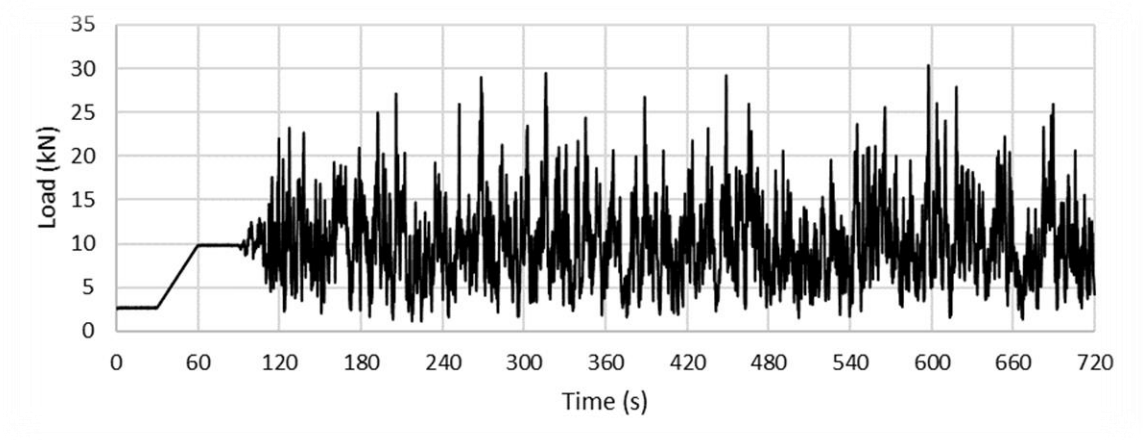

Figure D.35: The 70 m/s load time history of specimen HD2

Specimen HD3

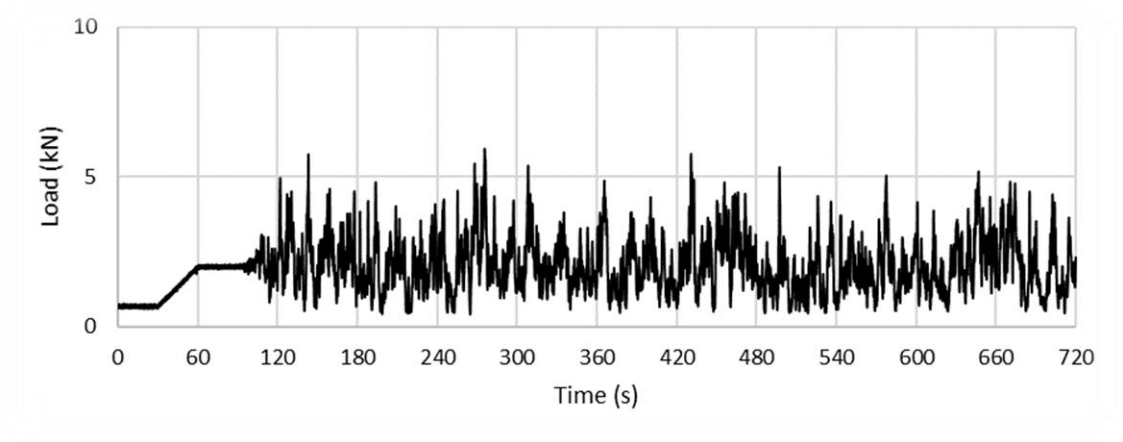

Figure D.36: The 30 m/s load time history of specimen HD3

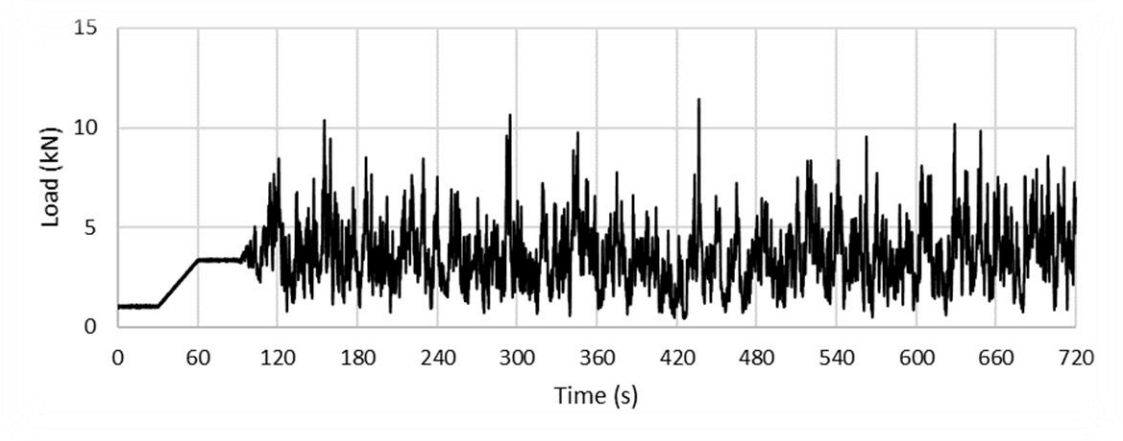

Figure D.37: The 40 m/s load time history of specimen HD3

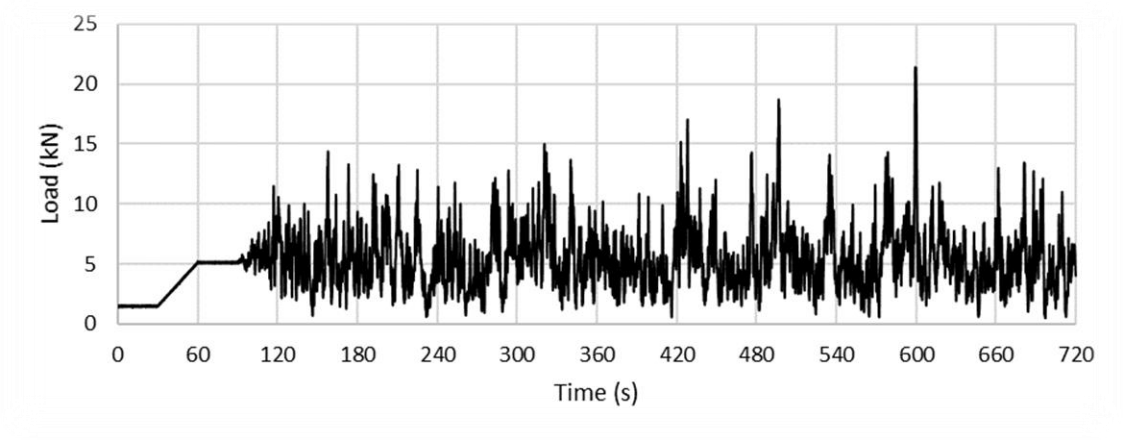

Figure D.38: The 50 m/s load time history of specimen HD3

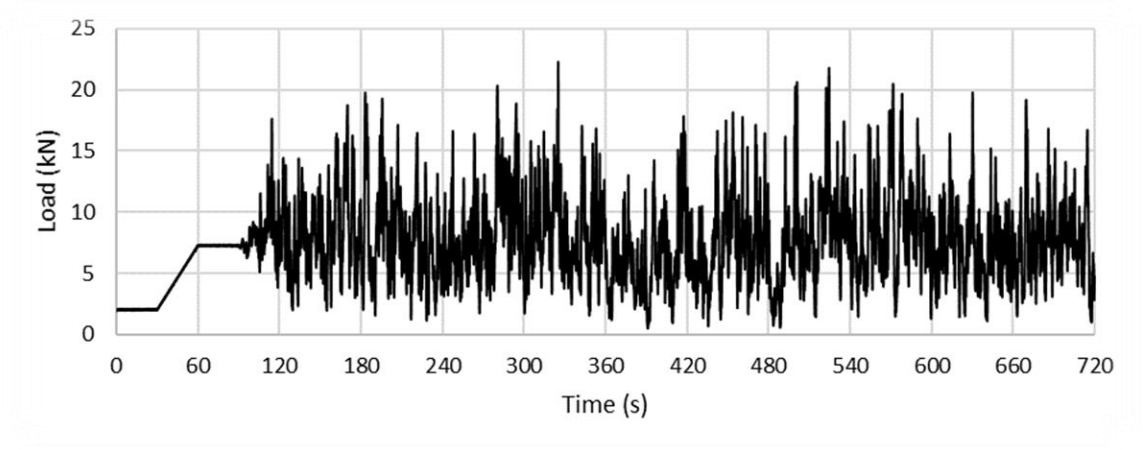

Figure D.39: The 60 m/s load time history of specimen HD3

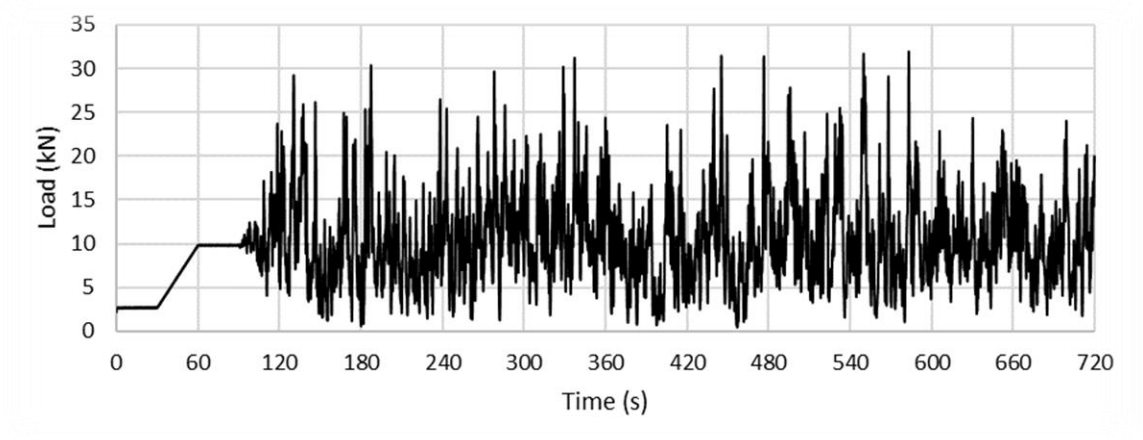

Figure D.40: The 70 m/s load time history of specimen HD3

Specimen HD4

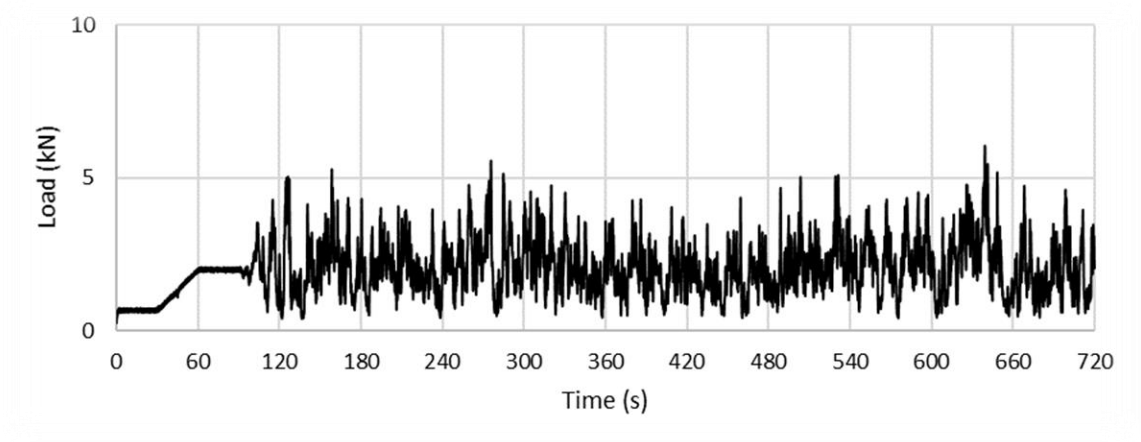

Figure D.41: The 30 m/s load time history of specimen HD4

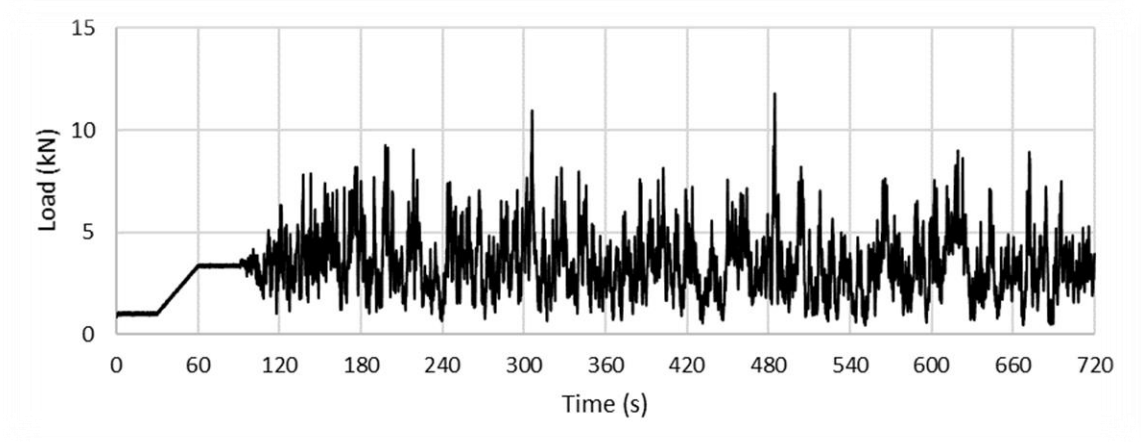

Figure D.42: The 40 m/s load time history of specimen HD4

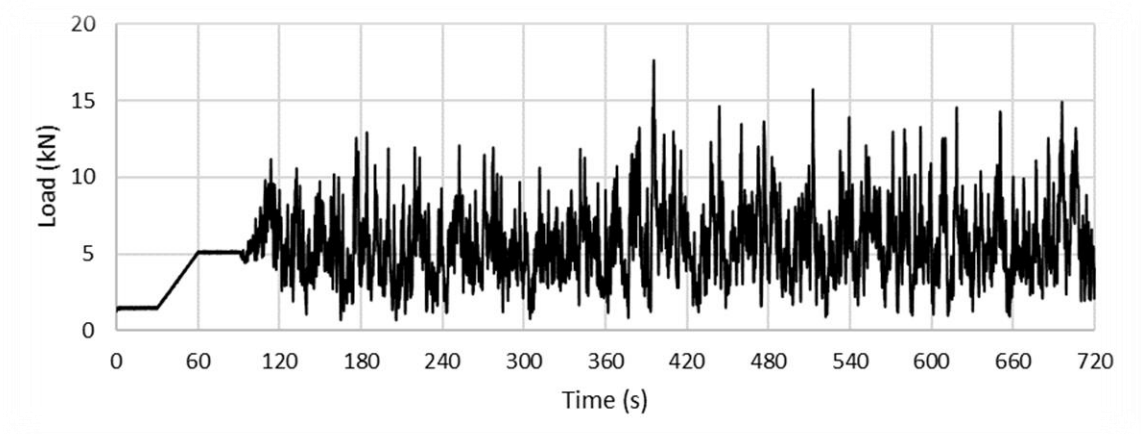

Figure D.43: The 50 m/s load time history of specimen HD4

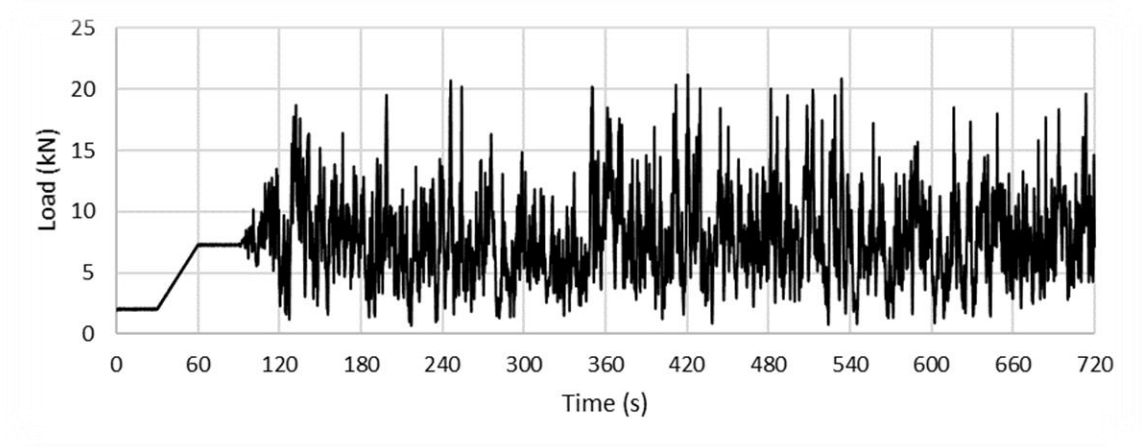

Figure D.44: The 60 m/s load time history of specimen HD4

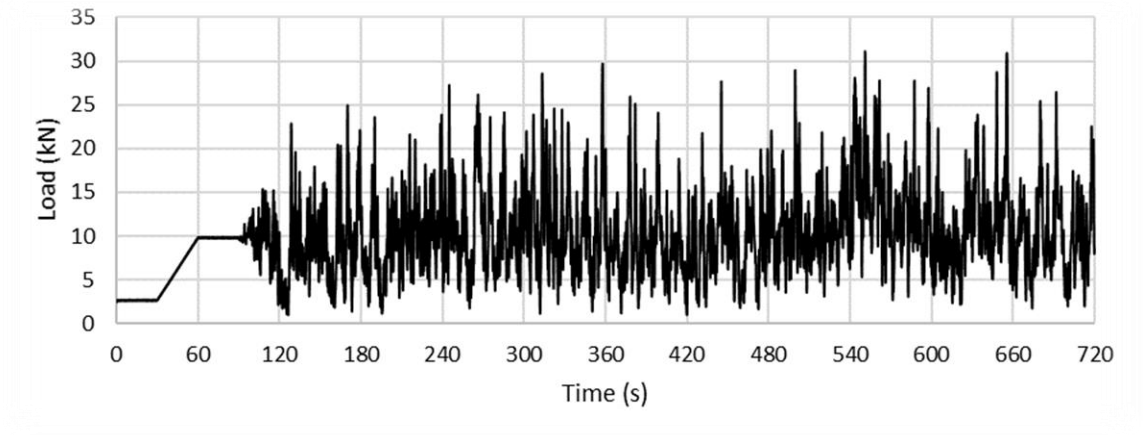

Figure D.45: The 70 m/s load time history of specimen HD4

Specimen HD5

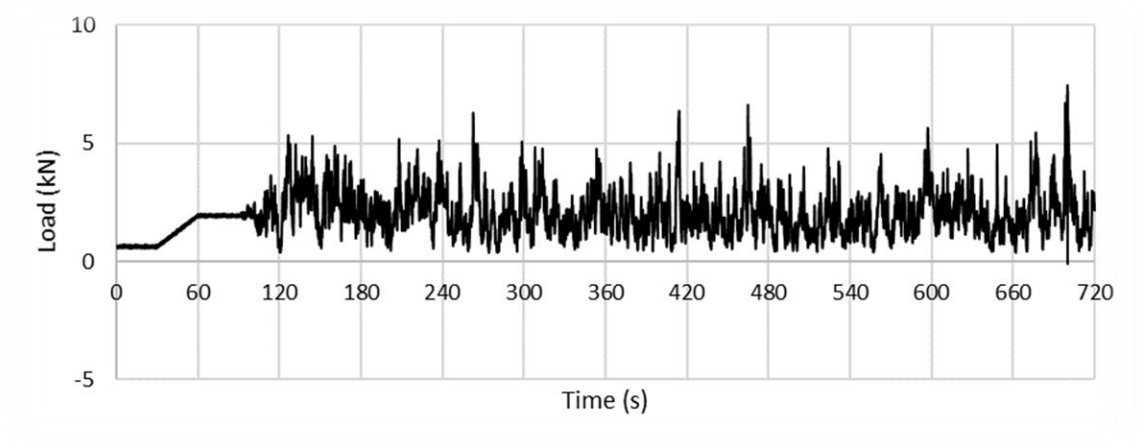

Figure D.46: The 30 m/s load time history of specimen HD5

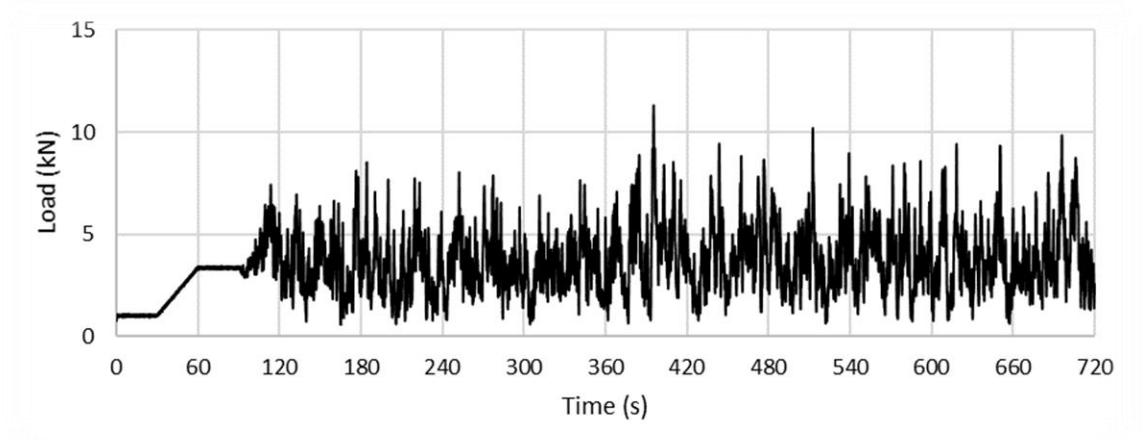

Figure D.47: The 40 m/s load time history of specimen HD5

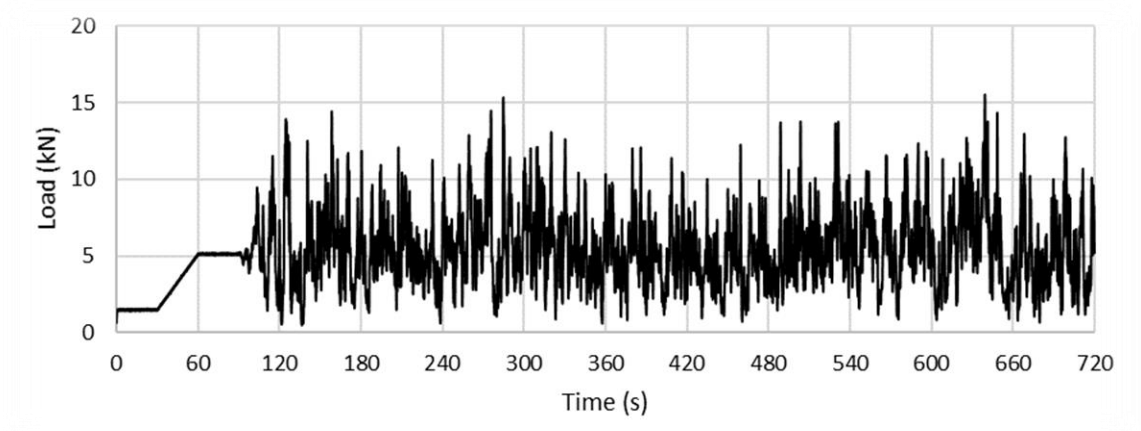

Figure D.48: The 50 m/s load time history of specimen HD5

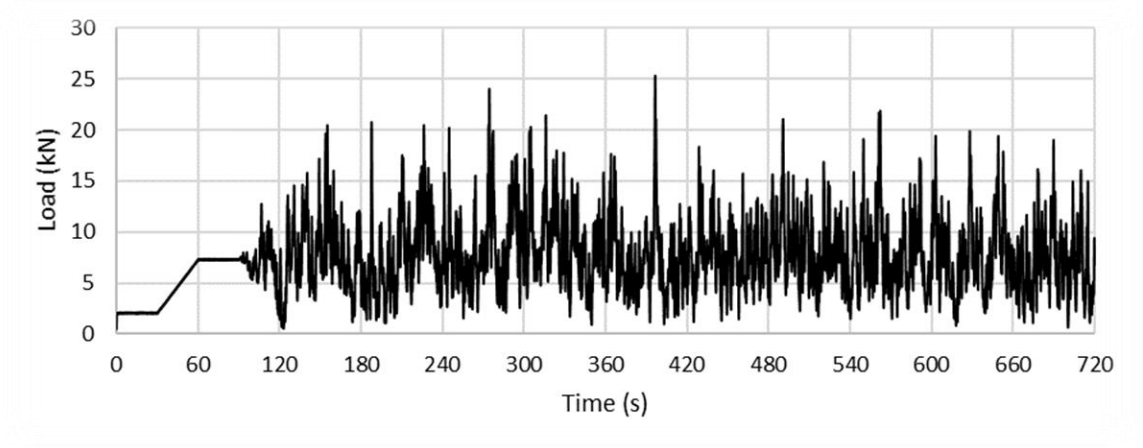

Figure D.49: The 60 m/s load time history of specimen HD5

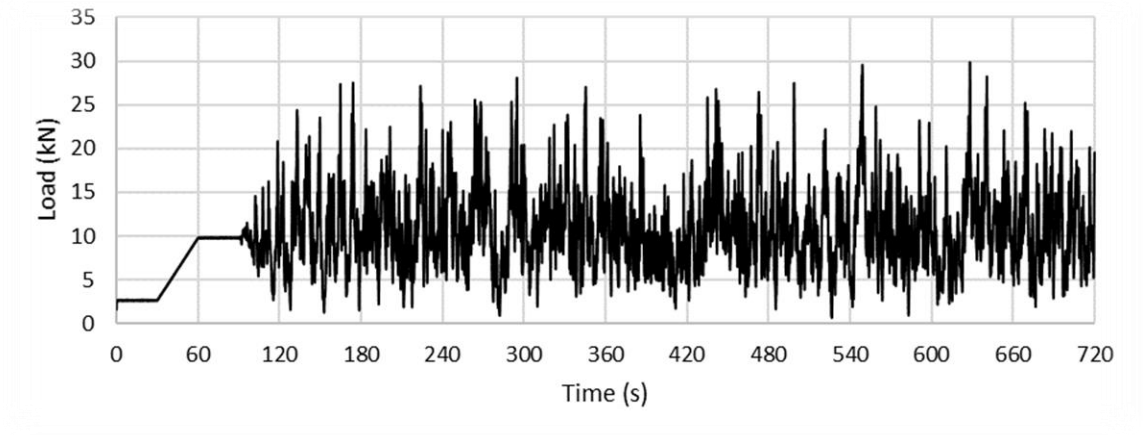

Figure D.50: The 70 m/s load time history of specimen HD5

Appendix E: Deflection Time Histories of the Dynamic Tests

Appendix E contains the deflection time histories that resulted from the wall specimens tested under dynamic loading conditions. *Figure E.1* to *Figure E.25* depict the results of the wall specimens with the low reinforcement ratio, while *Figure E.26* to *Figure E.50* depict the results of the wall specimens with the high reinforcement ratio.

The deflection in the diagrams represent the deflection at mid-height of the wall specimens. The measurements were taken using the Micro-Epsilon optoNCDT 1700-500 laser optical displacement measurement device.

Specimen LD1

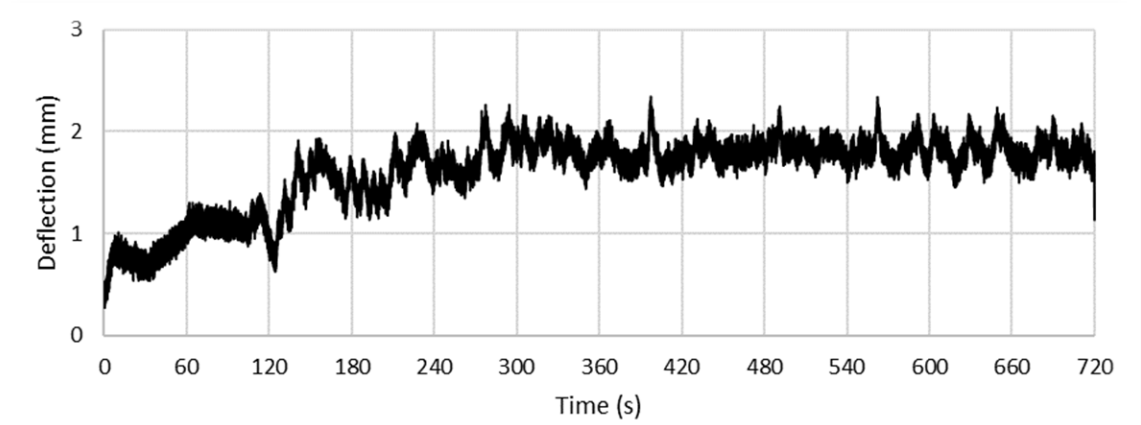

Figure E.1: The 30 m/s deflection time history of specimen LD1

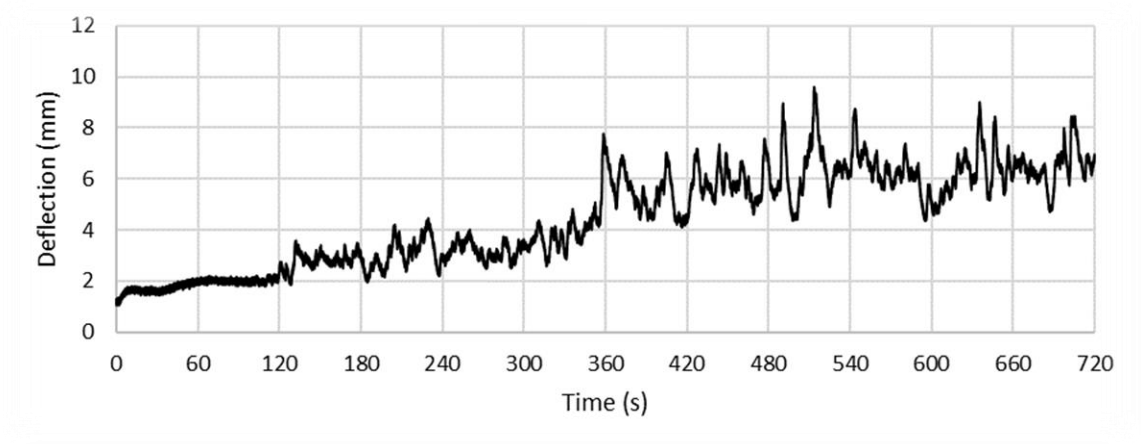

Figure E.2: The 40 m/s deflection time history of specimen LD1

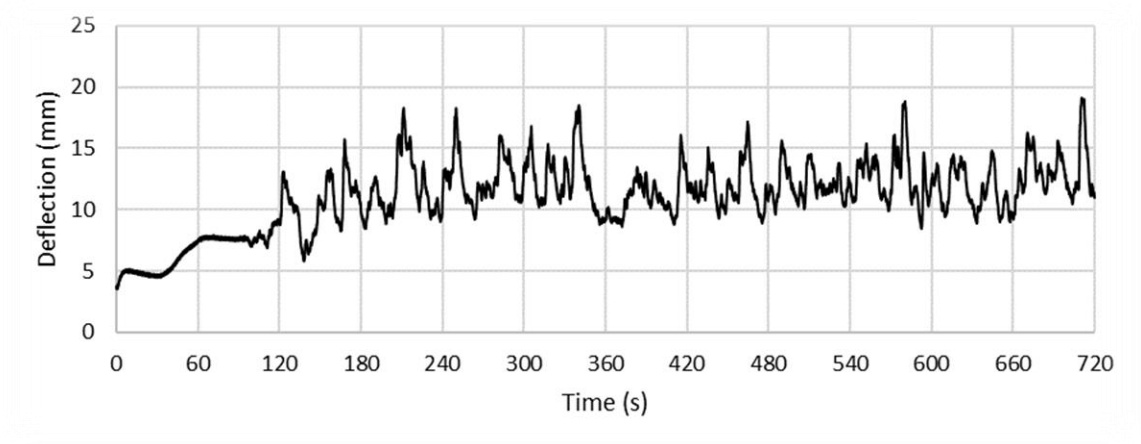

Figure E.3: The 50 m/s deflection time history of specimen LD1

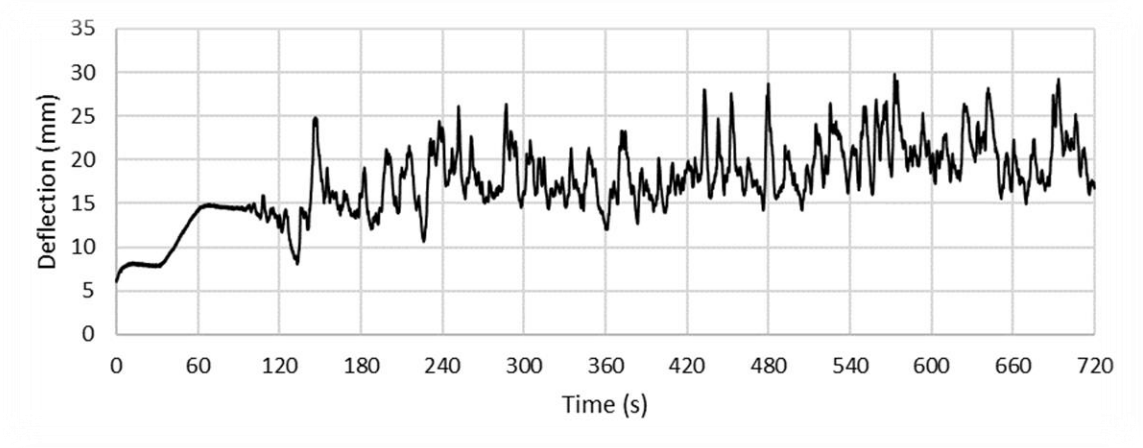

Figure E.4: The 60 m/s deflection time history of specimen LD1

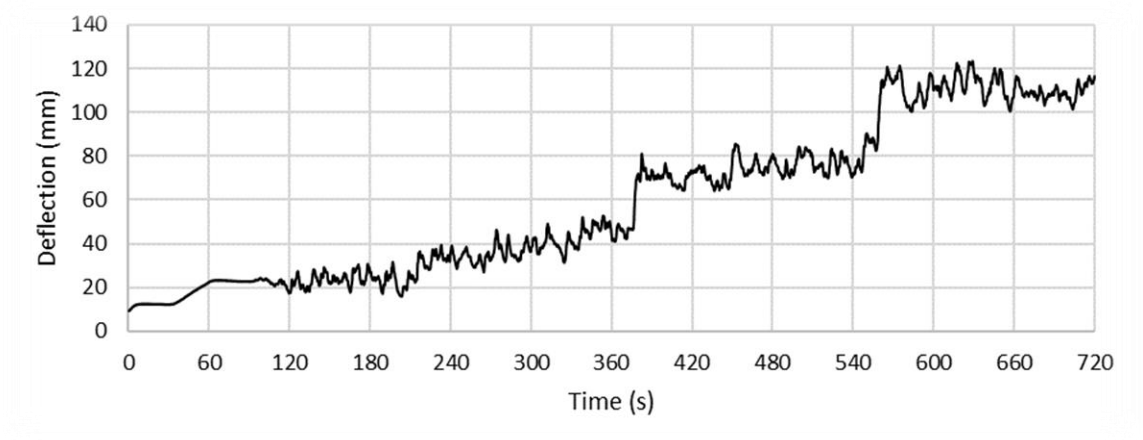

Figure E.5: The 70 m/s deflection time history of specimen LD1

Specimen LD2

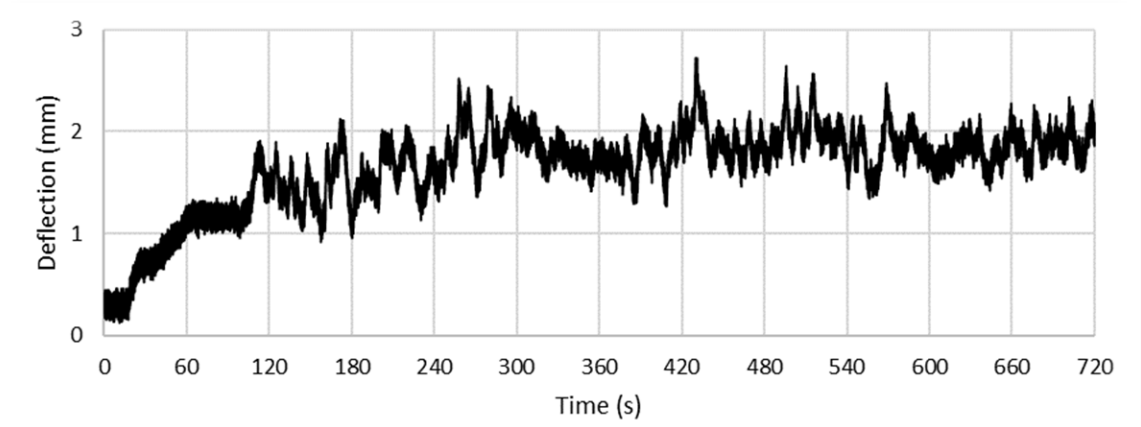

Figure E.6: The 30 m/s deflection time history of specimen LD2

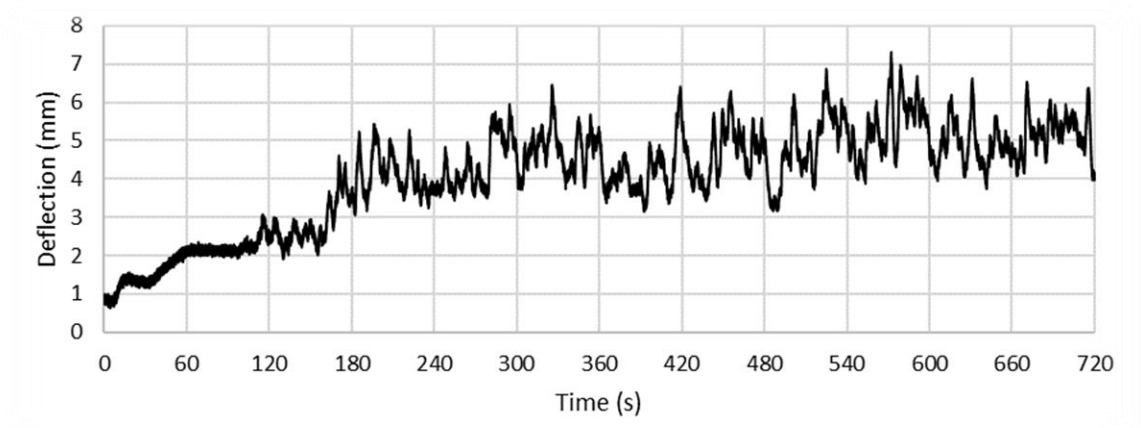

Figure E.7: The 40 m/s deflection time history of specimen LD2

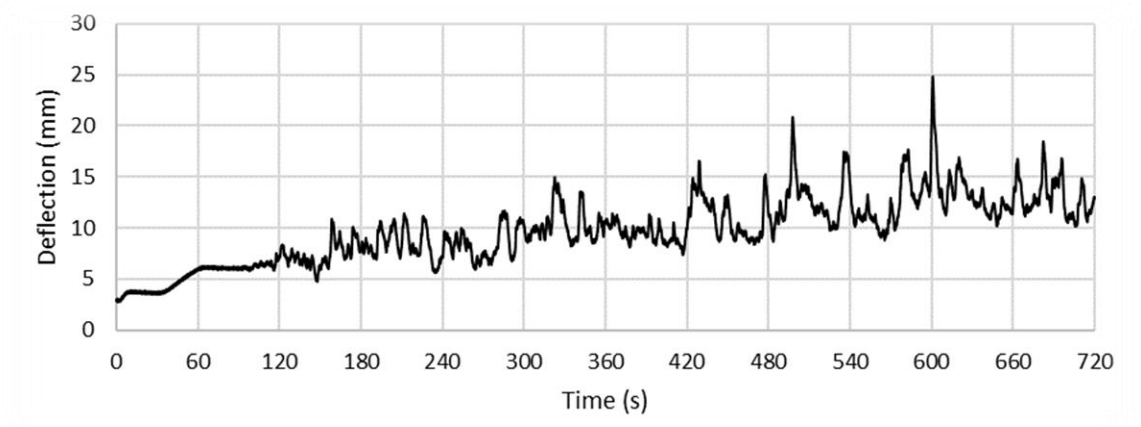

Figure E.8: The 50 m/s deflection time history of specimen LD2

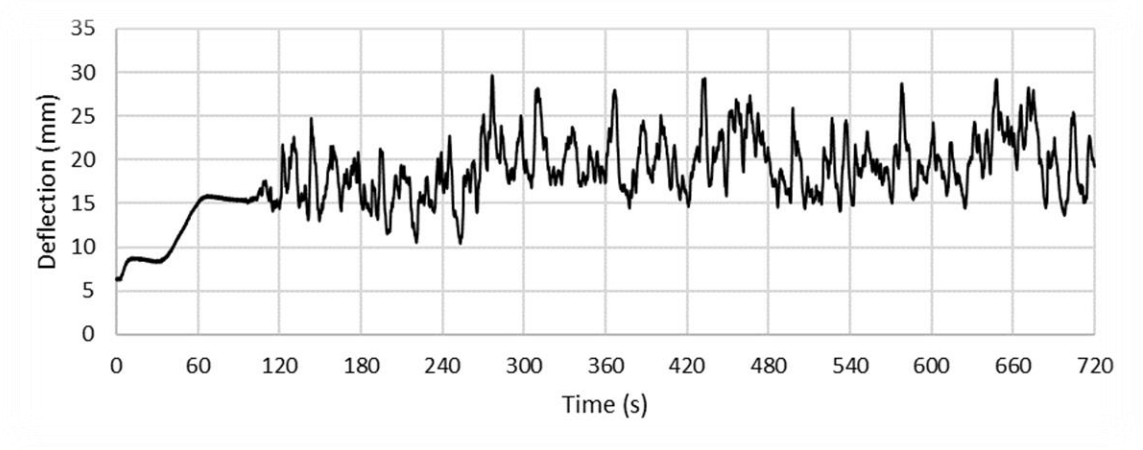

Figure E.9: The 60 m/s deflection time history of specimen LD2

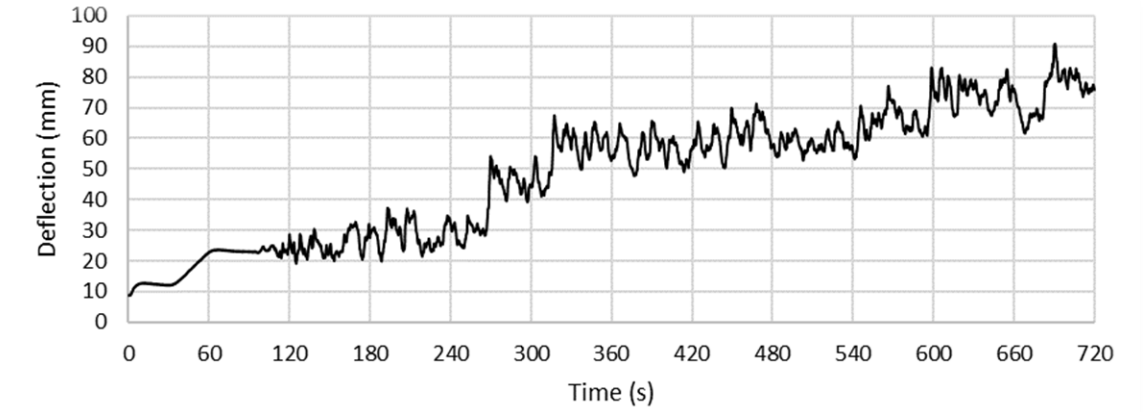

Figure E.10: The 70 m/s deflection time history of specimen LD2

Specimen LD3

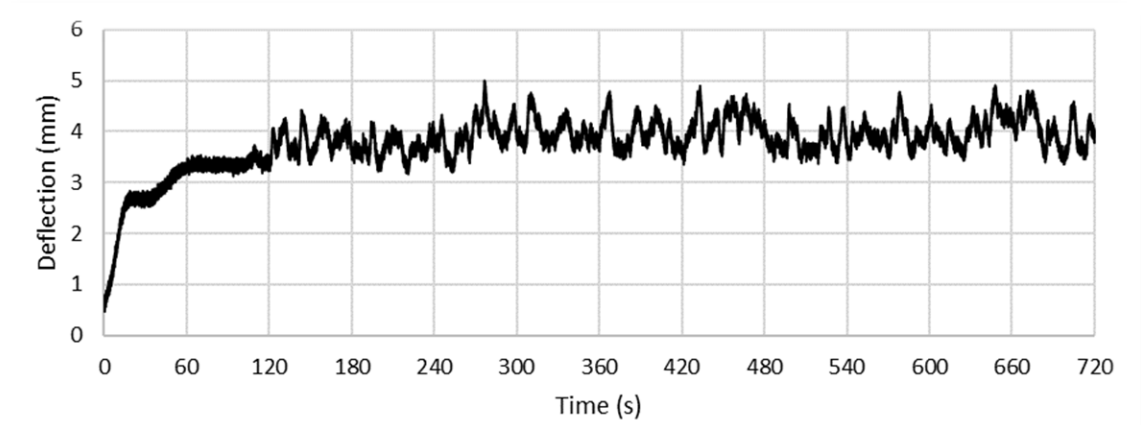

Figure E.11: The 30 m/s deflection time history of specimen LD3

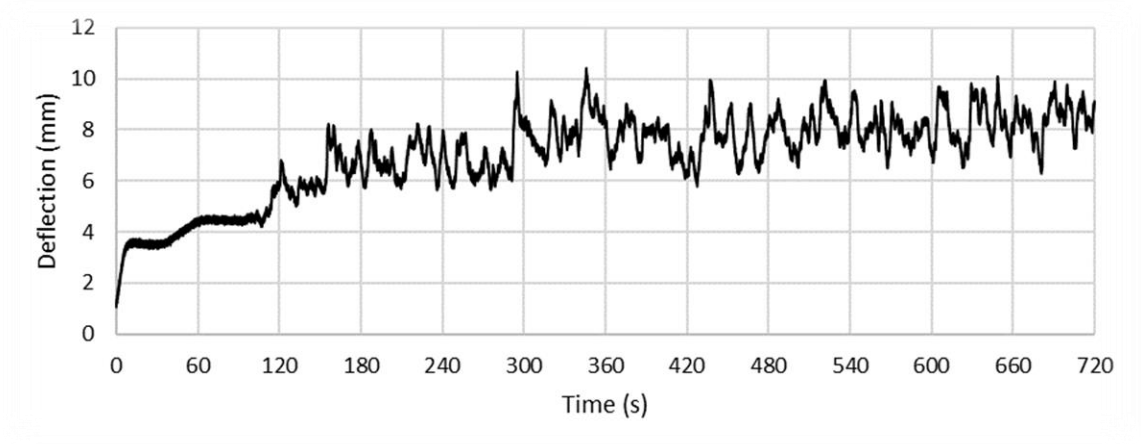

Figure E.12: The 40 m/s deflection time history of specimen LD3

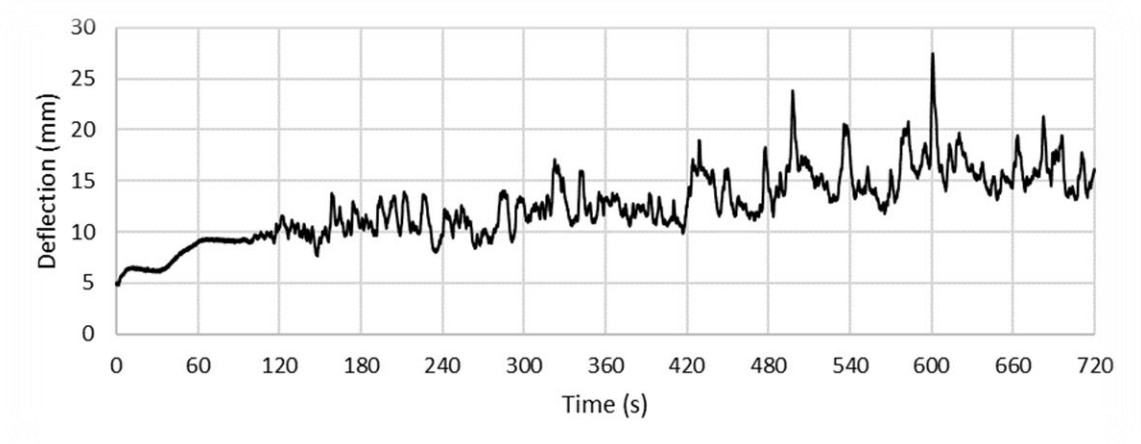

Figure E.13: The 50 m/s deflection time history of specimen LD3

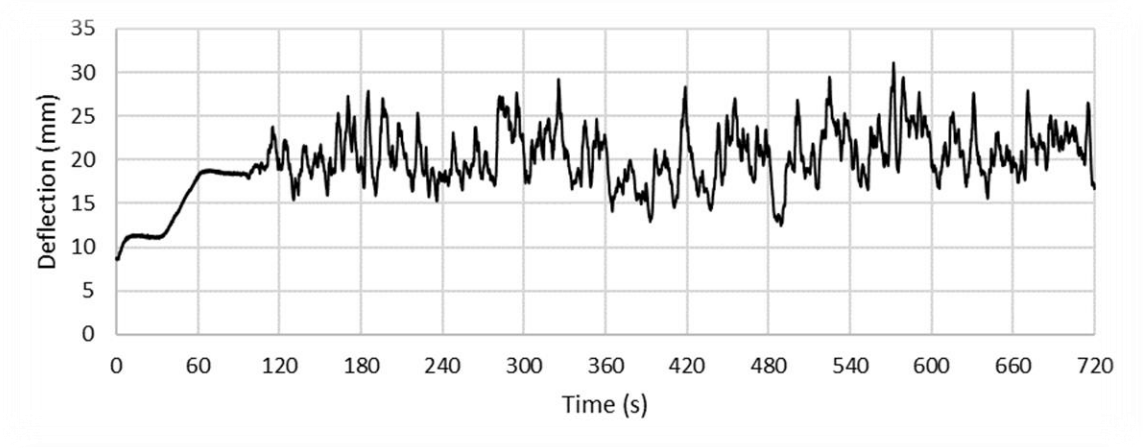

Figure E.14: The 60 m/s deflection time history of specimen LD3

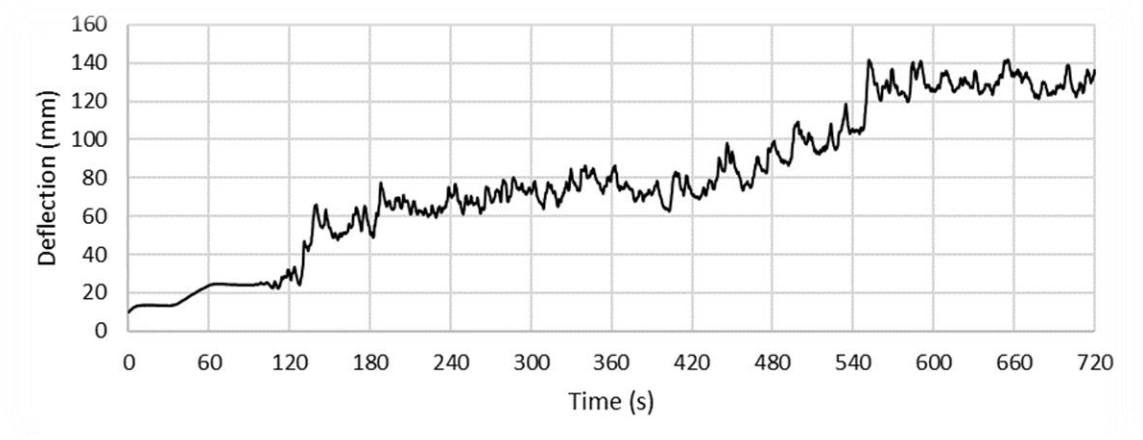

Figure E.15: The 70 m/s deflection time history of specimen LD3

Specimen LD4

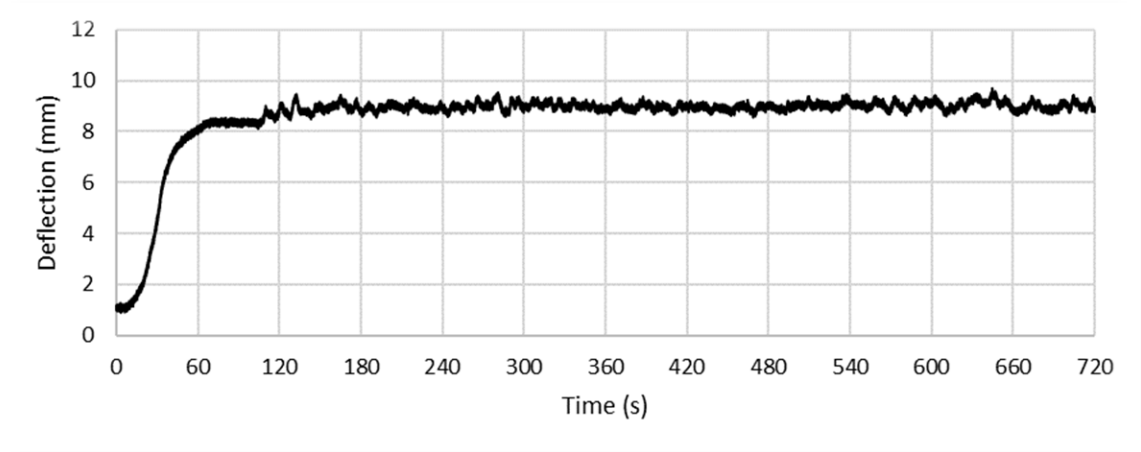

Figure E.16: The 30 m/s deflection time history of specimen LD4

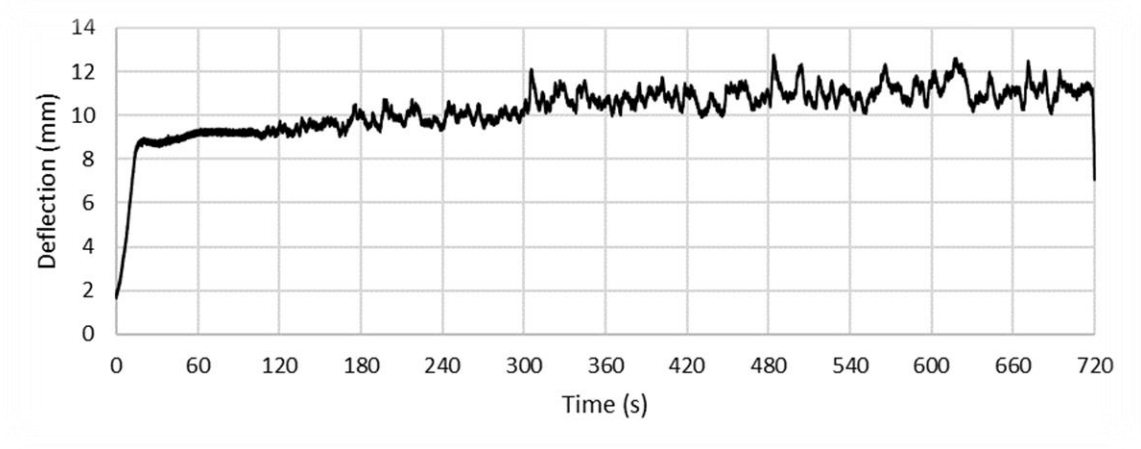

Figure E.17: The 40 m/s deflection time history of specimen LD4

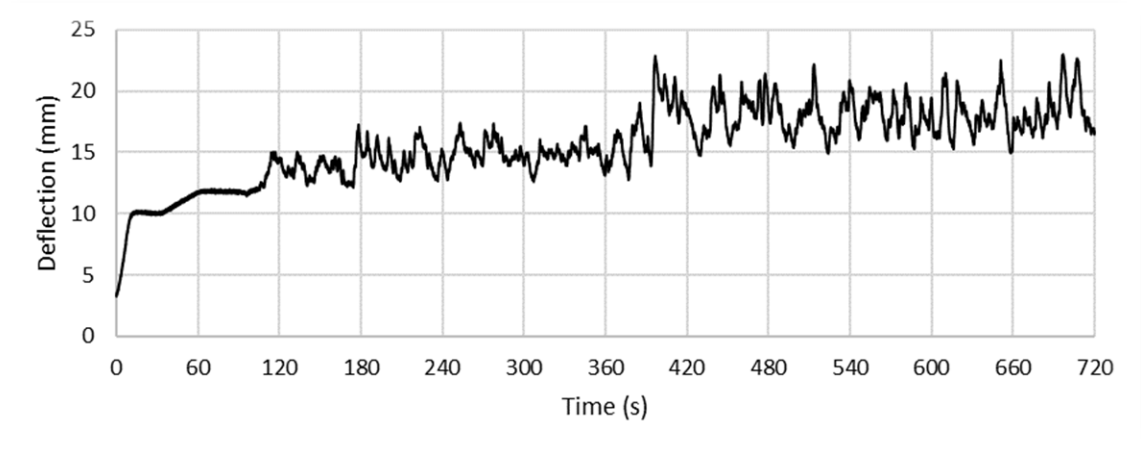

Figure E.18: The 50 m/s deflection time history of specimen LD4

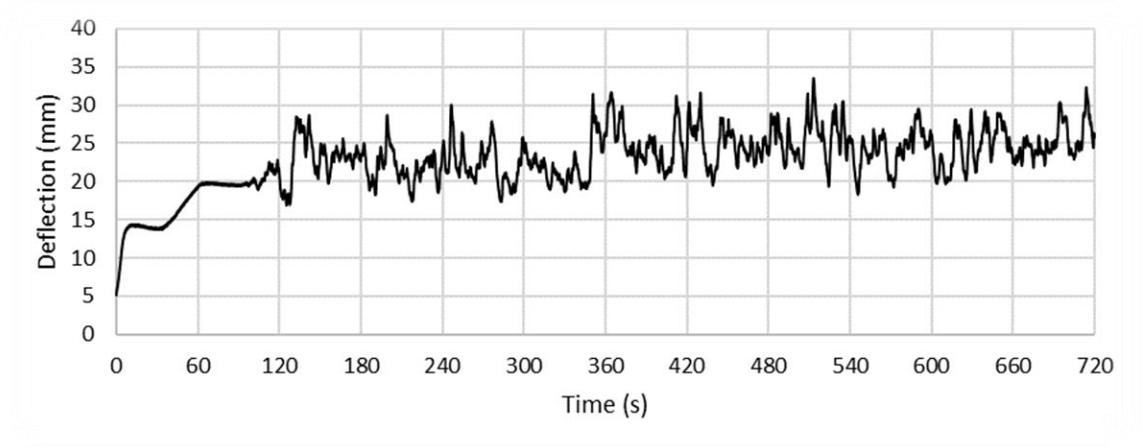

Figure E.19: The 60 m/s deflection time history of specimen LD4

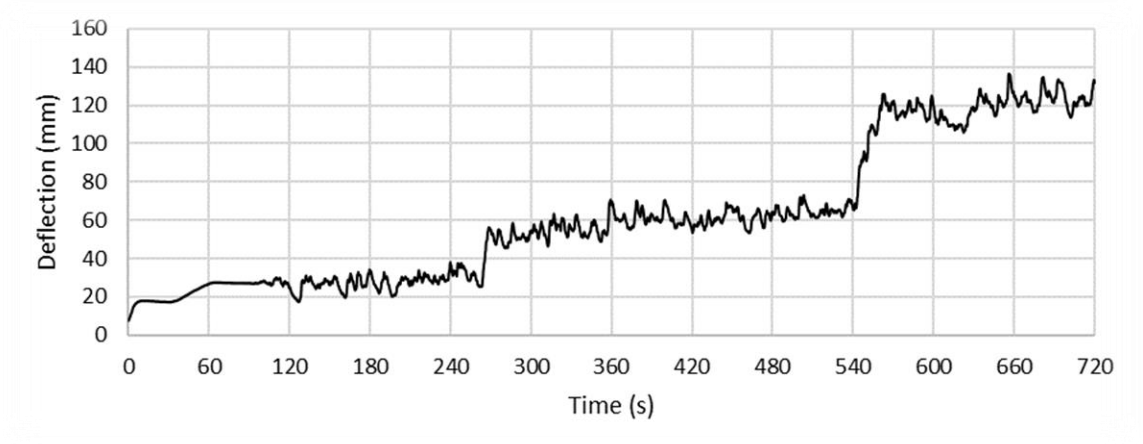

Figure E.20: The 70 m/s deflection time history of specimen LD4

Specimen LD5

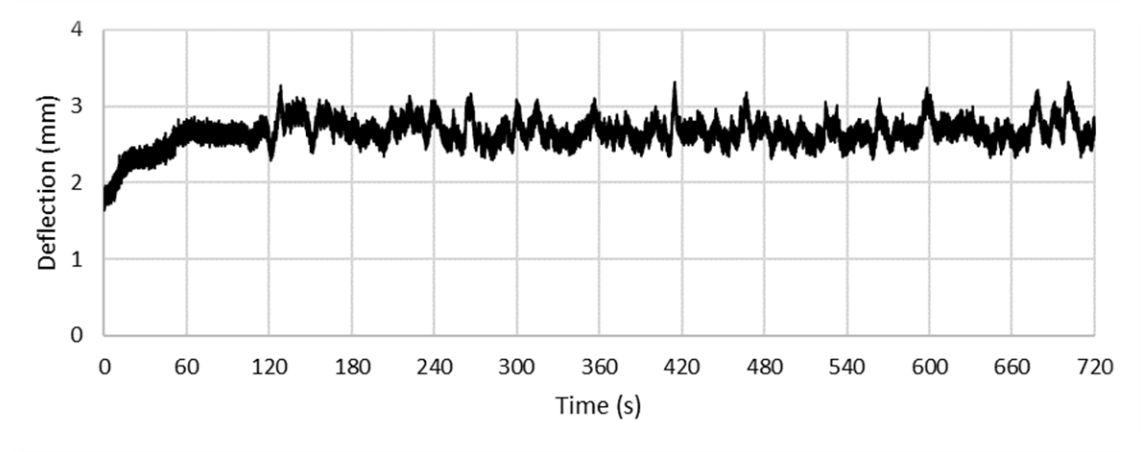

Figure E.21: The 30 m/s deflection time history of specimen LD5

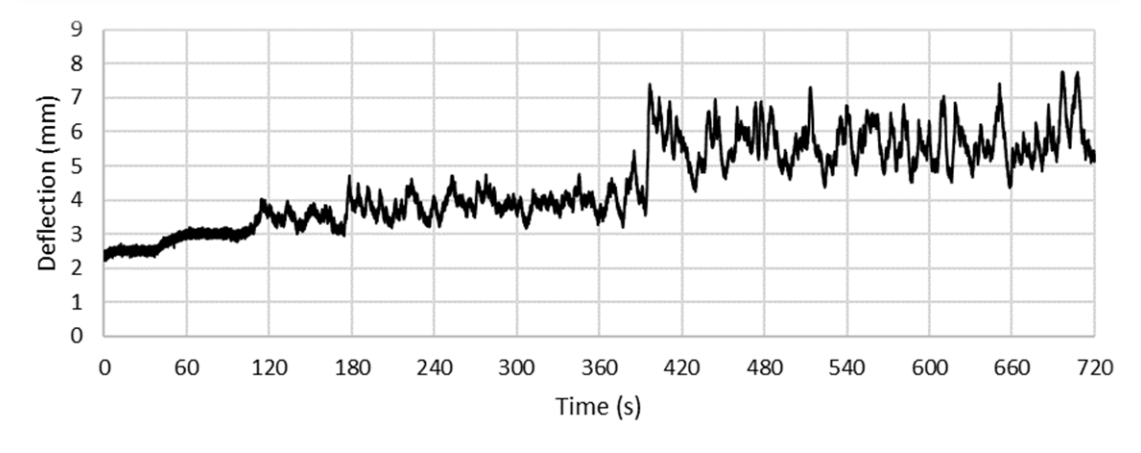

Figure E.22: The 40 m/s deflection time history of specimen LD5

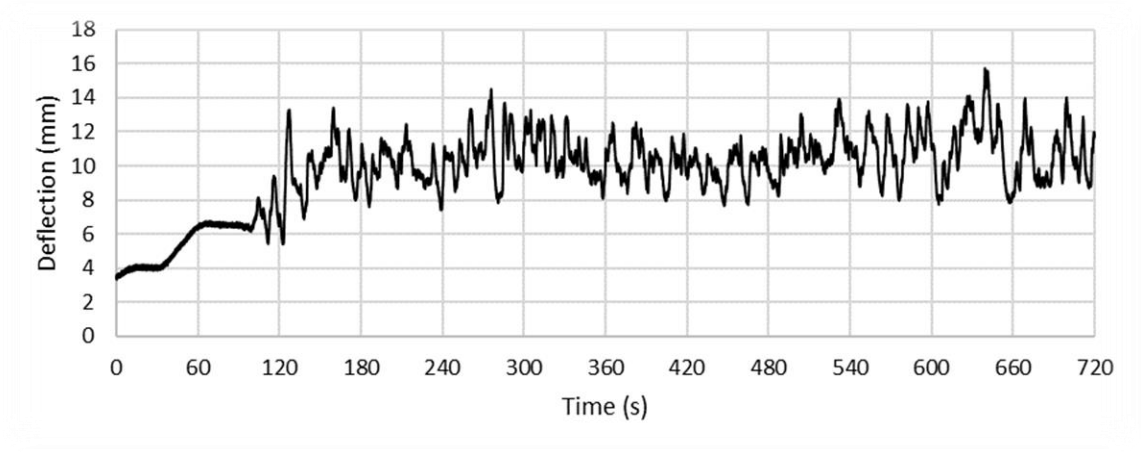

Figure E.23: The 50 m/s deflection time history of specimen LD5

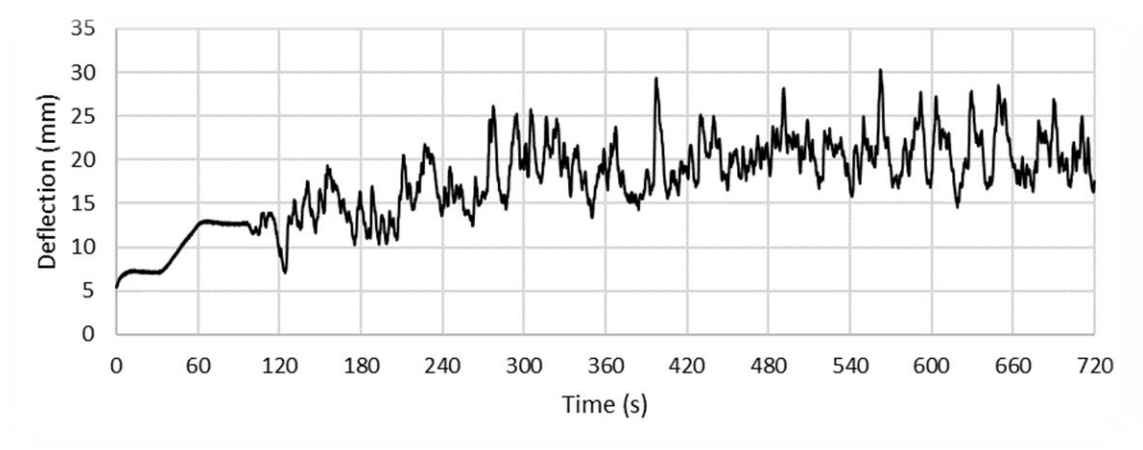

Figure E.24: The 60 m/s deflection time history of specimen LD5

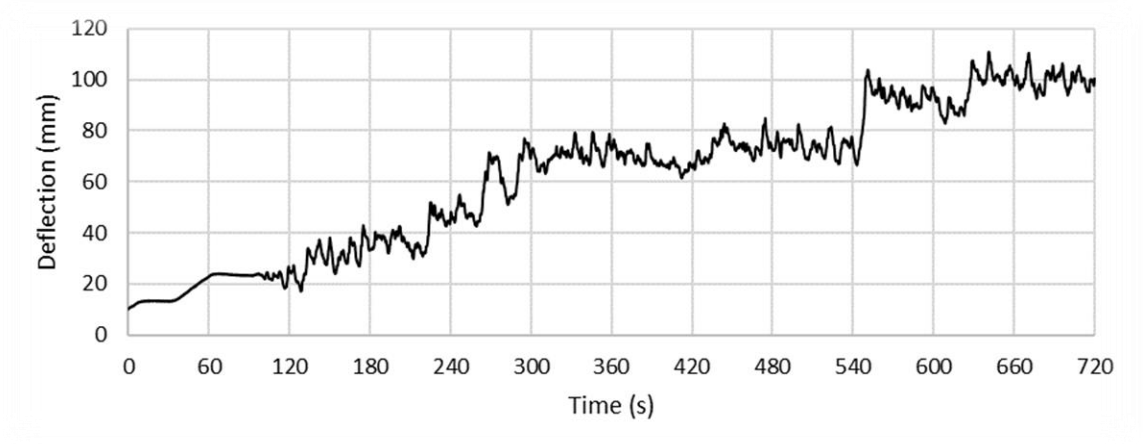

Figure E.25: The 70 m/s deflection time history of specimen LD5

Specimen HD1

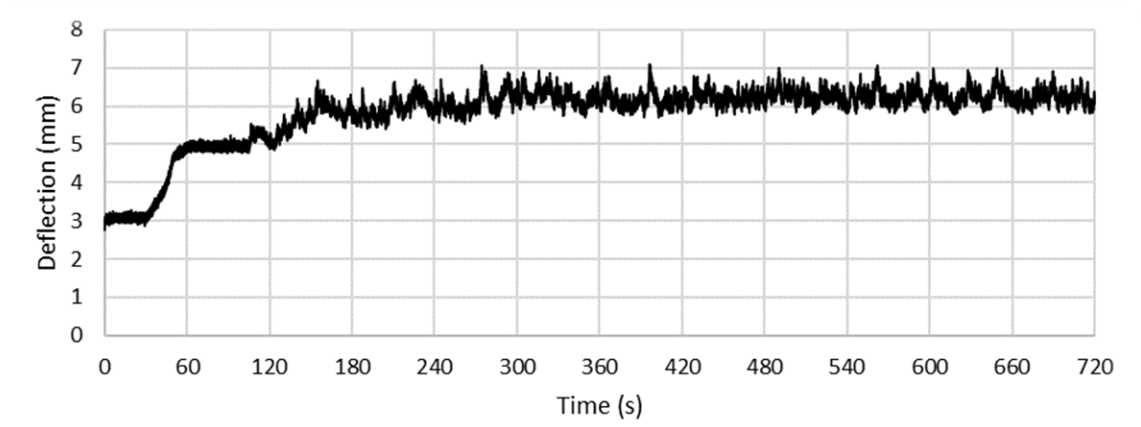

Figure E.26: The 30 m/s deflection time history of specimen HD1

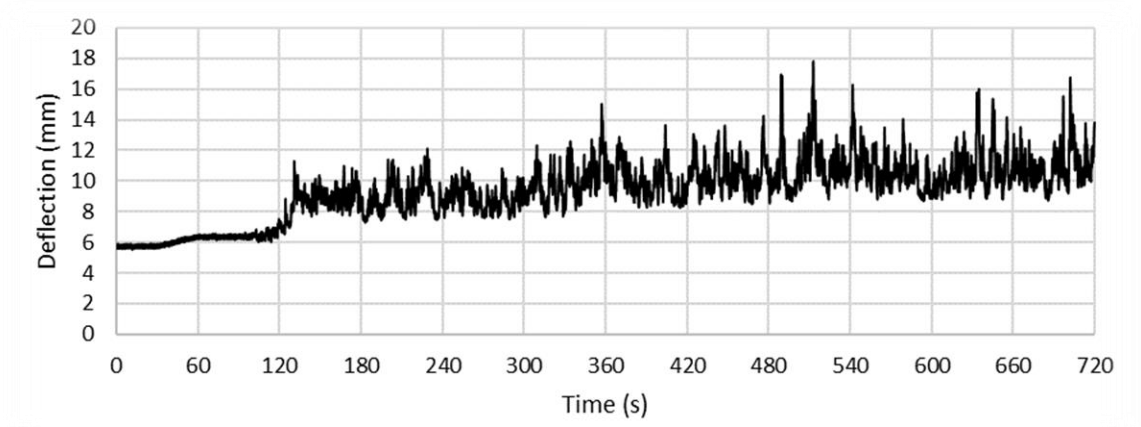

Figure E.27: The 40 m/s deflection time history of specimen HD1

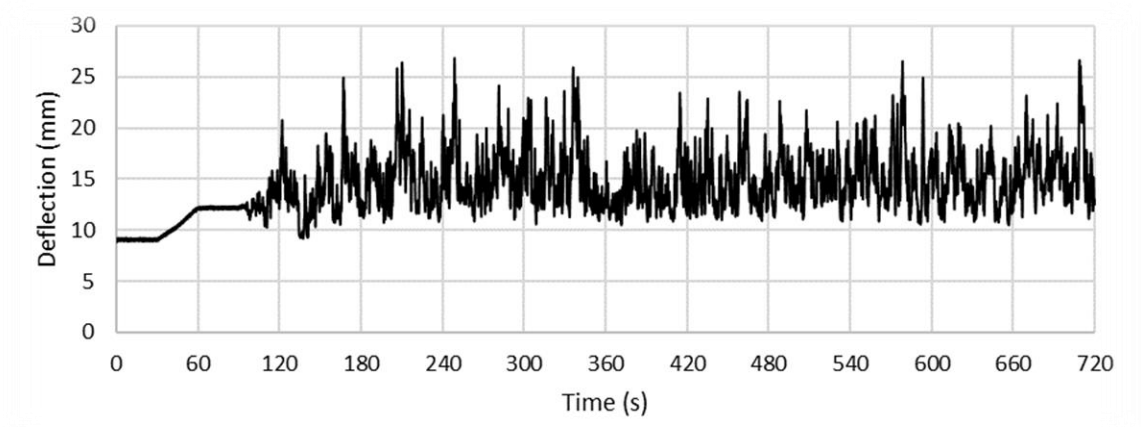

Figure E.28: The 50 m/s deflection time history of specimen HD1

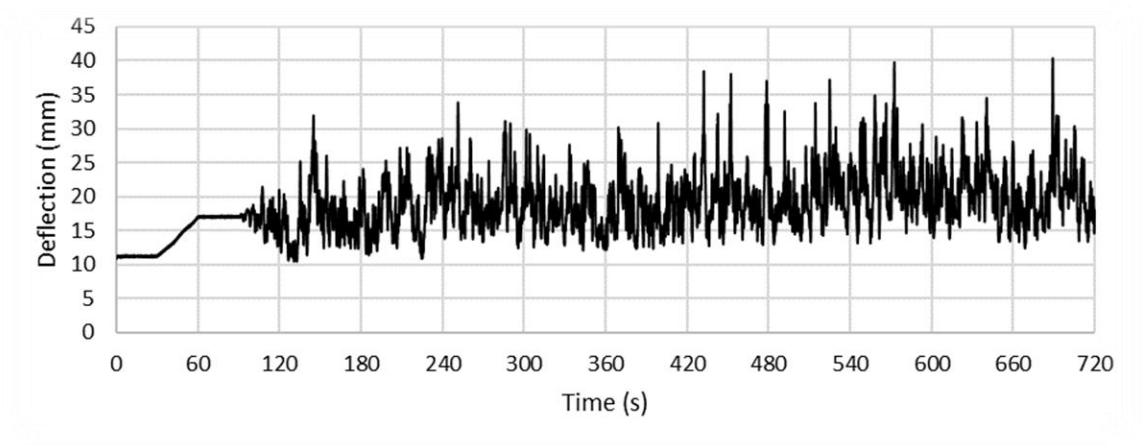

Figure E.29: The 60 m/s deflection time history of specimen HD1

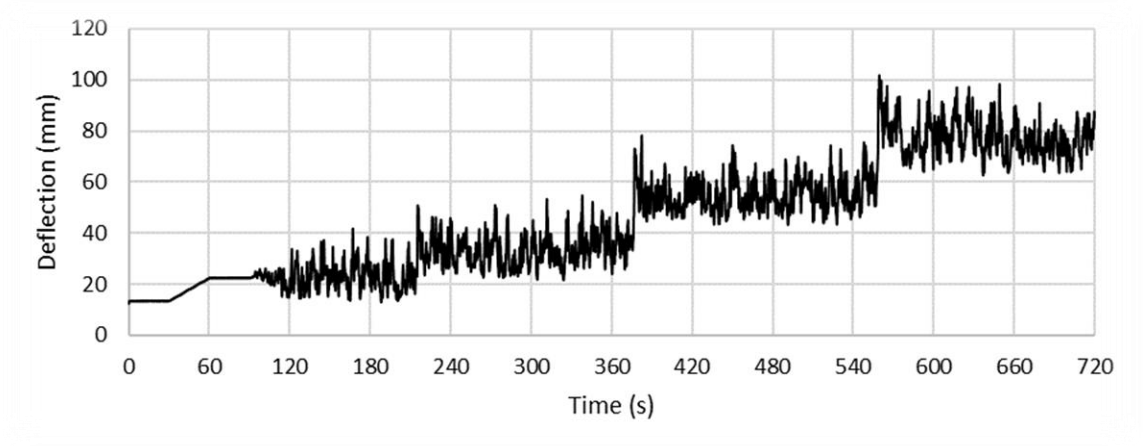

Figure E.30: The 70 m/s deflection time history of specimen HD1

Specimen HD2

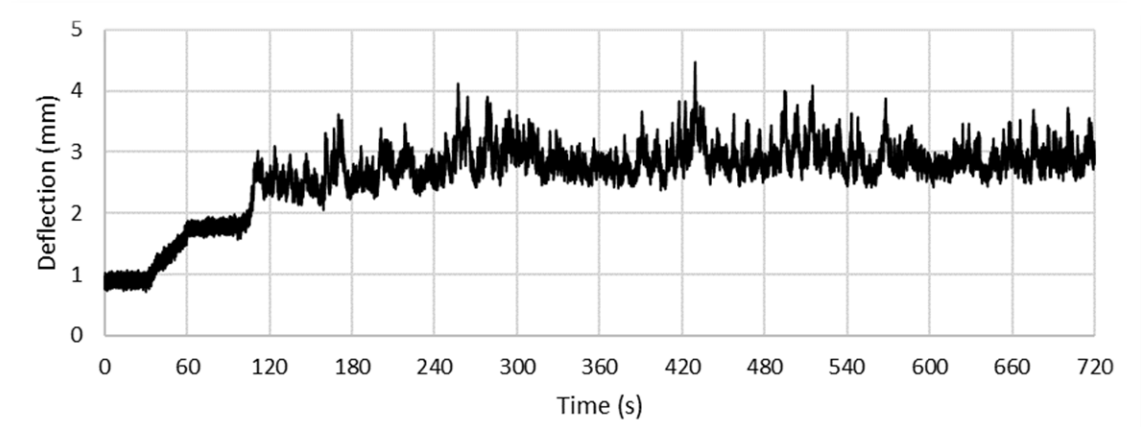

Figure E.31: The 30 m/s deflection time history of specimen HD2

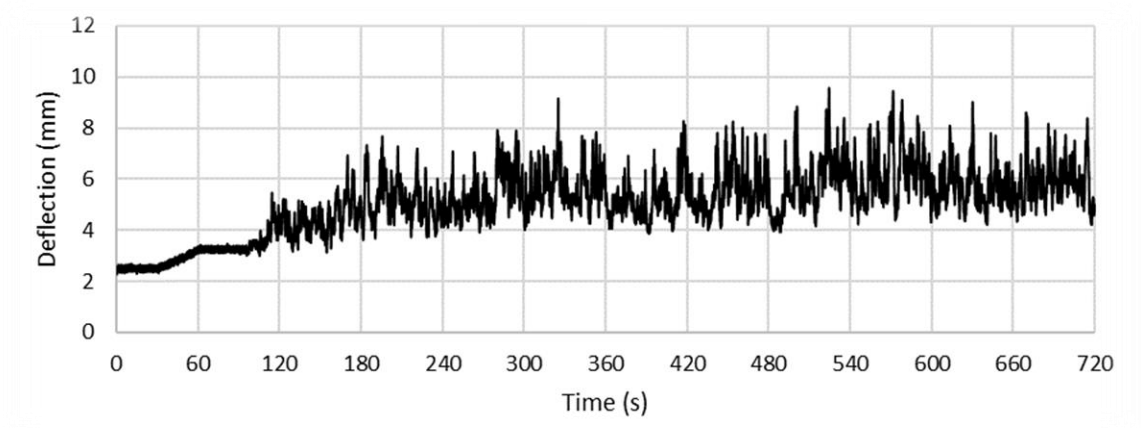

Figure E.32: The 40 m/s deflection time history of specimen HD2

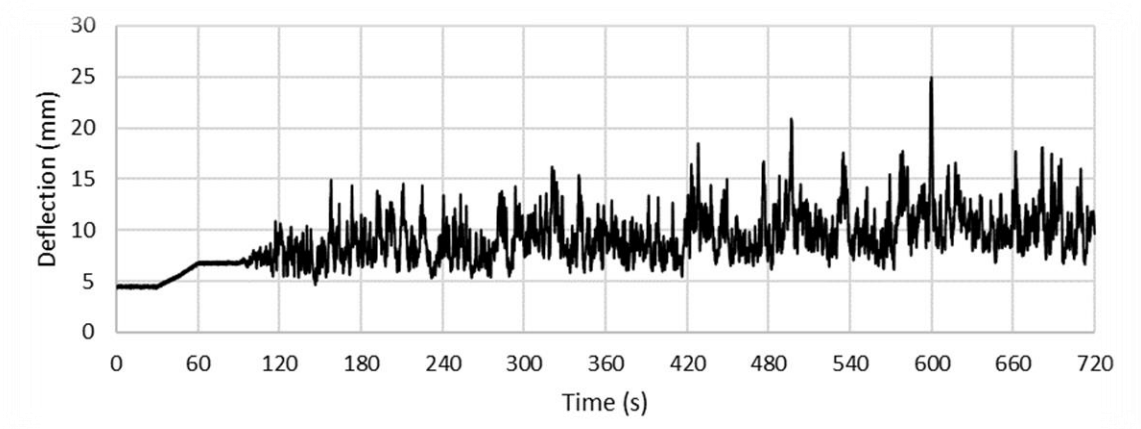

Figure E.33: The 50 m/s deflection time history of specimen HD2

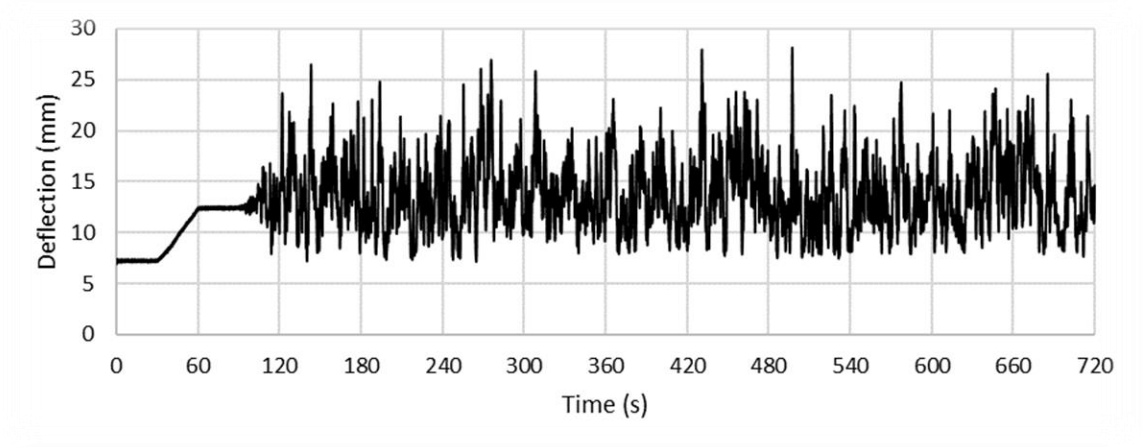

Figure E.34: The 60 m/s deflection time history of specimen HD2

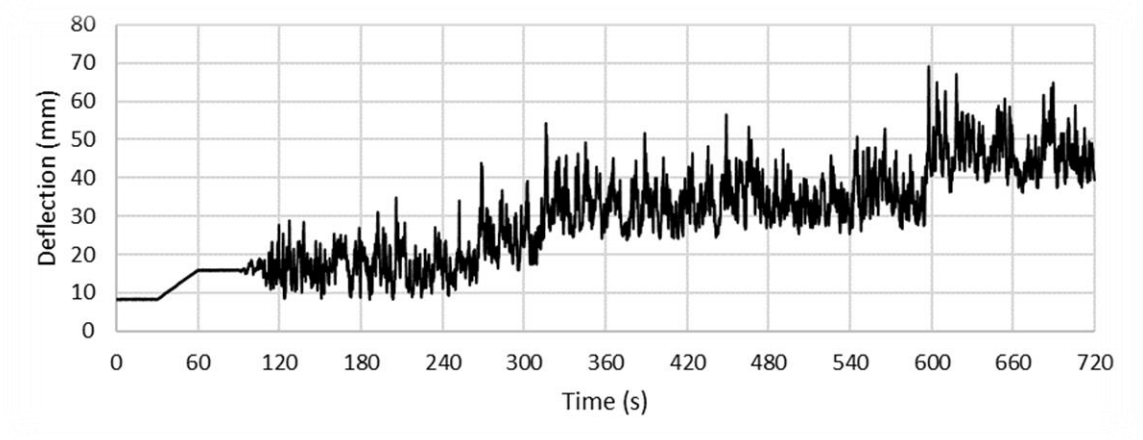

Figure E.35: The 70 m/s deflection time history of specimen HD2

Specimen HD3

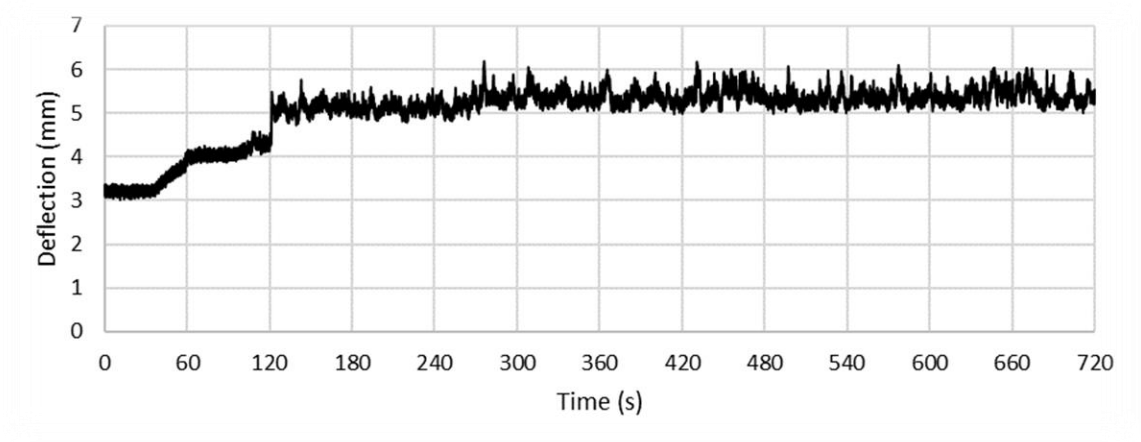

Figure E.36: The 30 m/s deflection time history of specimen HD3

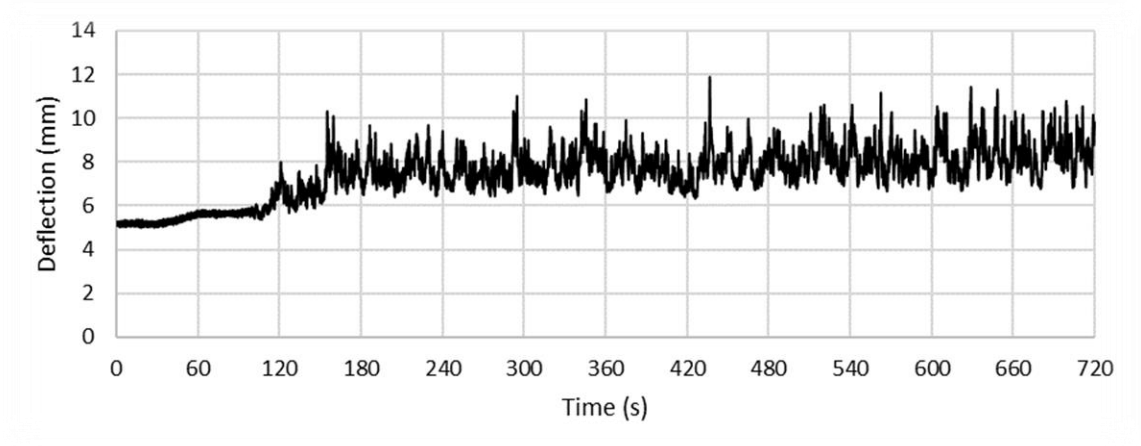

Figure E.37: The 40 m/s deflection time history of specimen HD3

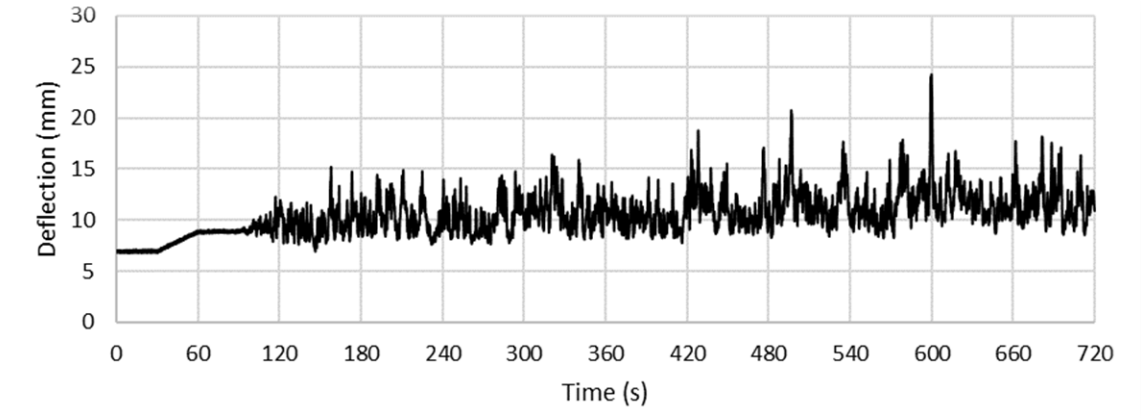

Figure E.38: The 50 m/s deflection time history of specimen HD3

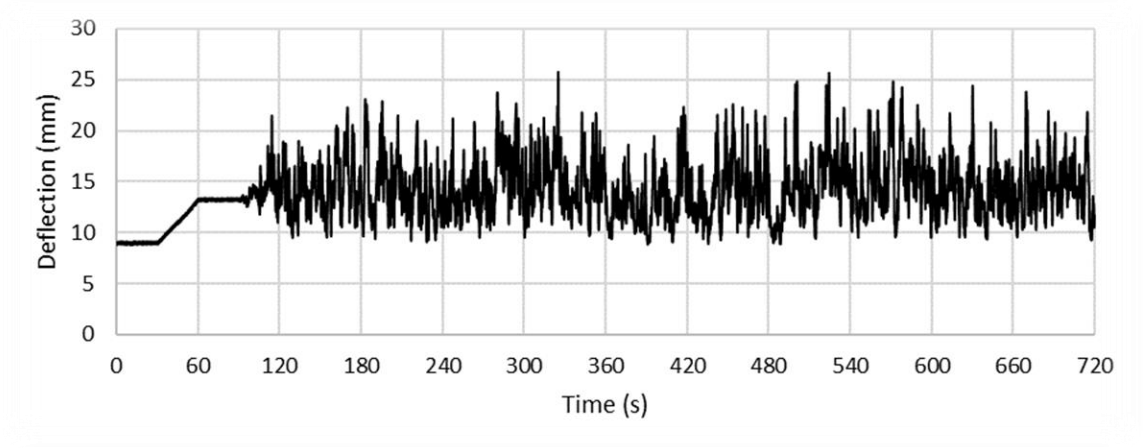

Figure E.39: The 60 m/s deflection time history of specimen HD3

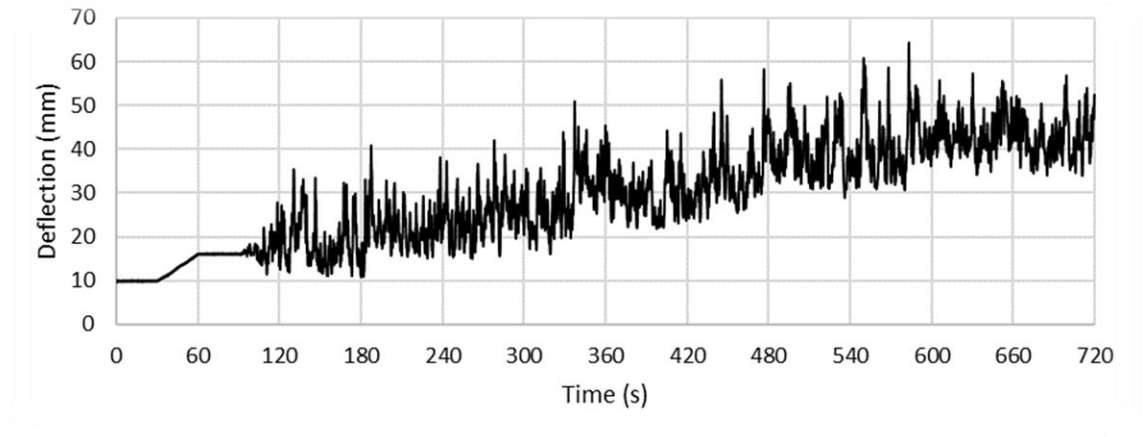

Figure E.40: The 70 m/s deflection time history of specimen HD3

Specimen HD4

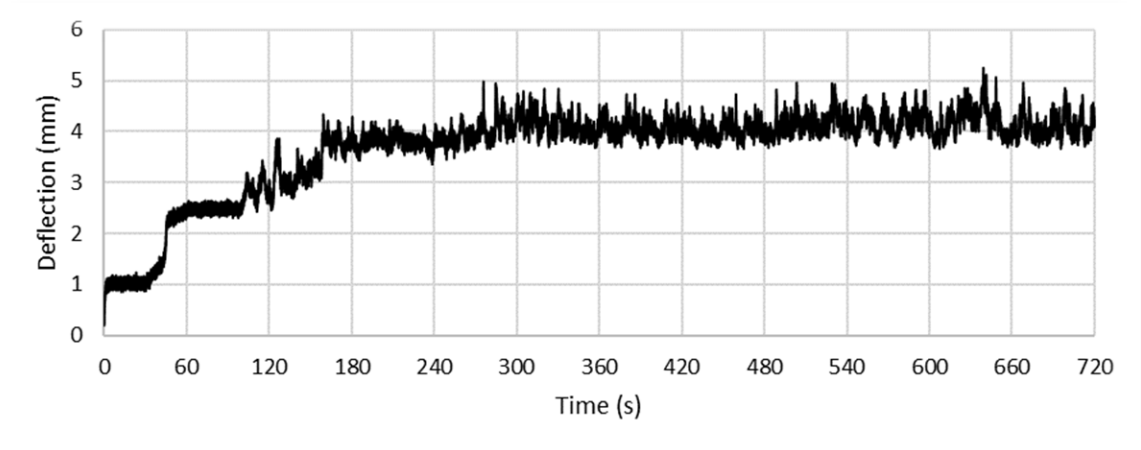

Figure E.41: The 30 m/s deflection time history of specimen HD4

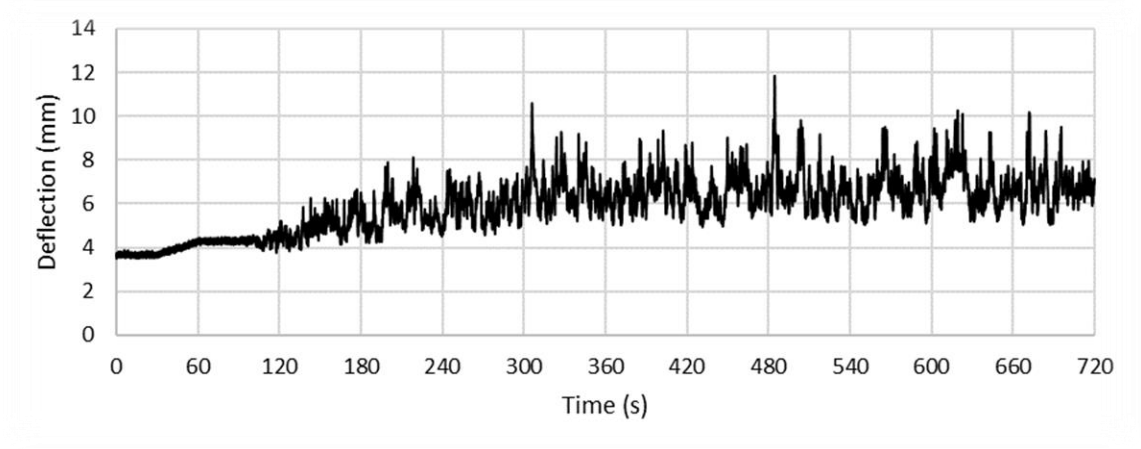

Figure E.42: The 40 m/s deflection time history of specimen HD4

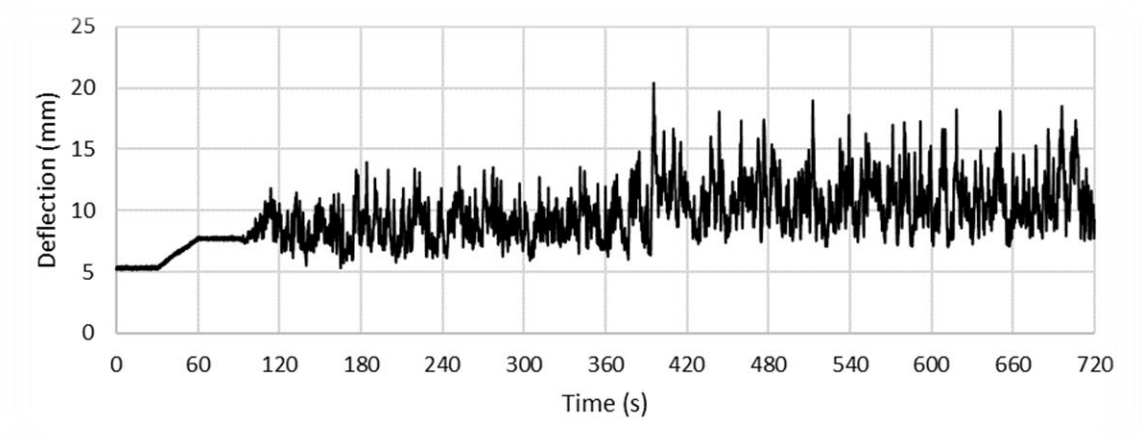

Figure E.43: The 50 m/s deflection time history of specimen HD4

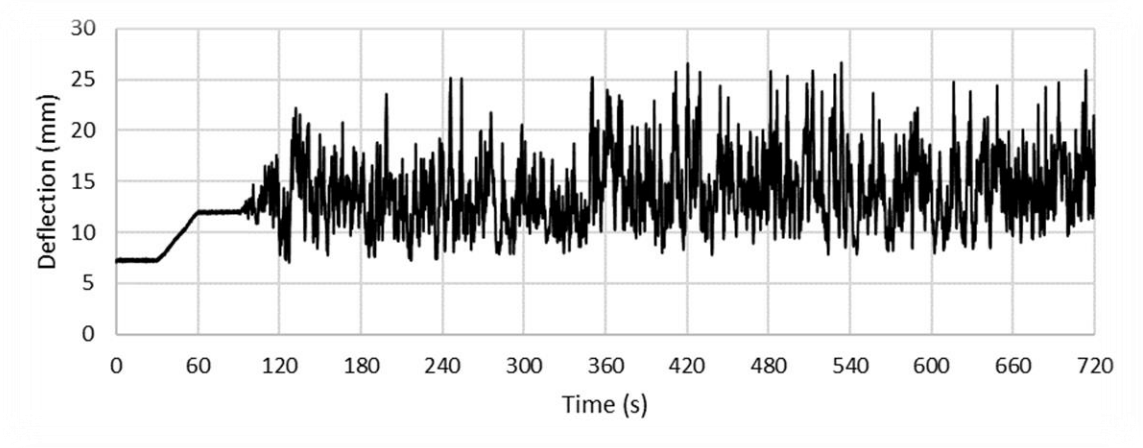

Figure E.44: The 60 m/s deflection time history of specimen HD4

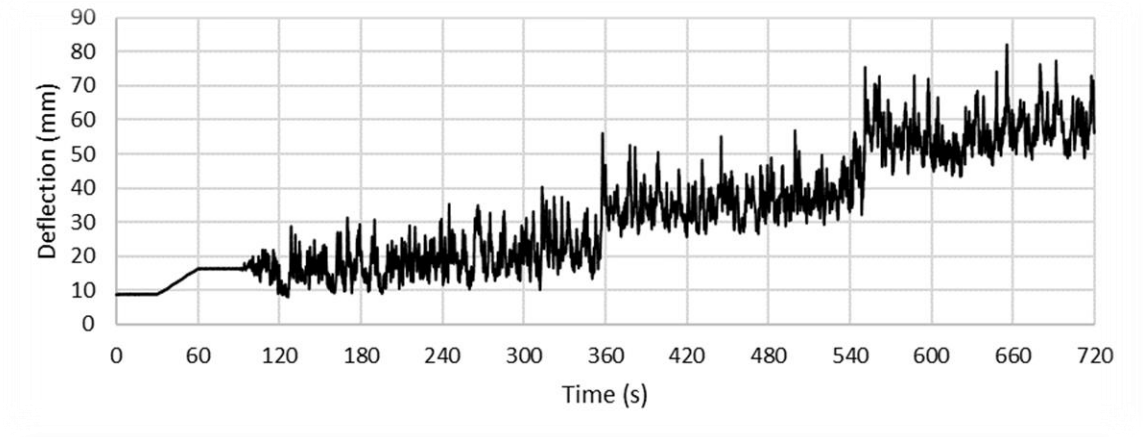

Figure E.45: The 70 m/s deflection time history of specimen HD4

Specimen HD5

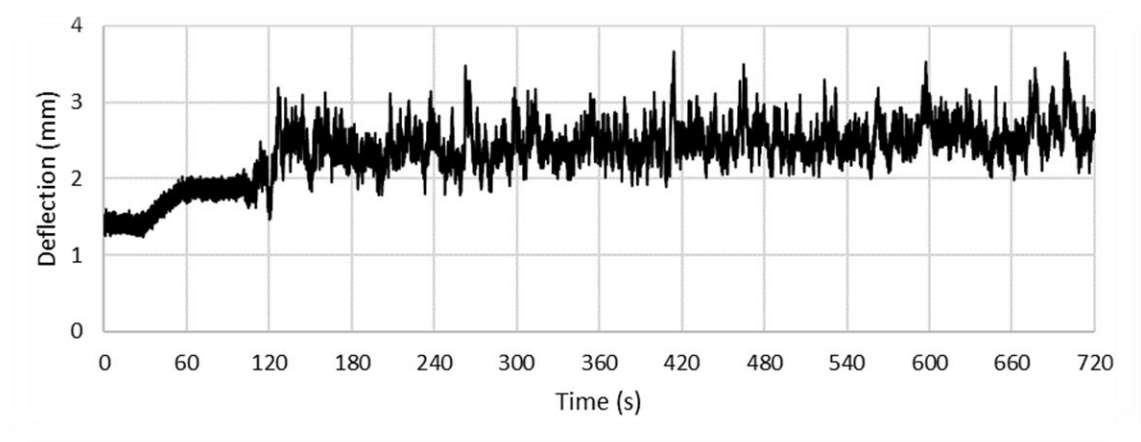

Figure E.46: The 30 m/s deflection time history of specimen HD5

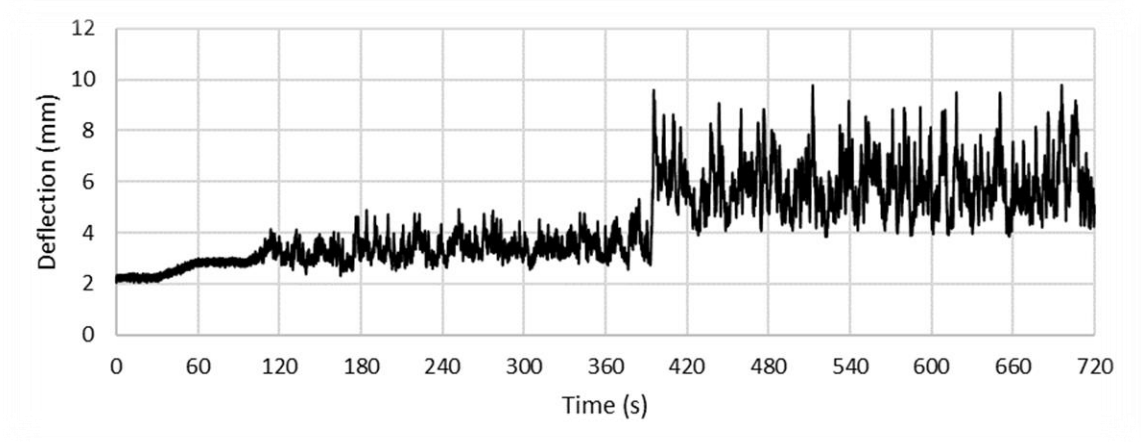

Figure E.47: The 40 m/s deflection time history of specimen HD5

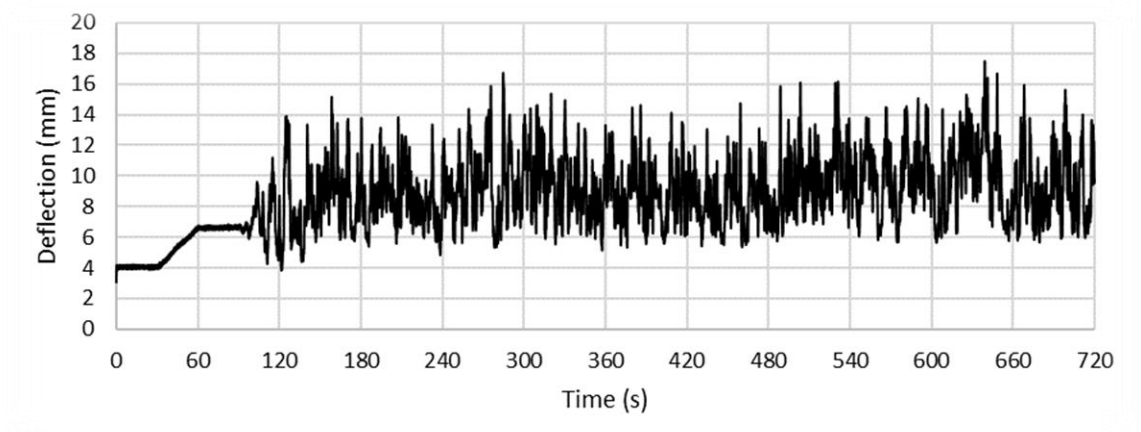

Figure E.48: The 50 m/s deflection time history of specimen HD5

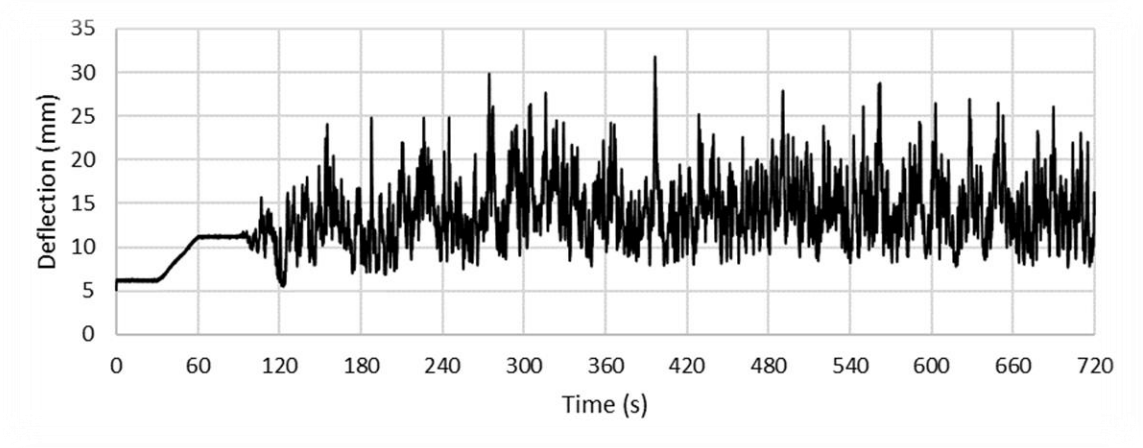

Figure E.49: The 60 m/s deflection time history of specimen HD5

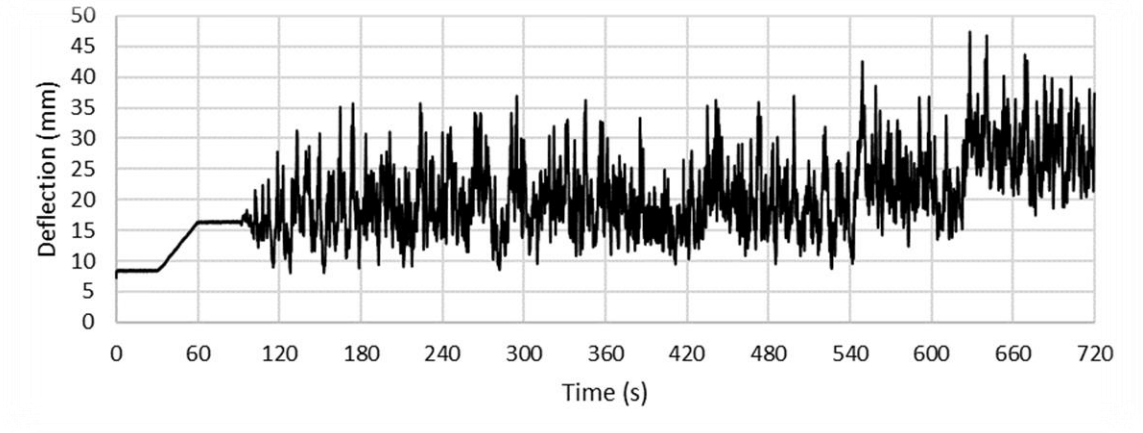

Figure E.50: The 70 m/s deflection time history of specimen HD5

Appendix F: Load vs. Deflection Hysteresis Plots of the Dynamic Tests

Appendix F contains the load-deflection hysteresis plots that resulted from the wall specimens tested under dynamic loading conditions. *Figure F.1* to *Figure F.25* depict the results of the wall specimens with the low reinforcement ratio, while *Figure F.26* to *Figure F.50* depict the results of the wall specimens with the high reinforcement ratio.

The load in the diagrams represent the total load applied by the MTS® Series 244 hydraulic actuator on the wall specimens. The load measurements were taken using the built-in force transducer of the actuator. The deflection in the diagrams represent the deflection at mid-height of the wall specimens. The deflection measurements were taken using the Micro-Epsilon optoNCDT 1700-500 laser optical displacement measurement device.

Specimen LD1

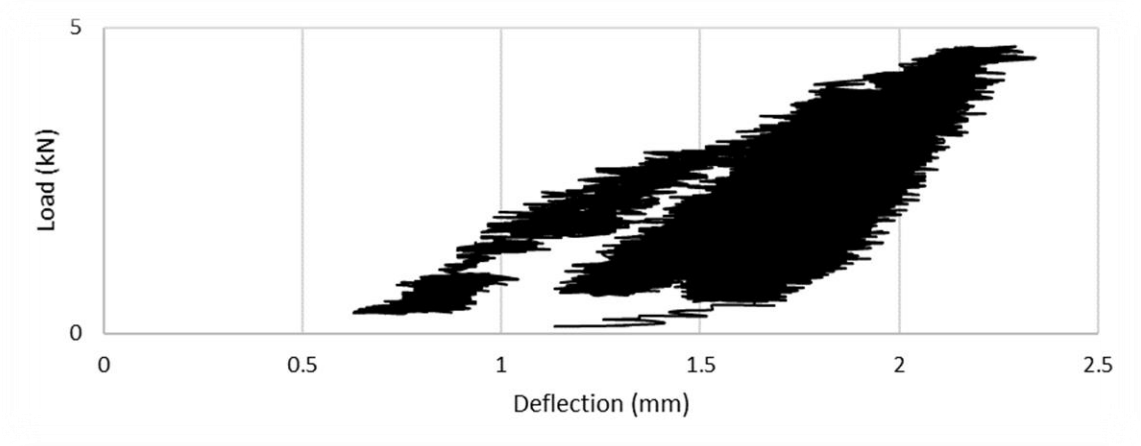

Figure F.1: The 30 m/s load-deflection hysteresis diagram of specimen LD1

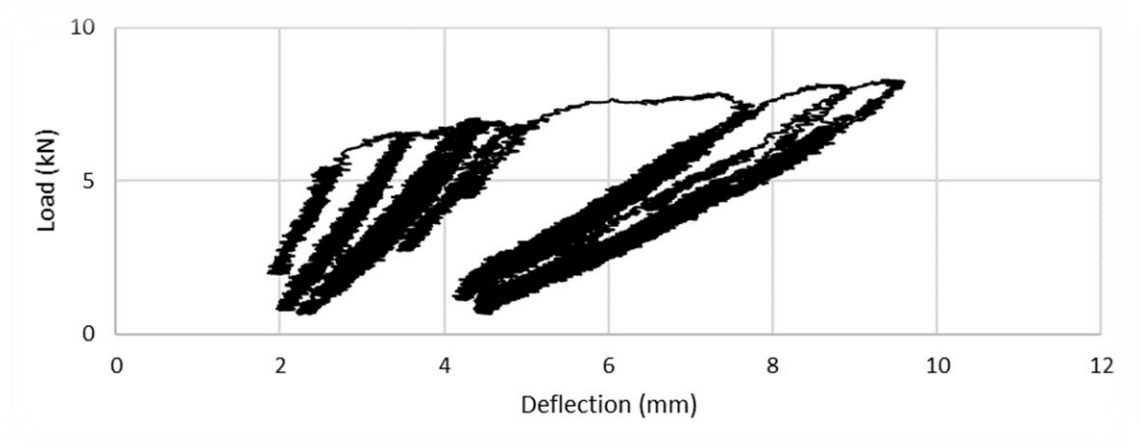

Figure F.2: The 40 m/s load-deflection hysteresis diagram of specimen LD1

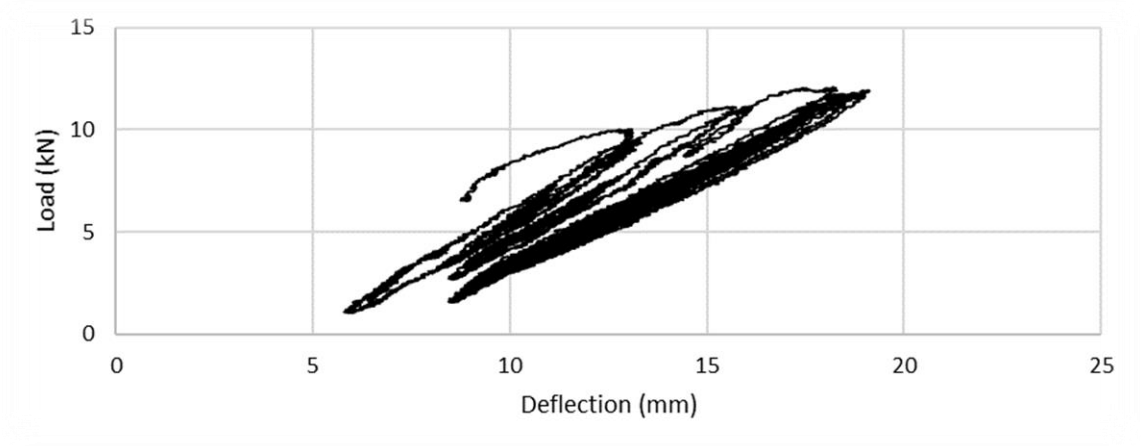

Figure F.3: The 50 m/s load-deflection hysteresis diagram of specimen LD1

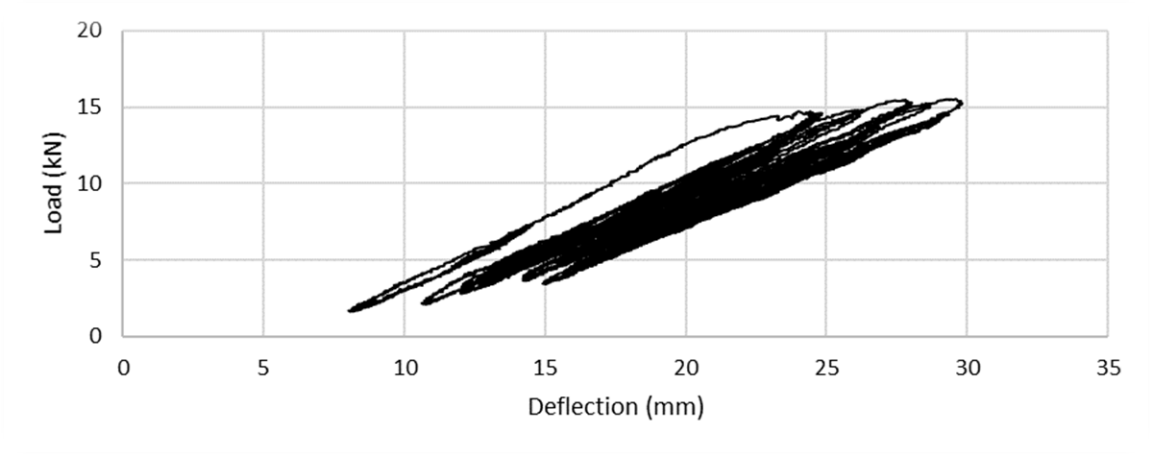

Figure F.4: The 60 m/s load-deflection hysteresis diagram of specimen LD1

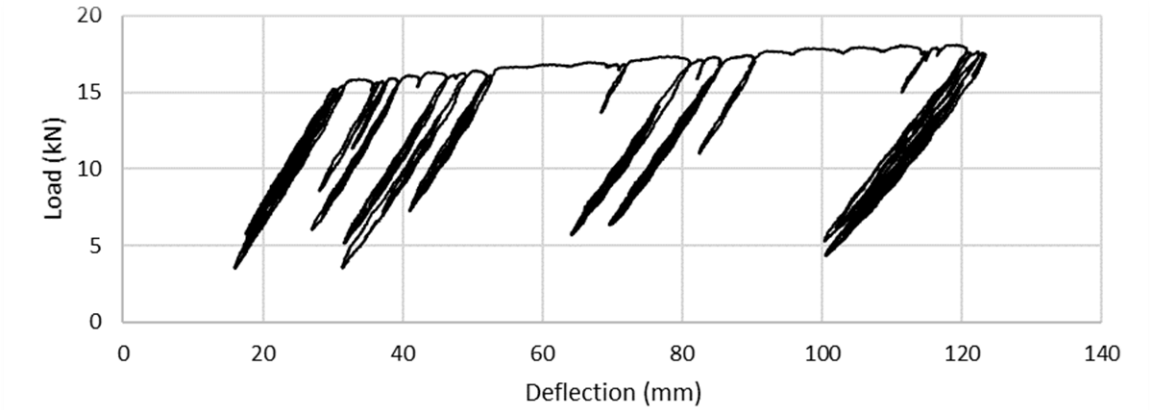

Figure F.5: The 70 m/s load-deflection hysteresis diagram of specimen LD1

Specimen LD2

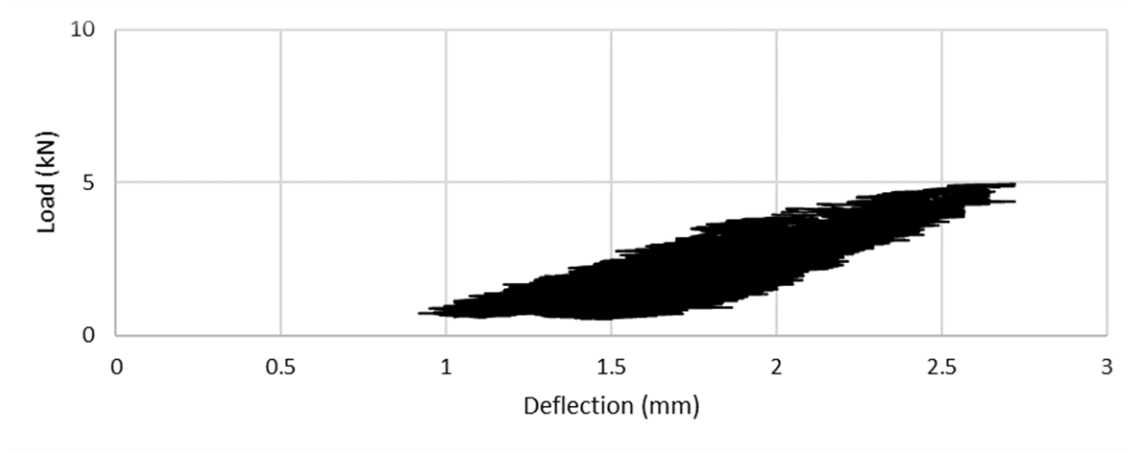

Figure F.6: The 30 m/s load-deflection hysteresis diagram of specimen LD2

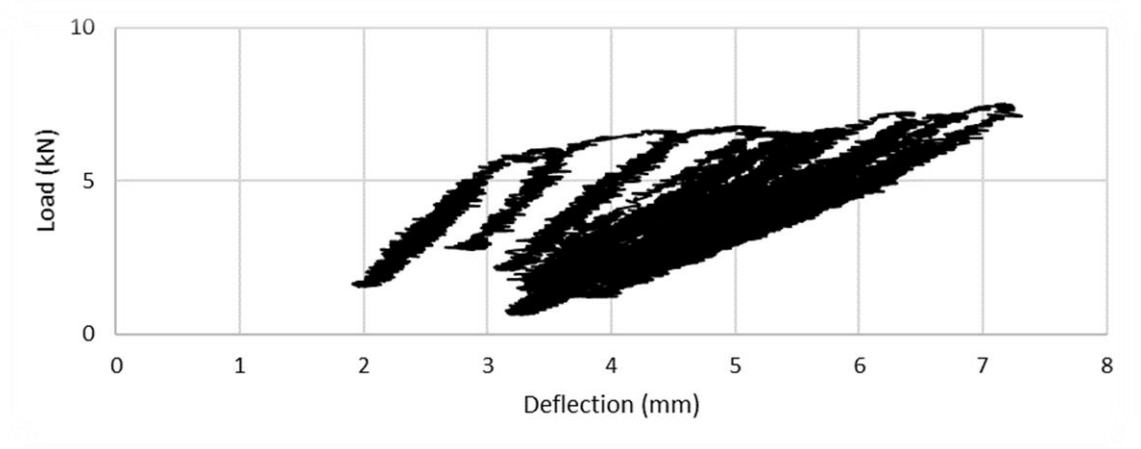

Figure F.7: The 40 m/s load-deflection hysteresis diagram of specimen LD2

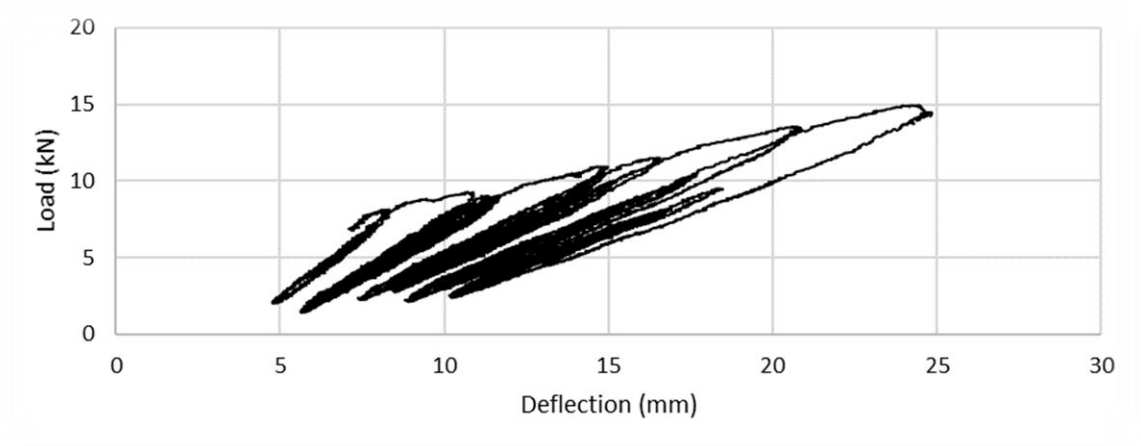

Figure F.8: The 50 m/s load-deflection hysteresis diagram of specimen LD2

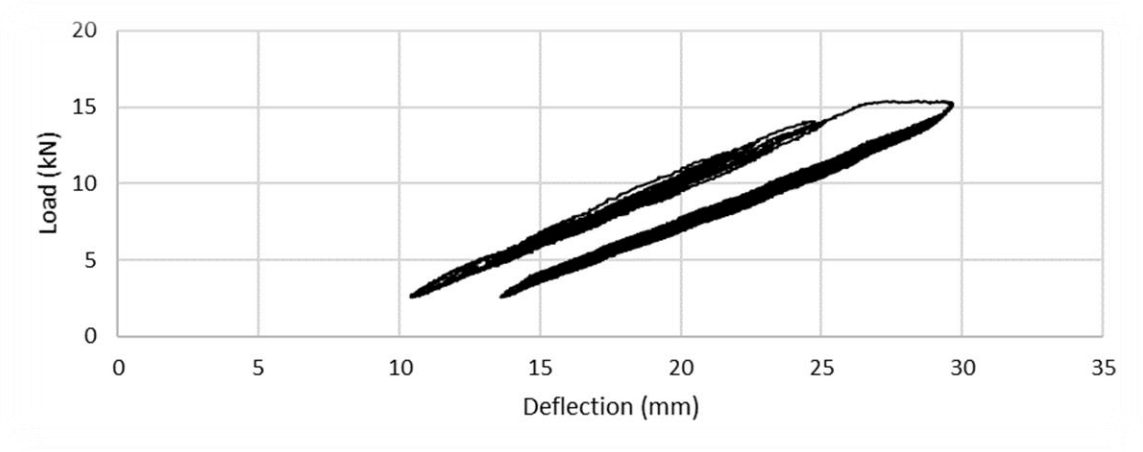

Figure F.9: The 60 m/s load-deflection hysteresis diagram of specimen LD2

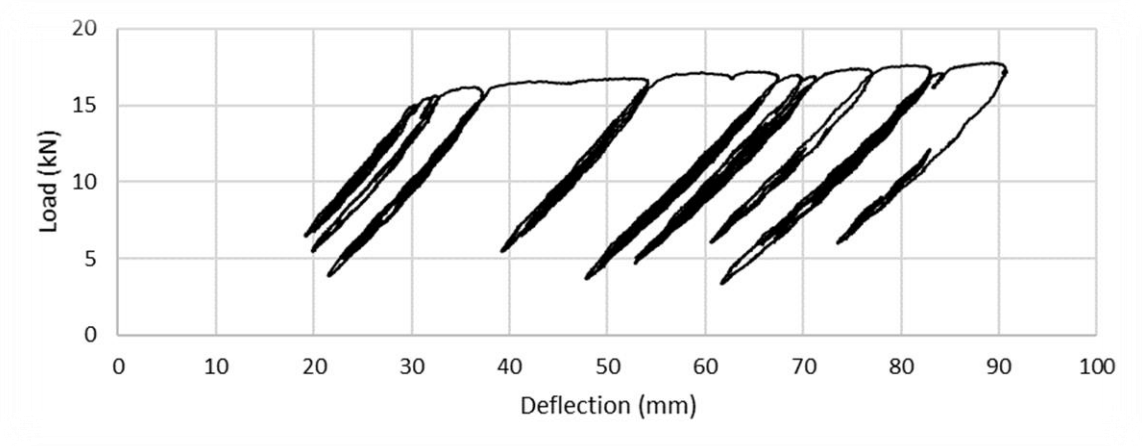

Figure F.10: The 70 m/s load-deflection hysteresis diagram of specimen LD2

Specimen LD3

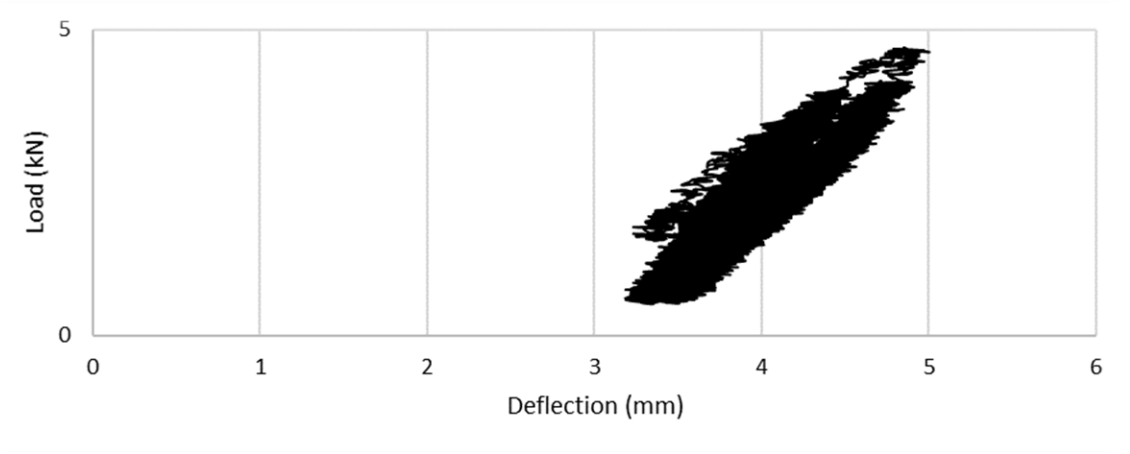

Figure F.11: The 30 m/s load-deflection hysteresis diagram of specimen LD3

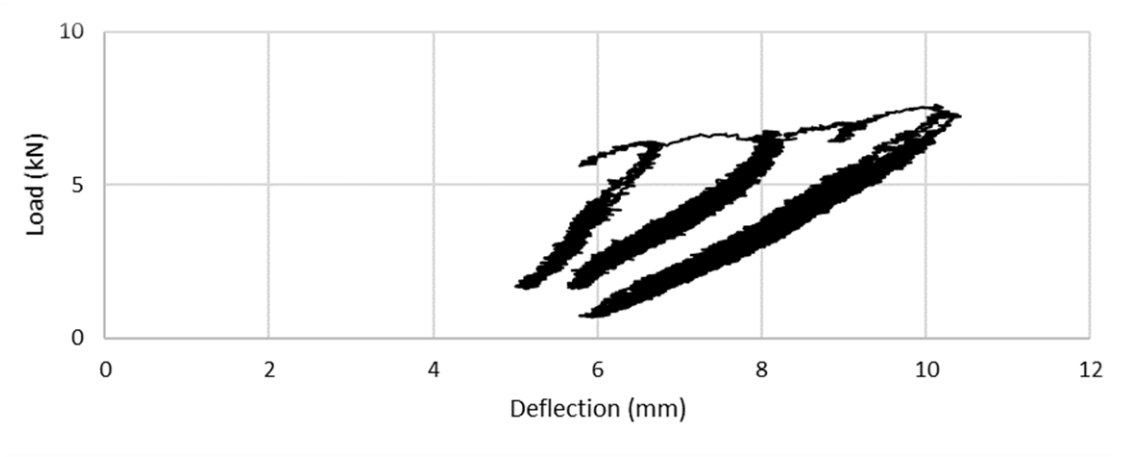

Figure F.12: The 40 m/s load-deflection hysteresis diagram of specimen LD3

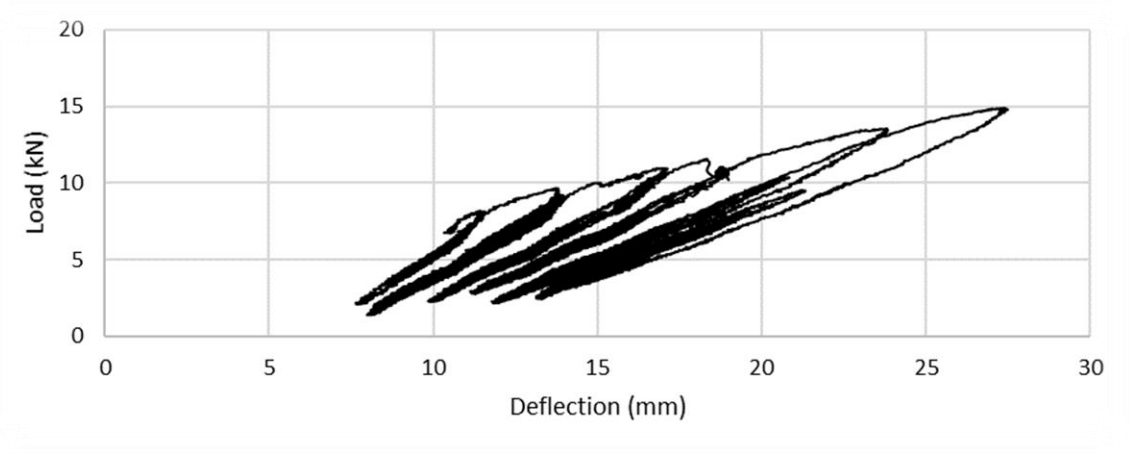

Figure F.13: The 50 m/s load-deflection hysteresis diagram of specimen LD3

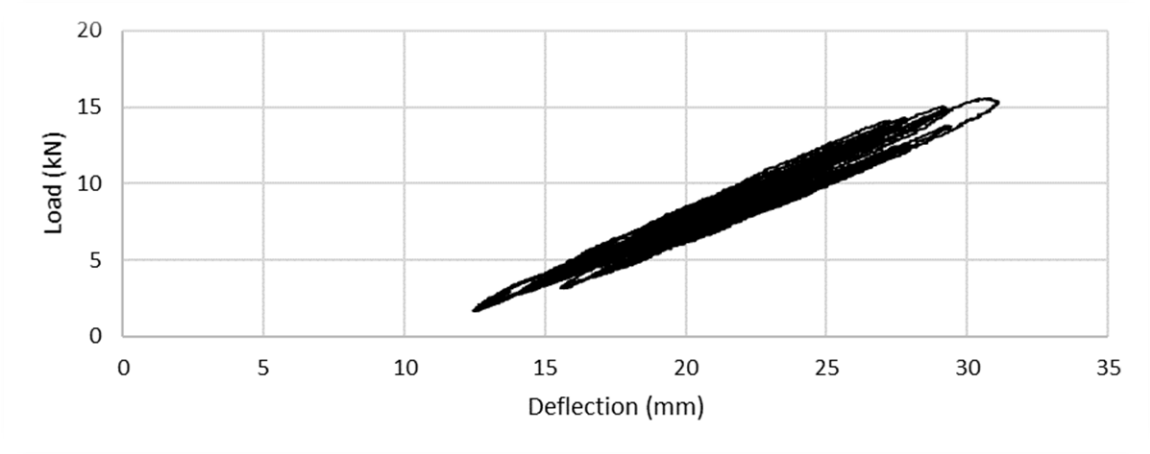

Figure F.14: The 60 m/s load-deflection hysteresis diagram of specimen LD3

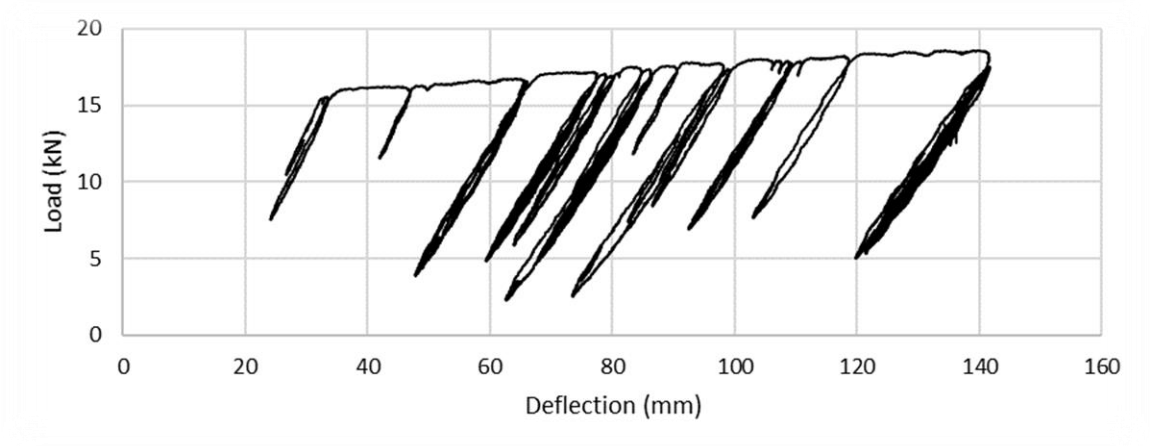

Figure F.15: The 70 m/s load-deflection hysteresis diagram of specimen LD3

Specimen LD4

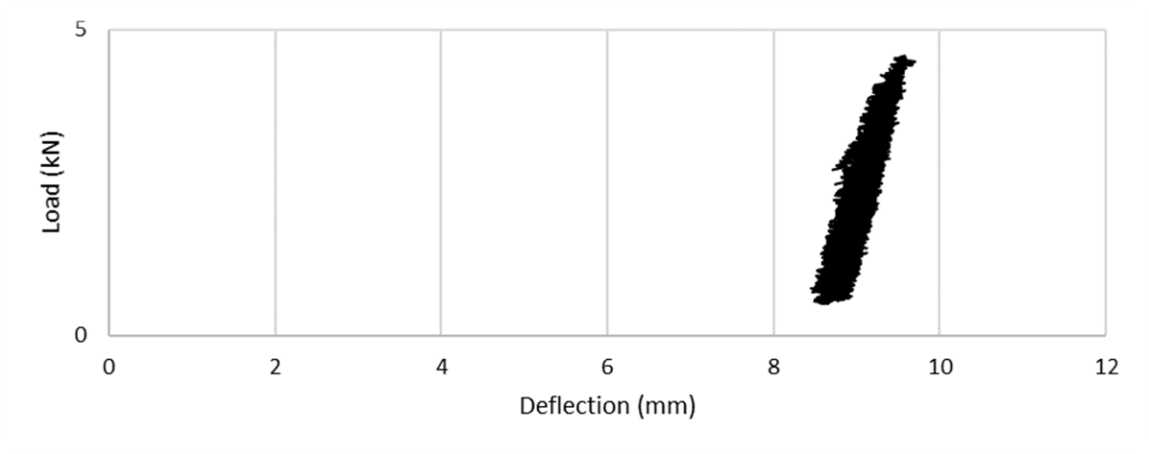

Figure F.16: The 30 m/s load-deflection hysteresis diagram of specimen LD4

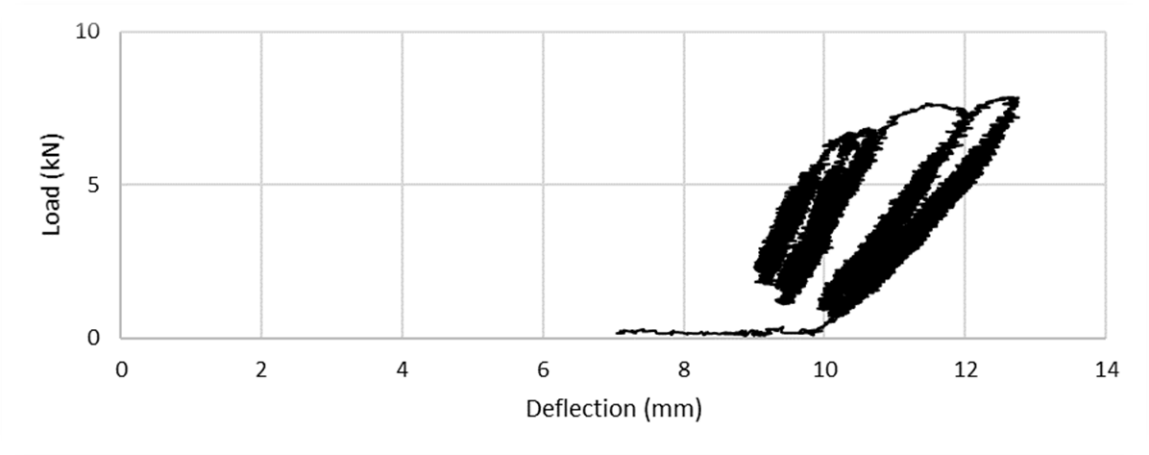

Figure F.17: The 40 m/s load-deflection hysteresis diagram of specimen LD4

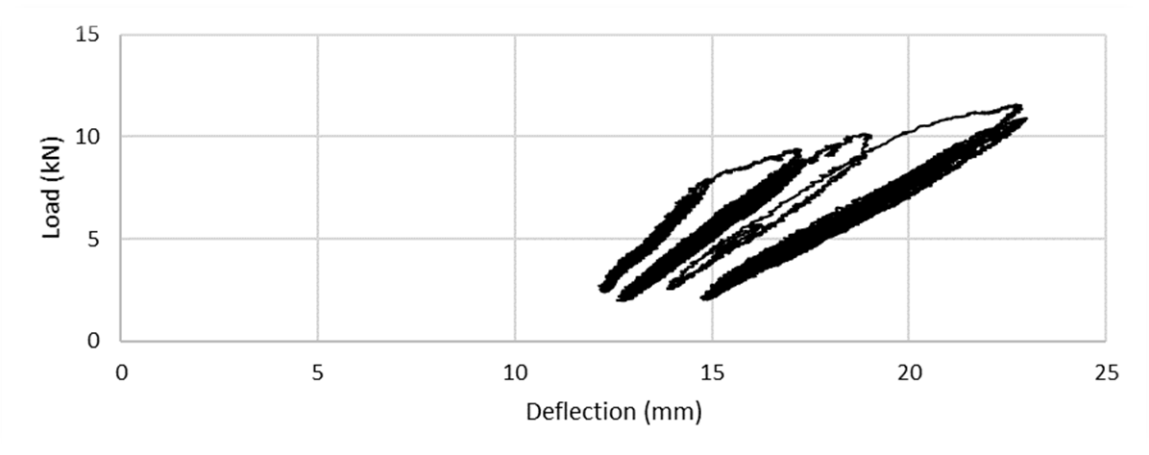

Figure F.18: The 50 m/s load-deflection hysteresis diagram of specimen LD4

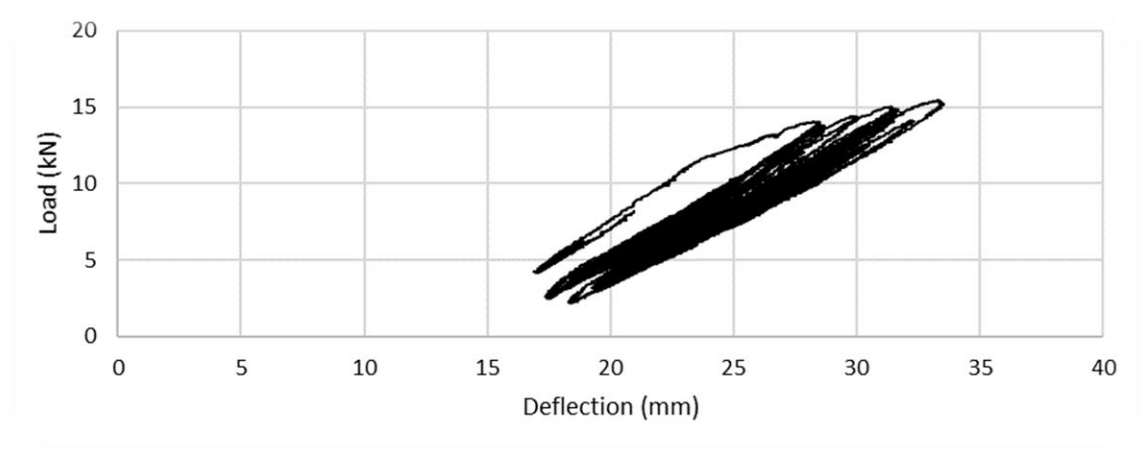

Figure F.19: The 60 m/s load-deflection hysteresis diagram of specimen LD4

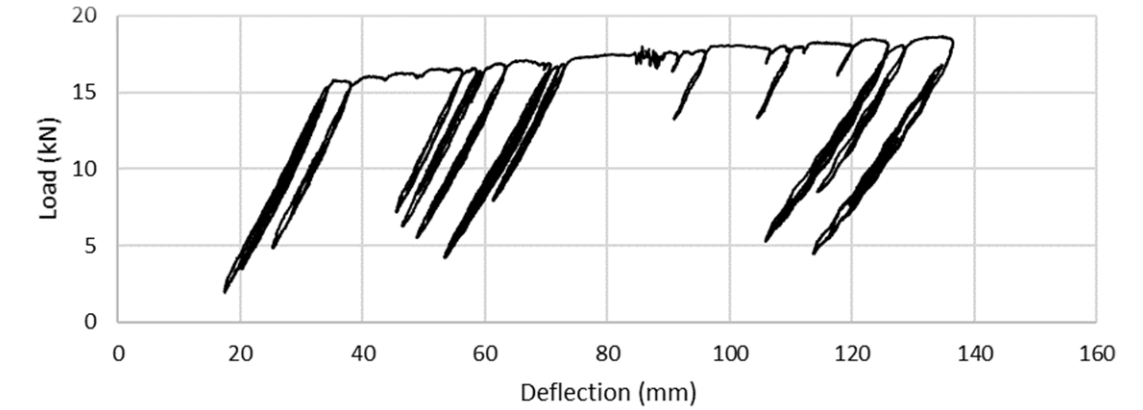

Figure F.20: The 70 m/s load-deflection hysteresis diagram of specimen LD4

Specimen LD5

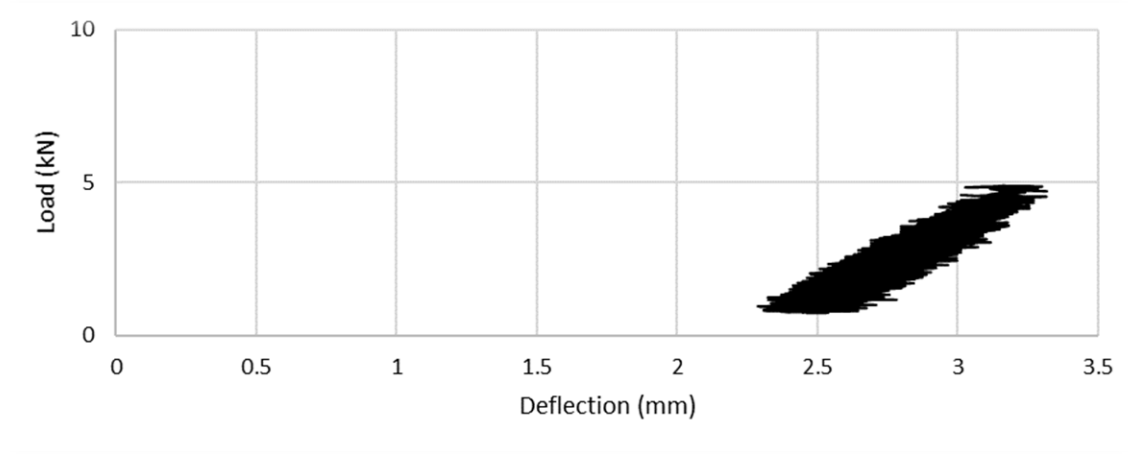

Figure F.21: The 30 m/s load-deflection hysteresis diagram of specimen LD5

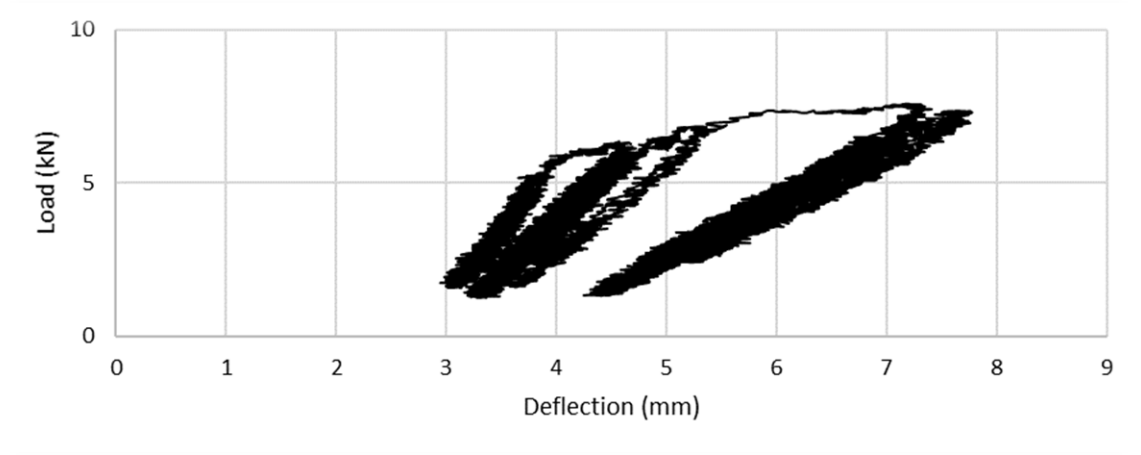

Figure F.22: The 40 m/s load-deflection hysteresis diagram of specimen LD5

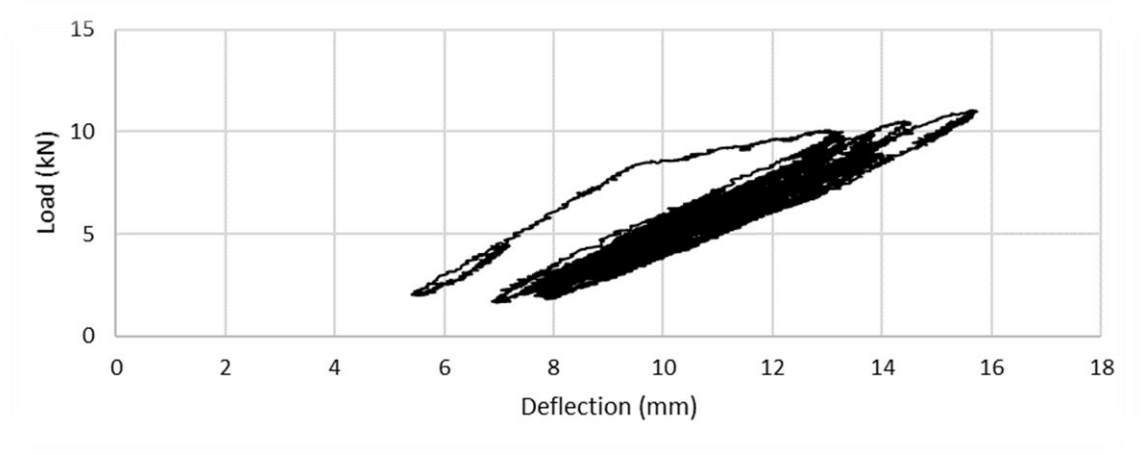

Figure F.23: The 50 m/s load-deflection hysteresis diagram of specimen LD5

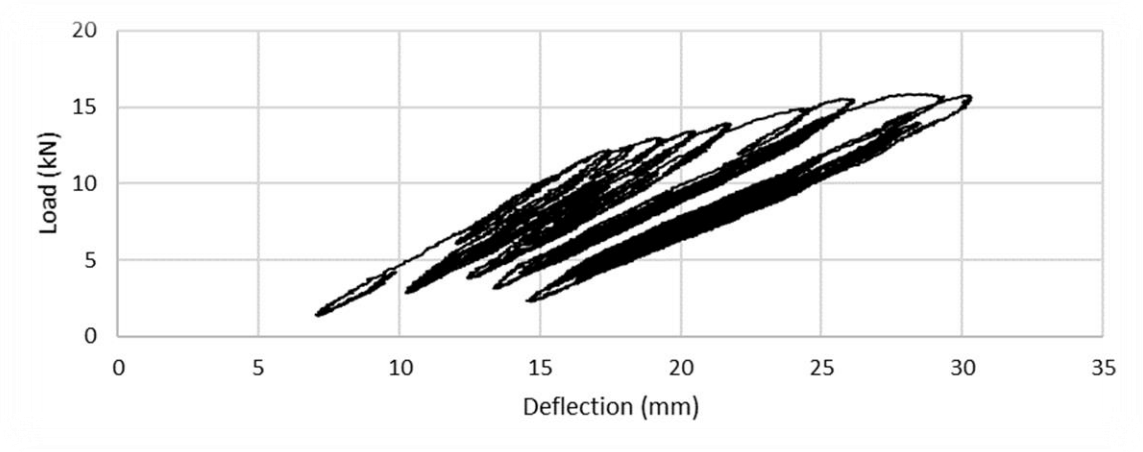

Figure F.24: The 60 m/s load-deflection hysteresis diagram of specimen LD5

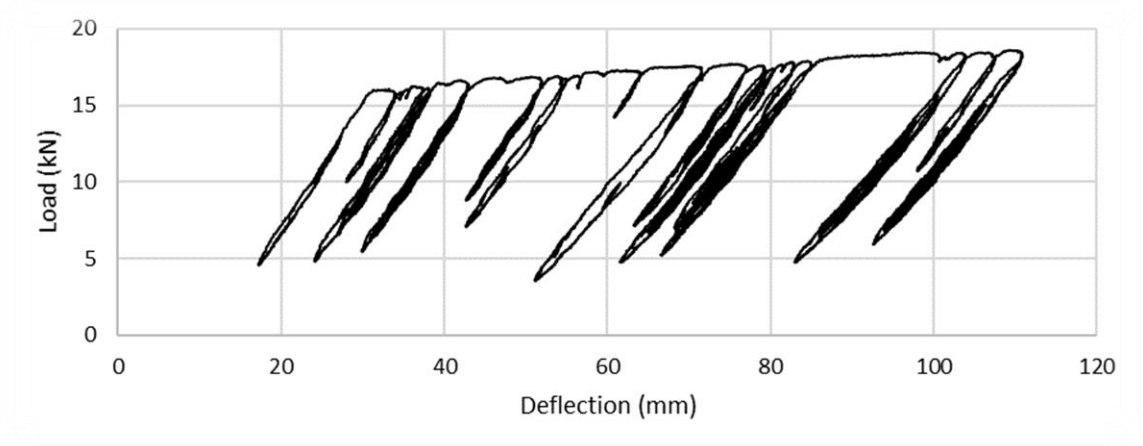

Figure F.25: The 70 m/s load-deflection hysteresis diagram of specimen LD5

Specimen HD1

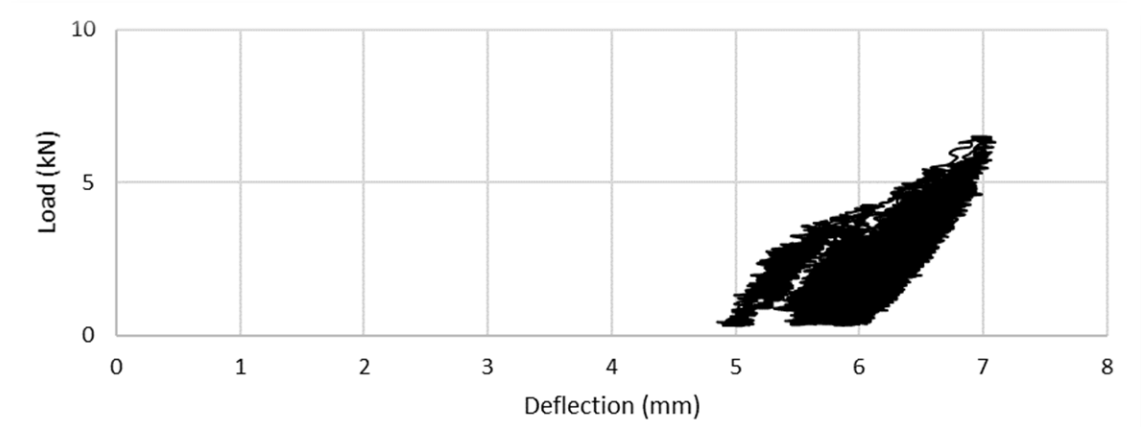

Figure F.26: The 30 m/s load-deflection hysteresis diagram of specimen HD1

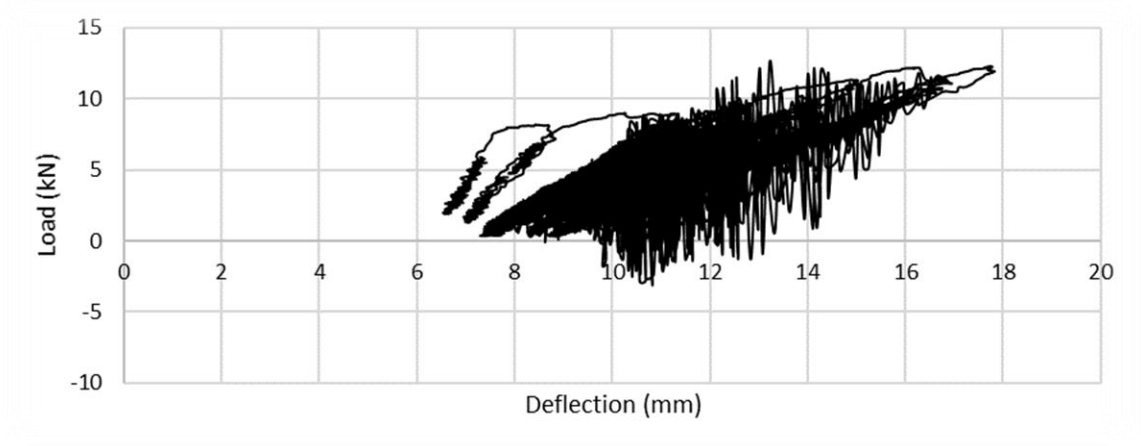

Figure F.27: The 40 m/s load-deflection hysteresis diagram of specimen HD1

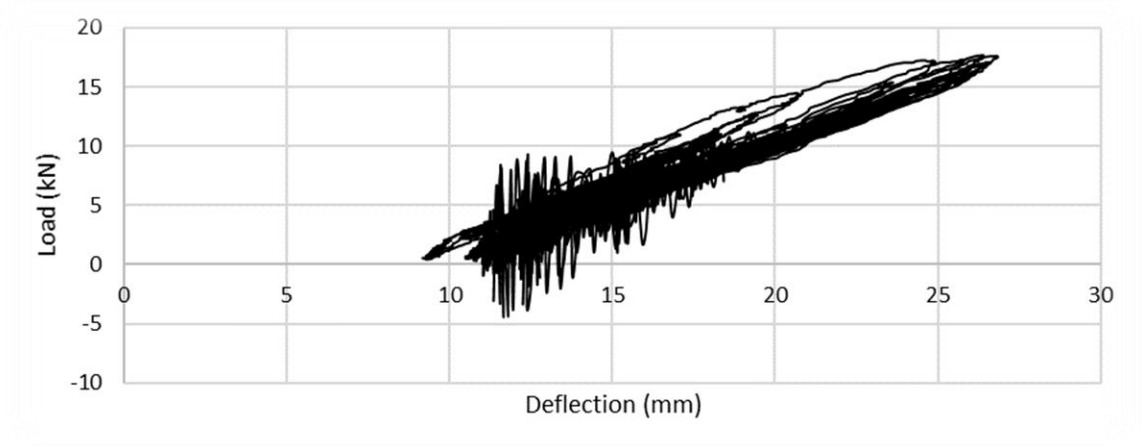

Figure F.28: The 50 m/s load-deflection hysteresis diagram of specimen HD1

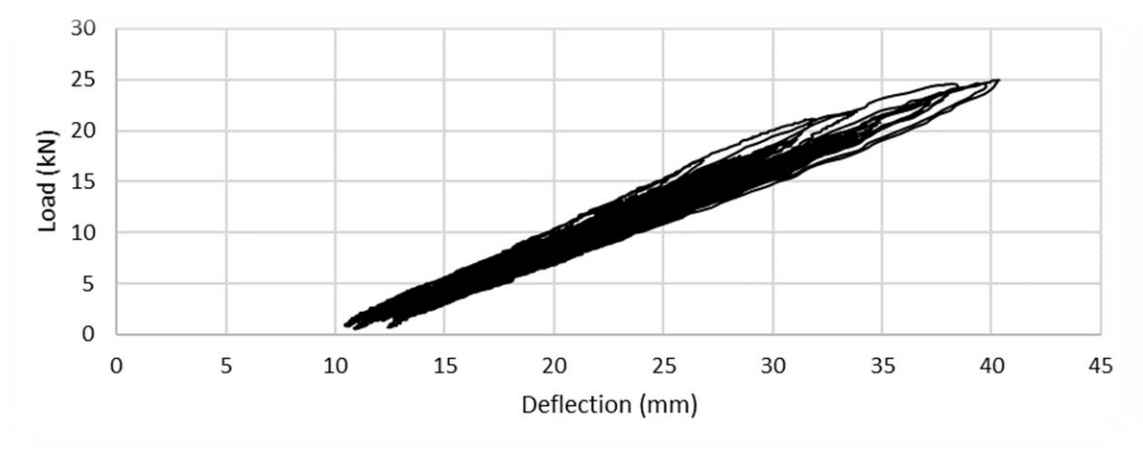

Figure F.29: The 60 m/s load-deflection hysteresis diagram of specimen HD1

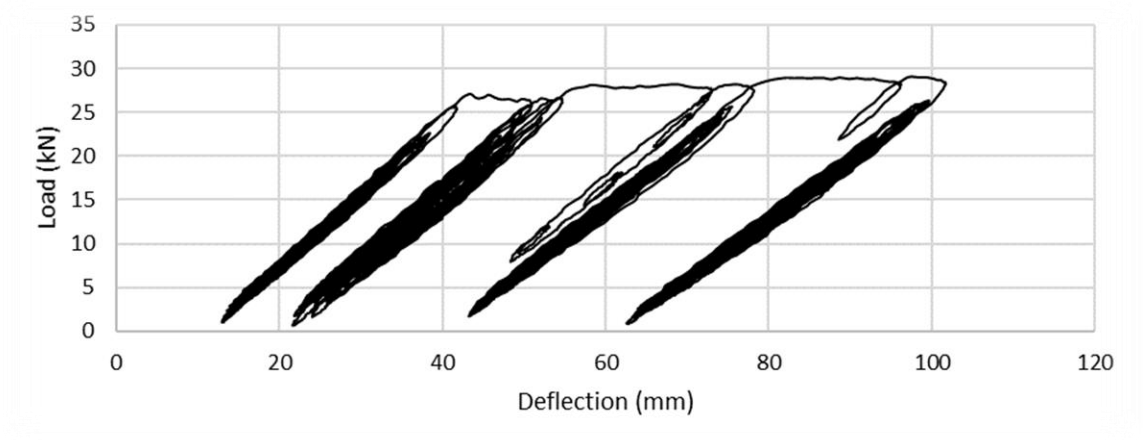

Figure F.30: The 70 m/s load-deflection hysteresis diagram of specimen HD1

Specimen HD2

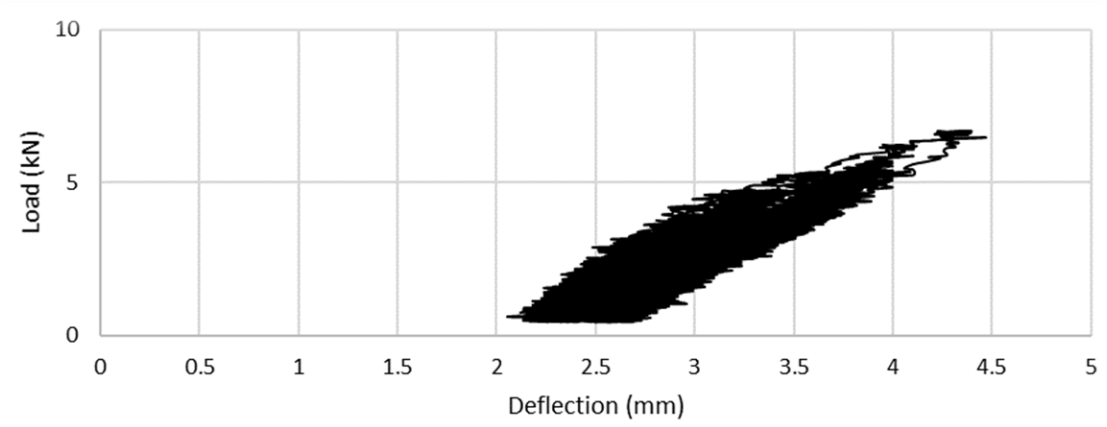

Figure F.31: The 30 m/s load-deflection hysteresis diagram of specimen HD2

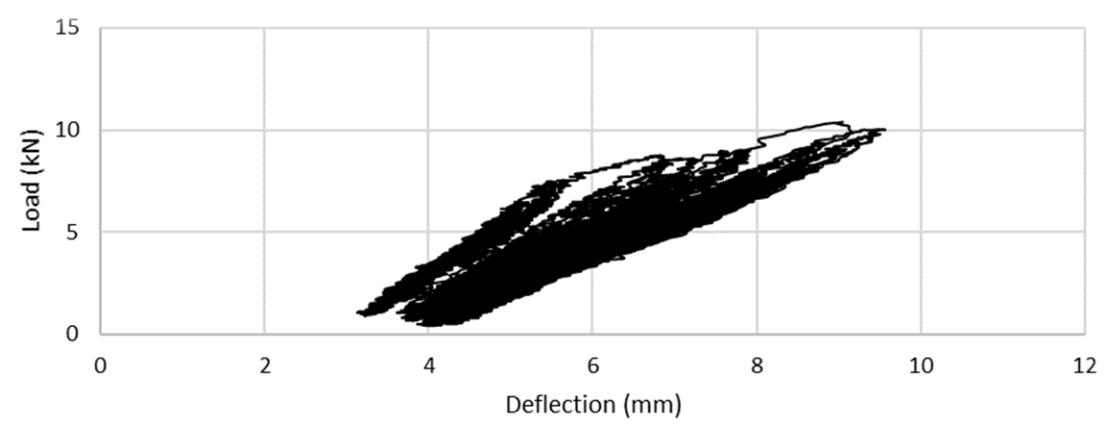

Figure F.32: The 40 m/s load-deflection hysteresis diagram of specimen HD2

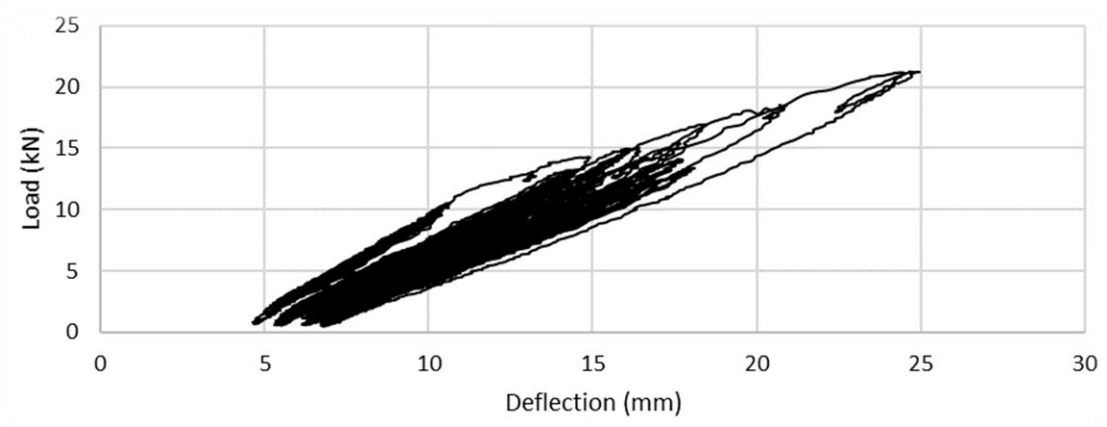

Figure F.33: The 50 m/s load-deflection hysteresis diagram of specimen HD2

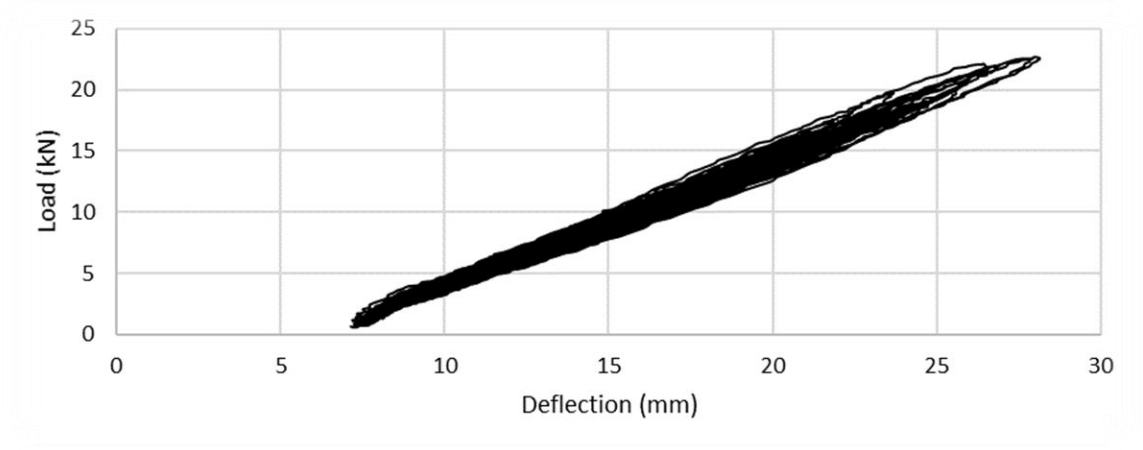

Figure F.34: The 60 m/s load-deflection hysteresis diagram of specimen HD2

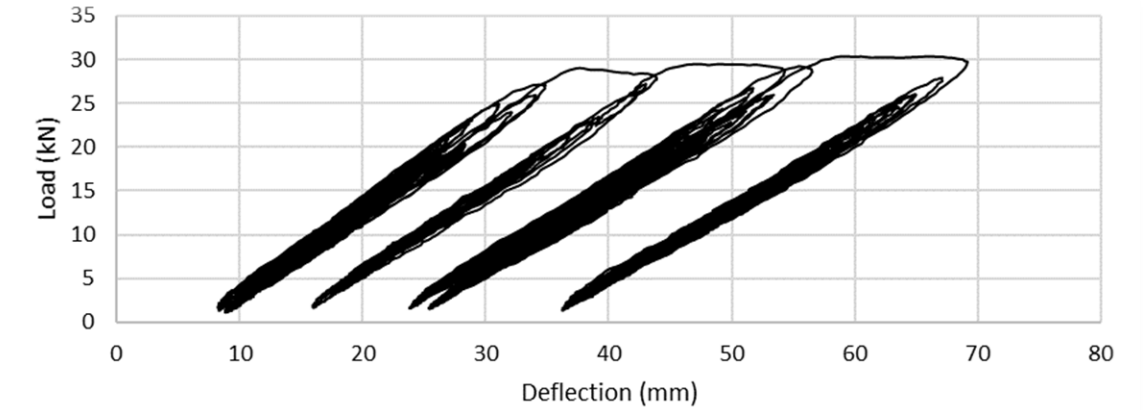

Figure F.35: The 70 m/s load-deflection hysteresis diagram of specimen HD2

Specimen HD3

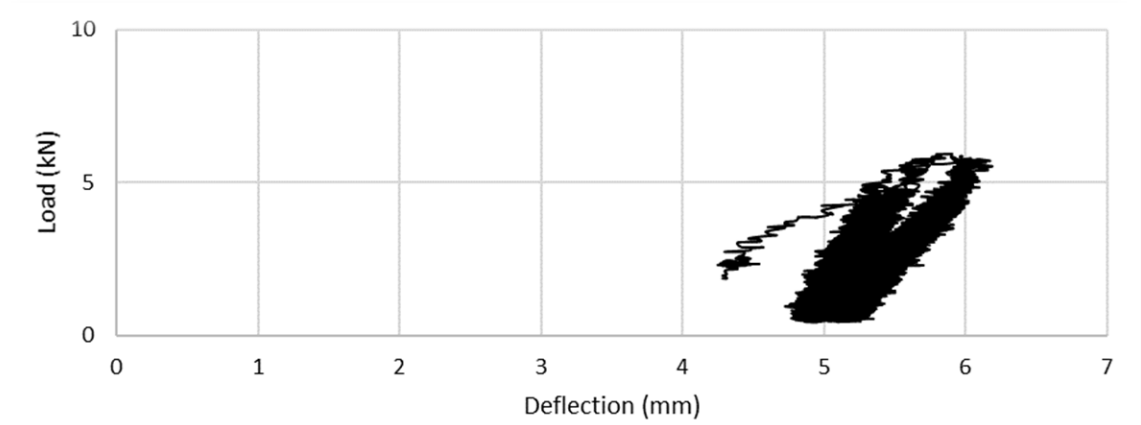

Figure F.36: The 30 m/s load-deflection hysteresis diagram of specimen HD3

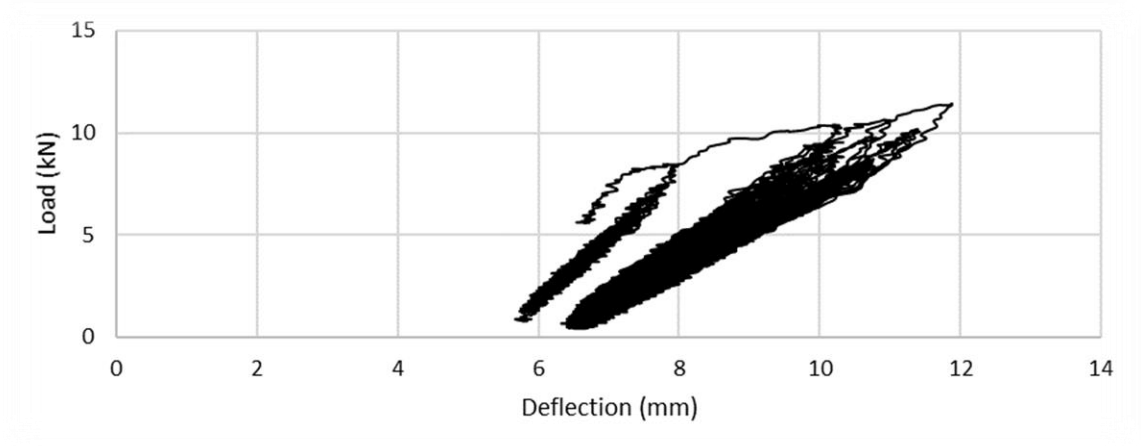

Figure F.37: The 40 m/s load-deflection hysteresis diagram of specimen HD3

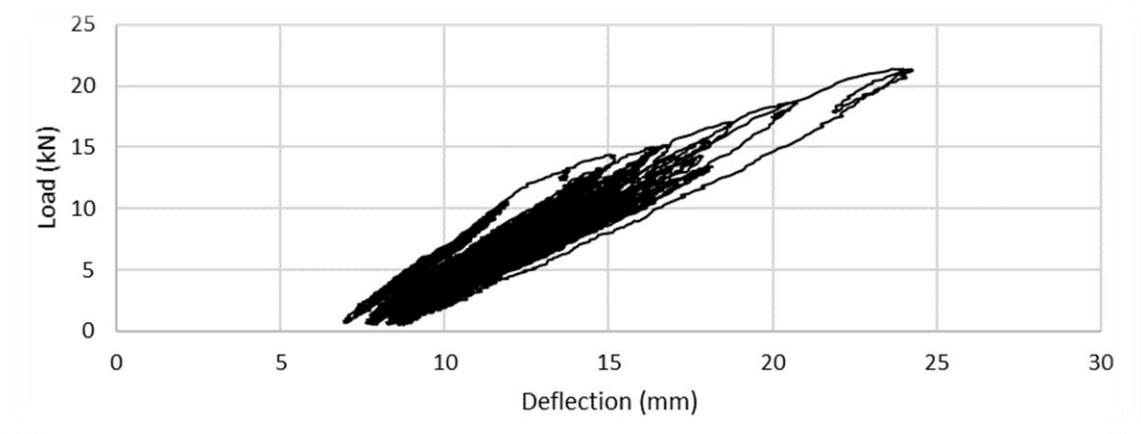

Figure F.38: The 50 m/s load-deflection hysteresis diagram of specimen HD3

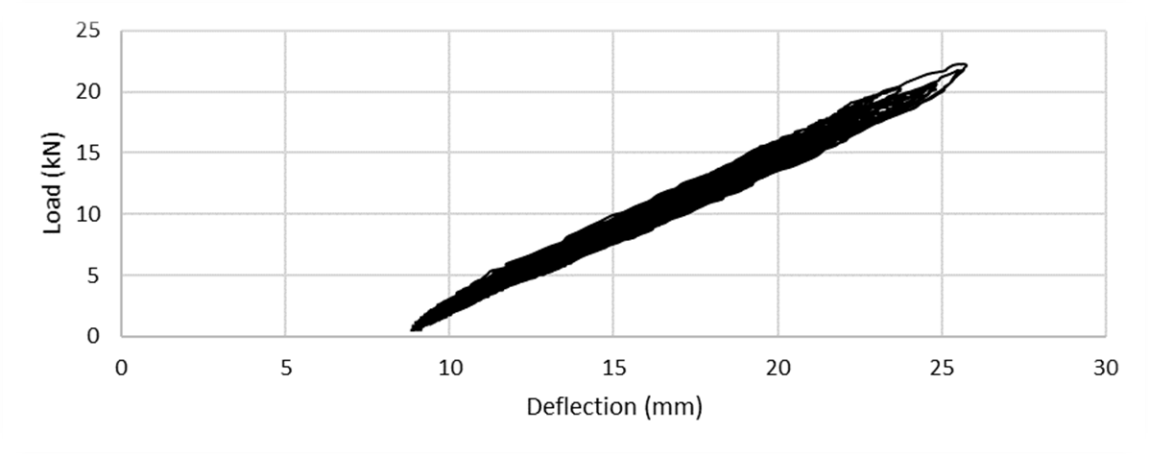

Figure F.39: The 60 m/s load-deflection hysteresis diagram of specimen HD3

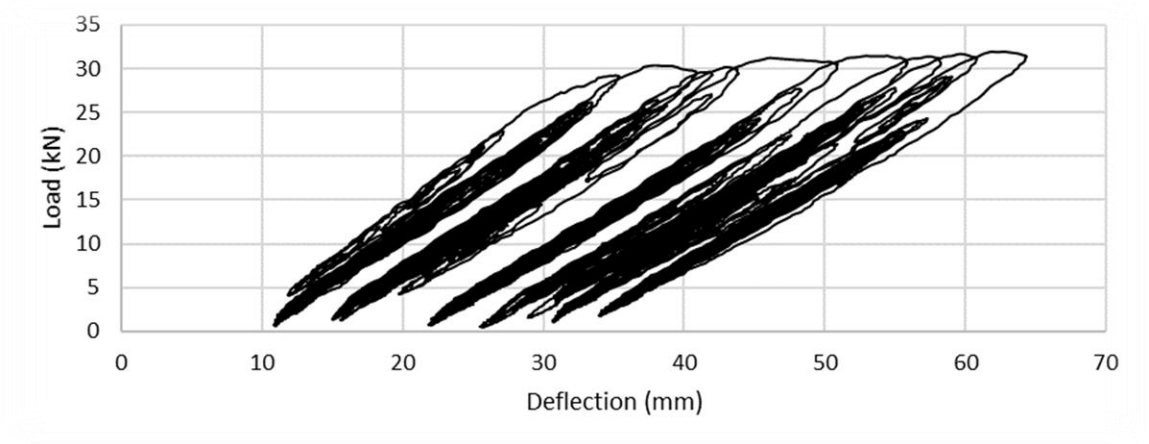

Figure F.40: The 70 m/s load-deflection hysteresis diagram of specimen HD3

Specimen HD4

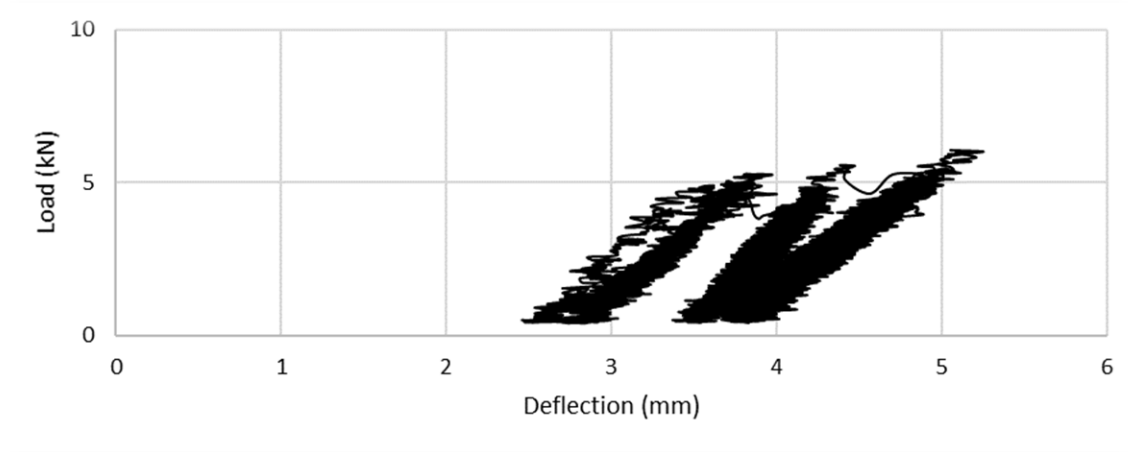

Figure F.41: The 30 m/s load-deflection hysteresis diagram of specimen HD4

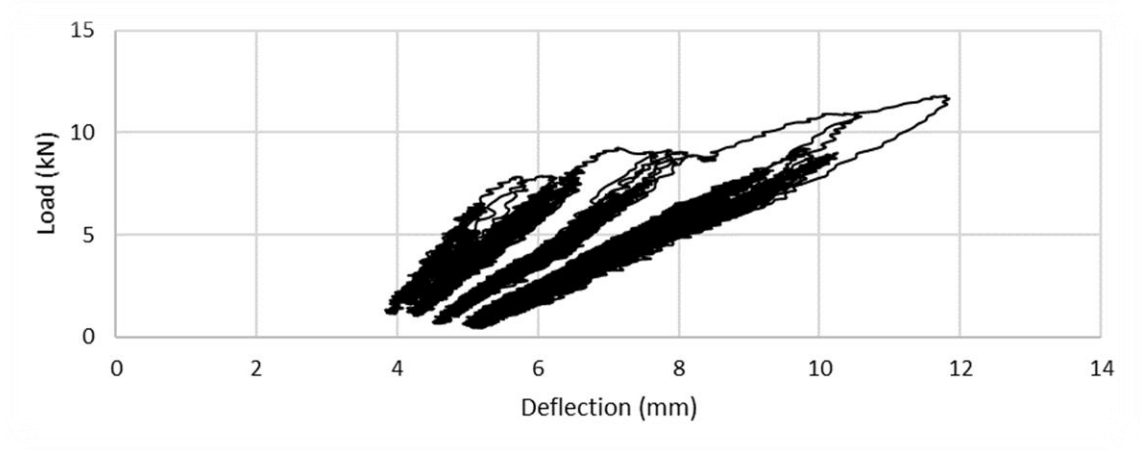

Figure F.42: The 40 m/s load-deflection hysteresis diagram of specimen HD4

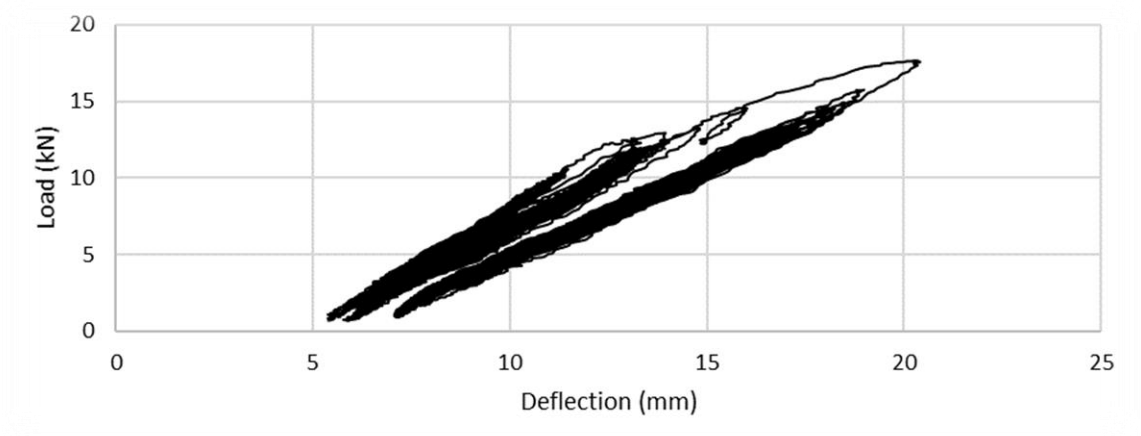

Figure F.43: The 50 m/s load-deflection hysteresis diagram of specimen HD4

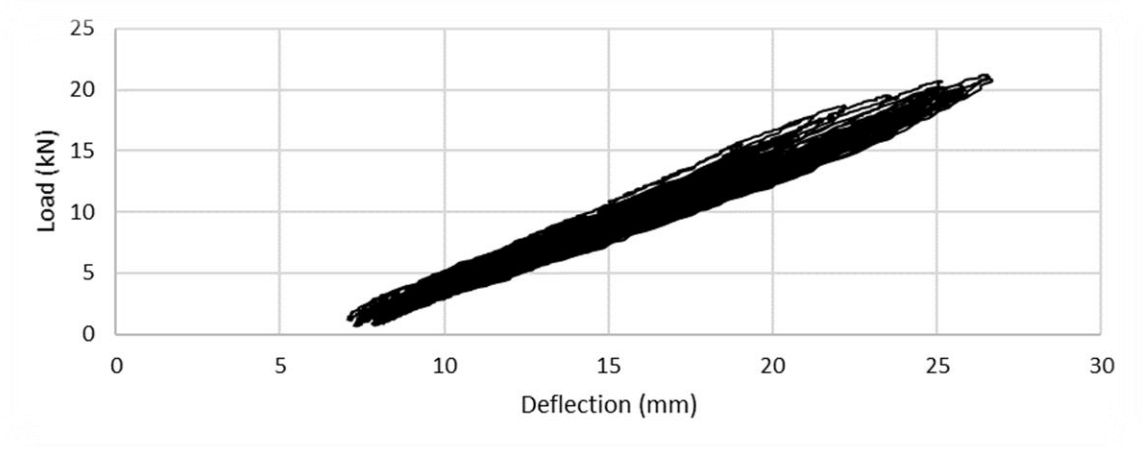

Figure F.44: The 60 m/s load-deflection hysteresis diagram of specimen HD4

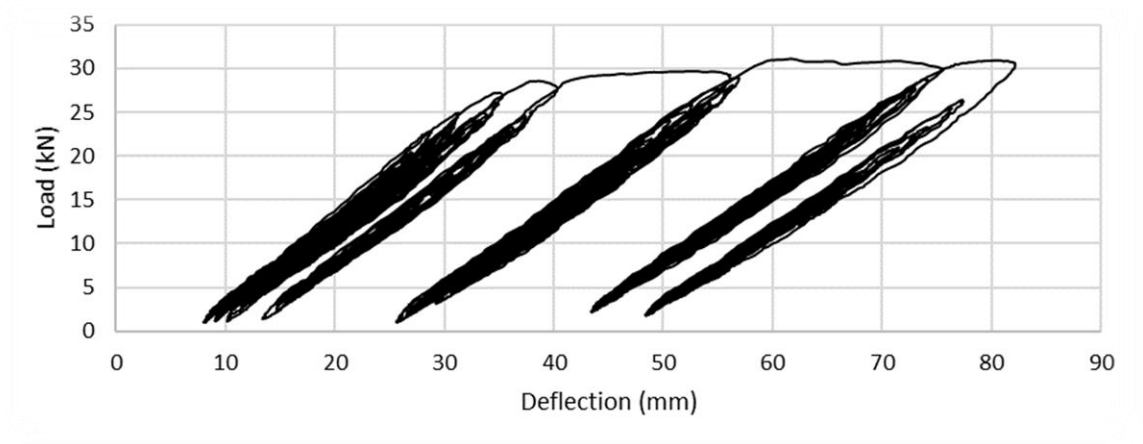

Figure F.45: The 70 m/s load-deflection hysteresis diagram of specimen HD4

Specimen HD5

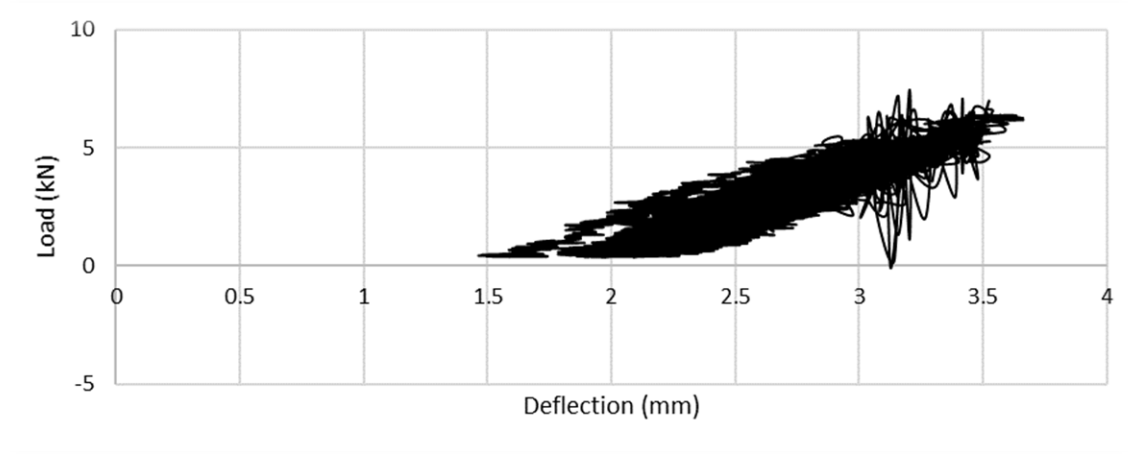

Figure F.46: The 30 m/s load-deflection hysteresis diagram of specimen HD5

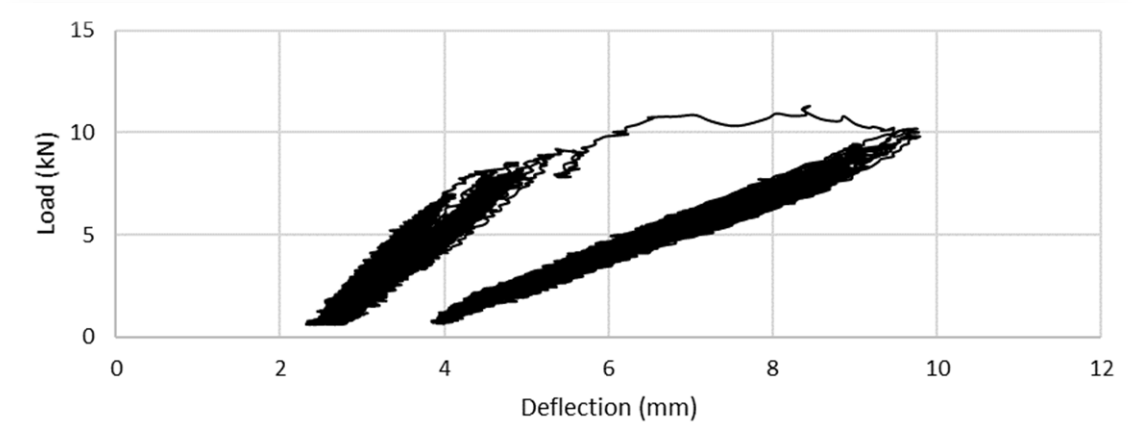

Figure F.47: The 40 m/s load-deflection hysteresis diagram of specimen HD5

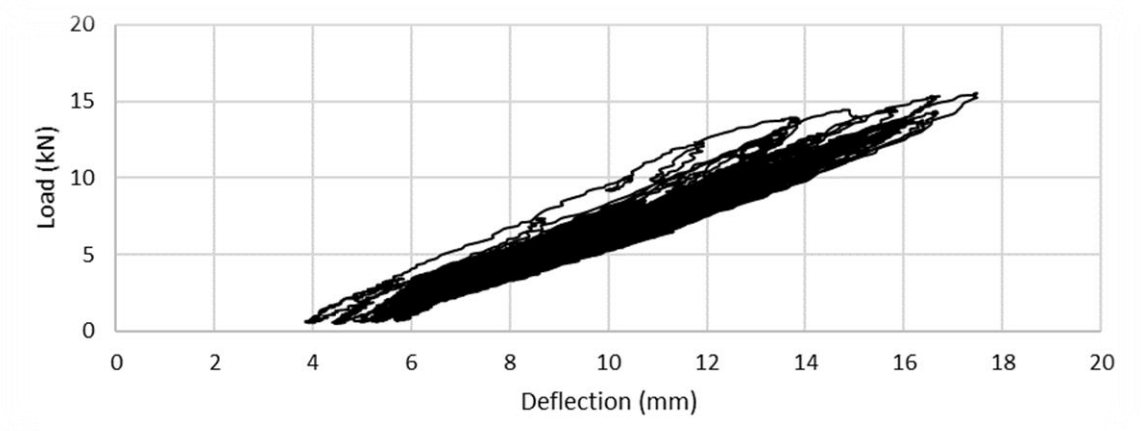

Figure F.48: The 50 m/s load-deflection hysteresis diagram of specimen HD5

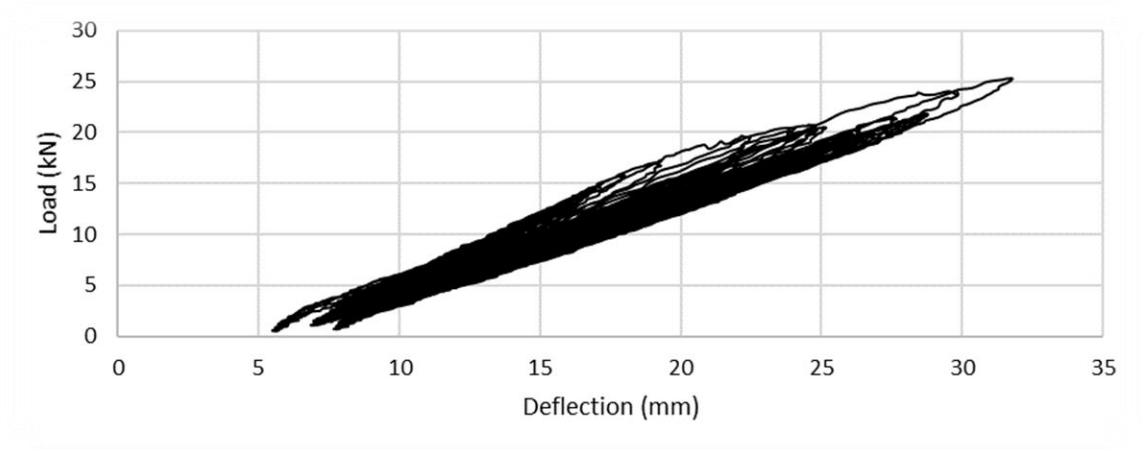

Figure F.49: The 60 m/s load-deflection hysteresis diagram of specimen HD5

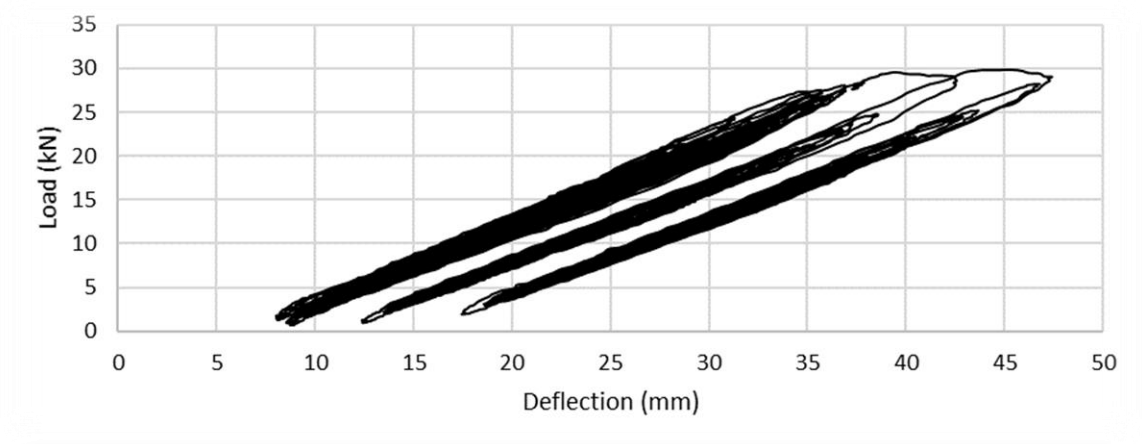

Figure F.50: The 70 m/s load-deflection hysteresis diagram of specimen HD5

Appendix G: Material Specimen Test Results

Appendix G contains the test results of the material that was used in the construction of the twenty large-scale wall specimens. This section provides a broader summary of the material specimen test results, while a detailed overview of the procedure and instrumentation is provided in Chapter 3.

Masonry Block Unit Strength

Two batches of masonry blocks were used in the construction of the wall specimens, where each batch consisted of a mixture of frog-ended and flat-ended standard concrete masonry blocks with a specified nominal strength of 15 MPa. Furthermore, batch B1 was used in the construction of the low reinforcement ratio wall specimens, whereas batch B2 was used in the construction of the high reinforcement ratio wall specimens.

Table G.1: Masonry block unit strength

Batch	Sample		Compressive Strength		
			Unit (MPa)	Mean (MPa)	CV (%)
B1	Frog ended	1	18.3	**17.0**	**16.9**
		2	19.1		
	Flat ended	1	12.8		
		2	17.6		
B2	Frog ended	1	16.8	**18.1**	**9.2**
		2	18.1		
	Flat ended	1	17.0		
		2	20.4		

Mortar Strength

Batches M1 to M15 were used in the construction of the low reinforcement ratio wall specimens, whereas batches M16 to M30 were used in the construction of the high reinforcement ratio wall specimens.

Table G.2: Mortar compressive strength

Batch	Compressive Strength of Samples (MPa)						Batch Mean	Batch CV	Mean	CV
	1	2	3	4	5	6	(MPa)	(%)	(MPa)	(%)
M1	15.0	16.8	14.7	14.7	16.5	16.3	15.7	6.0		
M2	13.1	15.0	12.8	12.1	14.5	14.1	13.6	8.1		
M3	14.7	15.0	15.3	15.0	16.4	15.1	15.2	4.0		
M4	16.6	16.7	17.3	16.4	15.5	16.8	16.5	3.6		
M5	16.8	19.0	17.3	16.6	16.7	15.9	17.1	6.1		
M6	14.5	15.3	16.1	15.4	15.6	16.6	15.6	4.5		
M7	14.0	15.5	16.2	15.6	14.7	14.2	15.0	5.7		
M8	23.4	24.2	25.6	25.1	24.3	25.8	24.7	3.8	**19.6**	**24.5**
M9	25.5	24.0	23.2	24.9	25.0	26.0	24.8	4.1		
M10	23.1	22.9	23.6	21.7	23.4	26.5	23.5	6.9		
M11	19.1	22.5	22.5	22.9	23.2	19.4	21.6	8.5		
M12	14.7	17.4	17.2	17.2	16.9	15.9	16.5	6.4		
M13	22.3	24.7	28.2	25.6	25.9	22.8	24.9	8.6		
M14	19.0	20.8	20.2	21.4	22.4	18.6	20.4	7.0		
M15	30.7	31.2	29.2	28.3	28.0	26.8	29.0	5.7		
M16	19.9	21.3	19.5	20.8	22.0	20.6	20.7	4.3		
M17	18.8	19.5	17.0	17.4	18.7	18.5	18.3	5.1		
M18	14.9	17.4	16.6	17.3	18.1	16.8	16.8	6.4		
M19	19.0	19.9	18.3	19.3	19.6	19.3	19.2	2.9		
M20	18.0	18.7	17.5	21.9	20.9	18.4	19.2	9.0		
M21	20.0	22.1	20.5	19.2	19.8	17.4	19.8	7.9		
M22	25.6	26.3	26.0	23.2	23.7	26.7	25.2	5.7		
M23	22.4	25.8	26.1	24.9	23.7	21.8	24.1	7.4	**20.7**	**12.7**
M24	21.1	24.4	22.5	27.1	25.6	24.4	24.2	8.8		
M25	23.0	20.7	21.5	20.7	22.8	21.7	21.7	4.5		
M26	18.7	19.2	18.9	18.3	18.9	17.4	18.5	3.3		
M27	21.1	20.8	19.1	18.5	19.6	19.5	19.8	5.0		
M28	20.7	20.8	19.4	18.5	18.8	19.7	19.7	4.9		
M29	22.0	22.4	20.1	20.0	19.5	18.9	20.5	6.8		
M30	24.5	24.3	21.5	19.9	19.8	21.6	21.9	9.3		

Grout Strength

Batches G1 to G12 were used in the construction of the low reinforcement ratio wall specimens, whereas batches G13 to G23 were used in the construction of the high reinforcement ratio wall specimens.

Table G.3: Grout compressive strength

Batch	Slump (cm)	Compressive Strength					
		Cylinder Samples			Absorbent Block Sample		
		Sample Mean (MPa)	Mean (MPa)	CV (%)	Sample Strength (MPa)	Mean (MPa)	CV (%)
G1	23.0	28.6			19.5		
G2	22.0	33.9			27.0		
G3	23.0	32.3			22.0		
G4	22.0	30.5			21.1		
G5	24.0	24.5			17.5		
G6	22.5	27.3	**28.3**	**13.8**	21.5	**22.4**	**14.0**
G7	23.0	28.4			23.5		
G8	21.0	27.2			23.4		
G9	22.0	33.6			28.1		
G10	22.5	27.9			18.8		
G11	25.0	23.9			24.5		
G12	22.5	21.2			21.7		
G13	17.0	27.5			18.0		
G14	22.0	26.3			20.2		
G15	19.0	29.6			23.2		
G16	24.0	26.5			18.6		
G17	19.5	27.3			20.6		
G18	22.0	28.3	**28.5**	**6.8**	21.7	**20.5**	**11.2**
G19	25.0	26.4			16.4		
G20	19.0	31.7			24.2		
G21	21.0	30.0			21.9		
G22	25.0	28.1			19.7		
G23	20.0	31.2			21.2		